การสังเคราะห์อนุภาคทองคำขนาดนาโนเมตรที่ดัดแปรด้วยพอลิเอไมด์นิวคลีอิกแอซิด

นางสาวจเรช กาญจนวรุณม์

SYNTHESIS OF GOLD NANOPARTICLES MODIFIED WITH POLYAMIDE NUCLEIC ACIDS

Miss Roejarek Kanjanawarut

A Thesis Submitted in Partial Fulfillment of the Requirements
for the Degree of Master of Science Program in Petrochemistry and Polymer Science
Faculty of Science
Chulalongkorn University
Academic Year 2007

501520

Thesis Title	SYNTHESIS OF GOLD NANOPARTICLES MODIFIED WITH POLYAMIDE NUCLEIC ACIDS
By	Miss Roejarek Kanjanawarut
Field of study	Petrochemistry and Polymer Science
Thesis Advisor	Associate Professor Tirayut Vilaivan, D.Phil.
Thesis Co-advisor	Assistant Professor Voravee P. Hoven, Ph.D.

Accepted by the Faculty of Science, Chulalongkorn University in Partial Fulfillment of the Requirements for the Master's Degree

.... Dean of the Faculty of Science

(Professor Supot Hannongbua, Dr.rer.nat.)

THESIS COMMITTEE

.... Chairman

(Associate Professor Sirirat kokpol, Ph.D.)

.... Thesis Advisor

(Associate Professor Tirayut Vilaivan, D.Phil)

.... Thesis Co-advisor

(Assistant Professor Voravee P. Hoven, Ph.D.)

.... Member

(Assistant Professor Warinthorn Chavasiri, Ph.D.)

.... Member

(Gamolwan Tumcharern, Ph.D.)

รจเรข กาญจนวรุตม์ : การสังเคราะห์อนุภาคทองคำขนาดนาโนเมตรที่ดัดแปรด้วย
พอลิเอไมด์นิวคลีอิกแอซิด. (SYNTHESIS OF GOLD NANOPARTICLES
MODIFIED WITH POLYAMIDE NUCLEIC ACID) อ. ที่ปรึกษา : รศ.ดร.
ธีรยุทธ วิไลวัลย์, อ. ที่ปรึกษาร่วม : ผศ.ดร. วรวีร์ โฮเว่น, 146 หน้า.

งานวิจัยนี้ได้ทำการสังเคราะห์อนุภาคทองคำขนาดนาโนเมตรที่ดัดแปรด้วยพอลิเอไมด์
นิวคลีอิกแอซิด (พีเอ็นเอ) ชนิดใหม่ที่มีประจุแตกต่างกันและศึกษาผลของประจุที่ส่งผลต่ออนุภาค
ทองคำนั้นด้วยเทคนิคยูวีวิซิเบิล โปตอนคอร์รีเรชั่นสเปกโตรสโกปีและกล้องจุลทรรศน์อิเล็คตรอ
นแบบส่องผ่านผลการทดลองแสดงให้เห็นว่าพีเอ็นเอที่มีการดัดแปรให้มีประจุบวกจะทำให้อนุภาค
ทองคำเกิดการรวมกลุ่มกัน ในทางตรงกันข้ามอนุภาคทองคำที่มีพีเอ็นเอที่เป็นกลางและมีประจุเป็น
ลบนั้นจะเสถียรกว่า รวมถึงพีเอ็นเอที่ตรึงอยู่บนอนุภาคทองคำที่สังเคราะห์ได้ไม่สามารถจับยึดกับดี
เอ็นเอที่มีลำดับเบสคู่สมกันไม่ว่าจะมีประจุแบบใด ในงานนี้ได้ยังนำเสนอแนวความคิดใหม่ในการ
ตรวจวัดลำดับเบสของดีเอ็นเอโดยอาศัยการรวมกลุ่มของอนุภาคทองคำที่เหนี่ยวนำด้วยพีเอ็นเอที่มี
การดัดแปร ที่ปลายข้างหนึ่งด้วยประจุบวกและไทออล ซึ่งพีเอ็นเอนี้จะไปปรับสภาพประจุจากเดิม
ของอนุภาคทองคำที่เป็นลบให้มีสภาพเป็นกลางจึงเป็นสาเหตุให้อนุภาคทองคำนั้นเกิดการรวมกลุ่ม
กันขึ้น ถ้านำพีเอ็นเอนี้จับยึดกับดีเอ็นเอก่อนที่จะตรึงลงบนอนุภาคทองคำ ประจุลบของหมู่ฟอสเฟต
บนดีเอ็นเอจะป้องกันไม่ให้อนุภาคทองคำนั้นเกิดการรวมกลุ่มกันในลักษณะที่จำเพาะเจาะจงกับ
ลำดับเบส โดยหลักการนี้สามารถนำไปตรวจสอบดีเอ็นเอที่มีลำดับเบสผิดไปหนึ่งตำแหน่งจากพี
เอ็นเอโพรบที่มีความยาว 9 ถึง 13 เบสได้

สาขาวิชา ปิโตรเคมีและวิทยาศาสตร์พอลิเมอร์ ลายมือชื่อนิสิต..............
ปีการศึกษา 2550 ลายมือชื่ออาจารย์ที่ปรึกษา..............
ลายมือชื่ออาจารย์ที่ปรึกษาร่วม..............

4872425823 : MAJOR PETROCHEMISTRY AND POLYMER SCIENCE

KEY WORD: POLYAMIDE NUCLEIC ACID / PNA / DNA

ROEJAREK KANJANAWARUT : SYNTHESIS OF GOLD NANOPARTICLES MODIFIED WITH POLYAMIDE NUCLEIC ACIDS. THESIS ADVISOR : ASSOC. PROF. TIRAYUT VILAIVAN, D.Phil., THESIS CO ADVISOR : ASST. PROF. VORAVEE P. HOVEN, Ph.D., 146 pp.

Gold nanoparticles (gold NPs) modified with thiolated polyamide nucleic acids (PNA) carrying different charge moieties were prepared and characterized by UV-VIS spectroscopy, Photon Correlation Spectroscopy (PCS), and Transmission Electron Microscopy (TEM). The results demonstrated that the positively charged PNA modifier causes aggregation of the gold nanoparticle. By contrast, the gold nanoparticles modified with neutral and negatively charged PNAs are more stable towards aggregation. In all cases, the gold nanoparticles-bond PNA could not hybridize with their complementary DNAs. A new concept of DNA sequences determination based on gold nanoparticles aggregation induced by positively charged thiol-modified PNA was proposed. The PNA causes aggregation by neutralization of the negatively charge of the gold nanoparticles. If the PNA is first hybridized with DNA, the negatively-charge phosphate group of the DNA prevents PNA-induced aggregation in a sequence-specific manner. This concept has been validated and the technique has been used to determine single base mismatch in the DNA target of 9-13 base pair in length.

Field of study Petrochemistry and Polymer Science   Student's signature...........

Academic year ....2007...............   Advisor's signature.......

Co-advisor's signature.......

ACKNOWLEDGEMENTS

ศูนย์วิทยทรัพยากร
จุฬาลงกรณ์มหาวิทยาลัย

CONTENT

LIST OF TABLES

ศูนย์วิทยทรัพยากร
จุฬาลงกรณ์มหาวิทยาลัย

LIST OF FIGURES

LIST OF SCHEMES

ศูนย์วิทยทรัพยากร
จุฬาลงกรณ์มหาวิทยาลัย

LIST OF ABBREVIATIONS

A	adenine
A^{Bz}	N^4-benzoyladenine
Abs	absorbance
ACPC	D-prolyl-2-aminocyclopentane-carboxylic acid
AFM	atomic force microscopy
B	nucleobase
Boc	*tert*-butoxycarbonyl
br	broad
Bz	benzoyl
BzS	benzoylthiol
c	concentration
C	cytosine
^oC	degree celcius
calcd	calculated
C^{Bz}	N^4-benzoylcytosine
CCA	α-cyano-4-hydroxy cinnamic acid
$CDCl_3$	deuterated chloroform
CH_3CN	acetonitrile
d	doublet
DIAD	diisopropylazodicarboxylate
DIEA	N, N'-dimethylaminopyridine
DMF	N, N'-dimethylformamide
DMSO-d_6	deuterated dimethylsulfoxide
DNA	deoxyribonucleic acid
DNPS	3-(2,4-dinitrophenylthio)
Dpm	diphenylmethyl
EDC	1-ethyl-3-(3-dimethylaminopropyl)-carbodiimide hydrochloride
EtOAc	ethyl acetate
Fmoc	9-fluorenylmethoxycarbonyl
FmocOSu	9-fluorenylmethyl N-succimidyl carbonate
g	gram

G	guanine
G^{ibu}	N^2-isobutyrylgaunine
h	hour
H	proton
HATU	O-(7-azabenzotriazol-1-yl)-N, N, N', N' -tetramethyluronium hexaflurophosphate
HOAt	1-hydroxy-7-azabenzotriazole
HPLC	high performance liquid chromatography
Hz	hertz
Ibu	isobutyryl
IR	infrared spectroscopy
J	coupling constant
KHz	kilohertz
Lys	lysine
m	multiplet
MALDI-TOF	matrix-assisted laser desorption/ionization-time of flight
mg	milligram
MHz	megahertz
min	minute
mL	milliliter
mmol	millimole
mm	millimeter
mp.	melting point
NHS	N-hydroxysuccinimide
nm	nanometer
NMR	nuclear magnetic resonance
NPs	nanopartilces
Pfp	pentafluorophenyl
PfpOTfa	pentafluorophenyl trifluoroacetic acid
Ph	phenyl
Phos	Phosphonium
pmol	picromole
PNA	polyamide nucleic acid or peptide nucleic acid
s	singlet

SAM	self assembly monolayer
SPPS	solid phase peptide synthesis
t	triplet
T	thymine
T^{Bz}	N^3-benzoylthymine
TEM	transmission electron microscopy
TFA	trifluoroacetic acid
THF	tetrahydrofuran
TLC	thin layer chromatography
T_m	melting temperature
t_R	retention time
v	volume
UV	ultraviolet
µL	microliter
µmol	micromole
δ	chemical shift

CHAPTER I

INTRODUCTION

1.1 Polyamide nucleic acid (PNA)

Polyamide nucleic acid or peptide nucleic acid (PNA), elegantly developed by Nielson's group[1], is one of the most interesting DNA analogues from both theoretical and practical points of view. The negatively charged sugar-phosphate backbone of DNA is totally replaced by an uncharged polyamide backbone (**Figure 1.1**) leading to the electronically neutral PNA which could still retain the binding specificity of DNA.
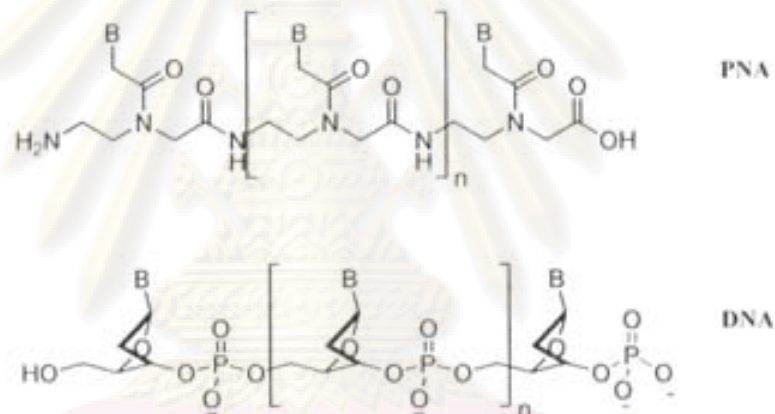
Figure 1.1 Structures of PNA and DNA: B = nucleobase

PNA offers several advantages over DNA in many applications including diagnostics and therapeutics. Firstly, the binding of PNA to its complementary DNA is highly sequence-specific. Secondly, The PNA·DNA hybrids are more stable than the corresponding DNA·DNA hybrids due to the absence of electrostatic repulsion between negative charge: and, a mismatch in a PNA·DNA hybrids is generally more destabilizing than a mismatch in a DNA·DNA duplex.[2] Furthermore, PNA is resistant to nucleases which should improve its in vivo.

These favorable properties of PNA have attracted wide attention in medicinal researchs for development of gene therapeutic (antisense and antigene) drugs[3] and

in biotechnology for development of diagnostic tools.[4] especially nucleic acid biosensor. A number of PNA systems have been developed but none of them had shown better properties than the original PNA. In 2005 Vilaivan et al.[5] have reported synthesis of a novel conformationally rigid pyrrolidinyl PNA based on D-prolyl-2-aminocyclopentane-carboxylic acid (ACPC) backbones. The precise stereochemistry of the backbone was found to be very important in determining the binding properties. Only the PNA containing (1S, 2S)-ACPC (**Figure 1.2a**) can form a very stable 1:1 complex with the complementary DNA in a sequence-specific manner. The thymine decamer (1S, 2S)-ACPC PNA can bind to the complementary DNA with a higher affinity and specificity than Nielsen's PNA (**Figure 1.2b**). The high specificity is also retained in the more complex mixed based sequences. This PNA system is therefore an interesting candidate for replacement of Nielsen's PNA in various applications, especially DNA sequences determination.
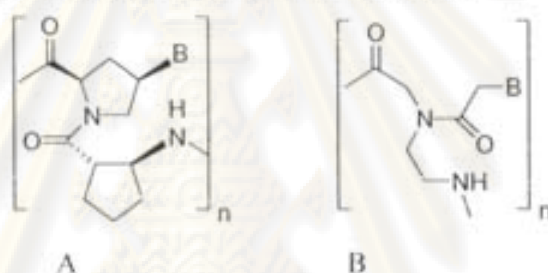
Figure 1.2 Structures of (A) (1S, 2S)-ACPC PNA or Vilaivan's PNA and (B) Nielsen's PNA

1.2 Nanotechnology

Recent advances in nanotechnology have provided a variety of nanostructured materials with highly controlled and interesting properties. The essence of nanotechnology is to produce and manipulate well-defined structures on the nanometer scale with high accuracy.[6] Nanoparticles are attractive probe candidates because of their small size (1-100 nm) and chemically tailorable physical properties, which directly relate to size, composition, and shape. The size of nanoparticles can be an advantage over a bulk structure because a target binding event involving the nanoparticles can have a significant effect on its physical and chemical properties.

Metal nanoparticles have attracted a lot of interests because of their unique optical properties. Nanoparticles of alkali noble metals such as copper, silver, and

gold have a broad absorption band in the visible region of the electromagnetic spectrum.[7-11] Gold (Au) nanoparticles have been the most widely studied class of metal nanoparticles because of tailorable optical properties, and availability of various chemistries to functionalize their surfaces. Solution of gold nanoparticles shows a very intense color, which depended strongly upon the size and shape of gold nanoparticles (**Figure 1.3**). The particles size can be manipulated during the preparation of the nanoparticles by adjusting the stoichiometric ratio of the gold nanoparticles precursor (hydrogen tetrachloroaurate) to the reducing agent (sodium citrate) [12,13].
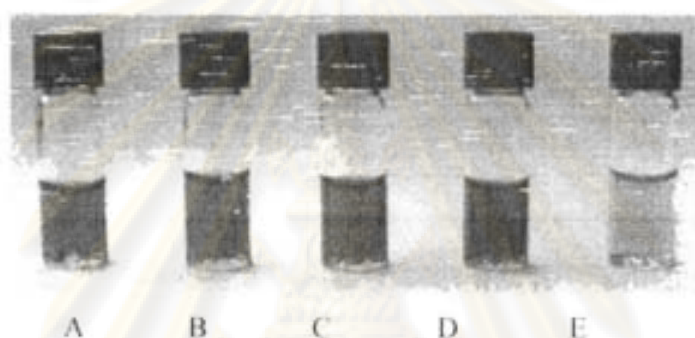
Figure 1.3 The color of gold nanoparticles sizes: (A) 18 nm, (B) 65 nm, (C) 150 nm, (D) 200 nm, and (E) 250 nm[12,13].

The color of gold nanoparticles is attributed to the collective oscillation of the free conduction electrons induced by an interacting electromagnetic field. These resonances are also denoted as surface plasmons (**Figure 1.4**)[14].
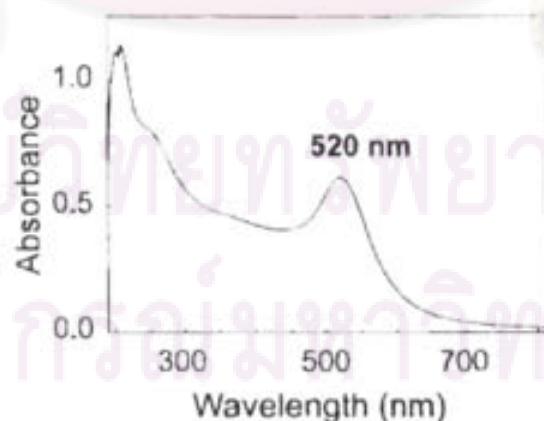
Figure 1.4 UV-VIS spectrum of an aqueous solution of 13-nm particles.

Gold binds to thiols with a high affinity to form a self-assembled monolayer (SAM). The use of functionalized thiol can introduce a variety of chemical functionalities with specific affinities onto the surface of gold nanoparticles (**Figure 1.5**)[15].
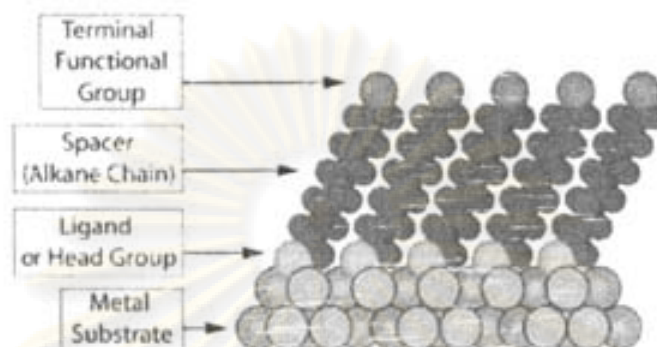
Figure 1.5 SAMs of alkanethiolates supported on a gold nanoparticles [15].

In general, the adsorbed density of the nanoparticles can be changed by modulating the surface functionality and the charge on the particles, the time of deposition, the pH and the salt concentration of the depositing solution, and the density of the active groups on the capture surface etc. In 1983, Nuzzo et al.[16] reported adsorption of bifunctional organic disulfides on gold surfaces. In 1993, Mulvaney and Giersig[17] reported the stabilization of gold nanoparticles with alkanethiols. Weisbecker and coworkers[18] described the preparation and characteristic of self-assembled monolayer (SAMs) of alkanethiolates via adsorption of alkanethiols onto the surfaces of gold colloids in aqueous dispersions. In 2002, Rongchao Jin et al.[19] reported the immobilization trithiol-capped oligodeoxyribonucleotide on gold nanoparticles. These DNA-gold nanoparticle conjugates exhibit substantially higher stability than analogs prepared from monothiol and cyclic disulfide-capped oligodeoxyribonucleotides. From this reports can bring to immobilization thiol-functionalized oligonucleotides on gold nanoparticles for detection of hybridization.

1.3 Optical Biosensor

The emergence and recent advance of nanoscience and nanotechnology present new opportunities for the application of nanoparticles in bioanalysis. Nanotechnology has helped the development of novel biosensors for biological and medical applications. Nanobioconjugates that consists of various functional nanoparticles linked to biological molecules have been used in many areas such as diagnostics[20-22], therapeutics[23-28], sensors[29-33], and bioengineering[34,35]. Detection methods based on these nanobioconjugates show increased selectivity and sensitivity as compared with many conventional assays that rely on molecular probes.

Gold nanoparticles may be easily modified with thiol-functionalized oligonucleotides. For examples Cardenas and co-workers[36] reported stability of gold nanoparticles before and after modification with thiol-ssDNA. A typical preparation consists of four steps. Step 1, gold nanoparticles were derivatized with disulfide-protected oligonucleotides (thiol-ssDNA) in aqueous solution overnight. The dispersion was incubated in NaCl (0.1 M) and sodium phosphate buffer (5 mM, pH 7) for another 2 h. The volume was then reduced at 40 °C over 3-4 h. In the last step, unbound oligonucleotides were removed by centrifugation washing. Cryo-TEM images of gold nanoparticles before and after modification by thiol-ssDNA (**Figure 1.6**) suggested that although some aggregation was observed due to centrifuge, the thiol-ssDNA-gold nanoparticles did stabilize the gold nanoparticles dispersion.
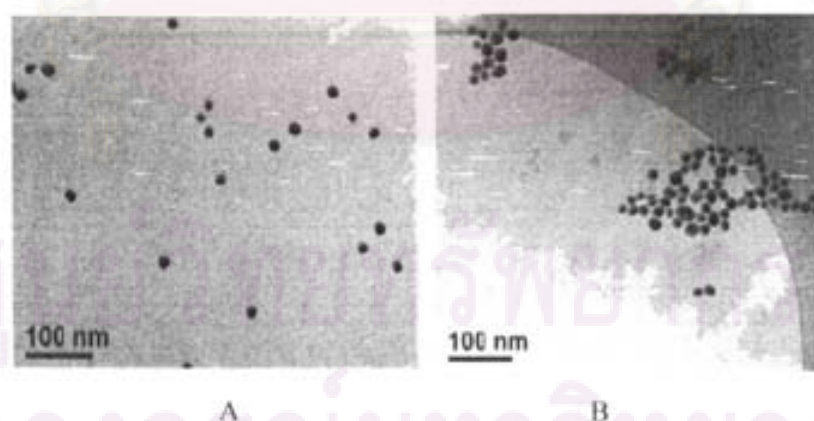
Figure 1.6 Cryo-TEM images of gold nanoparticles dispersed in water (A) and thiol-ssDNA-modified gold nanoparticles (B)[36].

In 1998 storhoff and co-workers[37] studied properties of gold nanoparticles derivatized with 12 base oligonucleotide functionalized with 5'-hexanethiol. The immobilization procedure was similar to the one described earlier. The UV-VIS spectra of the modified and unmodified gold nanoparticles in aqueous solution at 0.3 M NaCl are shown in **Figure 1.7**. The position of the SPR band suggested that partial aggregation also took place.
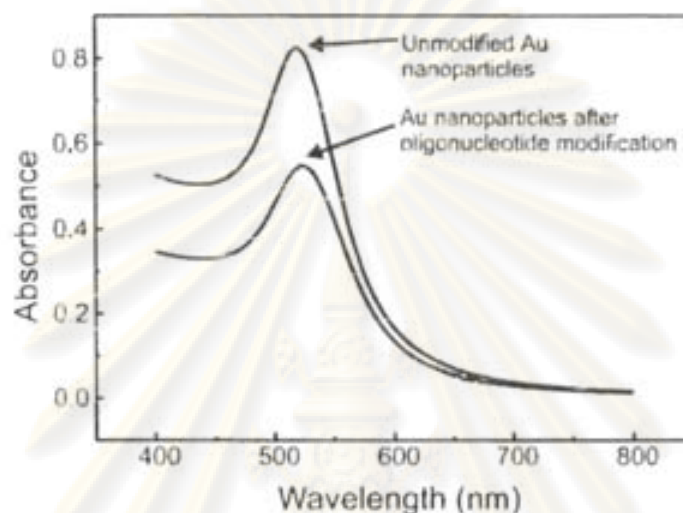
Figure 1.7 Comparison of UV-VIS spectra of 13 nm diameter gold nanoparticles before and after functionalized with 12 base oligonucleotide functionalized with 5'-hexanethiol at 0.3 M NaCl. 10 mM phosphate (pH 7)[37].

These gold nanoparticle-DNA conjugates were recently applied to polynucleotide detection in a manner that exploited the change in optical properties resulting from plasmon-plasmon interactions between locally adjacent gold nanoparticles.[38] It has long been known that the characteristic red color of gold colloid can be changed to a bluish-purple upon aggregation of the colloid particles. In the case of polynucleotide detection, modified with oligonucleotide probes were prepared as described earlier. When a single-stranded target oligonucleotide was introduced to hybridize with the nanoparticles-bond probes, the nanoparticles aggregated due to the binding between the probe and target oligonucleotides. This bring the nanoparticles close enough to each other to induce a dramatic red-to-blue color change as depicted in **Figure 1.8**. This behavior has been extensively exploited for DNA hybridization assays.
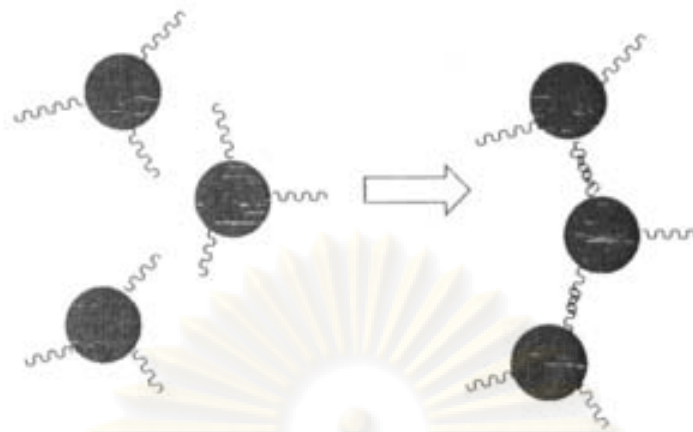
Figure 1.8 When gold nanoparticles come into close proximity, plasmon-plasmon interactions cause dramatic changes in optical properties.

Mirkin and co-workers[39] described a method to determine DNA sequences by aggregation of 13-nm gold nanoparticles. They attached two different DNA probes sequences to two batches of the gold nanoparticles. When the two solutions were brought in contact in the presence of a linker DNA molecule which carry a sequence complementary to both of the DNA probe strands, the nanoparticles aggregated and the color changed from red to purple (**Figure 1.9**).
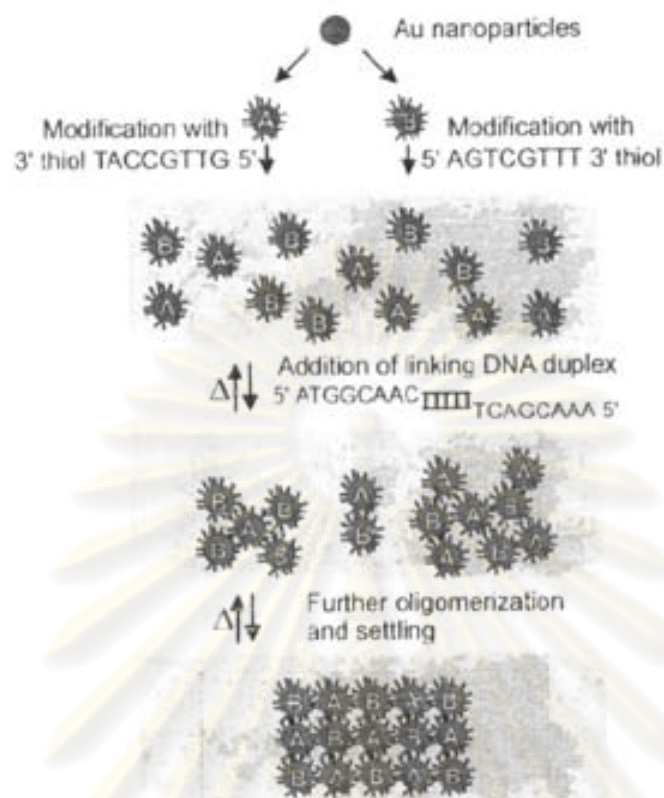
Figure 1.9 Schematic illustration of the DNA-directed assembly of colloidal nanoparticles [39].

Mucic and co-workers[40] reported a noncovalent method for assembling nanoparticles. Two different gold particles (8 and 31 nm in diameter) were modified with two thiol-functionalized 12 mer DNA. These solutions were incubated with a target 24 mer DNA. That is complementary to the two probes on the modified nanoparticles (**Figure 1.10**). They hoped that the use of bigger gold nanoparticles sizes may increase sensitivity of the nanoparticles.

Figure 1.10 Schemetric illustration of the HS(CH₃)₃O(O⁻)OPOATGCTCAACTCT DNA-modified gold nanoparticles 8 nm and TAGGACTTACGCOP(O)(O⁻)O(CH₂)₆SH DNA-modified gold nanoparticles 31 nm diameter and linking DNA (TACGAGTTGAGAATCCTGAATGCG) [40].

After both of the DNA modified gold nanoparticles were obtained, the solution appeared pink and the UV-VIS spectra did not significantly change. However a broadening and red shift in the particles surface plasmon resonance from 524 to 543 nm were clearly observed when a linker oligonucleotide was added in the solution. **Figure 1.11**
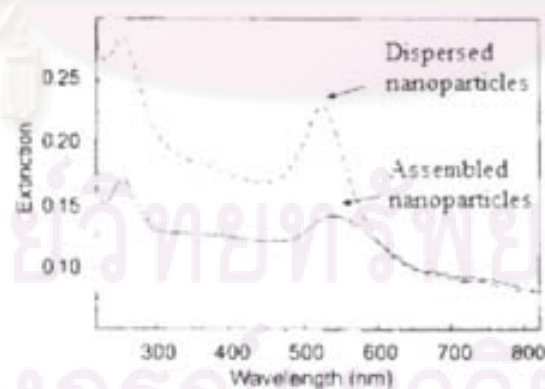
Figure 1.11 The UV-VIS spectra of a mixture DNA-modified 8-nm particles and DNA-modified 31-nm particles before and after incubation with linking DNA.

Furthermore the melting curves of these solutions were extremely sharp and reversible. This appears to be a common characteristic of all DNA-linked nanoparticles network structures studied thus far (**Figure 1.12**)[40]. Moreover Abigail et al.[41] have demonstrated the influence of the length of the poly-A spacers on T_m. The length of the spacer increased the distance between the particle and the DNA. This distance was necessary to achieve the maximum enhancement of the binding strength.
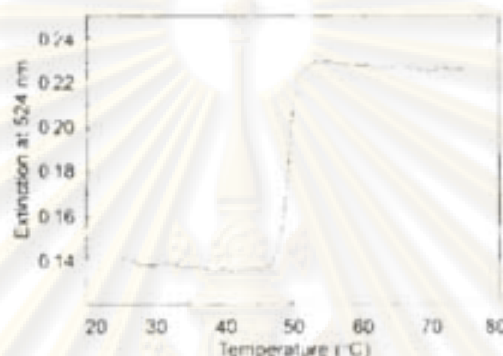
Figure 1.12 Thermal denaturation of the binary network materials (monitored at 524 nm)[40].

Besides the aggregation of gold nanoparticles as described above is induced by the cross-linking mechanism, the aggregation of gold nanoparticles by non-cross-linking DNA hybridization, is the formation of fully complementary dsDNA in the gold nanoparticle surfaces, is also observed. In this non-cross-linking system, Sato and co-workers[42] described a discovered aggregation phenomenon of DNA-functionalized gold nanoparticles induced by hybridization of target DNA. Gold nanoparticles modified with a 5′thiolated 15 mer DNA was hybridized with complementary target and single base mismatch target. The DNA-gold nanoparticles solution turned from red to purple color when adding the complementary DNA in the solution. On the contrary, when the DNA-gold nanoparticles solution were incubated with a single base mismatch target. No color change was observed as shown in **Figure 1.13**.
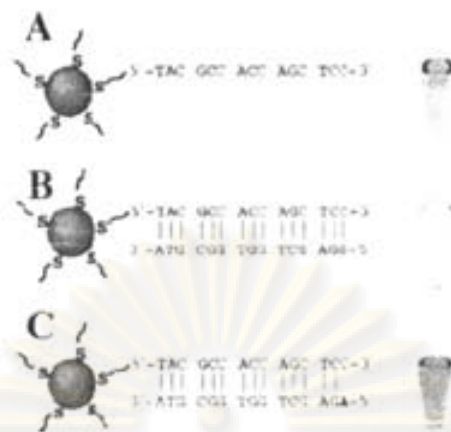
Figure 1.13 Aggregation behaviors of the DNA-gold nanoparticles at 0.5 M NaCl: (A) without DNA target, (B) with the complementary target, and (C) with a target containing a single base mismatch at its 5' terminus[42].

The UV-VIS spectra of corresponding **Figure 1.13A** and **1.13B** were shifted from 525 to 526 nm by the complementary target DNA.

Demers and co-workers[43] determined the number of thiol-derivatized single-stranded oligonucleotides bound to gold nanoparticles and their extent of hybridization with complementary oligonucleotides in solution. Quantity of alkanethiol-oligonucleotides loaded on nanoparticles were investigated by treatment with 2-mercaptoethanol to displace the fluorophore-labeled oligonucleotide initially immobilized on the nanoparticles. Then the solution containing the displaced oligonucleotides were determined for concentration by fluorescence spectroscopy. **Figure 1.14**

ศูนย์วิทยทรัพยากร
จุฬาลงกรณ์มหาวิทยาลัย
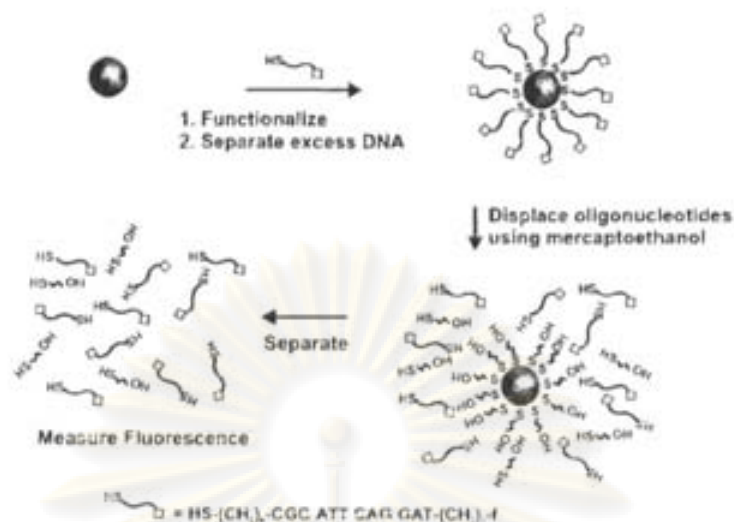
Figure 1.14 Measurement fluorophore-labeled DNA modified gold nanoparticles[43].

To determine the availability of adsorbed oligonucleotides for hybridization, a fluorophore-labeled oligonucleotide, which was complementary to the nanoparticle-bound oligonucleotides, was hybridized with oligonucleotide-modified gold surfaces. The fluorophore-labeled oligonucleotides were dehybridized by addition of NaOH. The concentration of the hybridized oligonucleotide and the corresponding hybridized target surface density were determined by fluorescence spectroscopy as shown in **Figure 1.15**
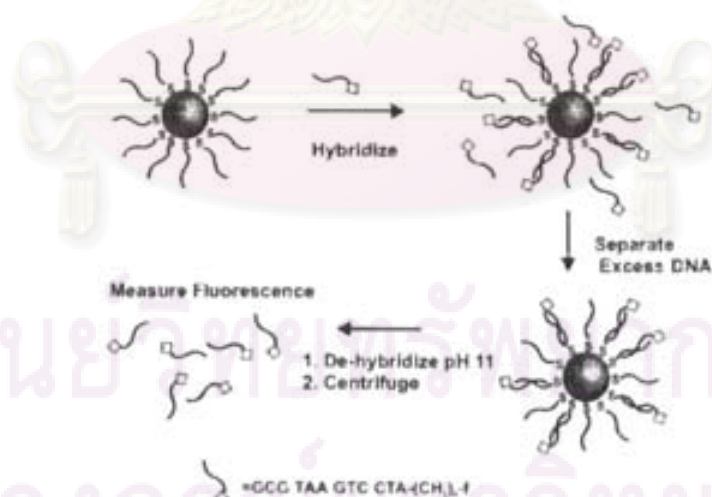
Figure 1.15 Measurement of fluorescent-labeled DNA hybridized with gold nanoparticles modified with DNA[43].

Furthermore fluorescence-labeled DNA was quenched upon imobilization the nanoparticles. When target binding occured, the fluorophore leaves the surface because of the structural rigidity of the hybridized DNA (double-stranded) (**Figure 1.16**) [44,45]. This resulted in re-generation of the fluorescent signal and has been used in detection of the hybridization event.
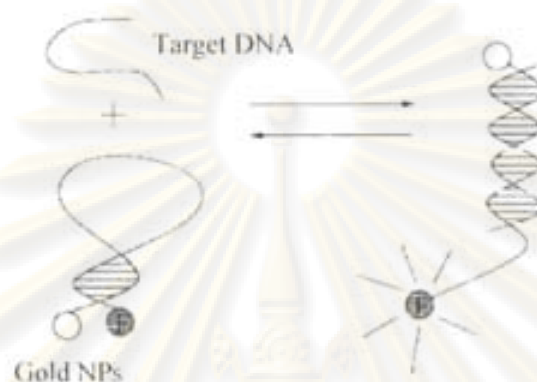
Figure 1.16 Schematic drawing of the two conformations of the dye-oligonucleotide gold conjugate and of the gold-quenched molecular beacon.

Although many research groups have reported the immobilization of DNA oligonucleotides on gold nanoparticles and subsequent hybridization with target DNA, there are a few research groups studying the hybridization of PNA-modified gold nanoparticles with target DNA.

Chakrabarti and co-workers[35] examined the properties of different peptide nucleic acids (PNAs) charge distributions to determine their effects on nanoparticles stability and studied their assembly. They demonstrated that the negatively charge PNAs can resisted to centrifugation-induced aggregation. On the other hand, neutral PNAs underwent immediate irreversible aggregation due to uncapped N-terminal amines. After gold nanoparticles were modified with two thiol-functionalized 18 mer PNA, linker PNA was added to the solution. No change in the surface plasmon band was detected over 12 h. However, over 5 days, all of the nanoparticles precipitated. Murphy et al.[46] examined hybridization between PNA-modified gold nanoparticles and the complementary DNA-modified gold nanoparticles. No hybridization was observed because either surface functionalization of the gold nanoparticles with PNA did not occur, or, if it did occur, then the DNA was not accessible. Gourishankar et

al.[47] reported that the PNA monomers bind much more strongly to the gold nanoparticles than the DNA bases and that a concentration 10 times smaller than that of the DNA bases is enough to bring about the saturation of the gold nanoparticle surface.

1.4 Objectives of this research

The objective of this research is to synthesize a novel thiol-modified Vilaivan's (1S, 2S)-ACPC-PNA and to determine the effect of these thiolated PNA carrying different charge modification on gold nanoparticles stability. The effect of thiolated PNA charge will be employed in the detection of PNA-DNA hybridization events by observing the aggregation the gold nanoparticles.
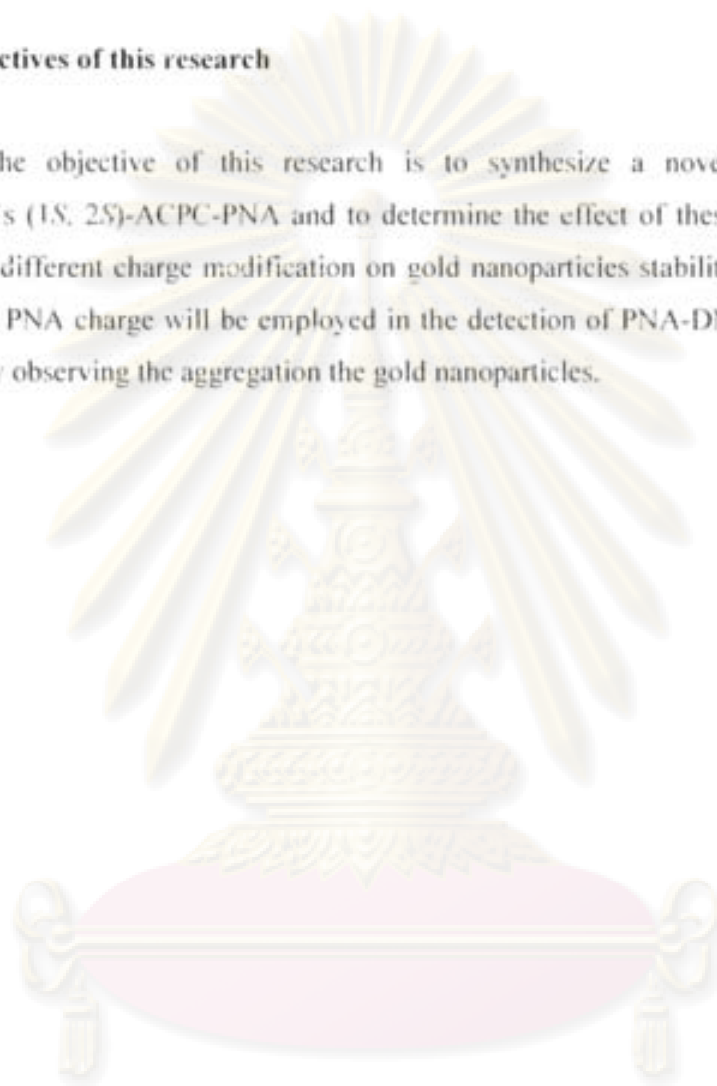
CHAPTER II

EXPERIMENTAL SECTION

2.1 General Procedures

2.1.1 Measurements

The weight of all substances chemical was determined on a Metler Toledo electrical balance. Melting points were recorded on an electrothermal melting point apparatus model 9100. Rotary evaporator was of Büchi Rotavapor R-200 with a water aspirator model B-490. UV cabinet for UV-visualization of TLC was made in-house by Mr. Chanchai Khongdeesameor. The magnetic stirrers were of Corning (USA). The high vacuum was delivered by a Refco Vacubrand pump. Thin layer chromatography (TLC) was performed on Merck D.C. silica gel 60 F_{254} 0.2 mm. precoated aluminium plates cat. no. 1.05554. Column chromatography was performed on silica gel 70-230 mesh (for general chromatography) or 230-400 mesh (for flash column chromatography). Reverse phase HPLC experiments were performed on Water 600™ system equipped with gradient pump and Water 996™ photodiode array detector; optionally alternate to Rheodyne 7725 manual sample loop (100 µL sample size for analytical scale). A Polaris™ C_{18} HPLC column 3 µm particle size 4.6 × 50 mm (Varian Inc., USA) was used for analytical purposes. Peak monitoring and data processing were avaliable for intergrated operating with the base Empower software. Fractions from HPLC were collected manually which was assisted by real-time HPLC chromatogram monitoring. The combined fractions were freezed and evaporated using Freeze dryer (Freezone 77520, Benchtop, Labconco). T_m experiment were recorded on a CARY 100 Bio UV-Visible spectrophotometer (Varian Inc., USA). ^1H and ^{13}C NMR spectra were recorded on Varian Mercury-400 plus operating at 400 and 100 MHz, respectively (Varian Inc., USA). MALDI-TOF mass spectra of thiol-modified PNA were collected on a Microflex MALDI-TOF mass spectrometry (Bruker Daltonics) in linear positive ion mode using doubly recrystallized α-cyano-4-hydroxy cinnamic acid (CCA) as matrix. Trifluoroacetic

acid (0.1%) in acetonitrile:water (1:2) was used as the diluents for preparation of MALDI-TOF samples.

2.1.2 Materials

All chemicals were purchased from Fluka (Switzerland), Merck (Germany) or Aldrich (USA), and were purified as appropriate depending on reaction conditions and purposes. Commercial grade solvents were distilled before use for column chromatography. Solvents for reactions and crystallization were reagent grade and used without purification. Acetonitrile for HPLC experiment was HPLC grade, obtained from BDH and was filtered through a membrane filter (13 mm φ, 0.45 μm Nylon Lida) before use. Anhydrous N,N-dimethylformamide (H$_2$O ≤ 0.01%) for solid phase peptide coupling reaction was obtained from Fluka and dried oven activated 3Å molecular sieves. The solid support for peptide synthesis (TentaGel S-RAM Fmoc resin) and trifluoroacetic acid were obtained from Fluka. The protected amino acids (Fmoc-L-Lys(Boc)-OPfp) was obtained from Novabiochem. Fmoc-Ser(tBu)-ODhbt and Fmoc-Asp(OtBu)-OH was obtained from Fluka and Novabiochem, respectively. 5(6)-Carboxyfluorescein N-hydroxysuccinimide ester for PNA labeling was purchased from Fluka. Nitrogen gas was obtained from TIG with high purity up to 99.5 %. MilliQ water was obtained from ultrapure water system with Millipak® 40 filter unit 0.22 μm, Millipore (USA). Oligonucleotides were purchased from Bioservice Unit, National Science and Technology Development Agency (Thailand) and fluorophore-labeled DNA was purchased from Bio Basic Inc (Canada). Gold nanoparticles with a diameter of 20 nm was purchased from Sigma Aldrich.

2.2 Experimental procedures

2.2.1 Synthesis of intermediate: proline derivatives modified with nucleobases

The intermediate proline derivatives of thymine (6), guanine (7), adenine (8), and cytosine (9) were synthesized as described previously (**Scheme 1**)[48-49] by Mr. Chaturong Supapprom, Miss Boonjira Boontha and Miss Cheeraporn Ananthanawat.
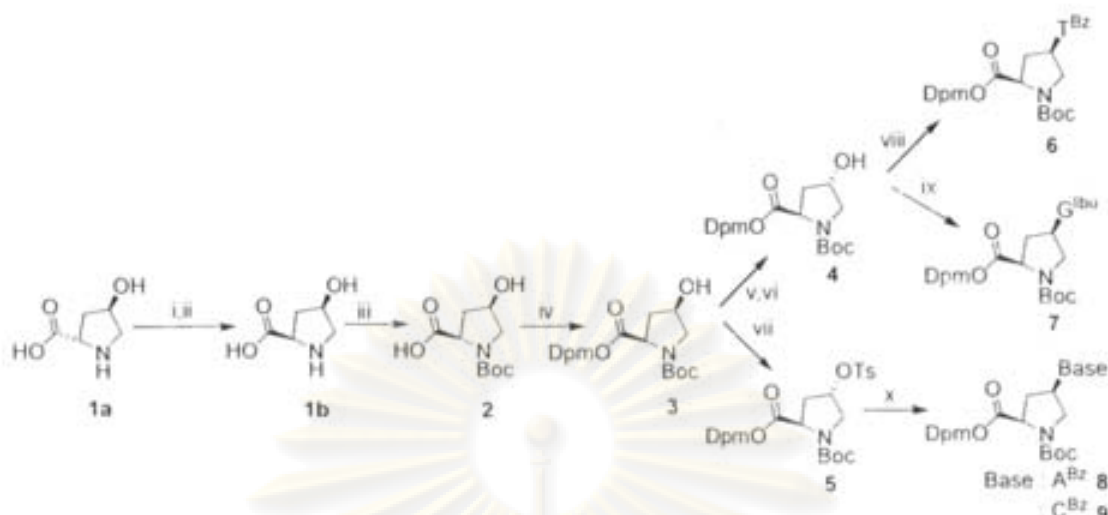
Scheme 1 i. Ac₂O, heat 90 °C 16 h; ii. 2 M HCl, reflux 5 h; iii. Boc₂O, ᵗBuOH, NaOH (aq), overnight; iv. Ph₂CN₂, EtOAc, overnight; v. HCO₂H, Ph₃P, DIAD, THF, overnight; vi. NH₃, MeOH, 2 h; vii. TsCl, Ph₃P, DIAD, THF, overnight; viii. N^3-T^{Bz}, Ph₃P, DIAD, THF, overnight; ix. N^2-IbuG(ONpe), Ph₃P, DIAD, dioxane, overnight; x. N^6-A^{Bz} or N^4-C^{Bz}, K₂CO₃, DMF, heat 90 °C, 5 h.

2.2.2 Synthesis of activated PNA monomers

(a) Thymine (T) monomer

N-Fluoren-9-ylmethoxycarbonylamino-cis-4-(thymin-1-yl)-D-proline   pentafluoro phenyl ester (11)
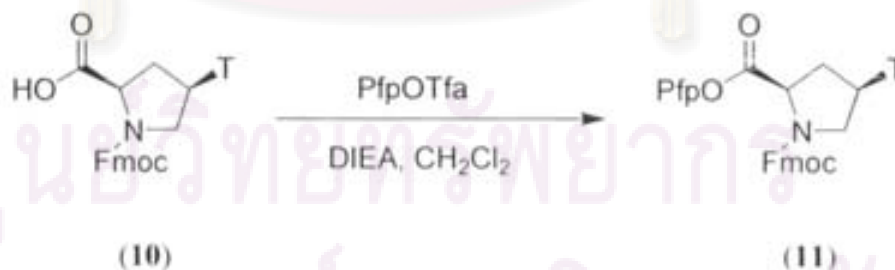
To a suspension of (N-fluoren-9-ylmethoxycarbonyl)-cis-4-(thymin-1-yl)-D-proline (10) (0.39 g, 0.86 mmol) and pentafluorophenyl trifluoroacetate (PfpOTfa) (445 μL, 2.58 mmol) in dichloromethane (3 mL) was added DIEA (588 μL, 3.44 mmol). The

resulting mixture was stirred at room temperature for one hour. The reaction was completed as indicated by TLC analysis and purified by flash column chromatography eluting with hexane: ethyl acetate (1:1) on silica gel to obtain the title compound (11) as white solid (0.42 g, 78 %).

^{1}H NMR (400 MHz, CDCl$_3$) δ_H 1.94 (3H, s, thymine C$\underline{H}_3$), 2.30-2.40 [1H, m, 1 × C$\underline{H}_2$(3')], 2.92-2.96 [1H, m, 1 × C$\underline{H}_2$(3')], 3.58-4.15 [2H, m, 2 × C$\underline{H}_2$(5')], 4.23 (1H, m, Fmoc aliphatic C$\underline{H}$), 4.48-4.56 (2H, m, Fmoc aliphatic C$\underline{H}_2$), 4.63-4.78 [1H, m, C$\underline{H}$(2')], 5.21-5.38 [1H, m, C$\underline{H}$(4')], 7.15 (1H, s, thymine C$\underline{H}$), 7.25-7.41 (2H, t, J = 7.2 Hz, Fmoc aromatic C$\underline{H}$), 7.58 (2H, d, J = 7.2 Hz, Fmoc aromatic C$\underline{H}$), 7.76-7.80 (2H, d, J = 7.6 Hz, Fmoc aromatic C$\underline{H}$)

2.2.3 Synthesis of *trans*-(1S,2S)-2-aminocyclopentanecarboxylic acid (ACPC) spacer

Ethyl (1S, 2S)-2-[(1'S)-phenylethyl]-aminocyclopentanecarboxylate (13) [50]
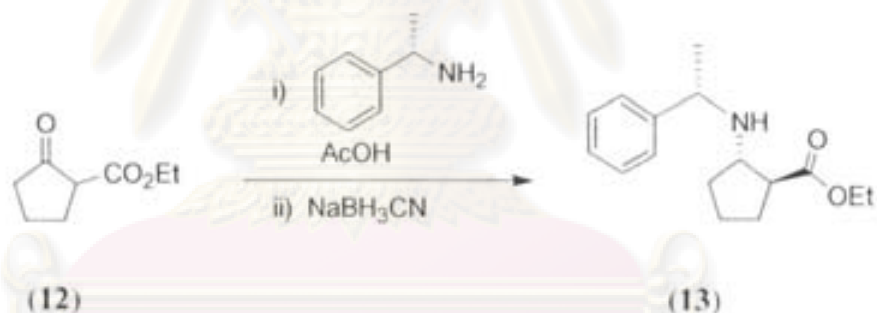
To a stirred solution of ethyl cyclopentanone-2-carboxylate (12) (4 mL, 27 mmol) in absolute ethanol (32 mL) was added (S)-(-)-α-methylbenzylamine (3.48 mL, 30.0 mmol) and glacial acetic acid (1.54 mL, 32.0 mmol). The reaction mixture was stirred at room temperature until the formation of enamine was complete (2 h, monitored by TLC, 7:3 hexane/EtOAc) The reaction mixture was heated to 72 °C and then gradually added sodium cyanoborohydride (3.14 g, 54.0 mmol) to the reaction mixture over a 5 h period. The disappearance of enamine was monitored by TLC. When the reaction was complete, the ethanol was removed by rotary evaporation heat at 78 °C and then added water (20 ml) The reaction mixture was adjusted a neutral solution by NaHCO$_3$. The resulting

mixture was extracted with dichloromethane. The dichloromethane was removed by rotary evaporation. The crude product can be purified by column chromatography, eluting with 100% hexane and followed 20:1 hexane:EtOAc on silica gel to obtain the title compound (13) as colorless liquid (1.40 g, 21 %).

^{1}H NMR (400 MHz, CDCl$_3$) δ_H 1.22 (3H, t, J = 7.0 Hz, CO$_2$CH$_2$CH$_3$), 1.39 (3H, d, J = 6.0 Hz, NHCHCH$_3$), 1.57-1.75 (2H, m, CH$_2$CH$_2$CH$_2$), 1.78-1.85 (2H, m, NHCHCH$_2$), 1.92-2.06 (2H, m, CH$_2$CHCO), 2.63 (1H, q, J = 7.0 Hz, CHCO$_2$Et), 3.25 (1H, q, J = 7.2 Hz, NHCHCH$_2$), 3.88 (1H, q, J = 6.4 Hz, NHCHCH$_3$), 4.15 (2H, m, CO$_2$CH$_2$CH$_3$) and 7.20-7.38 (5H, m, phenyl); $[\alpha]^{25}_D$ = +17.1 (c = 1.00 g/100 mL, CDCl$_3$).

(1S,2S)-2-Amino-cyclopentanecarboxylic acid ethyl ester (15) [51]

(13)   (14)   (15)
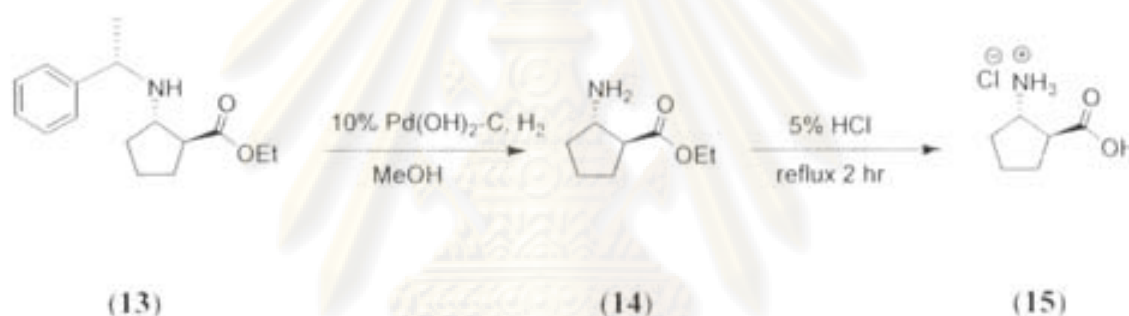
Ethyl (1S,2S)-2-[(1'S)-phenylethyl]-aminocyclopentane carboxylate (13) (1.14 g, 4.38 mmol) was dissolved in methanol (5 mL) and palladium hydroxide on charcoal (0.06 g) was added with stirring at room tempearture under H$_2$ atmosphere for three hour. The disappearance of compound (13) was monitored by TLC. The formation of ethyl (1S,2S)-2-aminocyclopentane carboxylate (14) were completed. The palladium catalyst was filtered off with the aid of celite and washed with methanol. The filtrate was evaporated by rotary evaporation to obtain compound (14). Without further purification, the compound (14) and 5% HCl (10 mL) was refluxed for 2 h at 110 °C. Then the mixture was allowed to cool down and the solvent was removed by rotary evaporation to obtain the title compound (15) as a white solid (0.33 g, 64% from 13).

^{1}H NMR (400 MHz, CDCl$_3$) δ_H 1.22 (3H, t, J = 7.0 Hz, CO$_2$CH$_2$CH$_3$), 1.59-1.62 (3H, d, J = 6.0 Hz, NHCHCH$_3$), 1.59-1.62 (2H, m, CH$_2$CH$_2$CH$_2$), 1.72-1.79 (2H, m,

NHCHC$\underline{H}_2$), 1.93-1.98 (2H, m, C$\underline{H}_2$CHCO), 2.21-2.32 (1H, q, J = 7.0 Hz, C$\underline{H}$CO$_2$Et), 3.40-3.45 (1H, q, J = 7.2 Hz, NHC$\underline{H}$CH$_2$), 4.16 (2H, m, CO$_2$C$\underline{H}_2$CH$_3$) and 7.36-7.45 (5H, m, phenyl); $[\alpha]^{25}_D$ = +61.3 (c = 1.00 g/100 mL H$_2$O).

(1*S*,2*S*)-2-(*N*-Fluoren-9-ylmethoxycarbonyl)-aminocyclopentanecarboxylic acid (16) [51]
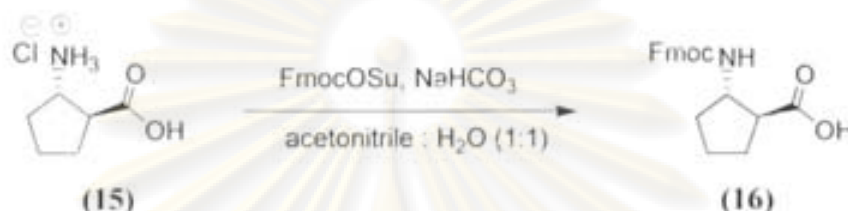
The (1*S*,2*S*)-2-aminocyclopentane carboxylic acid hydrochloride (15) (0.16 g, 1 mmol) was dissolved in acetonitrile : water (1:1, 2.5 mL) and NaHCO$_3$ (3 equiv excess) was added until the solution was basic (pH = 8). FmocOSu (0.37 g, 1.1 mmol) was slowly added with stirring at room temperature for 8 h. The disappearance of FmocOSu was monitored by TLC. When the reaction was complete, the residue was dilute with water (20 mL) and extracted with diethyl ether (3 × 20 mL). The aqueous phase was collected and the pH was adjusted to 2 with concentrated HCl. The white suspension was extracted with dichloromethane (3 × 20 mL). Solvent was removed by rotary evaporation and dried in vacuum to afford the title compound (16) as a white solid (0.32 g, 94 %).

^{1}H NMR (400 MHz, DMSO-d_6) δ_H 1.43-1.75 (4H, 2×m, CH$_2$C$\underline{H}_2$CH$_2$ and NHCHC$\underline{H}_2$), 1.90-1.95 (2H, m, C$\underline{H}_2$CHCO), 2.51 (1H, m, C$\underline{H}$CO), 4.02 (1H, t, J = 7.4 Hz, NHC$\underline{H}$), 4.21-4.29 (2H, m, Fmoc aliphatic C$\underline{H}$ and Fmoc aliphatic C$\underline{H}_2$) and 7.28-7.79 (8H, m, Fmoc aromatic C$\underline{H}$). $[\alpha]^{25}_D$ = + 36.4, c = 1.0 in MeOH

(1S,2S)-2-(N-Fluoren-9-ylmethoxycarbonyl)-aminocyclopentane pentafluorophenyl ester (17)
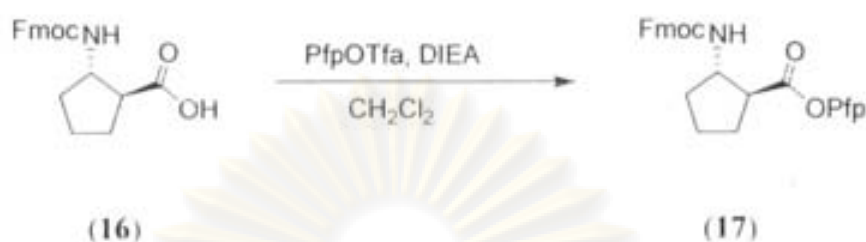
Synthesis of the titled compound (17) was accomplished using the same procedure as described for compound (11). Starting from N-fluoren-9-ylmethoxy-carbonyl-2-amino-cyclopentanecarboxylic acid (16) (200 mg, 0.5 mmol), PfpOTfa (258 µL, 1.5 mmol) and DIEA (194 µL, 1.5 mmol) in dichloromethane (3 mL) afforded compound (17) (0.1567 g, 30 %) as a white solid.

^{1}H NMR (400 MHz, CDCl$_3$) δ$_H$ 1.86 (2H, m, CH$_2$CH$_2$CH$_2$), 2.07 (2H, m, NHCHCH$_2$), 2.21 (2H, m, CH$_2$CHCO), 3.15 (1H, m, CHCO), 4.25 (1H, t, J = 6.2 Hz, NHCH), 4.36 (1H, t, J = 7.2 Hz, Fmoc aliphatic CH), 4.46 (2H, d, J = 6.4 Hz, Fmoc aliphatic CH$_2$), 4.92 (1H, s, NH) and 7.29-7.78 (8H, m, Fmoc aromatic CH); [α]$^{25}_D$ = +49.0 (c = 1.00 g/100 mL CHCl$_3$).

2.2.4 Synthesis of S-protected 3-mercaptopropionic acid

(a) 3-Benzhydrylthio-proanoic acid (19)
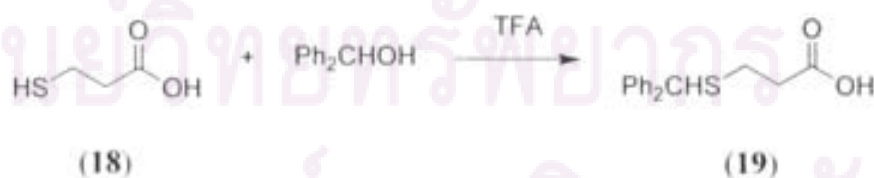
The title compound was synthesized according to the scheme above by Miss Cheeraporn Ananthanawat [52].

(b) 3-(2,4-Dinitrophenylthio)propanoic acid (21)

(20)   (21)
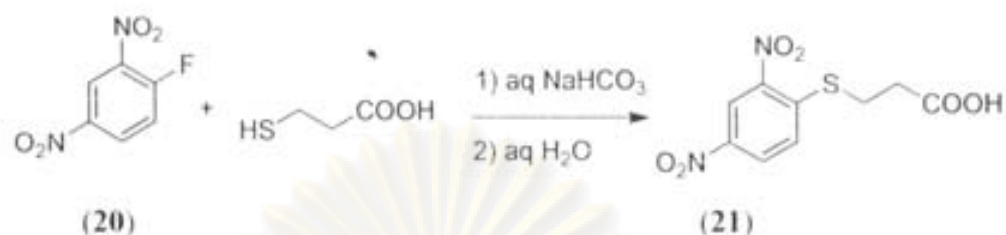
1-Fluoro-2,4-dinitrobenzene (20) (413.7 mg, 2 mmol) was reacted with 3-mercaptopropanoicacid (211.7 mg, 2 mmol) in aqueous $NaHCO_3$ (376.7 mg, 2 mmol) and MeCN. The reaction was stirred at room temperature for 3 h. The reaction was extracted by dichloromethane, the aqueous phase acidified with 10% HCl and extracted with EtOAc to obtain the 3-(2,4-dinitrophenylthio)propanoic acid (21) as a yellow solid (463.5 mg, 85%).

^{1}H NMR (400 MHz, DMSO-$d6$) δ_H 8.84 (1H, d, J=2.4 Hz, ArH), 8.41 (1H, dd, J=2.4 and 8.8 Hz, ArH), 7.87 (1H, d, J=8.8 Hz, ArH), 3.33 (2H, t, J=7.2 Hz, SCH_2CH$_2$), 2.80 (2H, t, J=7.2 Hz, CH$_2$CH_2CO); ^{13}C NMR (100 MHz, CDCl$_3$) δ_C 172.75 (C=O), 145.59 (C), 144.94 (C), 144.04 (C), 128.48 (CH), 128.01 (CH), 121.78 (CH), 32.48 (CH$_2$), 27.50 (CH$_2$), m.p. = 174.7-175.2 °C, Anal. Calcd for C$_9$H$_8$NO: C, 41.2; H, 2.9; N, 10.4. Found: C, 41.22; H, 2.9; N, 10.4%. IR (neat): v_{max} 3343.48, 1704.93, 1591.94, and 1335.52 cm^{-1}.

(c) 3-(2,4-Dinitrophenylthio)propanoic acid pentafluorophenyl ester (22)

(21)   (22)
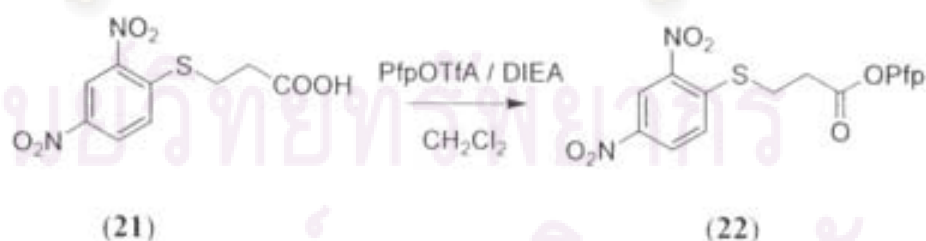
3-(2,4-Dinitrophenylthio)propanoic acid (21) (0.1 g, 0.37 mmol) was reacted with PfpOTfa (63.77 µL, 0.37 mmol) and DIEA (47.82 µL, 0.37 mmol) as decribed

previously. The reaction was complete within 1 h according to TLC analysis. The product was again quickly purified by column chromatography eluting with hexane:ethyl acetate (2:1) on silica gel to obtain the 3-(2,4-dinitrophenylthio)propanoic acid pentafluorophenyl ester (**22**) as a yellow solid (0.293 g, 79 %).

^{1}H-NMR (400 MHz, CDCl$_3$) δ_H 9.11 (1H, d, J=2.4 Hz, ArH), 8.44 (1H, dd, J=2.4 and 8.7 Hz, ArH), 7.61 (1H, d, J=8.7 Hz, ArH), 3.46 (2H, t, J=7.3 Hz, SCH_2CH$_2$), 3.17 (2H, t, J=7.3 Hz, CH$_2$CH_2CO); ^{13}C-NMR (100 MHz, CDCl$_3$) δ_C 172.75 (C=O), 145.06 (2xC), 144.14 (C), 127.46 (CH), 126.61 (CH), 121.94 (CH), 31.58 (CH$_2$), 26.97 (CH$_2$), m.p. = 125.0-126.5 °C, Anal. Calcd for C$_x$H$_x$NO: C, 41.2; H, 1.6; N, 6.4. Found: C, 41.2; H, 1.6; N, 6.4%. IR (neat): ν_{max} 1783.16, 1522.40, 1344.00, and 1105.18 cm^{-1}.

(d) 3-(Benzoylthio)propanoic acid (24)

(23)　　　　　　　　　　　　　　　(24)
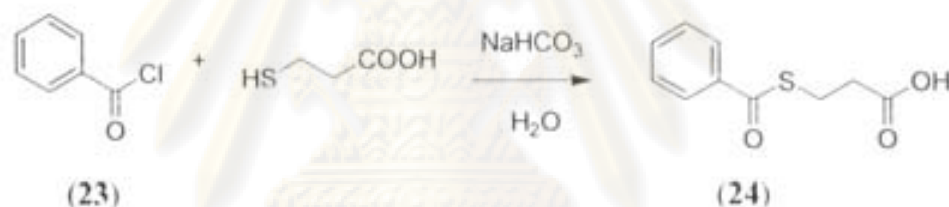
Benzoyl chloride (**23**) (329.2 mg, 2 mmol) was reacted with 3-mercaptopropanoic acid (251.3 mg, 2.37 mmol) and NaHCO$_3$ (385.3 mg, 2 mmol) in H$_2$O (2 ml). The reaction was stirred at room temperature for 1 h. The reaction mixture was extracted with dichloromethane. The aqueous phase was acidified and extracted with dichloromethane to obtain the 3-(benzoylthio)propanoic acid (**24**) as a white solid (0.206 g, 42 %).

^{1}H-NMR (400 MHz, CDCl$_3$) δ_H 7.93 (2H, d, J=8.8 Hz, ArH), 7.52-7.45 (1H, m, ArH), 7.45-7.39 (2H, m, ArH), 3.31 (2H, t, J=6.8 Hz, SCH_2CH$_2$), 2.80 (2H, t, J=6.8 Hz, CH$_2$CH_2CO); ^{13}C-NMR (100 MHz, CDCl$_3$) δ_C 191.50 (C=O), 178.04 (C=O), 133.58 (CH), 128.66 (2xCH), 127.74 (2xCH), 34.30 (CH$_2$), 23.62 (CH$_2$), m.p. = 96.3-97.2 °C. Anal. Calcd for C$_x$H$_x$NO: C, 56.9; H, 4.8. Found: C, 56.9; H, 4.8 %. IR (neat): ν_{max} 3356.43, 1704.93, 1681.47, and 1209.48 cm^{-1}.

(e) 3-(Benzoylthio) propanoic acid pentafluorophenyl ester (25)

(24)   (25)
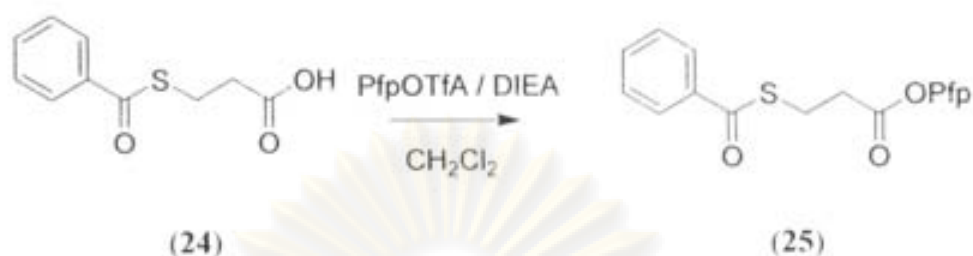
3-(Benzoylthio)propanoic acid (24) (0.1 g, 0.488 mmol) was reacted with PfpOTfa (0.1367 g, 0.488 mmol) and DIEA (63.1 µL, 0.488 mmol) in dichloromethane 4 µL. The resulting mixture was stirred at room temperature for one hour. The reaction was completed as indicated by TLC analysis and purified by flash column chromatography eluting with hexane:ethyl acetate (2:1) on silica gel to obtain the 3-(benzoylthio)propanoic acid pentafluorophenyl ester (25) as a colorless oil (0.293 g, 62 %).

^{1}H-NMR(400 MHz, CDCl$_3$) δ_H 7.90 (2H, d, J=7.2 Hz, ArH), 7.57-7.47 (1H, m, ArH), 7.45-7.37 (2H, m, ArH), 3.35 (2H, t, J=7.2 Hz, SCH_2CH$_2$), 3.04 (2H, t, J=7.2 Hz, CH$_2$CH_2CO); ^{13}C-NMR (100 MHz, CDCl$_3$) δ_C 191.21 (C=O), 167.78 (C=O), 136.50 (C), 133.75 (CH), 128.71 (2xCH), 127.28 (2xCH), 33.79 (CH$_2$), 23.60 (CH$_2$). Anal. Calcd for C$_x$H$_y$NO: C, 51.1; H, 2.4. Found: C, 51.1; H, 2.4 %. IR (neat): ν_{max} 3356.43, 1787.51, 1661.47, 1518.05, and 1209.48 cm^{-1}.

2.2.5 Synthesis of gold nanoparticles

(a) 13 nm diameter gold nanoparticles [53]

HAuCl$_4$.3H$_2$O (1mM, 50 mL) was refluxed while stirring at 60 °C. After the solution boiling, tri-sodium citrate (38.8 mM, 5 mL) was rapidly added until the color of the solution turned from pale yellow to deep red and the reflux was continued for another 15 min.

(b) 16 nm diameter gold nanoparticles [36]

HAuCl$_4$.3H$_2$O (1%, 0.5 mL) in water (49.5 mL) was heated up to 60 °C for 10 min. Tri-sodium citrate (1 %, 2 mL) was rapidly added in the stirring solution and keep to heat for 5 min. The color changed from deep blue to pale purple then to burgundy red.

(c) 40 nm diameter gold nanoparticles [54]

HAuCl$_4$.3H$_2$O (1 mg/mL, 1 mL) in water (18 mL) was heated to boiling. Tri-sodium citrate (10 mg/mL, 1 mL) was rapidly added in the stirring solution for 30 min. After that H$_2$O was added to the solution to bring volume back 20 mL. The boiling solution turned to deep red color within about 20 min of boiling.

2.3 Synthesis of thiolated PNA carrying different charge

2.3.1 Preparation of the reaction pipette and apparatus for solid phase peptide synthesis

All peptide syntheses were carried out using a custom-made peptide synthesis column from Pasteur pipette which was plugged with a small amount of glass powder and sintered on a small flame as described previously [55,56]. The resin was weighed accurately into the pipette. The resin in the pipette was swollen in DMF solvent for at least 1 h before use. For each reaction, the reagent was directly sucked in, ejected out by manual control for the specified period of time. After the reaction was complete, the reaction was washed by DMF solvent for 3 time in order to eliminate the excess reagent.

Synthesis of each thiol-modified PNA was carried out on 1.5 μmol scale in three stock reagents. The general synthesis protocol was divided into steps as follows.

i   Removing Fmoc protecting group form the resin

The reaction pipette containing TentaGel S RAM Fmoc resin (4.2 mg, 1.0 μmol) was prepared as described above. The resin was treated 100 μL of deprotection solution (piperidine 20 μL, 1.8-diazabicyclo[5.4.0] undec-7-ene (DBU) 20 μL, and DMF 960 μL) in a 1.5 mL Eppendorf tube for 15 min at room temperature occasional agitation. After the specified period of time, the reagent was squeezed off and the reaction column was washed exhaustively with DMF.

ii) Anchoring of the first amino acid residue

The first amino acid (lysine, aspartic acid, or serine) was attached to the free amino group on the Tentagel-S-RAM resin. The activated amino acid (Fmoc-L-Lys(Boc)-OPfp) and Fmoc-Ser(tBu)-ODhbt were used with HOAt (1.4 mg, 10 μmol), Fmoc-Asp(OtBu)-OH was used HATU (3.8 mg, 10 μmol). The prepared resin was soaked in a solution of activated amino acids in DMF (10 μmol, 30 μL) with occasional agitation for 1 h at room temperature. After the specified period of time, the reagent was squeezed off and the reaction column was washed exhaustively with DMF.

iii) Deprotection of the Fmoc protection group at N-terminal

After the coupling was completed, the resin was treated with 100 μL of the deprotection solution in a 1.5 mL Eppendorf tube for 5 min at room temperature occasional agitation. After the specified period of time, the reagent was squeezed off and the reaction column was washed exhaustively with DMF. The used deprotecting reagent can be used to determine the coupling efficiency by diluting with an appropriate volume of methanol and then the UV-absorbance of dibenzofulvene-piperidine adduct at 264 nm measured. The first UV-absorbance of the adduct was assumed to be 100%. Such determination of coupling efficiency was advantageous in terms of determining how the solid phase reaction progress. The efficiency should be >95 % for each step in order to give acceptable yield of the 9-15 mer PNA oligomer.

iv) Coupling with pyrrolidinyl monomer

The free amino group, generated from the deprotection step (iii) above, was further coupled with a designated PNA monomer. PNA Pfp monomer (6.0 µmol) in 15 µL of DIEA solution (DIEA 70 µL and DMF 930 µL) and 15 µL of HOAt solution (HOAt 5.5 mg and DMF 100 µL). The resin in the reaction pipette was treated with this solution for 30 min at room temperature with occasional agitation. After reaction the column was washed exhaustively with DMF.

v) End capping

After coupling step, the free amino residue was capped with 2 µL acetic acid in 30 µL of DIEA solution (DIEA 70 µL and DMF 930 µL) in a 1.5 mL Eppendorf tube to prevent formation of deletion sequences and facilitate purification for 10 min.[55]

vi) Coupling with SS-ACPC spacer monomer

In the same way as described for (iii)– (iv), ssACPC-spacer monomer (17) (3.10 mg, 6 µmol) was coupled next to the pyrrolidinyl monomer after removal of the Fmoc gruop. This constituted one unit of cis-D-ssACPC PNA. Alternate couplings of the pyrrolidinyl monomer and ssACPC spacer were performed in the subsequent steps until the complete sequence was obtained.

vii) Modifying the PNA oligomer with 2-[2-(Fmoc-amino)ethoxy]ethoxy acetyl linker

The synthesis cycle was repeated until the growing peptide chain was extended to the desired sequences. The terminal Fmoc group was removed by treatment with the deprotection solution as in (iii). If the sequences contain G, C, or A, the nucleobase side-chain protecting groups were removed by treatment with dioxane:ammonia 1:1 (2 mL) at 60 °C overnight. The PNA was further coupled with 2-[2-(Fmoc-amino)ethoxy]ethoxy

acetic acid pentafluorophenyl ester (5.5 mg, 10.0 µmol) dissolved in 30 µL anhydrous DMF without addition of HOAt and DIEA. The resin was treated with this solution for 30 min at room temperature with occasional agitation.

viii)   Modifying the N-terminus of PNA oligomer with thiol

After the final cleavage of Fmoc, the PNA oligomer was treated with a solution of the activated S-protected mercaptopropanoic acid. DpmS(CH$_2$)$_2$CO$_2$H (**19**) (2.5 mg, 4.0 µmol) and HATU (1.3 mg, 3.5 µmol) was dissolved in 30 µl anhydrous DMF. Then DIEA (1.4 µL, 8.0 µmol) was added to the reaction mixture. The resin carrying free amino group was treated with the solution for 30-60 min at room temperature followed by normal washing. Other thiol modifiers were coupled similarly. In the case of lipoic acid (4.2 mg, 4.0 µmol), DNP-S(CH$_2$)$_2$CO$_2$Pfp (**22**) (4.4 mg, 4.0 µmol) and BzS(CH$_2$)$_2$CO$_2$Pfp (**25**) (3.7 mg, 4.0 µmol) were accomplished in the same way DpmS(CH$_2$)$_2$CO$_2$H (**19**).

ix) Method for cleavage PNA oligomer from the resin
and deprotection at S-atom

The cleavage of PNA oligomer from the resin was done by treatment with anisole in trifluoroacetic acid (10:90) (for S-Dpm) or TFA (for lipoic acid, S-DNP and S-Bz) at room temperature for 1 h with occasional agitation. After one hour, the trifluoroacetic acid in the cleavage solution was removed by a nitrogen stream in fume hood. The resin was treated with another portion of TFA to ensure a complete cleavage of the peptide from the resin. The sticky residue was treated with diethyl ether to precipitate the crude PNA. The suspension was the centrifuged and decanted. The crude peptide was centrifugally washed with diethyl ether (3-4 times). Finally the crude peptide was air dried at room temperature and stored dried at -20 °C until used.

x) Purification and Identification

The crude peptide was prepared for HPLC analysis by dissolving a mixture in 200 µL deionized water. The solution was filtered through a nylon membrane filter (0.45 µm). Analysis and purification was performed by reverse phase HPLC, monitoring by UV-absorbance at 260 nm and eluting with a gradient system of 0.1% TFA in acetonitrile/water. The HPLC gradient system used two solvent systems which are solvent A (0.1% trifluoroacetic acid in acetonitrile) and solvent B (0.1% trifluoroacetic acid in milliQ water). The elution began with A:B (10:90) for 5 min followed by a linear gradient up to A:B (90:10) over a period of 30 min, then hold for 5 min before reverted back to A:B (10:90). After freeze drying, the identity of the PNA oligomer was verified by MALDI-TOF mass spectrometry.

2.3.2 Solid phase peptide synthesis of $HS(CH_2)_2CO$-egl-T_9-LysNH$_2$ (P1)

Synthesis of $HS(CH_2)_2CO$-egl-T_9-LysNH$_2$ (**P1**) began with step i and ii. A cycle of PNA monomer attachment (deprotection (step iii), coupling with the desired PNA monomer (step iv), and end capping (step v)) was then performed alternately with a cycle of spacer attachment (deprotection (step iii), coupling with spacer (step vi), and end capping (step v)). After PNA nonamer were obtained, step vii, viii (S-Dpm), ix, and x were consecutively followed. After purification, the HPLC peak of $HS(CH_2)_2CO$-egl-T_9-LysNH$_2$ (**P1**) appeared at t_R = 22.9 min. MALDI-TOF mass spectrum showed $M \cdot H^+_{obs}$ = 3373.64; $M \cdot H^+_{calcd}$ = 3369.39

2.3.3 Solid phase peptide synthesis of $HS(CH_2)_2CO$-egl-T_9-SerNH$_2$ (P2)

Synthesis of $HS(CH_2)_2CO$-egl-T_9-SerNH$_2$ (**P2**) differs from $HS(CH_2)_2CO$-egl-T_9-LysNH$_2$ (**P1**) in anchoring of the first amino acid (step ii). Fmoc-Serine was first attached to the free amino group on the RAM resin employing Fmoc-Ser(tBu)-ODhbt (5.3 mg, 10 µmol), HOAt (1.4 mg, 10 µmol), and DIEA (3.4 µL, 20 µmol) dissolved in anhydrous DMF (30 µL) in a 1.5 mL Eppendorf tube. Other steps were performed using

a similar step as described for $HS(CH_2)_2CO$-egl-T_9-LysNH$_2$ (**P1**) above. After purification by HPLC, the peak of $HS(CH_2)_2CO$-egl-T_9-SerNH$_2$ (**P2**) appeared at t_R = 22.9 min. MALDI-TOF mass spectrum showed $M \cdot H^+_{obs}$ = 3330.83; $M \cdot H^+_{calcd}$ = 3329.30

2.3.4 Solid phase peptide synthesis of $HS(CH_2)_2CO$-egl-T_9-AspNH$_2$ (P3)

Synthesis of $HS(CH_2)_2CO$-egl-T_9-AspNH$_2$ (**P3**) differs from $HS(CH_2)_2CO$-egl-T_9-LysNH$_2$ (**P1**) in anchoring of the first amino acid (step ii). Fmoc-Aspartate was first attached to the free amino group on the RAM resin employing Fmoc-Asp(OtBu)-OH (4.1 mg, 10 µmol), HOAt (1.4 mg, 10 µmol), and DIEA (3.4 µL, 20 µmol) dissolved in anhydrous DMF (30 µL) in a 1.5 mL Eppendorf tube. Other steps were performed using a similar step as described for $HS(CH_2)_2CO$-egl-T_9-LysNH$_2$ (**P1**) above. After purification by HPLC, the peak of $HS(CH_2)_2CO$-egl-T_9-AspNH$_2$ (**P3**) appeared at t_R = 22.4 min. MALDI-TOF mass spectrum showed $M \cdot H^+_{obs}$ = 3339.25; $M \cdot H^+_{calcd}$ = 3339.79

2.3.5 Solid phase peptide synthesis of $HS(CH_2)_2CO$-egl$_3$-T_9-SerNH$_2$ (P4), $HS(CH_2)_2CO$-egl$_5$-T_9-SerNH$_2$ (P5)

Synthesis of $HS(CH_2)_2CO$-egl$_3$-T_9-SerNH$_2$ (**P4**) and $HS(CH_2)_2CO$-egl$_5$-T_9-SerNH$_2$ (**P5**) were similar to $HS(CH_2)_2CO$-egl-T_9-SerNH$_2$ (**P2**) above. However, the coupling with 2-[2-(Fmoc-amino)ethoxy]ethoxy acetic acid pentafluoro phenyl ester (step vii) was repeated for 3 cycle and 5 cycle in $HS(CH_2)_2CO$-egl$_3$-T_9-SerNH$_2$ (**P4**), $HS(CH_2)_2CO$-egl$_5$-T_9-SerNH$_2$ (**P5**), respectively. After purification by HPLC, the peak of $HS(CH_2)_2CO$-egl$_3$-T_9-SerNH$_2$ (**P4**) appeared at t_R = 20.8 min. MALDI-TOF mass spectrum showed $M \cdot H^+_{obs}$ = 3619.00; $M \cdot H^+_{calcd}$ = 3619.30 and the HPLC peak of $HS(CH_2)_2CO$-egl$_5$-T_9-SerNH$_2$ (**P5**) appeared at t_R = 22.6 min. MALDI-TOF mass spectrum showed $M \cdot H^+_{obs}$ = 3913.36; $M \cdot H^+_{calcd}$ = 3909.94

2.3.6 Solid phase peptide synthesis of Ac-T$_9$-LysNH$_2$ (P6), Ac-T$_9$-SerNH$_2$ (P7)

Synthesis of Ac-T$_9$-LysNH$_2$ (P6) and Ac-T$_9$-SerNH$_2$ (P7) were accomplished in the same way as described for HS(CH$_2$)$_2$CO-egl-T$_9$-LysNH$_2$ (P1) and HS(CH$_2$)$_2$CO-egl-T$_9$-SerNH$_2$ (P2) from step i to step vi. After final cleavage of the Fmoc group, the nonamer PNA (P6) and PNA (P7) were treated with Ac$_2$O 2 µl in 30 µl DIEA solution in a 1.5 Eppendorf tube. After purification by HPLC, the peak of Ac-T$_9$-LysNH$_2$ (P6) appeared at t_R = 26.8 min. MALDI-TOF mass spectrum showed M·H$^+_{obs}$ = 3181.00; M·H$^+_{calcd}$ = 3179.44 and the peak of Ac-T$_9$-SerNH$_2$ (P7) appeared at t_R = 25.0 min. MALDI-TOF mass spectrum showed M·H$^+_{obs}$ = 3139.32; M·H$^+_{calcd}$ = 3138.35

2.3.7 Solid phase peptide synthesis of lipoic-T$_9$-LysNH$_2$ (P8)

Synthesis of lipoic-T$_9$-LysNH$_2$ (P8) was similar to HS(CH$_2$)$_2$CO-egl-T$_9$-LysNH$_2$ (P1) from step i to step vi. After final cleavage of Fmoc, the nonamer PNA (P8) was coupled with DL-α lipoic acid (1.1 mg, 0.5 µmol), HATU (1.7 mg, 10 µmol), and DIEA (1.7 µL, 10 µmol) dissolved in anhydrous DMF (30 µL) in a 1.5 mL Eppendorf tube. After purification by HPLC, the peak of lipoic-T$_9$-LysNH$_2$ (P8) appeared at t_R = 23.7 min. MALDI-TOF mass spectrum showed M·H$^+_{obs}$ = 3325.76; M·H$^+_{calcd}$ = 3325.39

2.3.8 Solid phase peptide synthesis of lipoic-egl-T$_9$-LysNH$_2$ (P9) and lipoic-egl-T$_9$-SerNH$_2$ (P10)

Syntheses of lipoic-egl-T$_9$-LysNH$_2$ (P9) and lipoic-egl-T$_9$-SerNH$_2$ (P10) were similar to HS(CH$_2$)$_2$CO-egl-T$_9$-LysNH$_2$ (P1) and HS(CH$_2$)$_2$CO-egl-T$_9$-SerNH$_2$ (P2) from step i to step vii, respectively. After final cleavage of Fmoc, the nonamer PNA (P9) and the PNA (P10) were coupled with DL-α lipoic acid (1.1 mg, 0.5 µmol), HATU (1.7 mg, 10 µmol), and DIEA (1.7 µL, 10 µmol) dissolved in anhydrous DMF (30 µL) in a 1.5 mL eppendorf tube. After purification by HPLC, the peak of lipoic-egl-T$_9$-LysNH$_2$ (P9) appeared at t_R = 24.1 min. MALDI-TOF mass spectrum showed M·H$^+_{obs}$ = 3469.64;

$M \cdot H^+_{calcd}$ = 3470.39 and the peak of lipoic-egl-T_9-SerNH$_2$ (**P10**) appeared at t_R = 25.3 min. MALDI-TOF mass spectrum showed $M \cdot H^+_{obs}$ = 3433.86; $M \cdot H^+_{calcd}$ = 3429.34

2.3.9 Solid phase peptide synthesis of lipoic-egl-T_9-Lys(Fluorescein)NH$_2$ (P11)

Synthesis of lipoic-egl-T_9-Lys(Fluorescein)NH$_2$ (**P11**) was accomplished in the same way as described for lipoic-egl-T_9-LysNH$_2$ (**P9**) above. After cleavage from resin. this PNA (**P9**) (A_{260} = 21, 20 µL) was coupled with 5(6)-Carboxyfluorescein N-hydroxysuccinimide (0.2 mg, 10 eq) in acetonitrile containing DIEA (3.42 µL, 10 equiv). After purification by gel electrophoresis. MALDI-TOF mass spectrum showed $M \cdot H^+_{obs}$ = 3929.01; $M \cdot H^+_{calcd}$ = 3929.39

2.3.10 Solid phase peptide synthesis of DNP-S(CH$_2$)$_2$CO-egl-T_9-LysNH$_2$ (P12)

Synthesis of DNP-S(CH$_2$)$_2$CO-egl-T_9-LysNH$_2$ (**P12**) was accomplished in the same way as described for lipoic-egl-T_9-LysNH$_2$ (**P9**) above but the thiol modifier was changed from lipoic acid to -(2,4-dinitrophenylthio)propanoic acid pentafluorophenyl ester (**22**) in the last step. After deprotection of Fmoc-egl-T_9-LysNH$_2$, this PNA was coupled with 3-(2,4-dinitrophenylthio)propanoic pentafluorophenyl ester (**22**) (4.4 mg, 0.5 µmol) in anhydrous DMF (30 µL) without addition of DIEA. The PNA was cleaved from the resin as usual. After purification by HPLC, the peak of DNP-S(CH$_2$)$_2$CO-egl-T_9-LysNH$_2$ (**P12**) appeared at t_R = 21.2 min. MALDI-TOF mass spectrum showed $M \cdot H^+_{obs}$ = 3516.22; $M \cdot H^+_{calcd}$ = 3519.39

2.3.11 Solid phase peptide synthesis of BzS(CH$_2$)$_2$CO-egl-T_4GT$_4$-LysNH$_2$ (P13)

Synthesis of BzS(CH$_2$)$_2$CO-egl-T_4GT$_4$-LysNH$_2$ (**P13**) started with solid phase peptide synthesis of Fmoc-T_4-Lys at 1.5 µmol scale. It was divided to three parts (0.5 µmol scale). One part, was coupled with G and T monomers until the sequence Fmoc-T_4GT$_4$-Lys was obtained. The Fmoc and side chain protections were removed by treatment with the deprotection solution and aqueous ammonia/dioxane 1:1 at 60 °C

overnight, repectively. The resin-bound PNA was coupled with 2-[2-(Fmoc-amino)ethoxy] ethoxy acetic acid pentafluorophenyl ester (vii) (2.6 mg, 0.5 μmol) and then with 3-(benzoylthio)propanoic pentafluorophenyl ester (25) (1.8 mg, 0.5 μmol) in anhydrous DMF (15 μL). After usual cleavage purification by HPLC, the peak of $BzS(CH_2)_2CO$-egl-T_4GT_4-LysNH$_2$ (P13) appeared at t_R = 21.2 min. MALDI-TOF mass spectrum showed M·H$^+$$_{obs}$ = 3499.00; M·H$^+$$_{calcd}$ = 3496.52

2.3.12 Solid phase peptide synthesis of $BzS(CH_2)_2CO$-egl-T_4CT_4-LysNH$_2$ (P14)

Synthesis of $BzS(CH_2)_2CO$-egl-T_4CT_4-LysNH$_2$ (P14) started with solid phase peptide synthesis of Fmoc-T_4-Lys at 1.5 μmol scale as described in 2.3.11. The second parts (0.5 μmol), was coupled with C and T monomers until the sequence Fmoc-T_4CT_4-Lys was obtained. The Fmoc and side chain protections were removed by treatment with the deprotection solution and aqueous ammonia/dioxane 1:1 at 60 °C overnight, repectively. The resin-bound PNA was coupled with 2-[2-(Fmoc-amino)ethoxy] ethoxy acetic acid pentafluorophenyl ester (vii) (2.6 mg, 0.5 μmol) and then with 3-(benzoylthio)propanoic pentafluorophenyl ester (25) (1.8 mg, 0.5 μmol) in anhydrous DMF (15 μL). After purification by HPLC, the peak of $BzS(CH_2)_2CO$-egl-T_4CT_4-LysNH$_2$ (P14) appeared at t_R = 22.3 min. MALDI-TOF mass spectrum showed M·H$^+$$_{obs}$ = 3460.01; M·H$^+$$_{calcd}$ = 3456.52

2.3.13 Solid phase peptide synthesis of $BzS(CH_2)_2CO$-egl-T_4AT_4-LysNH$_2$ (P15)

Synthesis of $BzS(CH_2)_2CO$-egl-T_4AT_4-LysNH$_2$ (P15) started with solid phase peptide synthesis of Fmoc-T_4-Lys at 1.5 μmol scale as described in 2.3.11. The third parts (0.5 μmol), was coupled with A and T monomers until the sequence Fmoc-T_4AT_4-Lys was obtained. The Fmoc and side chain protections were removed by treatment with the deprotection solution and aqueous ammonia/dioxane 1:1 at 60 °C overnight, repectively. The resin-bound PNA was coupled with 2-[2-(Fmoc-amino)ethoxy] ethoxy acetic acid pentafluorophenyl ester (vii) (2.6 mg, 0.5 μmol) and then with 3-(benzoylthio)propanoic pentafluorophenyl ester (25) (1.8 mg, 0.5 μmol) in anhydrous

DMF (15 µL). After purification by HPLC. the peak of BzS(CH$_2$)$_2$CO-egl-T$_4$AT$_4$-LysNH$_2$ (**P15**) appeared at t_R = 21.9 min. MALDI-TOF mass spectrum showed M·H$^+_{obs}$ = 3484.06: M·H$^+_{calcd}$ = 3480.53

2.3.14 Solid phase peptide synthesis of BzS(CH$_2$)$_2$CO-egl-T$_9$-LysNH$_2$ (P16)

Synthesis of BzS(CH$_2$)$_2$CO-egl-T$_9$-LysNH$_2$ (**P16**) was similar to lipoic-egl-T$_9$-LysNH$_2$ (**P9**) from step i to step vii. After final cleavage of Fmoc. the nonamer PNA (**P16**) were coupled with 3-(benzoylthio)propanoic pentafluorophenyl ester (**25**) in a 1.5 Eppendorf tube. After usual cleavage and purification by HPLC, the peak of BzS(CH$_2$)$_2$CO-egl-T$_9$-LysNH$_2$ (**P16**) appeared at t_R = 21.8 min. MALDI-TOF mass spectrum showed M·H$^+_{obs}$ = 3476.13: M·H$^+_{calcd}$ = 3474.39

2.3.15 Solid phase peptide synthesis of BzS(CH$_2$)$_2$CO-egl-T$_4$GT$_4$-Lys(Phos)NH$_2$ (P17)

Synthesis of BzS(CH$_2$)$_2$CO-egl-T$_4$GT$_4$-Lys(Phos)NH$_2$ (**P17**) began with step i and ii by using Fmoc-Lys(Mtt)-OH (9.4 mg. 10 µmol), HATU (5.7 mg. 10 µmol), and DIEA (3.4 µL, 20 µmol) during the first loading. After final Fmoc-removal the sequence T$_4$GT$_4$ was through further treated with aqueous ammonia:dioxane 1:1 at 60 °C for 6 h. This resin-bound PNA was coupled with 2-[2-(Fmoc-amino)ethoxy] ethoxy acetic acid pentafluorophenyl ester (vii) (2.6 mg. 0.5 µmol) and then with 3-(benzoylthio)propanoic pentafluorophenyl ester (**25**) (1.8 mg. 0.5 µmol) in anhydrous DMF (15 µL). The Mtt group was removed with 2% TFA (1 ml. 7 times) in dichloromethane until the cleavage solution color changed from yellow to colorless. The resin was then treated with DIEA/DMF to neutralize the TFA. Next the resin-bound PNA was coupled with carboxybutyltriphenylphosphonium succidimidyl ester (4.6 mg. 10 µmol), DIEA (3.4 µL, 20 µmol) in anhydrous DMF (30 µL) for 1 hour. After usual cleavage and purification by HPLC, the peak of BzS(CH$_2$)$_2$CO-egl-T$_4$GT$_4$-Lys(Phos)NH$_2$ (**P17**) appeared at t_R = 25.9 min. MALDI-TOF mass spectrum showed M·H$^+_{obs}$ = 3844.00; M·H$^+_{calcd}$ = 3843.52

2.3.16 Solid phase peptide synthesis of BzS(CH₂)₂CO-egl-T₄CT₄-Lys(Phos)NH₂ (P18)

Synthesis of $BzS(CH_2)_2CO$-egl-T_4CT_4-Lys(Phos)NH_2 (**P18**) was accomplished in the same way as described for $BzS(CH_2)_2CO$-egl-T_4GT_4-Lys(Phos)NH_2 (**P17**) above. After usual cleavage and purification by HPLC, the peak of $BzS(CH_2)_2CO$-egl-T_4CT_4-Lys(Phos)NH_2 (**P18**) appeared at $t_R = 26.4$ min. MALDI-TOF mass spectrum showed $M \cdot H^+_{obs} = 3804.88$; $M \cdot H^+_{calcd} = 3803.52$

2.3.17 Solid phase peptide synthesis of BzS(CH₂)₂CO-egl-T₄AT₄-Lys(Phos)NH₂ (P19)

Synthesis of $BzS(CH_2)_2CO$-egl-T_4AT_4-Lys(Phos)NH_2 (**P19**) was accomplished in the same way as described for $BzS(CH_2)_2CO$-egl-T_4CT_4-Lys(Phos)NH_2 (**P18**) above. After usual cleavage and purification by HPLC, the peak of $BzS(CH_2)_2CO$-egl-T_4AT_4-Lys(Phos)NH_2 (**P19**) appeared at $t_R = 26.4$ min. MALDI-TOF mass spectrum showed $M \cdot H^+_{obs} = 3827.00$; $M \cdot H^+_{calcd} = 3827.53$

2.3.18 Solid phase peptide synthesis of BzS(CH₂)₂CO-egl-T₉-Lys(Phos)NH₂ (P20)

Synthesis of $BzS(CH_2)_2CO$-egl-T_9-Lys(Phos)NH_2 (**P20**) was accomplished in the same way as described for $BzS(CH_2)_2CO$-egl-T_4CT_4-Lys(Phos)NH_2 (**P18**) above. After usual cleavage and purification by HPLC, the peak of $BzS(CH_2)_2CO$-egl-T_9-Lys(Phos)NH_2 (**P20**) appeared at $t_R = 27.1$ min. MALDI-TOF mass spectrum showed $M \cdot H^+_{obs} = 3819.88$; $M \cdot H^+_{calcd} = 3818.52$

2.3.19 Solid phase peptide synthesis of BzS(CH₂)₂CO-egl-T₉-Lys(Ac)NH₂ (P21)

Synthesis of $BzS(CH_2)_2CO$-egl-T_9-Lys(Ac)NH_2 (**P21**) began with step i and ii using Fmoc-Lys(Mtt)-OH during the first loading as described for $BzS(CH_2)_2CO$-egl-T_9-Lys(Phos)NH_2 (**P20**) above. After the Mtt group was removed with 2% TFA in

dichloromethane, the resin-bound PNA was treated with Ac$_2$O 2 μl in 30 μl DIEA solution in a 1.5 Eppendorf tube and was coupled with 2-[2-(Fmoc-amino)ethoxy] ethoxy acetic acid pentafluorophenyl ester followed by 3-(benzoylthio)propanoic pentafluoro phenyl ester (25), respectively. After usual cleavage and purification by HPLC, the peak of BzS(CH$_2$)$_2$CO-egl-T$_9$-Lys(Ac)NH$_2$ (P21) appeared at t_R = 21.8 min. MALDI-TOF mass spectrum showed M·H$^+$$_{obs}$ = 3516.00; M·H$^+$$_{calcd}$ = 3514.54

2.3.20 Solid phase peptide synthesis of Bz-egl-T$_9$-Lys(Phos)NH$_2$ (P22)

Synthesis of Bz-egl-T$_9$-Lys(Phos)NH$_2$ (P22) began with step i to viii as described for BzS(CH$_2$)$_2$CO-egl-T$_9$-Lys(Phos)NH$_2$ (P20) above. After the N-terminus of PNA was modified with 2-[2-(Fmoc-amino)ethoxy]ethoxy acetic acid pentafluorophenyl ester, the Fmoc group was deprotected and coupled with benzoic anhydride (2.3 mg, 10 μmol), DIEA (3.4 μL, 20 μmol) in anhydrous DMF (15 μL) for 30 min. The Mtt group was removed with 2% TFA in dichloromethane until the cleavage solution color changed from yellow to colorless. The resin was then treated with DIEA/DMF to neutralize the TFA. Next the resin-bound PNA was coupled with carboxybutyltriphenylphosphonium succidimidyl ester (4.6 mg, 10 μmol), DIEA (3.4 μL, 20 μmol) in anhydrous DMF (30 μL) for 1 hour. After usual cleavage and purification by HPLC, the peak of Bz-egl-T$_9$-Lys(Phos)NH$_2$ (P22) appeared at t_R = 26.2 min. MALDI-TOF mass spectrum showed M·H$^+$$_{obs}$ = 3733.00; M·H$^+$$_{calcd}$ = 3729.39

2.3.21 Solid phase peptide synthesis of BzS(CH$_2$)$_2$CO-egl-TTCCCCCTCCCAA Lys(Phos)NH$_2$ (P23)

Synthesis of BzS(CH$_2$)$_2$CO-egl-TTCCCCCTCCCAA-Lys(Phos)NH$_2$ (P23) was accomplished in the same way as described for BzS(CH$_2$)$_2$CO-egl-T$_4$XT$_4$-Lys(Phos)NH$_2$ above. After usual cleavage and purification by HPLC, the peak of BzS(CH$_2$)$_2$CO-egl-TTCCCCCTCCCAA-Lys(Phos)NH$_2$ (P23) appeared at t_R = 24.4 min. MALDI-TOF mass spectrum showed M·H$^+$$_{obs}$ = 5047.1; M·H$^+$$_{calcd}$ = 5045.14

2.3.22 Solid phase peptide synthesis of BzS(CH$_2$)$_2$CO-egl-TTCCCCTTCCCAA Lys(Phos)NH$_2$ (P24)

Synthesis of BzS(CH$_2$)$_2$CO-egl-TTCCCCTTCCCAA-Lys(Phos)NH$_2$ (**P24**) was accomplished in the same way as described for BzS(CH$_2$)$_2$CO-egl-T$_4$XT$_4$-Lys(Phos)NH$_2$ above. After usual cleavage and purification by HPLC, the peak of BzS(CH$_2$)$_2$CO-egl-TTCCCCTTCCCAA-Lys(Phos)NH$_2$ (**P24**) appeared at t_R = 24.3 min. MALDI-TOF mass spectrum showed M·H$^+_{obs}$ = 5060.1; M·H$^+_{calcd}$ = 5060.14

2.4 T_m experiments of thiol-modified PNA : DNA hybrids in solution[57]

T_m experiments were performed on a CARY 100 Bio UV-Visible spectrophotometer (Varian Ltd.) equipped with a thermal melt system. The sample for T_m measurement was prepared by mixing calculated amounts of stock DNA and PNA solutions together to give a final concentration of 1 µM at a ratio of PNA:DNA = 1:1 and 0.5 mM sodium phosphate buffer (pH 7.0) and the final volumes were adjusted to 3.0 mL by an addition of deionized water. The samples were transferred to a 10 mm quartz cell with a Teflon stopper and equilibrated at the starting temperature for 10 min. The A$_{260}$ was recorded in steps from 20→90→20→90 °C (block temperature) with a temperature increment of 1 °C/min and hold time of 10 min after each cycle. The heating only the result taken from the last heating cycle was used and was normalized by dividing the absorbance at each temperature by the initial absorbance. Analysis of the data was performed on a PC compatible computer using Microsoft Excel XP (Microsoft Corp.) (See Appendix A for detail of data analysis)

2.5 Immobilization and hybridization with target DNA of thiolated PNA carrying with different charge modification on gold nanoparticles

Immobilization of thiolated PNA carrying different charge modifications on gold nanoparticles was monitored by UV-VIS and fluorescence spectrophotometry, respectively. Furthermore surface functionality, topography and stabilities of the PNA-

capped nanoparticles were characterized by Photon Correlation Spectrocropy, and Transmission Electron Microscopy (TEM). Both of them can detect size of particles, however, TEM technique focuses on one particles size but Photon Correlation Spectrocropy technique detect total particles sizes. T_m experiments were used to determine PNA-capped gold nanoparticles - DNA hybridization by optimum conditions for hybridization and also fluorescence spectrophotometry was performed for detection of hybridization.

(a) UV-VIS spectrophotometry

UV-VIS experiment was performed on a CARY 100 Bio UV-Visible spectrophotometer (Varian Ltd.) using the same conditions as 2.4. The sample for UV-VIS experiment was prepared as follows.

i) Effects of mole ratio of PNA:gold nanoparticles (500:1 and 1500:1)

Gold nanoparticles (0.98 nM, 450 μL) were incubated with $HS(CH_2)_2CO$-egl-T_9-$SerNH_2$ (P2) and $HS(CH_2)_2CO$-egl-T_9-$AspNH_2$ (P3) (mole ratio of PNA:gold nanoparticles (500:1 and 1500:1)), respectively for 24 h. The solutions were centrifugally washed by 5 mM phosphate buffer (pH 7) twice and then incubated with 5 mM phosphate buffer (pH 7) (115 μL). The PNA-modified gold nanoparticles (115 μL) was hybridized with complementary DNA (dA_9 and A_{50}) (final concentration of 1 μM at a ratio of PNA : DNA = 1:1 and 10 mM sodium phosphate buffer (pH 7.0) at the final volume of 3.0 mL. The melting temperature was then observed at 260 nm.

ii) Effect of NaCl concentration

$HS(CH_2)_2CO$-egl-T_9-$AspNH_2$ (P3) modified gold nanoparticles (3.89 nM, 115 μL) were incubated with at various NaCl concentration (150 mM, 100 mM, and 50 mM) in total volume 125 μL. The PNA-modified gold nanoparticles (125 μL) was hybridized with complementary DNA (dA_9 and A_{50}) (final concentration of 1 μM at a ratio of PNA :

DNA = 1:1 and 10 mM sodium phosphate buffer (pH 7.0) at the final volume of 3.0 ml.. The melting temperature was then observed at 260 nm.

iii) Effect of length of 2-[2-(Fmoc-amino)ethoxy]ethoxy acetyl linker

The length of the linker was investigated by using PNA $HS(CH_2)_2CO$-egl$_n$-T$_9$-SerNH$_2$ PNA with different linker units (**P4, P5**) (n = 3, 5, respectively). These PNA were immobilized on gold nanoparticles (0.98 nM, 450 μL) (mole ratio of PNA:gold nanoparticles (500:1 and 1500:1)) as usual. The solutions were centrifugally washed by 5 mM phosphate buffer (pH 7) twice. The PNA-modified gold nanoparticles (115 μL) was hybridized with complementary DNA (dA$_9$) (final concentration of 1 μM at a ratio of PNA : DNA = 1:1 and 10 mM sodium phosphate buffer (pH 7.0) at the final volume of 3.0 mL.. The melting temperature was then observed at 260 nm.

iv) Effect of blocking thiol

Two different procedures were employed for $HS(CH_2)_2CO$-egl-T$_9$-AspNH$_2$ (**P3**).

→ First procedures. $HS(CH_2)_2CO$-O-T$_9$-AspNH$_2$ (**P3**) was immobilized on gold nanoparticles (0.98 nM, 450 μL) (mole ratio of $HS(CH_2)_2CO$-O-T$_9$-AspNH$_2$ (**P3**) to gold nanoparticles = 250:1 and 500:1). The excess PNA was removed by centrifugation wash with 5 mM phosphate buffer (pH 7) twice and then incubated with 5 mM phosphate buffer (pH 7) (115 μL). 2-Mercaptoethanol (1 mM, 200 μL) was added centrifugal to the gold nanoparticles (3.89 nM, 115 μL). After 1 h, the solution nanoaprticles were with 5 mM phosphate buffer (pH 7) twice in order to eliminate the excess 2-mercaptoethanol and then incubated with 5 mM phosphate buffer (pH 7) (315 μL). The nanoparticles solution (1.42 nM, 315 μL) was hybridized with complementary DNA (dA$_9$) (final concentration of 1 μM at a ratio of PNA : DNA = 1:1 and 10 mM sodium phosphate buffer (pH 7.0) at the final volumes of 3.0 mL. The melting temperature was then observed at 260 nm.

HS(CH$_2$)$_2$CO-egl-T$_9$-SerNH$_2$ (**P2**) was immobilized on gold nanoparticles according to the HS(CH$_2$)$_2$CO-O-T$_9$-AspNH$_2$ (**P3**) as described above.

→ Second procedures. HS(CH$_2$)$_2$CO-egl-T$_9$-AspNH$_2$ (**P3**), gold nanoparticles (mole ratio of HS(CH$_2$)$_2$CO-O-T$_9$-AspNH$_2$ (**P3**) to gold nanoparticles = 250:1 and 500:1) and blocking thiol (1 mM, 200 µL) were mixed at the same time. The reaction was incubated for 24 h. The excess PNA and blocking thiol were washed by centrifugation with 5 mM phosphate buffer (pH 7) twice and then incubated with 5 mM phosphate buffer (pH 7) (315 µL). The nanoparticles solution (1.42 nM, 315 µL) was hybridized with complementary DNA (dA$_9$) (final concentration of 1 µM at a ratio of PNA : DNA = 1:1 and 10 mM sodium phosphate buffer (pH 7.0) at the final volumes of 3.0 mL. The melting temperature was then observed at 260 nm.

(b) Fluorescence spectrophotometry

Fluorescence experiment, a CARY ECLIPSE Fluorescence spectrophotometer (Varian Inc.), was used for the determination % efficiency both of immobilization of thiolated PNA on gold nanoparticles and hybridization of thiolated PNA-capped gold nanoparticles and labeled target DNA.

(i) Immobilization

To Quantitate the immobilization of Lipoic-egl-T$_9$-Lys(Fluorescein)NH$_2$ (**P11**) on gold nanoparticles, the PNA (**P11**) (33.17 µM, 6.7 µL) and gold nanoparticles (0.98 nM, 450 µL) (mole ratio PNA:gold nanoparticles = 500:1) were incubated at room temperature for 24 h. The gold nanoparticles were then centrifugally at 14,000 rpm with 5 mM phosphate buffer (pH 7) twice in order to eliminate the excess PNA. Potassium cyanide solution (6 µL, final concentration 0.05 M) was added to the gold nanoparticles solution (final concentration 4.22 nM, 106 µL) to digest PNA-capped gold nanoparticles for 1 hour. The amount of thiolated PNA immobilized on gold nanoparticles (106 µL, in

total volume 2000 μL of 5 mM phosphate buffer pH 7) was determined by fluorescence spectroscopy (extinction wave length 490 nm).

(ii) Hybridization

The lipoic-egl-T_9-SerNH$_2$ (**P10**) (24.2 μM, 9.1 μL) was immobilized on gold nanoparticles (0.98 nM, 450 μL) (mol ratio PNA:gold nanoparticles = 500:1) for 24 h as described above. The modified nanoparticles were treated with the target DNA (13.9 μL, final concentration 2 μM) (mole ratio of PNA: DNA fluorescien-labeled (5'FAM AAA AAA AAA) = 1:1) (The labeled DNA was purchased from Bio Basic Inc.) in sodium phosphate buffer pH 7 (10 mM). After 1 hour, nanoparticles were centrifugally washed with 5 mM phosphate buffer twice to eliminate the unhybridized DNA. The nanoparticles (110 μL, final concentration 4.68 μM) mixed with a potassium cyanide solution (6 μL, final concentration 0.05 M KCN and 3.88 nM gold nanoparticles) in total volume 116 μL for 1 hour. Quantitation of the hybridized DNA (116 μL in total volume 2000 μL with 5 mM phosphate buffer pH 7) was performed by fluorescence spectroscopy (extinction wave length 490 nm).

(c) MALDI-TOF mass spectrometry

The PNA-modified gold nanoparticles (50 μL) were treated with dithiothreitol (final concentration 10 mM DTT) for 16 h at room temperature or KCN (final concentration 0.05 M) for 1 h. This solution (1 μL) was mixed with CCA (Saturated solution in 2:1 H$_2$O:MeCN containing 0.1% TFA) and spotted on the target. The MALDI-TOF spectra were collected on a Bruker Microflex MALDI-TOF mass spectrometry.

(d) Transmission electron microscopy (TEM)

TEM micrographs of nanoparticle aggregates were obtained on a Hitachi 8100 transmission electron microscopy operating at 200 keV. The PNA-modified gold

nanoparticles were prepared by depositing approximately 10 μL of the aggregate solutions onto carbon-coated grids and wicking away any excess solution. Grids were allowed to dry for at least 1 h prior to imaging. The sample preparation and measurement were carried out at the Material Technology Center (MTEC).

(e) Photon Correlation spectroscopy

Zeta potential data was obtained on a Malven Instrument Nano Ziser at the Material Technology Center (MTEC). The PNA-modified gold nanoparticles (3.89 nM, 20 μL) were added into cuvette and then volume adjusted to 2.0 mL by an addition of deionized water.
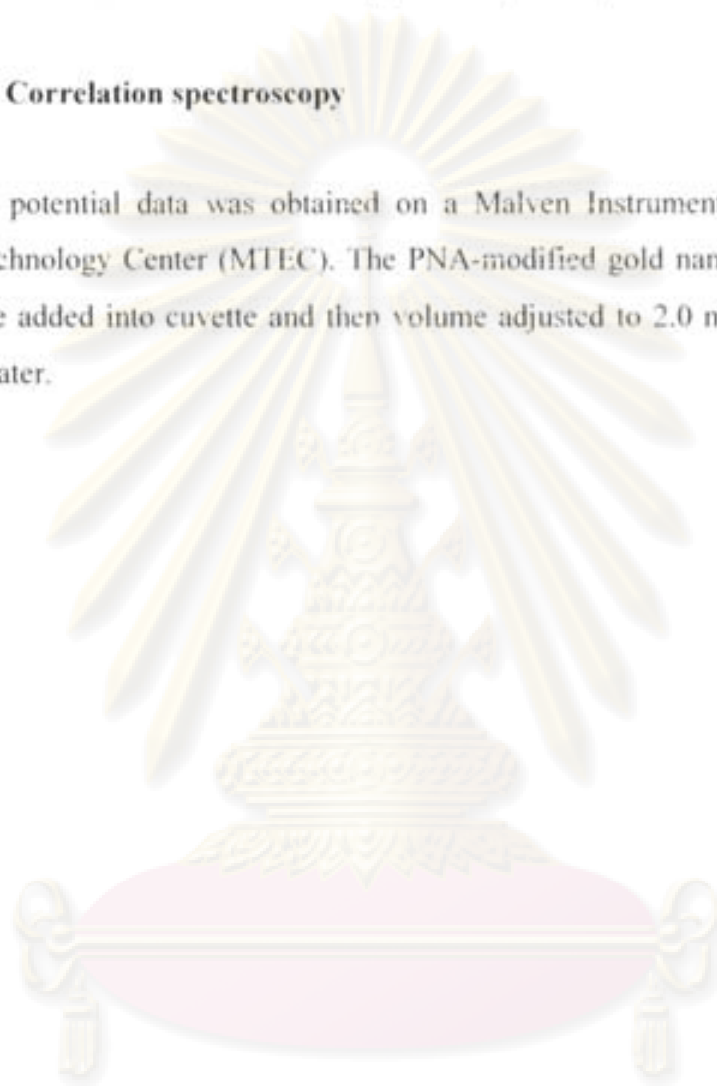
CHAPTER III

RESULTS AND DICUSSION

3.1 Synthesis of activated PNA monomers

The four Pfp-PNA monomers were synthesized as previously described by Mr. Chaturong Suparpprom, Miss Boonjira Boonta, Miss Cheeraporn Ananthanawat, and Mrs. Choladda Srisuwannaket[5]. They were purified by column chromatography and were obtained as white solids showing NMR spectra consistent with literature values.

3.2 Synthesis of ACPC spacer

Synthesis of the β-amino acid spacer (ssACPC) followed the procedure previously reported by Gellman [58]. Ethyl cyclopentanone-2-carboxylate (12) was reacted with (S)-(-)-α-methybenzylamine in the presence of glacial acetic acid to give an enamine intermediate. The enamine was stereoselectively reduced with sodium cyanoborohydride to give the (S,S)-*trans* β-aminoester (13) along with other stereoisomers, which could be separated by column chromatography. At the end, 21 % yield of ethyl (1S,2S)-2-[(1'S)-phenylethyl]-aminocyclopentane carboxylate (13) was obtained (**Figure 3.1**). The correct (1S,2S,1'S)-isomer was identified by comparison of NMR spectrum and the specific rotation value ([α]$_D$ +17.1, c = 1.0 in CHCl$_3$) with that reported by Gellman. (**Figure 3.2**)
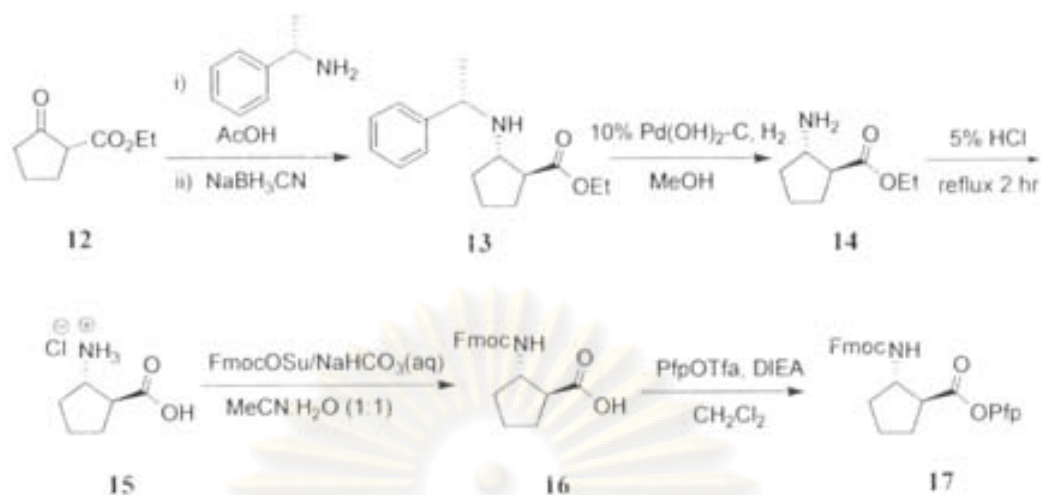
Figure 3.1 Synthesis of ACPC spacer.
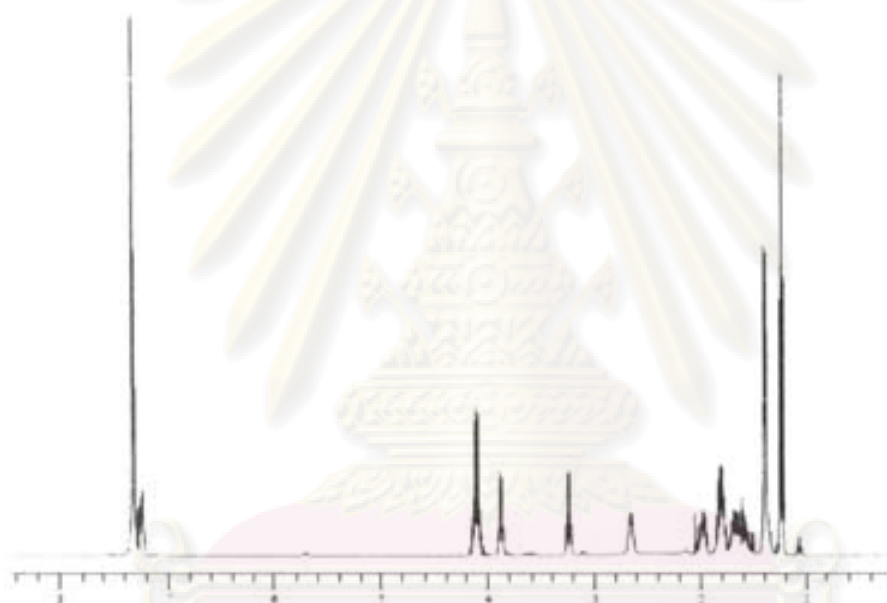
Figure 3.2 ¹H-NMR spectrum of ethyl (1*S*,2*S*)-2-[(1'*S*)-phenylethyl]-aminocyclopentane carboxylate (**13**)

The *S*-methylbenzylamine auxiliary was removed by hydrogenation over a palladium-hydroxide to afford the free amine (**14**). Acid hydrolysis gives the amino acid as hydrochloride salt (**15**) in 21 % yield from (**13**). Protection of the amino group with FmocOSu was accomplished under mildly basic condition as described previously [5,58]. This resulted in the free acid (**16**) in 63 % yield (**Figure 3.1**).

The ¹H NMR spectrum of compound (**16**) showed the following important signals: 4.26 ppm (Fmoc CH), 4.48 ppm (Fmoc CH₂), 7.34 ppm (Fmoc Ar CH), 7.42

ppm (Fmoc Ar C<u>H</u>). 7.62 ppm (Fmoc Ar C<u>H</u>) and 7.80 ppm (Fmoc Ar C<u>H</u>) (**Figure 3.2**). The identity and optical purity of the product was further confirmed by comparison of the specific rotation value ($[\alpha]_D$ +36.4, c = 1.0 in MeOH) with the value reported in the literature ($[\alpha]_D$ +36.3, c = 1.21 in MeOH).[58]

The Fmoc free acid (**16**) reacted with PfpOTfa and DIEA as decribed previously for the PNA monomers [59]. This reaction was complete within 1 h according to TLC analysis. The product was quickly purified by flash column chromatography to avoid decomposition of the product on the column. The product (**17**) was obtained in 78 % yield as a white solid (**Figure 3.1**). The identity of the product was confirmed by ^{1}H, ^{13}C and elemental analysis which are fully consistent with the expected structure. The optical rotation ($[\alpha]^{25}_D$ = + 49.0, c = 1.0 in CHCl$_3$) also corresponded to the authentic samples prepared previously in this laboratory ($[\alpha]^{25}_D$ = + 51.4, c = 1.0 in CHCl$_3$).

3.3 Synthesis of S-protected thiol modifiers

It was planned to incorporate the thiol group *via* 3-mercaptopropaonic acid. Since the thiol groups are nucleophilic, they require protection during the PNA synthesis. Initially it was protected as S-Dpm which could be removed by TFA treatment at the same time of cleaving the PNA from the solid support. However, the so-obtained free thiol PNA was not stable enough to allow proper purification. Other protecting groups which are stable toward TFA were therefore investigated. These include S-2,4-dinitrophenyl (S-DNP) and S-benzoyl (S-Bz).

3-(2,4-Dinitrophenylthio)propanoic acid (**21**) was synthesized by reacting 1-fluoro-2,4-dinitrobenzene (**20**) and 3-mercaptopropanoic acid in aqueous NaHCO$_3$. The product (**21**) was obtained in 85% yield as a yellow solid after simple acid-base extraction (**Figure 3.3**). The acid (**21**) was activated as its Pfp ester by reaction with PfpOTfa and DIEA. The Pfp ester (**22**) was obtained in 79% yield as a yellow solid (**Figure 3.3**). The structure of which was verified by ^{1}H, ^{13}C and elemental analysis which are fully consistent with the expectation. (**Figure 3.4**)
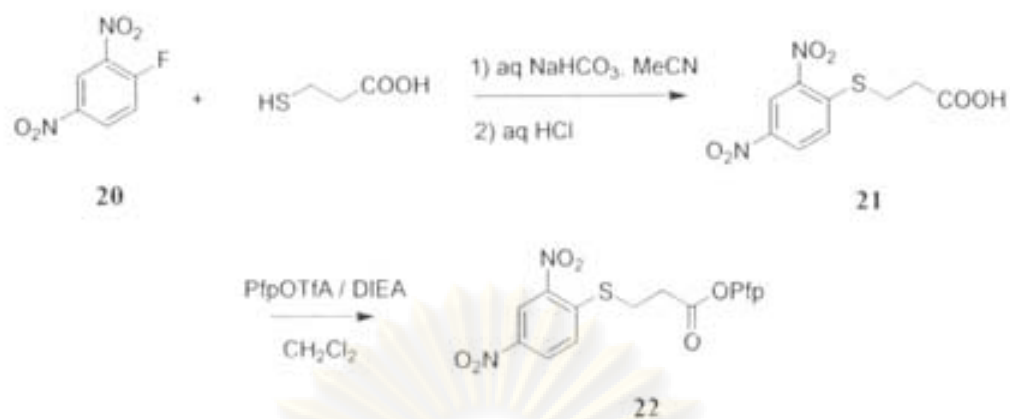
Figure 3.3 Synthesis of 3-(2,4-dinitrophenylthio)propanoic acid pentafluorophenyl ester (**22**)
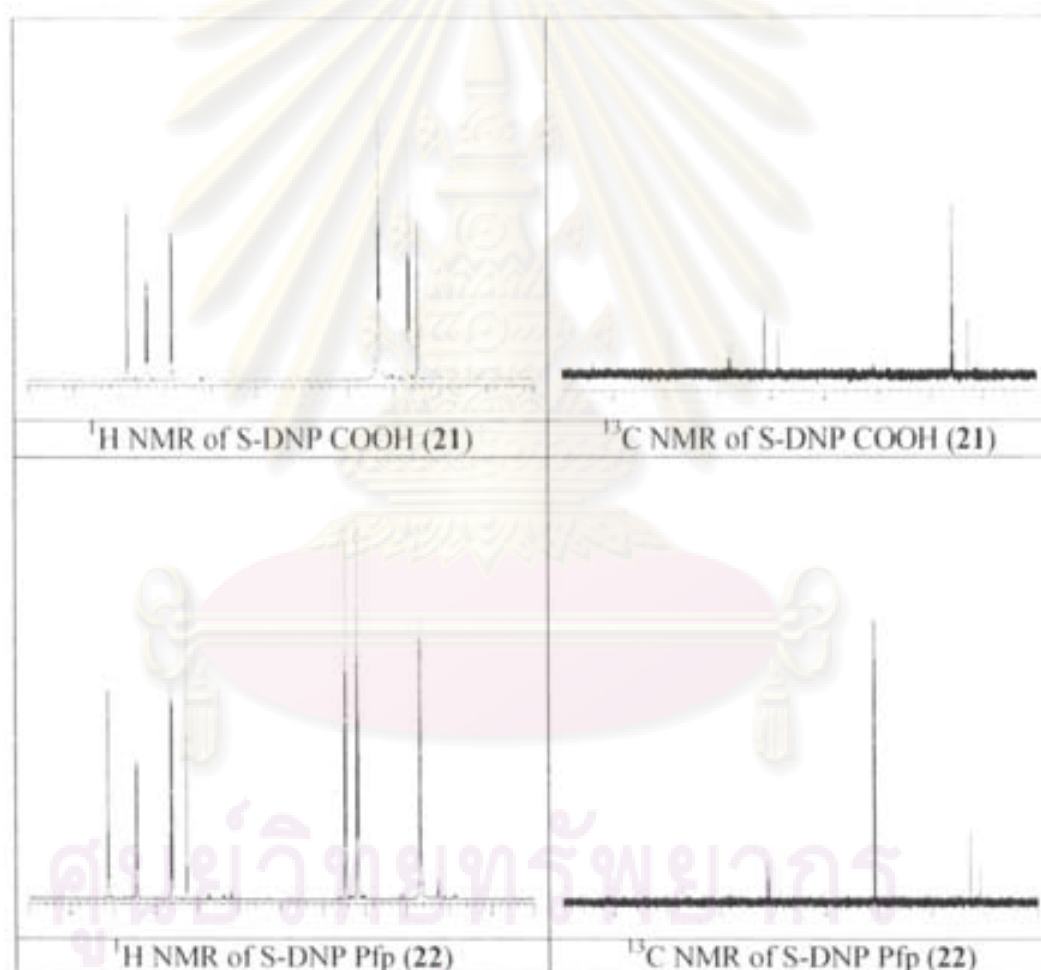
Figure 3.4 ¹H NMR and ¹³C NMR spectrum of both 3-(2,4-dinitrophenylthio)propanoic acid (**21**) and 3-(2,4-dinitrophenylthio)propanoic acid pentafluorophenyl ester (**22**), respectively.

3-(Benzoylthio)propanoic acid (**24**) was synthesized from the reaction of benzoyl chloride (**23**) and 3-mercaptopropanoic acid in aqueous NaHCO₃. The product (**24**) was obtained in 42% yield as a white solid and was further reacted with PfpOTfa and DIEA. The Pfp ester (**25**) was obtained in 62% yield as a colorless oil (**Figure 3.5**). The structure of product was confirmed by ¹H, ¹³C NMR and elemental analysis (**Figure 3.6**).
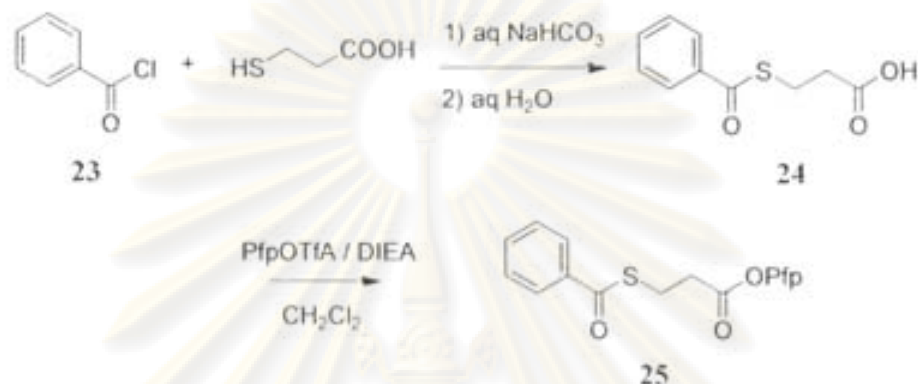
Figure 3.5 Synthesis of 3-(benzoylthio)propanoic acid pentafluorophenyl ester (**25**)
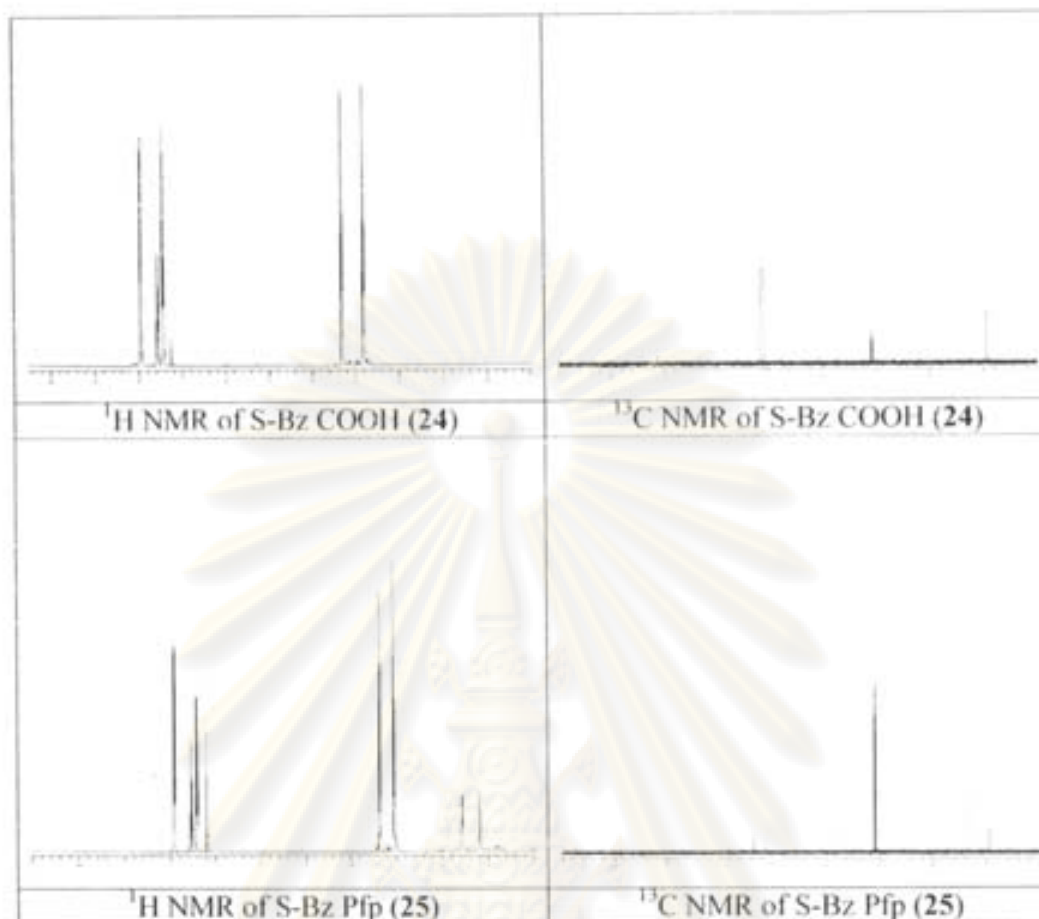
Figure 3.6 ^{1}H NMR and ^{13}C NMR spectrum of both 3-(benzoylthio)propanoic acid (24) and 3-(benzoylthio)propanoic acid pentafluorophenyl ester (25) respectively.

3.4 Synthesis of gold nanoparticles

Preparation of gold nanoparticles was attempted by citrate reduction of hydrogen tetrachloroaurate following literature procedures. In principle, the size of the nanoparticles depends upon the stoichiometric ratio of hydrogen tetrachloroaurate to sodium citrate. The higher the ratio, the larger the particle size. **Figure 3.7** displays TEM images of the gold nanoparticles prepared using a stoichiometric ratio of hydrogen tetrachloroaurate to sodium citrate of 0.065, 0.164, and 0.26 which should yield the gold nanoparticles with a theoretical diameter of 13, 16, and 40 nm, respectively. Most of the gold nanoparticles were round in shape. As opposed to other two samples, the shape of the 40-nm diameter gold nanoparticles seems to be more defined with narrower size distribution. The size and size distribution of the gold

nanoparticles were further verified by photon correlation spectroscopy. As can be seen from Table 3.1, the preparation of the gold nanoparticles with the theoretical diameter less than 20 nm cannot be well controlled. The diameters of the gold nanoparticles determined by PCS were much larger than the theoretical ones. This difference implied that there may be some aggregation of the gold nanoparticles.

(A) (B) (C)
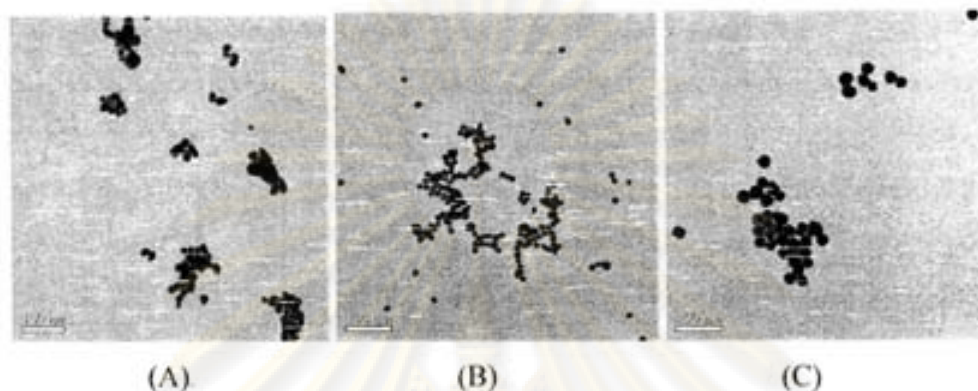
Figure 3.7 TEM images of gold nanoparticles with theoretical diameter of 13 nm (A), 16 nm (B), and 40 nm (C).

Table 3.1 Particle sizes of gold nanoparticles analyzed by photon correlation spectroscopy (PCS).

Theoretical diameter (nm) [53,36,54]	Diameter analyzed by PCS (nm)	PDI*	Zeta potential	SD
13 nm	19.2	0.59	-40.5	3.8
16 nm	28.2	0.52	-44.0	0.35
40 nm	37.8	0.16	-47.4	2.4

*PDI = poly dispersity index

Although the preparation of gold nanoparticles with the theoretical diameter of 40 nm could be accomplished, the stability of the nanoparticles varied from batch to batch. And the size is too large particularly for sensing applications. Thus, it was preferred to use the commercially available 20 nm gold nanoparticles (Sigma) for subsequent experiments. The concentration of the nanoparticle could be determined based on its molar extinction coefficient which is 1×10^9 $M^{-1}cm^{-1}$.

3.5 Synthesis of thiol-modified PNA nonamer by solid phase peptide synthesis

Solid Phase Peptide Synthesis (SPPS) of PNA was carried out according to the standard protocol previously developed in this laboratory [55,56]. An appropriate Fmoc-protected amino acid (Ser, Asp, Lys) was first coupled to the resin followed by the PNA monomer and spacer alternately until the desired PNA sequence was obtained. After completion of the synthesis, N-terminal Fmoc group was removed. If the PNA contains nucleobases other than thymine, the nucleobase protecting groups should be removed at this stage by treatment with 1:1 aqueous ammonia:dioxane at 60 °C for 6 h. The completely deprotected PNA was then coupled with a hydrophilic diethyleneglycol ("egl") linker to increase the solubility and also increase the distance between the PNA and the gold nanoparticles. This was reported to facilitate hybridization with DNA[58] before coupling of the linker. The thiol modifier was then coupled after another Fmoc deprotection to obtain the thiol-modified PNA.

For PNA containing C-terminal fluorescein [lipoic-egl-T_9-LysNH$_2$ Fluorescein (**P11**)], the amine reactive label [5(6)-carboxyfluorescein succinimidyl ester] was attached to the PNA bearing a C-terminal lysine residue in the solution after cleavage from resin. The PNA was purified from any excess fluorescein by gel electrophoresis.

Synthesis of C-terminal phosphonium modified PNA was carried out on the solid support using carboxybutyl triphenylphosphonium succinimidyl ester (Prepared by Miss Boonjira Boontha). To enable C-terminal functionalization on the solid support, Fmoc-Lys(Mtt)-OH must be first introduced before the PNA synthesis. Following the standard PNA synthesis, including protecting group removal, attachment of linker and thiol modifiers, the PNA was ready for functionalization. The Mtt protecting group of the lysine side-chain was first removed under mildly acidic condition (2% TFA in CH$_2$Cl$_2$). After the deprotection was completed as shown by disappearance of the yellow color from the deprotection solution, the PNA was coupled with the amine reactive phosphonium to give the desired doubly-modified PNA. The PNA was then cleaved from the solid support using TFA and purified by HPLC. The presence of hydrophobic DNP-S and BzS had beneficial effects in increasing the retention time of the desired PNA relative to the deletion sequences, hence facilitating the purification.

A complete synthesis cycles for a thiol-modified PNA nonamer can be readily performed in only a few days (excluding purification). The coupling efficiency

calculated from UV-absorption revealed that the synthesis was reasonably efficient (average coupling yield per step >90%). Retention time (t_R) and MALDI-TOF mass spectral data of all PNA synthesized in this work are shown in **Table 3.2**.

Table 3.2 Percent coupling efficiency, t_R and mass spectral data of the thiol-modified PNA nonamers

thiol-modified PNA nanomer	scale (μmol)	% efficiency* (overall)	t_R (min)	mass	
				M·H⁺ (calcd)	M·H⁺ (found)
HS(CH₂)₂CO-egl-T₉-LysNH₂ (P1)	1.0	77	24.0	3370.4	3373.6
HS(CH₂)₂CO-egl-T₉-SerNH₂ (P2)	1.0	74	22.9	3329.3	3330.83
HS(CH₂)₂CO-egl-T₉-AspNH₂ (P3)	1.0	60	22.4	3339.8	3339.2
HS(CH₂)₂CO-egl₃-T₉-SerNH₂ (P4)	0.5	69	20.8	3619.3	3619.0
HS(CH₂)₂CO-egl₅-T₉-SerNH₂ (P5)	0.5	67	22.6	3909.9	3913.4
Ac-T₉-LysNH₂ (P6)	0.5	74	26.8	3179.4	3181.0
Ac-T₉-SerNH₂ (P7)	0.5	69	25.0	3138.3	3139.3
Lipoic-T₉-LysNH₂ (P8)	1.0	75	23.7	3325.4	3325.7
Lipoic-egl-T₉-LysNH₂ (P9)	1.0	72	24.1	3470.4	3469.6
Lipoic-egl-T₉-SerNH₂ (P10)	1.0	66	25.3	3429.3	3433.9
Lipoic-egl-T₉-Lys(Fluorescien)NH₂ (P11)	0.5	48	-	3929.39	3929.01
DNP-S(CH₂)₂CO-	0.5	75	21.2	3519.35	3516.22

egl-T$_9$-LysNH$_2$ (P12)					
BzS(CH$_2$)$_2$CO-egl-T$_4$GT$_4$-LysNH$_2$ (P13)	0.5	82	21.2	3496.5	3499.0
BzS(CH$_2$)$_2$CO-egl-T$_4$CT$_4$-LysNH$_2$ (P14)	0.5	62	22.3	3456.5	3460.0
BzS(CH$_2$)$_2$CO-egl-T$_4$AT$_4$-LysNH$_2$ (P15)	0.5	55	21.9	3480.5	3484.1
BzS(CH$_2$)$_2$CO-egl-T$_9$-LysNH$_2$ (P16)	1.0	68	21.8	3474.4	3476.1
BzS(CH$_2$)$_2$CO-egl-T$_4$GT$_4$-Lys(Phos)NH$_2$ (P17)	0.37	80	25.9	3843.5	3844.0
BzS(CH$_2$)$_2$CO-egl-T$_4$CT$_4$-Lys(Phos)NH$_2$ (P18)	0.37	67	26.4	3803.5	3804.9
BzS(CH$_2$)$_2$CO-egl-T$_4$AT$_4$-Lys(Phos)NH$_2$ (P19)	0.37	89	26.4	3827.5	3827.0
BzS(CH$_2$)$_2$CO-egl-T$_9$-Lys(Phos)NH$_2$ (P20)	0.37	63	27.1	3818.5	3819.9
BzS(CH$_2$)$_2$CO-egl-T$_9$-Lys(Ac)NH$_2$ (P21)	0.37	71	21.8	3514.5	3516.0
Bz-egl-T$_9$-Lys(Phos)NH$_2$ (P22)	0.37	78	26.2	3729.4	3733.0

BzS(CH₂)₂CO-egl-TTCCCCCTCCCAA-Lys(Phos)NH₂ (P23)	0.5	71	24.4	5045.14	5047.1
BzS(CH₂)₂CO-egl-TTCCCCTTCCCAA-Lys(Phos)NH₂ (P24)	0.5	63	24.3	5060.14	5060.1

* calculated from the initial absorbance of dibenzofulvene-piperidine adduct from deprotection of Fmoc lysine with the absorbance obtained from Fmoc deprotection of the last cycle.

The thiol-modified PNA containing free thiol and lipoic acid were not stable upon storage and no HPLC purification could be performed. The use of more stable S-DNP and S-Bz derivatives allow purification and storage. However these protecting groups may require separate treatment to liberate the free thiol groups. In the case of S-DNP PNA, treatment with mercaptoethanol was reported to provide the free thiol PNA [60] as shown in **Figure 3.8**.
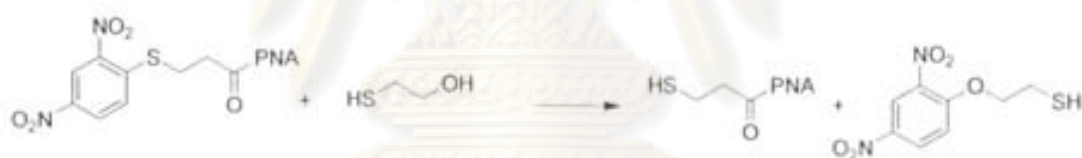
Figure 3.8 Deprotection of 1,3-dinitrobenzene by mrecaptoethanol.

In our hands, the DNP group could not be removed from the DNP-S(CH₂)₂CO-egl-T₉-LysNH₂ (P12) after treatment with mercaptoethanol under various conditions. MALDI-TOF mass spectrometric analysis (**Figure 3.9**) showed that the original mass of the PNA was observed in all cases (Mass 3535 [3512+Na]⁺).
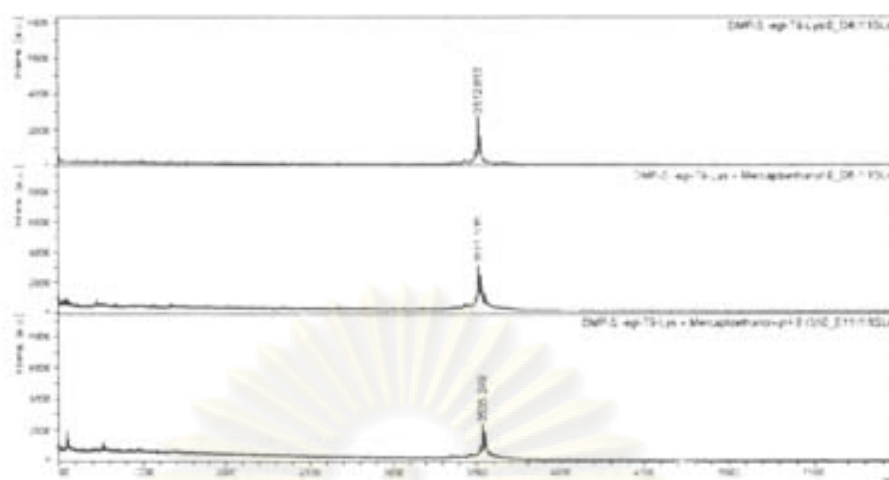
Figure 3.9 Mass spectra of DNP-S(CH₂)₂CO-egl-T₉-LysNH₂ (**P12**) before (A) and after treated with mercaptoethanol (B) and adjusted pH 8 (C).

On the other hand, the S-Bz group could be deprotected within 15 minutes at room temperature by treatment with aqueous ammonia. However, this free thiol PNA solution must be used immediately because it was unstable. After only a few hours at room temperature, the intensity of the free thiol PNA peak decreased and a new peak with had a mass twice of the original PNA was observed. This was attributed to the formation of a PNA dimer linked by a disulfide bond. The disulfide was formed from air oxidation of the thiol (**Figure 3.10**).
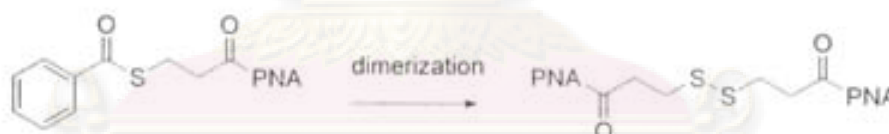
Figure 3.10 Dimerization of the S-Bz group.

The PNA were therefore stored in S-Bz protected form. In fact, it was subsequently shown that the deprotection was not necessary and the S-Bz protected PNA could be directly immobilized onto the gold nanoparticles.
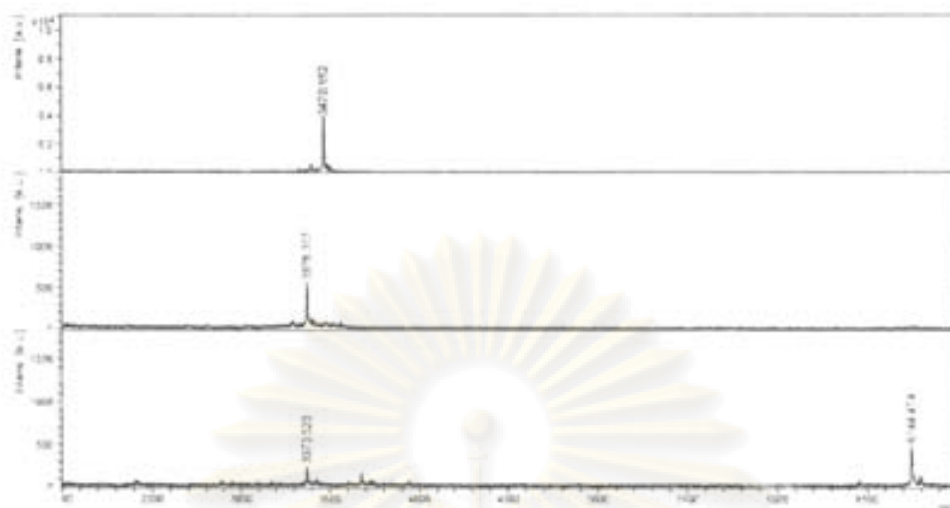
Figure 3.11 Mass spectra of deprotection of BzS(CH$_2$)$_2$CO-egl-T$_9$-LysNH$_2$ (**P16**) before (A) and after treated with ammonia (B) and (C).

Typical HPLC chromatogram and mass spectra BzS(CH$_2$)$_2$CO-egl-T$_9$-Lys(Phos)NH$_2$ (**P20**) are shown in **Figure 3.12a** and **Figure 3.12b**.

(A)

(B)
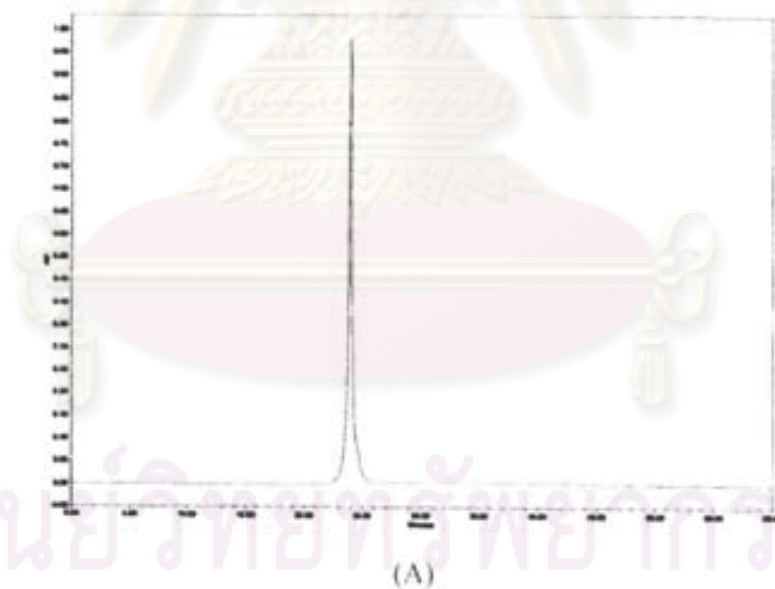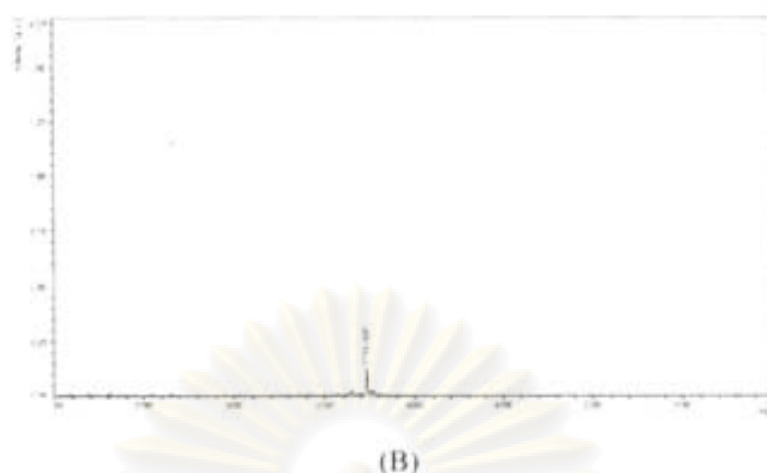
Figure 3.12 (A) HPLC chromatogram of BzS(CH$_2$)$_2$CO-egl-T$_9$-Lys(Phos)NH$_2$ **(P20)** and (B) MALDI-TOF MS of BzS(CH$_2$)$_2$CO-egl-T$_9$-Lys(Phos)NH$_2$ **(P20)**.

3.6 T_m experiments of thiol-modified PNA:DNA hybrids in solution

The binding properties of thiol-modified PNA nonamer BzS(CH$_2$)$_2$CO-egl-T$_9$-Lys(Phos)NH$_2$ **(P20)** with complementary DNA d(AAAAAAAAA) in solution was investigated by T_m measurement at 260 nm.

The T_m value of 82 °C was comparable to that of non-thiolated PNA[5]. This indicated that the thiol modifier had no adversed effects on the PNA-DNA hybridization and the BzS(CH$_2$)$_2$CO-egl-T$_9$-Lys(Phos)NH$_2$ **(P20)** could still form stable hybrids with dA$_9$. Repeating the T_m experiments between BzS(CH$_2$)$_2$CO-egl-T$_9$-Lys(Phos)NH$_2$ **(P20)** and different oligonucleotide nonamers containing one mismatch bases resulted in lowered T_m values of the complex by 29-37 °C per mismatch (**Figure 3.13** and **Table 3.3**, entry 45-48). Thus these thiol-modified PNAs shows high specificity in DNA recognition.
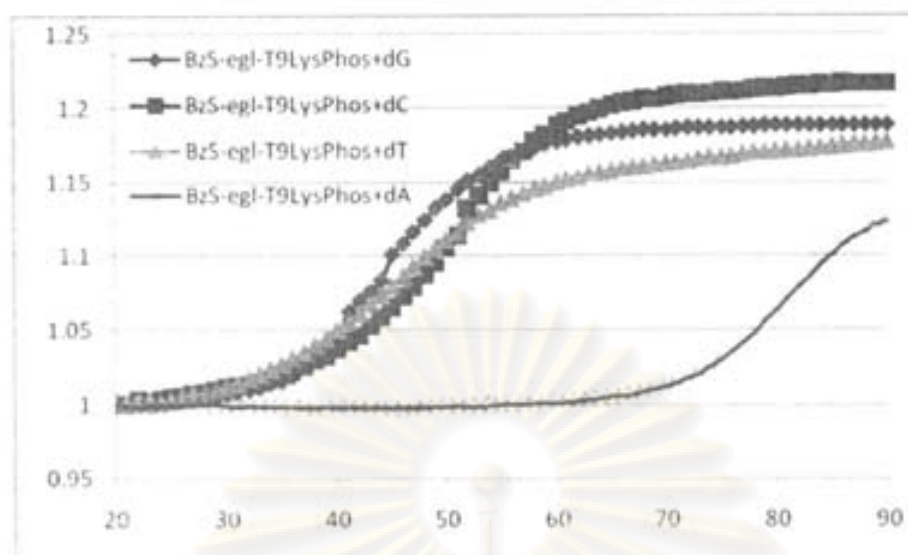
Figure 3.13 Melting curves of BzS(CH₂)₂CO-egl-T₉-Lys(Phos)NH₂ (**P20**) with d(AAAAAAAAA) (perfect match) and d(AAAAXAAAA) (single mismatch, X = G, C, and T). The T_m was measured at molar ratio of PNA:DNA = 1:1; concentration of PNA strand = 1 μM; 10 mM sodium phosphate buffer pH 7; heating rate 1 °C/min.

Table 3.3 T_m values of hybrids between thiol-modified PNA nonamer and oligo – nucleotides.

entry	PNA	oligonucleotide[a] (condition)	T_m[b] (°C)	note
1	**Dpm-S (P1)**	d(AAAAAAAAA)	79	perfect match
2	**Dpm-S (P1)**	d(AAAATAAAA)	30	single mismatch
3	**Dpm-S (P2)**	d(AAAAAAAAA)	69	perfect match
4	**Dpm-S (P2)**	d(AAAATAAAA)	44	single mismatch
5	**Dpm-S (P3)**	d(AAAAAAAAA)	65	perfect match
6	**Dpm-S (P3)**	d(AAAATAAAA)	34	single mismatch
7	**Dpm-S (P4)**	d(AAAAAAAAA)	68	perfect match
8	**Dpm-S (P4)**	d(AAAATAAAA)	33	single mismatch
9	**Dpm-S (P5)**	d(AAAAAAAAA)	69	perfect match
10	**Dpm-S (P5)**	d(AAAATAAAA)	43	single mismatch
11	**Lipoic (P8)**	d(AAAAAAAAA)	78	perfect match
12	**Lipoic (P8)**	d(AAAATAAAA)	50	single mismatch

13	**Lipoic (P9)**	d(AAAAAAAAA)	76	perfect match
14	**Lipoic (P9)**	d(AAAATAAAA)	45	single mismatch
17	**BzS (P13)**	d(AAAAAAAAA)	27	single mismatch
18	**BzS (P13)**	d(AAAATAAAA)	39	single mismatch
19	**BzS (P13)**	d(AAAACAAAA)	58	perfect match
20	**BzS (P13)**	d(AAAAGAAAA)	26	single mismatch
21	**BzS (P14)**	d(AAAAAAAAA)	34	single mismatch
22	**BzS (P14)**	d(AAAATAAAA)	27	single mismatch
23	**BzS (P14)**	d(AAAACAAAA)	-	single mismatch
24	**BzS (P14)**	d(AAAAGAAAA)	56	perfect match
25	**BzS (P15)**	d(AAAAAAAAA)	42	single mismatch
26	**BzS (P15)**	d(AAAATAAAA)	72	perfect match
27	**BzS (P15)**	d(AAAACAAAA)	31	single mismatch
28	**BzS (P15)**	d(AAAAGAAAA)	28	single mismatch
29	**BzS (P16)**	d(AAAAAAAAA)	81	perfect match
30	**BzS (P16)**	d(AAAATAAAA)	53	single mismatch
31	**BzS (P16)**	d(AAAACAAAA)	43	single mismatch
32	**BzS (P16)**	d(AAAAGAAAA)	45	single mismatch
33	**BzS (P17) (Phos)**	d(AAAAAAAAA)	34	single mismatch
34	**BzS (P17) (Phos)**	d(AAAATAAAA)	-	single mismatch
35	**BzS (P17) (Phos)**	d(AAAACAAAA)	57	perfect match
36	**BzS (P17) (Phos)**	d(AAAAGAAAA)	-	single mismatch
37	**BzS (P18) (Phos)**	d(AAAAAAAAA)	-	single mismatch
38	**BzS (P18) (Phos)**	d(AAAATAAAA)	-	single mismatch
39	**BzS (P18) (Phos)**	d(AAAACAAAA)	-	single mismatch
40	**BzS (P18) (Phos)**	d(AAAAGAAAA)	56	perfect match
41	**BzS (P19) (Phos)**	d(AAAAAAAAA)	43	single mismatch
42	**BzS (P19) (Phos)**	d(AAAATAAAA)	73	perfect match
43	**BzS (P19) (Phos)**	d(AAAACAAAA)	39	single mismatch
44	**BzS (P19) (Phos)**	d(AAAAGAAAA)	-	single mismatch
45	**BzS (P20) (Phos)**	d(AAAAAAAAA)	80	perfect match
46	**BzS (P20) (Phos)**	d(AAAATAAAA)	45	single mismatch
47	**BzS (P20) (Phos)**	d(AAAACAAAA)	51	single mismatch

48	**BzS (P20) (Phos)**	d(AAAA<u>G</u>AAAA)	42	single mismatch
49	**BzS (P23) (Phos)**	d(TTGGGAGGGGGAA)	64	perfect match
50	**BzS (P23) (Phos)**	d(TTGGGAAGGGGAA)	39	single mismatch
51	**BzS (P24) (Phos)**	d(TTGGGAGGGGGAA)	41	single mismatch
52	**BzS (P24) (Phos)**	d(TTGGGAAGGGGAA)	67	perfect match

[a]The T_m was measured at a ratio of PNA : DNA = 1:1: concentration of PNA strand =

1 μM: 10 mM sodium phosphate buffer pH 7: heating rate 1 °C/min.

[b]T_m was determined from first derivative plot.

3.7 Immobilization of thiol-modified PNA nonamer on gold nanoparticles

Thiolated PNA-gold nanoparticles conjugates were prepared by incubating 0.22-1.3 nmol of free thiolated PNA carrying different charge modification including HS(CH$_2$)$_2$CO-egl-T$_9$-LysNH$_2$ (**P1**), HS(CH$_2$)$_2$CO-egl-T$_9$-SerNH$_2$ (**P2**), HS(CH$_2$)$_2$CO-egl-T$_9$-AspNH$_2$ (**P3**) and Ac-T$_9$-SerNH$_2$ (**P7**) with 0.98 nM gold nanoparticles (20 nm particles size). After centrifugal-washing (15 min at 14,000 rpm, three times) to remove any unimmobilized PNA, the gold nanoparticles modified with PNA were characterized by UV-VIS-spectrophotometry, Photon Correlation Spectroscopy, and Transmission Electron Microscopy (TEM).

3.7.1 UV-VIS spectrophotometry

The UV-VIS spectra of unmodified gold nanoparticles before and after modification with the three thiolated PNAs are shown in the **Figure 3.14**. After modification, HS(CH$_2$)$_2$CO-egl-T$_9$-LysNH$_2$ (**P1**) bearing positively charged side-chain caused immediate and irreversible aggregation. This process can be visualized in solution by naked eye (red to purple color change) (**Figure 3.15A**). This color change can be attributed to the formation of large aggregates of gold nanoparticles caused by neutralization of the surface negative charge of the gold nanoparticles. In HS(CH$_2$)$_2$CO-egl-T$_9$-AspNH$_2$ (**P3**), a single anionic aspartate residue was incorporated and hence the PNA is negatively charged. Modification of gold nanoparticles of gold nanoparticles with this PNA did not result in aggregation. Only a slight shift of surface plasmon band from 520 to 527 nm which may be due to

centrifugation-induced aggregation was observed (**Figure 3.14**). The same behavior was also observed when neutral $HS(CH_2)_2CO$-egl-T_9-$SerNH_2$ (**P2**) was used. Both of PNA-functionalized gold nanoparticles did not exhibit any visible color change as shown in **Figure 3.15B** and **Figure 3.15C**, respectively. In the case of the Ac-T_9-$SerNH_2$ (**P7**) carrying acetyl group instead of the thiol, only a small surface plasmon band shift from 520 to 523 nm was also observed without any visible color change (**Figure 3.14 and 3.15D**).
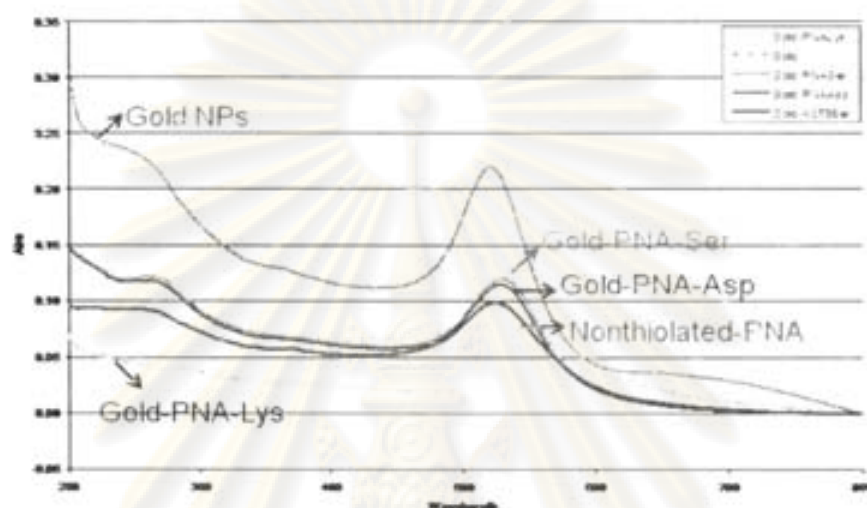
Figure 3.14. Comparison of UV-VIS spectra of gold nanoparticles immobilized with $HS(CH_2)_2CO$-egl-T_9-$SerNH_2$ (**P2**), $HS(CH_2)_2CO$-egl-T_9-$AspNH_2$ (**P3**), Ac-T_9-$SerNH_2$ (**P7**) and $HS(CH_2)_2CO$-egl-T_9-$LysNH_2$ (**P1**) before and after modification.
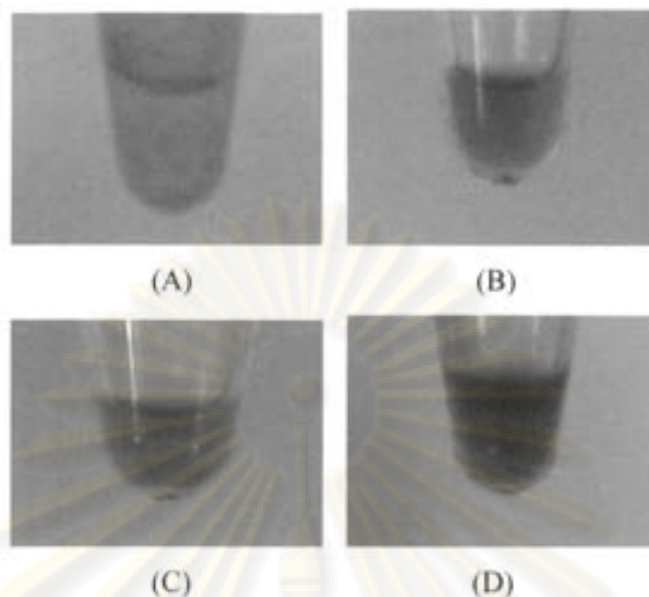
Figure 3.15. Aggregation behavior of thiolated PNA carrying different charge modification: (A) HS(CH$_2$)$_2$CO-egl-T$_9$-LysNH$_2$ (**P1**), (B) HS(CH$_2$)$_2$CO-egl-T$_9$-AspNH$_2$ (**P3**), (C) HS(CH$_2$)$_2$CO-egl-T$_9$-SerNH$_2$ (**P2**), and (D) Ac-T$_9$-SerNH$_2$ (**P7**) with gold nanoparticles.

3.7.2 MALDI-TOF mass spectrometry

To ensure that the PNA were immobilized on gold nanoparticles through thiolated the thiol group, MALDI-TOF mass spectrometry was used to follow the immobilization process. After standing for 24 h of HS(CH$_2$)$_2$CO-egl-T$_9$-LysNH$_2$ (**P1**) with gold nanoparticles, the solution was centrifuged for 15 min at 14,000 rpm to remove non-thiolated PNA and excess thiolated PNA that were not immobilized. The first time, MALDI-TOF analysis of the solution showed both incomplete non-thiolated and excess thiolated PNA (m/z = 3371.9) in the solution (**Figure3.16A**). In the second wash with followed by centrifugation, MALDI-TOF mass spectrum analysis revealed no signal of these PNA indicating that washing twice could remove all unbound PNA from the nanoparticles (**Figure 3.16B**).
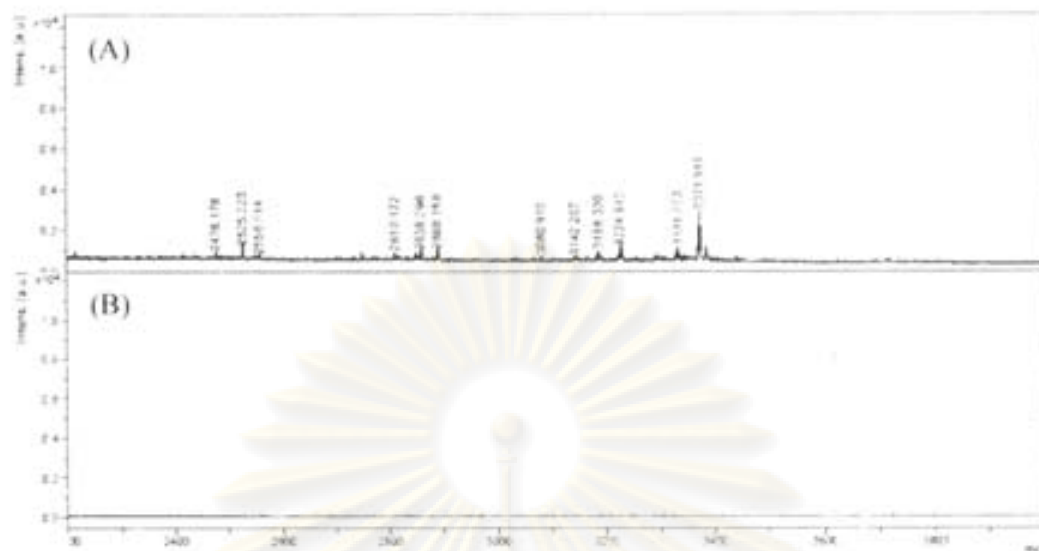
Figure 3.16. Mass spectrometric analysis results obtained from cleaned gold nanoparticles (A) first time, and (B) second time.

The HS(CH₂)₂CO-egl-T₉-LysNH₂ (**P1**) capped gold nanoparticles obtained after washing was incubated with DTT for 16 h at room temperature to release the PNA from the nanoparticles. Analysis of this solution showed the expected MALDI-TOF mass spectrum at m/z = 3370 indicating that the immobilization was successful. This also confirmed that the immobilization was selective for thiolated PNA because no signals of non-thiolated PNA were observed even though the PNA was used as a crude reaction product. Other PNA-modified gold nanoparticles give similar signals corresponding to the immobilized PNA. The same treatment of fresh gold nanoparticles with DTT gave no signals in this region. Likewise, no signal was observed in gold nanoparticles treated with the non-thiolated PNA Ac-T₉-SerNH₂ (**P7**) (**Figure 3.17**).
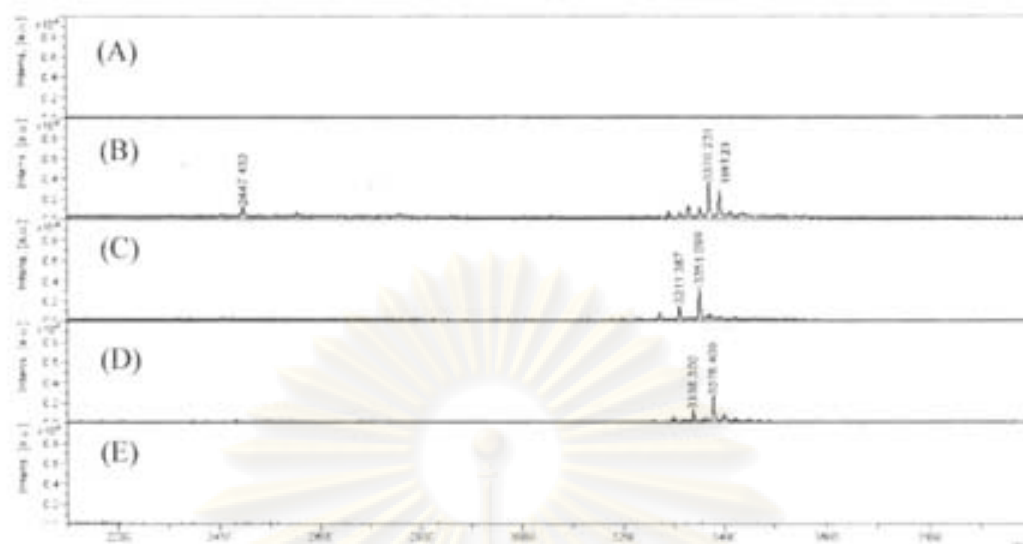
Figure 3.17 Mass spectrometric analysis results obtained from (A) gold nanoparticles and (B) HS(CH$_2$)$_2$CO-egl-T$_9$-LysNH$_2$ (**P1**) M·H$^+$ (calcd) = 3370.2 (3393.2 [M+Na$^+$]), (C) HS(CH$_2$)$_2$CO-egl-T$_9$-SerNH$_2$ (**P2**) M·H$^+$ (calcd) = 3329.3 (3351.1 [M+Na$^+$]), (D) HS(CH$_2$)$_2$CO-egl-T$_9$-AspNH$_2$ (**P3**) M·H$^+$ (calcd) = 3339.8 (3378.4 [M+K$^+$]), and (E) Ac-T$_9$-SerNH$_2$ (**P7**) M·H$^+$ (calcd) = 3138.3 modified gold nanoparticles treated with DTT.

3.7.3 Transmission Electron Microscopy (TEM) and Photon Correlation Spectroscopy (PCS)

The gold nanoparticles modified with the thiolated PNA P1-P3 were examined by TEM technique and compared with the unmodified gold nanoparticles (**Figure 3.18 (A)**). As can be seen in **Figure 3.18 (B)**, the positively charged HS(CH$_2$)$_2$CO-egl-T$_9$-LysNH$_2$ (**P1**) induced extensive aggregation of the gold nanoparticles whereas the neutral HS(CH$_2$)$_2$CO-egl-T$_9$-SerNH$_2$ (**P2**) modified gold nanoparticles, and the negatively charged HS(CH$_2$)$_2$CO-egl-T$_9$-AspNH$_2$ (**P3**) modified gold nanoparticles were randomly distributed with small aggregation and did not show a sign of extensive aggregation (**Figure 3.18 (C), (D)**).
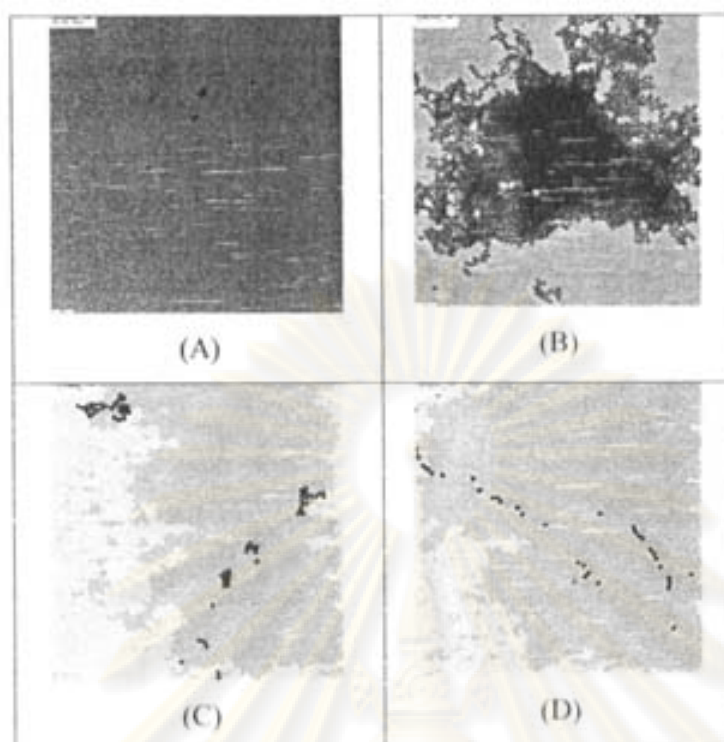
Figure 3.18 TEM images of gold nanoparticles (A) before and after immobilization with (B) HS(CH₂)₂CO-egl-T₉-LysNH₂ **(P1)**. (C) HS(CH₂)₂CO-egl-T₉-SerNH₂ **(P2)**. and HS(CH₂)₂CO-egl-T₉-AspNH₂ **(P3)**.

The aggregation of gold nanoparticles by PNA was further studied by photon correlation spectroscopy. Data in **Table 3.4** confirm the relationships between PNA charge stage and average particle size of the thiolated-modified PNA obtained from TEM studies. HS(CH₂)₂CO-egl-T₉-LysNH₂ **(P1)** caused extensive aggregation of the gold nanoparticles because the positive charge of PNA neutralized the negative charge of the citrate ion on the surface of gold nanoparticles so that the size determined by PCS was correspondingly larger. The neutral HS(CH₂)₂CO-egl-T₉-SerNH₂ **(P2)**. on the other hand, was ~ 2.5 times larger in size implying possible aggregation induced by centrifugation and/or the reduction of negative charge density on the gold nanoparticles due to the shielding effect. As opposed to other two systems. HS(CH₂)₂CO-egl-T₉-AspNH₂ **(P3)** showed particle size in a similar range to the unmodified gold nanoparticles. Because **(P3)** carries the same charge as citrate ion, it should not reduce the charge density of the gold nanoparticles. The modified gold nanoparticles remained stable and did not aggregate.

Table 3.4 Particle sizes of gold nanoparticles before and after modification.

PNA sequences	Diameter analyzed by PCS (nm)	PDI	Zeta potential	SD
Gold nanoparticles	38.6	0.14	-31.7	6.1
(P1) modified gold nanoparticles	458.7	0.26	-23.5	3.7
(P2) modified gold nanoparticles	97.3	0.17	-19.46	3.4
(P3) modified gold nanoparticles	31.5	0.16	-24.7	2.8

3.7.4 Stability of thiolated PNA modified gold nanoparticles

This set of experiments was designed to investigate the stability of thiolated PNA capped gold nanoparticles in various media. The PNA sequences studied included: (P2) neutral and (P3) negative. The PNA (P1) was not studied because it caused immediate aggregation of the gold nanoparticles.

i) Effect of phosphate buffer (pH 7.0) concentration

The stability of the $HS(CH_2)_2CO$-egl-T_9-$SerNH_2$ (P2) modified gold nanoparticles was evaluated by observing the color change at different phosphate buffer concentrations (0.05, 0.1, 2.0, and 5.0 mM).
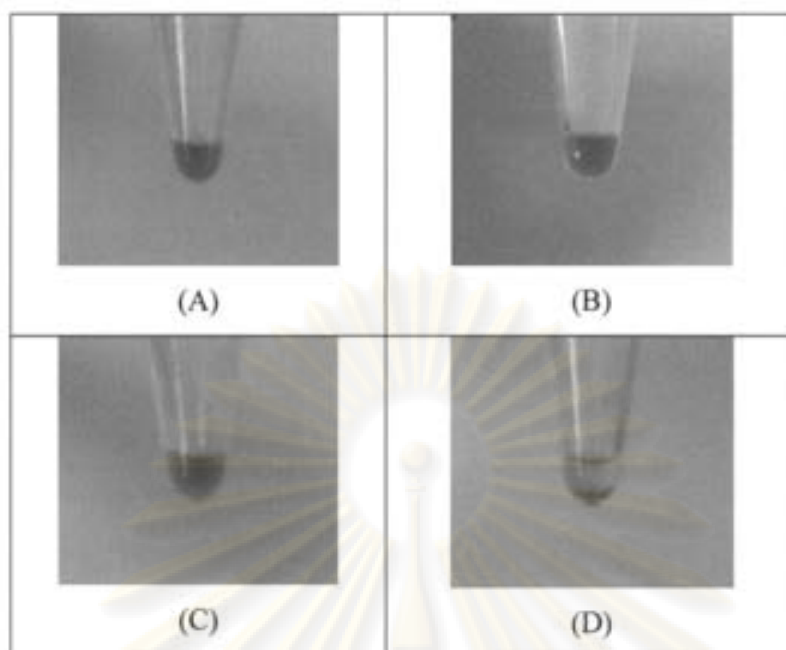
Figure 3.19 Effect of phosphate buffer pH7 (A) 0.05 mM, (B) 0.1 mM, (C) 2mM, and (D) 5 mM of $HS(CH_2)_2CO$-egl-T_9-SerNH$_2$ (**P2**) modified gold nanoparticles.

The results in **Figure 3.19** show that the neutral $HS(CH_2)_2CO$-egl-T_9-SerNH$_2$ (**P2**) modified gold nanoparticles was stable in phosphate buffer up to a concentration of 2 mM. On the other hand, $HS(CH_2)_2CO$-egl-T_9-AspNH$_2$ (**P3**) modified gold nanoparticles was stable under these conditions and also at 10 mM phosphate buffer (pH 7) (**Figure 3.20**). No aggregation was observed for over a period of two days. It could be explained that the negatively charged aspartate in $HS(CH_2)_2CO$-egl-T_9-AspNH$_2$ (**P3**) provided protection to the particles from the salt-induced aggregation at high buffer concentration.

Figure 3.20 $HS(CH_2)_2CO$-egl-T_9-AspNH$_2$ (**P3**) modified gold nanoparticles in 10 mM phosphate buffer (pH 7).

ii) Effect of NaCl concentration

The stability of PNA-modified gold nanoparticles at different NaCl concentrations (0.01 M, 0.05 M, 0.1 M, and 0.3 M) was also investigated. The addition of salt to the particles will result in a decrease in interparticle distance, due to charge screening effects. This results in the particle aggregation and the solution color turn from red to blue. $HS(CH_2)_2CO$-egl-T_9-$SerNH_2$ (**P2**) modified gold nanoparticles can resist aggregation up to 0.05 M NaCl concentration (**Figure 3.21**).

Figure 3.21 Effect of NaCl concentration on $HS(CH_2)_2CO$-egl-T_9-$SerNH_2$ (**P2**) modified gold nanoparticles (A) 0.01 M, (B) 0.05 M, (C) 0.1 M, and (D) 0.3 M.

The results in **Figure 3.22** showed that $HS(CH_2)_2CO$-egl-T_9-$AspNH_2$ (**P3**) modified gold nanoparticles are stable up to a salt concentration of 0.5 M, with no detectable color change even after leaving for 5 days.

(A)   (B)   (C)
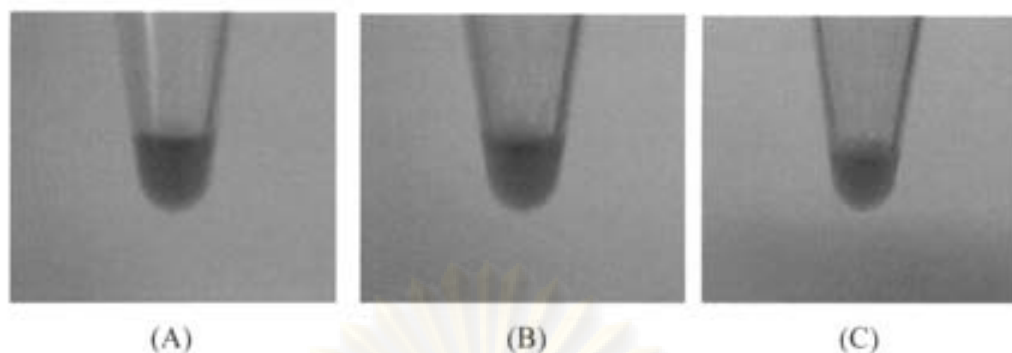
Figure 3.22 Effect of NaCl concentration on $HS(CH_2)_2CO$-egl-T_9-AspNH$_2$ (**P3**) modified gold nanoparticles (A) 0.1 M, (B) 0.3 M, and (C) 0.5 M.

These results indicated that the charge of the *C*-teminus amino acid contributes significantly to the stability of the PNA-modified gold nanoparticles. The $HS(CH_2)_2CO$-egl-T_9-AspNH$_2$ (**P3**) modified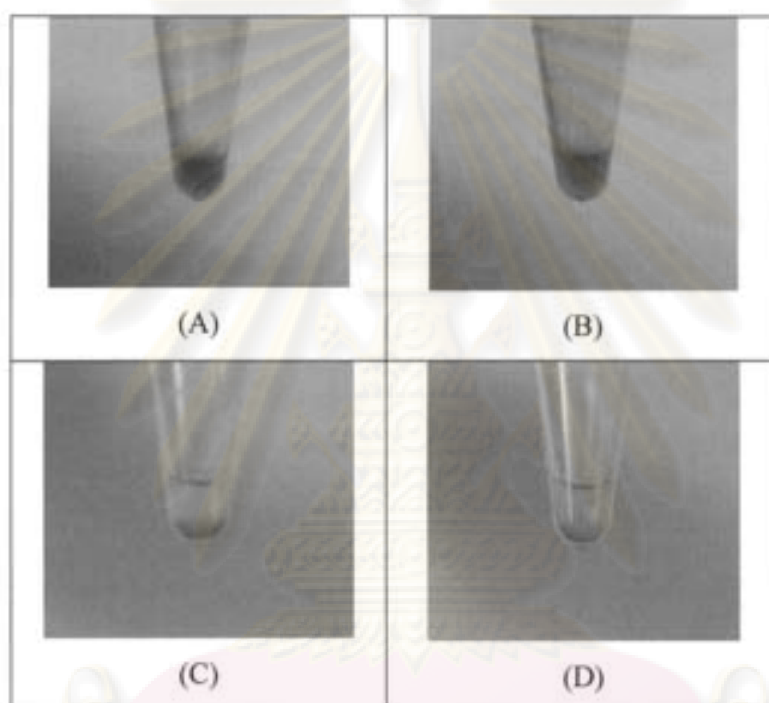 gold nanoparticles appeared to be more stable than $HS(CH_2)_2CO$-egl-T_9-SerNH$_2$ (**P2**) modified gold nanoparticles and $HS(CH_2)_2CO$-egl-T_9-LysNH$_2$ (**P1**) modified gold nanoparticles, respectively. This is in good agreement with prediction based on the charge state of the PNA modifiers.

3.8 Attempted detection of hybridization of PNA-modified gold nanoparticles with DNA

3.8.1 Melting temperature

Four different conditions were employed for hybridization of $HS(CH_2)_2CO$-egl-T_9-SerNH$_2$ (**P2**) modified gold nanoparticles and $HS(CH_2)_2CO$-egl-T_9-AspNH$_2$ (**P3**) modified gold nanoparticles with target DNA.

In the first set of experiments, the mole ratio of $HS(CH_2)_2CO$-egl-T_9-SerNH$_2$ (**P2**) to gold nanoparticles was varied (500:1 and 1500:1) during the immobilization step. The modified nanoparticles (11 nM, 23.8 μM PNA) were mixed with dA$_9$ at a concentration of 1 μM). The T_m was then measured at 260 nm. In both cases no melting curve could be obtained suggesting that no hybridization took place.

It was thought that increasing the DNA length might help increasing T_m observed for free PNA-DNA hybridization[5]. However increasing the length of DNA to dA$_{50}$ still resulted in no hybridization both with $HS(CH_2)_2CO$-egl-T_9-SerNH$_2$

(P2) and also HS(CH₂)₂CO-egl-T₉-AspNH₂ (P3)-capped gold nanoparticles

To determine the effect of increasing salt concentration on the melting temperature, the HS(CH₂)₂CO-egl-T₉-AspNH₂ (P3)-modified gold nanoparticles (mol ratio PNA:gold nanoparticles = 500:1), were hybridized with complementary DNA (dA₉) at various salt concentrations (150 mM, 100 mM, and 50 mM). Again, the melting analyses showed that salt concentration did not improve the T_m of the nanoparticle aggregates. Although salt concentration affects charge of gold nanoparticles and stability of DNA-DNA hybrids, it did not work to hybridization between PNA-modified gold nanoparticles and DNA due to PNA's neutrality.

It was thought that if the PNA lies to close to the gold nanoparticles, hybridization will be difficult. One diethyleneglycol linker unit (8 atoms) inserted between the PNA and the thiol group may not be sufficient to separate the PNA from the gold nanoparticles. To investigate the relationship between the poly(ethyleneglycol) linker length and T_m of PNA-DNA hybrids, the thiolated PNA carrying different numbers of poly(ethyleneglycol) units (n = 3, 5) were prepared. Under standard experimental conditions, the melting analyses of gold nanoparticles modified with these PNA showed that poly(ethyleneglycol) length did not have positive effects to the hybridization. No melting curve could still be observed in all cases. In order to confirm that the PNA was indeed immobilized in the functional state, ie without decomposition or denaturation, the PNA modified gold nanoparticles was treated with KCN solution. [61] The presence of cyanide and air cause dissolution of the nanoparticles, liberating the free thiolated PNA HS(CH₂)₂CO-egl₃-T₉-SerNH₂ (P4) into the solution. T_m experiment of this KCN-treated HS(CH₂)₂CO-egl₃-T₉-SerNH₂ (P4)-functionalized gold nanoparticles with dA₉ showed a clear T_m value of 78° C (**Figure 3.23**).
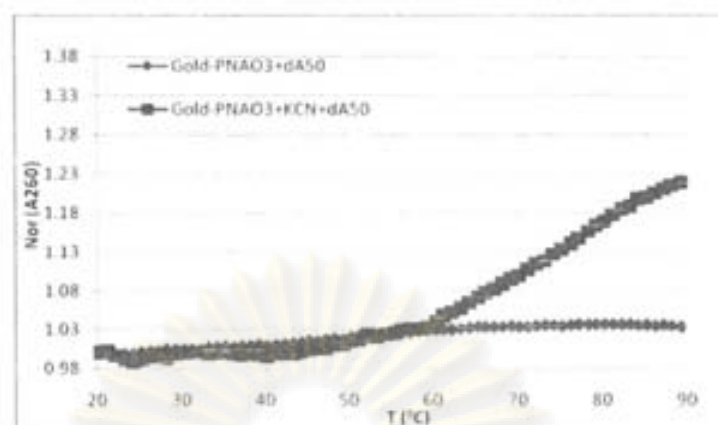
Figure 3.23 Melting temperature of HS(CH$_2$)$_2$CO-egl$_3$-T$_9$-SerNH$_2$ (**P4**)-modified gold nanoparticles before (A) and after (B) treatment with KCN.

This suggested that the PNA could be immobilized and released reversible without losing the binding properties. Although PNA was added linker length, PNA could not set up far away from gold nanoparticles. So DNA could not hybridize with PNA-modified gold nanoparticles. It can be further concluded that the morphology of PNA-modified gold nanoparticles were unsuitable for hybridization. Likewise, no hybridization was observed in the case of PNA-modified gold nanoparticles hybridized with DNA-modified gold nanoparticles [37]. From this result was corresponded with our results.

In a related study of immobilization of thiolated PNA on gold surface, addition of a small thiol was shown to improve the hybridization properites of the surface-immobilized PNA [61]. It was thought that if PNA and blocking thiol were immobilized on gold nanoparticles, the blocking thiol may be prevent the PNA lied on gold nanoparticles [52]. The effect of blocking thiol to the hybridization was also investigated. The PNA-modified gold nanoparticles [HS(CH$_2$)$_2$CO-egl-T$_9$-SerNH$_2$ (**P2**), mole ratios 500:1 and 1500:1] were treated with mercaptoethanol (1 mM, 200 uL). After 1 hour, the gold nanoparticles were hybridized with dA$_9$. Again no melting curves could be obtained. Similar experiments with HS(CH$_2$)$_2$CO-egl-T$_9$-AspNH$_2$ (**P3**) modified gold nanoparticles also gave the same results. Next, the PNA HS(CH$_2$)$_2$CO-egl-T$_9$-AspNH$_2$ (**P3**), gold nanoparticles and the blocking thiol were mixed at the same time. After washing, T_m experiment was carried out as usual. Again no melting curve could be obtained indicating that high surface coverage may not be

the important factors that contribute to the inability of gold nanoparticles-PNA to hybridize with DNA.

3.8.2 Quantitation of immobilized PNA and of hybridization by fluorescence experiment

Fluorescence is defined as the emission of radiation given out as a molecule returns to its ground state from an excited electronic state and fluorescence can be investigated by the analysis of changes in the emission. The emission from oligonucleotides is very weak at room temperature. As a result, synthetic fluorophores can be introduced earlier into an oligonucleotides or PNA by specific covalent or non-covalent addition.
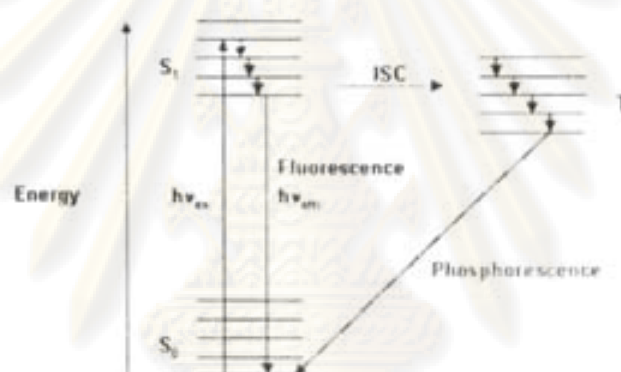

Figure 3.24 A simplified Jablonski diagram illustrating the principles of fluorescence and phosphorescence.

Fluorescence energy transfer (FRET) is a spectroscopic process by which energy is passed non-radiatively between molecules over long distances (10-100 Å). The non-radiative transfer of excited-state energy from a fluorescence donor molecule to an unexcited acceptor molecule *via* dipole-dipole coupling between the donor and the acceptor. The rate of this energy transfer depends on the spectral properties of the donor and acceptor. In general, the donor molecule is a fluorophore which has an absorption maximum at a shorter wavelength, can be excited selectively, and transfer the energy of an adsorbed photon non-radiatively to an acceptor molecule. The acceptor usually has an excitation λ_{max} at the longer wavelength. The result is that the

energy of a photon absorbed by donor can be lost by fluorescence photon emission from donor or by radiationless transition to acceptor leading to photon emission from acceptor at a longer wavelength.

Gold is known to be an effective quencher for many fluorophores including fluorescein according to the principle of FRET shown above [43,44]. If a fluorescein labelled PNA is immobilized onto gold nanoparticles, the fluorescence will be quenched. Upon release of the PNA from the gold, the fluorescence signal appears again. This can be applied in determination of PNA surface coverage and in measuring hybridization efficiency with DNA [43].

Figure 3.25 Illustration of detection the fluorescence signal.

i) Quantitation of surface coverage [43]

In quantitation of surface coverage a purified fluorophore-labelled PNA must be used as standard. As a result, the unstability and difficulty to purify, free thiolated PNA were not suitable for this purpose. Instead, a more stable lipoic acid modified PNA was chosen. The fluorophore, [5(6)-carboxyfluorescein], as a donor was introduced to the PNA sequence lipoic-egl-T_9-LysNH$_2$ at the C-terminal lysine residue in solution. This was purified by gel electrophoresis to give the pure fluorescein-labelled PNA. The PNA sequence was immobilized on gold nanoparticles (mole ratio PNA:gold nanoparticles = 500:1) in the dark at room temperature for 24 h. The PNA-immobilized gold nanoparticles were cleaned by centrifugal wash with 5 mM phosphate buffer pH 7 twice. The gold nanoparticles were digested by cyanide

solution (final concentration 0.05 M) to liberate the free labeled PNA. The fluorescence associated with the fluorescein at 524 nm was measured by spectroscopy (excited at 490 nm). To quantitate the amount of immobilized PNA, a calibration curve was also prepared by serial dilution of fluorophore-labeled PNA of known concentration. The calibration curve was linear over the concentration range of 10-70 nM (**Figure 3.26**).
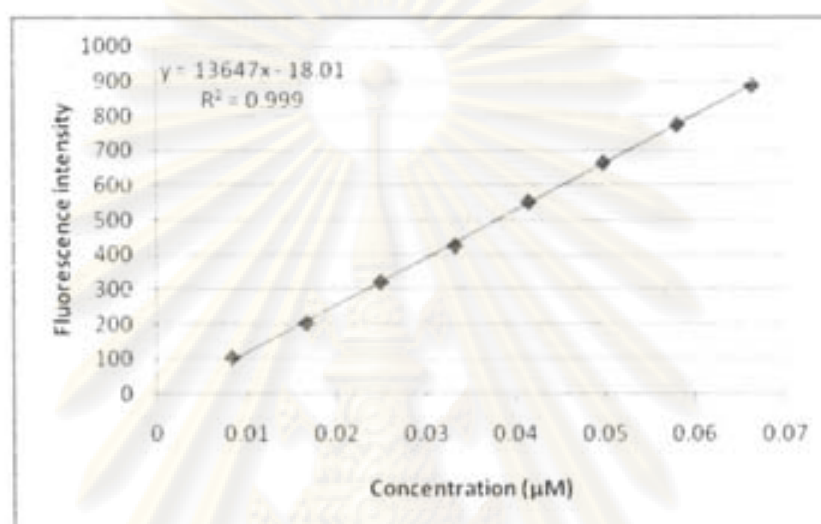

Figure 3.26 The calibration curve of lipoic-egl-T$_6$-LysNH$_2$ Fluorescein (**P11**).

The measured fluorescence intensity of the sample was 475.216 (106 µL in total volume 2000 µL of 5 mM phosphate buffer pH 7). The concentration of the PNA, and the surface density could be calculated from the equation shown in **Figure 3.26**.

$$475.216 = 13647\,X - 18.01$$

$$X = 0.03614\ \mu M$$

Dilution factor: $(0.03614 \times 2000) / 106 = 0.682\ \mu M$

PNA probe / one particle $= 0.682\ \mu M / 4.24\ nM$; $A_{520} = \varepsilon bc$

$$= 160.85 \qquad (0.984 = 1 \times 10^9\ M^{-1}cm^{-1} \times 1\ cm \times C)$$

$$(C\ start = 0.984\ nM)$$

$$(0.984\ nM)(456.67\ \mu L) = C(106\ \mu L)$$

$$C = 4.24\ nM$$

$$6.02 \times 10^{23}\ molecules = 1\ mole$$

$$160.85 \text{ molecules} \qquad = 26.72 \times 10^{-23} \text{ mole}$$

From circumference $(4\pi r^2)$ of gold nanoparticles : $4\pi(10 \times 10^{-7} \text{ cm})^2$

$$= 1.257 \times 10^{-11} \text{ cm}^2$$

PNA coverage on surface area of 20 nm diameter gold nanoparticles :

One particle with a surface area of $1.257 \times 10^{-11} \text{ cm}^2$ contains 26.72×10^{-23} mole of PNA probe

$$= 21.26 \times 10^{-12} \text{ mole / cm}^2 \ (21.26 \text{ pmol / cm}^2)$$

The average surface coverage of lipoic-egl-T_9-LysNH$_2$ Fluorescein (P11) on gold nanoparticles was 160.85 PNA probes per one nanoparticle, which corresponds to 21.26 pmol/cm^2. This measurement was repeated twice and the results showed similar values (154.5 PNA probes per one nanoparticles, 17.36 pmol/cm^2). Sato, K et al.[41] have reported 200 DNA probes per one 15 nm nanoparticle. Since diameter of DNA·DNA duplex was 20 A^0 (2 nm)[62]. The total coverage area could be calculated as follows.

$$\text{DNA: } 200\pi(r)^2 = 200\pi(1\text{nm})^2$$
$$= 628.6 \text{ nm}^2$$

Circumference $(4\pi r^2)$ of gold nanoparticles (15 nm diameter):
$$= 4\pi(7.5 \text{ nm})^2$$
$$= 707.1 \text{ nm}^2$$

Compare the two figures, it appears that DNA could form monolayer on the gold nanoparticles. In our case, similar calculation revealed that the amount of PNA probes was corresponded with DNA probes (assuming the PNA have similar dimension to DNA).

$$\text{PNA: } 160.85\pi(r)^2 = 160.85\pi(1\text{nm})^2$$
$$= 505.5 \text{ nm}^2$$

Circumference $(4\pi r^2)$ of gold nanoparticles (20 nm diameter):
$$= 4\pi(10 \text{ nm})^2$$
$$= 1257.1 \text{ nm}^2$$

ii) Quantitation of the hybridized target [43]

The PNA sequence lipoic-egl-T$_9$-SerNH$_2$ (P10) was used in this experiment because the surface coverage data of lipoic-egl-T$_9$-Lys(Fluorescein)NH$_2$ (P11) was available (see above). A fluorescein-labeled DNA (dA$_9$) was hybridized with the thiolated PNA (P10)-modified gold nanoparticles (final concentration of DNA 2 µM, of gold nanoparticles = 4.11 nM) in 10 mM phosphate buffer (pH 7) for 1 h. After the hybridization, the gold nanoparticles were cleaned by centrifugal wash with 5 mM phosphate buffer pH 7 twice in order to remove the excess flurophore-labeled oligonucleotides. The gold nanoparticles was digested by cyanide solution (final concentration 0.05 M) to liberate the free labeled DNA. The absorbance associated with the fluorescein at 516 nm was measured to quantitate the hybridization efficiency between PNA-modified gold nanoparticles and flurophore-labeled DNA against a calibration curve prepared by serial dilution of fluorophore-labeled DNA of known concentration (Figure 3.27).
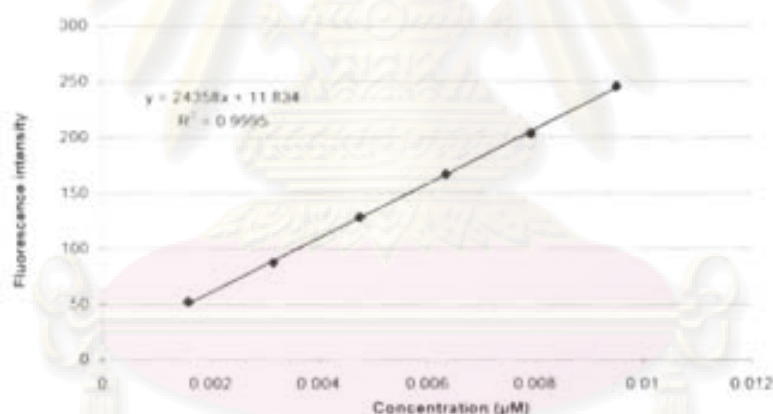

Figure 3.27 The calibration curve of flurophore-labeled oligonucleotides.

Intensity of the sample was 71.62 (116 µL) in total volume 2000 µL with 5 mM phosphate buffer (pH 7). The concentration was then calculated from the equation shown on the chart in Figure 3.27.

$$71.62 = 24358 \text{ X} + 11.834$$

$$\text{X} = 0.00245 \ \mu\text{M}$$

Dilution factor: $(0.00245(2000)) / 116 = 0.042 \ \mu\text{M}$

PNA probe / one particles $= 0.042 \ \mu\text{M} / 3.88 \ \text{nM} : A_{520} = \varepsilon bc$

$$= 10.82 \qquad (0.984 = 1 \times 10^9 \ \text{M}^{-1}\text{cm}^{-1} \times 1 \ \text{cm} \times \text{C})$$

$$(\text{C start} = 0.984 \ \text{nM})$$

$$(0.984 \ \text{nM})(459.15 \ \mu\text{L}) = \text{C}(116 \ \mu\text{L})$$

$$\text{C} = 3.88 \ \text{nM}$$

$$6.02 \times 10^{23} \ \text{molecules} = 1 \ \text{mole}$$

$$10.82 \ \text{molecules} \qquad = 1.80 \times 10^{-23} \ \text{mole}$$

Circumference $(4\pi r^2)$ of gold nanoparticles: $4\pi(10 \times 10^{-7} \ \text{cm})^2$

$$= 1.257 \times 10^{-11} \ \text{cm}^2$$

PNA coverage on surface area of 20 nm diameter gold nanoparticles :

One particle with a surface area of $1.257 \times 10^{-11} \ \text{cm}^2$ contains 1.80×10^{-23} mole of PNA probe

$$= 1.43 \times 10^{-12} \ \text{mole} / \ \text{cm}^2 \ (1.43 \ \text{pmol} / \ \text{cm}^2)$$

Comparison of the figures obtained above and the previous experiment clearly revealed that less than 1% of the PNA immobilized onto the gold nanoparticles could successfully form hybrid with DNA. From the calculation of the free labeled oligonucleotides suggested that the fluorophore's signal has 3.6×10^{-4} mole while the beginning of the fluorophore-labeled DNA has 1.82×10^{-2} mole. Therefore, it can be concluded that no hybridization fluorescein-labled oligonucleotides and lipoic-egl-T$_9$-SerNH$_2$ (**P10**)-modified gold nanoparticles took place. This is consistent with T_m experiments described in section 2.4.

3.9 Colorimetric detection of hybridization of thiolated PNA carrying positive charge with target DNA by gold nanoparticles

Since the PNA immobilized on gold nanoparticles failed to show binding to DNA targets, a new concept for detection of the hybridization event was developed based on the discovery that gold nanoparticles can aggregate in the presence of thiolated PNA bearing positive charge. The principle is summarized in **Figure 3.28**.
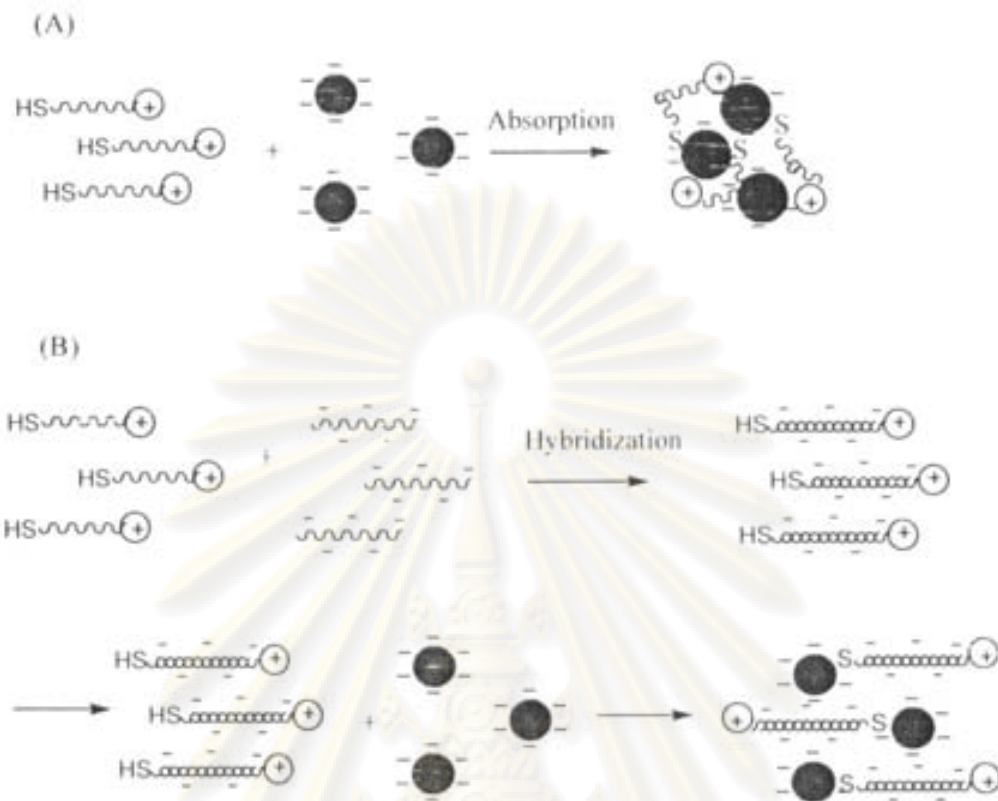
Figure 3.28 Illustration of (A) the aggregation of gold nanoparticles by positively charged thiolated PNA and (B) the presence of (negatively charged) complementary DNA should prevent the aggregation.

The aggregation was believed to be the result of charge neutralization of the gold nanoparticle upon functionalization with the (positively charged) PNA. However, if the PNA is first hybridized with DNA, the hybrid formed will be negatively charged because DNAs are polyanionic. If this PNA·DNA hybrid is now mixed with the nanoparticles, no aggregation should take place because the nanoparticles are still negatively charged after the functionalization.

This concept brought about a novel colorimetric detection of PNA·DNA hybridization based on gold nanoparticles aggregation, which will later be discussed in detail.

a) Concept validation using lipoic acid modifed PNA

Initially three different lipoic acid-modified T_9 PNA were used to validate the concept. The PNA sequences were: lipoic-T_9-LysNH$_2$ (**P8**), lipoic-egl-T_9-LysNH$_2$ (**P9**), and lipoic-egl-T_9-SerNH$_2$ (**P10**).

In the first set of experiment, a minimum amount of PNA that is sufficient to cause aggregation of the gold nanoparticles, as observed by color change from red to purple, was determined. Lipoic acid-T_9-Lys (**P8**) was mixed with gold nanoparticles at different ratio. The amounts of lipoic acid-T_9-Lys (**P8**) (1, 5, 10, 20 and 50 pmol) were varied in 10 mM phosphate buffer pH 7, while the gold nanoparticles concentration was kept constant at (0.70 nM) in a total volume 35 μL. As shown in **Figure 3.29**, when the concentration of lipoic acid-T_9-Lys (**P8**) was higher than 5 pmol in 35 μL (final concentration of PNA 0.26 μM, concentration of PNA:gold nanoparticles = 405:1), a definite color change from red to purple was observed within 5 min because the positive charge of PNA induced aggregation of the gold nanoparticles as described above.

(A)   (B)   (C)   (D)   (E)
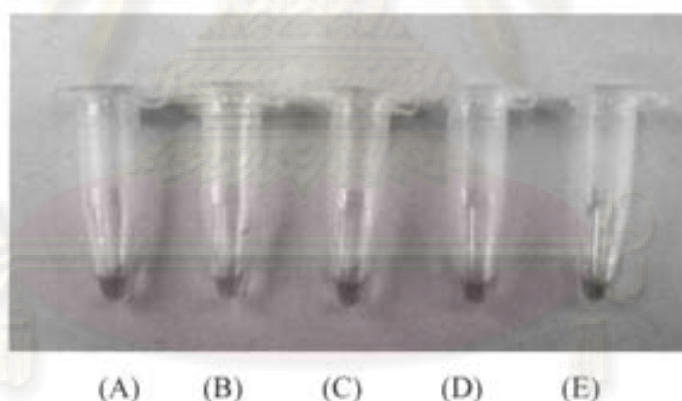
Figure 3.29 Aggregation behaviors of the lipoic acid-T_9-Lys (**P8**)-gold nanoparticles at various amounts of lipoic acid-T_9-Lys (**P8**) at room temperature: (A) 50 pmol, (B) 20 pmol, (C) 10 pmol, (D) 5 pmol, and (E) 1 pmol.

In the next experiments, the PNA were hybridized with DNA before treatment with the nanoparticles. Two different lipoic acid-T_9-Lys (**P8**) concentrations were employed for the detection of DNA hybridization by the aggregation of gold

nanoparticles. When 10 pmol of lipoic acid-T_9-Lys (**P8**) was used under the conditions described earlier (concentration PNA:gold nanoparticles = 405:1), no visible color changes were observed both for the full match (dA_9) and single mismatch (dA_8T) DNA targets (**Figure 3.30**).
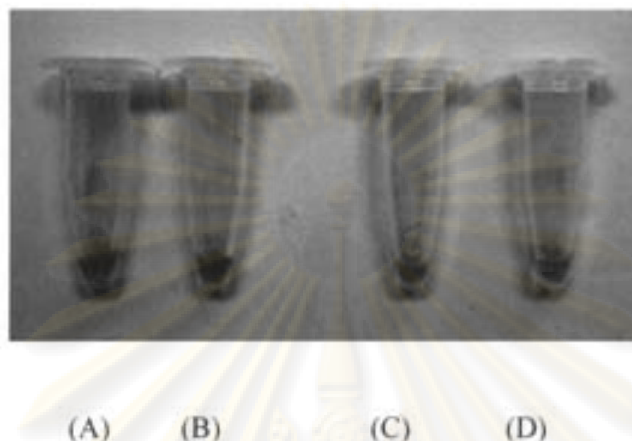

(A) (B) (C) (D)

Figure 3.30 Aggregation behaviors of hybridization of the 10 pmol lipoic acid-T_9-Lys (**P8**) and DNA with gold nanoparticles at various quantity of DNA: (A) 10 pmol of complementary target, (B) 10 pmol of single base mismatch target, (C) 20 pmol of a complementary target, and (D) 20 pmol of single base mismatch target.

At 20 pmol of the PNA (concentration PNA:gold nanoparticles = 810:1), however, the color change from red to purple was evidenced within a few minutes when 20 pmol single mismatched DNA (dA_8T) was present. No color change was observed with 20 pmol of complementary DNA (dA_9) during the same period. When the amount of the DNA was decreased to 10 pmol, the gold nanoparticles were aggregated for both complementary and single mismatch DNA targets. This may be explained by the fact that there is not enough DNA to neutralize the charge on the PNA and therefore the excess PNA induced gold nanoparticles aggregation (**Figure 3.31**).
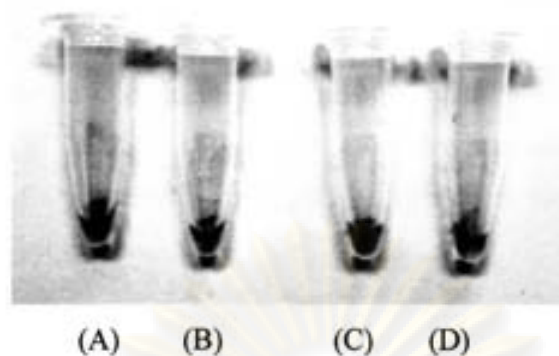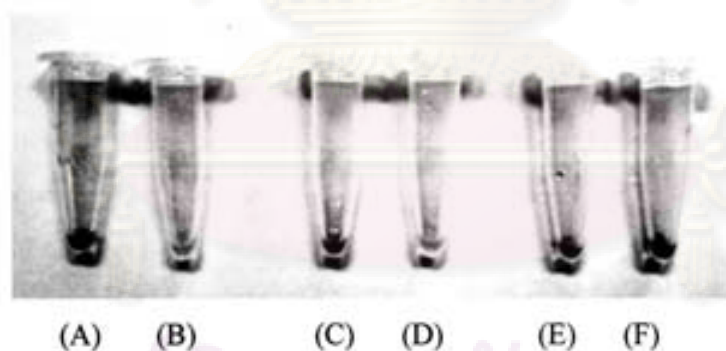
Figure 3.31 Aggregation behaviors of the 20 pmol lipoic acid-T_9-Lys (**P8**)-DNA hybridization on gold nanoparticles at various quantity of DNA: (A) 10 pmol of complementary target, (B) 10 pmol of single base mismatch target, (C) 20 pmol of complementary target, and (D) 20 pmol of single base mismatch target.

The amounts of the PNA and DNA were then varied to the high range (20, 100 and 200 pmol). In all cases, clear color difference could be observed for complementary (dA_9) and single mismatch (dA_8T) DNA targets as long as at least equimolar quantities of the DNA targets to the thiolated PNA probes were present (**Figure 3.32**).

Figure 3.32 Aggregation behaviors of the 20 pmol lipoic acid-T_9-Lys (**P8**)-DNA hybridization in gold nanoparticles at various quantity of DNA: (A) 20 pmol of a complementary target, (B) a single base mismatch, (C) 100 pmol of a complementary target, (D) a single base mismatch, (E) 200 pmol of a complementary target, and (F) a single base mismatch.

The same experiments were also carried out with the non-thiolated PNA Ac-T_9-Ser (**P7**). In this cases, both complementary (dA_9) and single base mismatch (dA_8T) caused no visible change at 20 pmol of both PNA and DNA suggesting that the aggregation of the gold nanoparticles was indeed caused by the immobilization of the positively charged PNA on the gold nanoparticles via the thiol group (**Figure 3.33**).

(A)   (B)

Figure 3.33 Aggregation behaviors of gold nanoparticles in the presence of 20 pmol of the nonthiolated PNA Ac-T_9-Ser (**P7**) and equimolar amounts of complementary (dA_9) (A) or single base mismatch (dA_8T) (B).

To investigate the specificity of this new assay, 20 pmol of Lipoic-egl-T_9-LysNH$_2$ (**P9**) were hybridized with four different target DNAs (dA_9, dA_8T, dA_8C, dA_8G) under the optimal conditions obtained above (concentration PNA:gold nanoparticles = 810:1, and 20 pmol DNA, 10 mM phosphate buffer pH 7.0). In this experiment, the diethyleneglycol linker was inserted between the lipoic acid and the PNA sequence to improve hybridization efficiency. The photograph taken following addition of the gold nanoparticles is shown in **Figure 3.34**. The results showed clear discrimination between hybridization of lipoic-egl-T_9-LysNH$_2$ (**P9**) with full match and all other single mismatched (T-T, T-C and T-G) DNA. No visible color change was observed with the full match target DNA (dA_9). In contrast, obvious color change to purple or blue due to the aggregation of gold nanoparticles were observed for all single mismatch cases, indicating the high specificity of the test.

A$_4$XA$_4$: A T C G
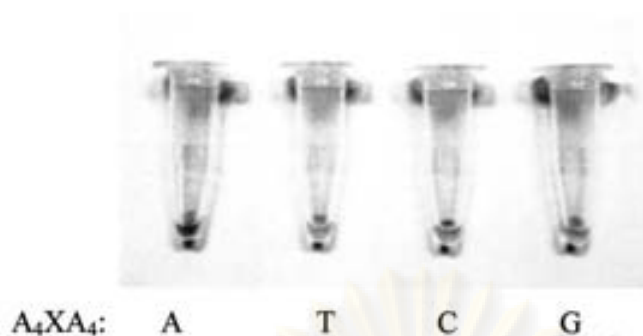
Figure 3.34 Aggregation behaviors of gold nanoparticles in the presence of equimolar quantities of lipoic-egl-T$_9$-LysNH$_2$ (**P9**) with various DNA targets dA$_4$XA$_4$ (X=A, T, C, G) at 20 pmol.

b) Colorimetric detection of hybridization of S-protected thiolated PNA with DNA

Although the use of lipoic acid modified PNA have solved the problem of instability of thiolated PNA to some extent, it was still problematic in attempting to prepare Lipoic acid modified PNA with sequences other than T9. This was primarily due to the instability of the lipoic acid under the nucleobase side-chain deprotection conditions. It was therefore necessary to find a new thiol PNA surrogate. At first dinitrophenyl (DNP) group was chosen because of its stability and hydrophobicity, which facilitate HPLC purification. However, attempts to remove the DNP group by treatment with mercaptoethanol according to the literature[59] failed as shown by MALDI-TOF analysis. Therefore this protecting group was not investigated further. The next protecting group considered was S-Benzoyl. The S-Benzoyl group could be easily removed by treatment with base such as NH$_3$[64]. It is also conceivable that the S-benzoyl PNA could be directly immobilized onto the gold nanoparticles. The same experiments as lipoic-egl-T$_9$-LysNH$_2$ (**P9**) were repeated using four new PNA probes carrying four differnt nucleobases in the middle of the strand, BzS(CH$_2$)$_2$CO-egl-T$_4$XT$_4$-LysNH$_2$, under the same conditions. At 20 pmol, the color change because aggregation of gold nanoparticles were readily detected with high specificity as previously observed in lipoic-egl-T$_9$-LysNH$_2$ (**P9**) (**Figure 3.35**).
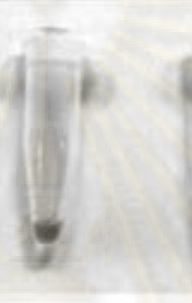
Figure 3.35 Aggregation behaviors of gold nanoparticles in the presence of 20 pmol BzS(CH$_2$)$_2$CO-egl-T$_4$XT$_4$-LysNH$_2$ and 20 pmol of DNA targets dA$_4$YA$_4$ (X,Y=C,G,T,A)

Unfortunately, the results were not quite reproducible. It was thought that this could be the result of different charge state of Lys-PNA (pKa side chain = 9.74) at different pH. If one could make this positive charge permanent, it should be possible to improve the sensitivity and reproducibility of the test. The C-terminal Lys on the PNA was therefore modified with a permanent charge group in the next experiments.

c) Colorimetric detection of hybridization of permanent charge-labelled thiolated PNA with DNA

In these experiments, the four PNA with sequences BzS(CH$_2$)$_2$CO-egl-T$_4$XT$_4$-Lys(Phos)NH$_2$ (X= T,A,C,G) (P17-P20) were synthesized as described in section 3.5. Basically, a phosphonium charge tag was incorporated at the amino group of Lys at 3'-termini of the PNA via the reactive monomer shown in **Figure 3.36**. Two other negative controls PNA – one without the BzS group Bz-egl-T$_9$-Lys(Phos)NH$_2$ (P22) and the other without the phosphonium group BzS(CH$_2$)$_2$CO-egl-T$_9$-Lys(Ac)NH$_2$ (P21) – were also prepared for comparison. The use of phosphonium salt was hoped to produce a permanent positive charge irrespective of operating pH which should increase reproducibility and perhaps also sensitivity of the present DNA sequence detection method based on aggregation of gold nanoparticles.
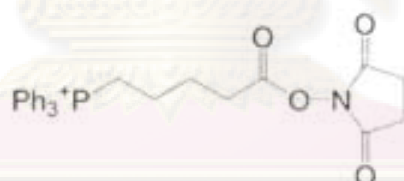

Figure 3.36. Structure of phosphonium salt.

In the first set of experiments, BzS(CH$_2$)$_2$CO-egl-T$_9$-Lys(Phos)NH$_2$ (P20) was compared with the negative control BzS(CH$_2$)$_2$CO-egl-T$_9$-Lys(Ac)NH$_2$ (P21) in order to demonstrate the role of the positive charge. Without adding the DNA, gold nanoparticles were aggregated with (P20) but not (P21) under identical reaction conditions (concentration PNA:gold nanoparticles = 810:1) as shown in the **Figure 3.37**.

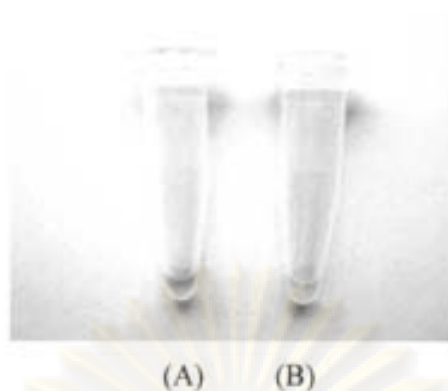**Figure 3.37** Aggregation behaviors of $BzS(CH_2)_2CO$-egl-T_9-Lys(Ac)NH_2 (**P21**) (A) and $BzS(CH_2)_2CO$-egl-T_9-Lys(Phos)NH_2 (**P20**) (B) to gold nanoparticles.

The aggregation behaviors of gold nanoparticels in the presence of the three PNA sequences: $BzS(CH_2)_2CO$-egl-T_9-Lys(Phos)NH_2 (**P20**), $BzS(CH_2)_2CO$-egl-T_9-Lys(Ac)NH_2 (**P21**), and Bz-egl-T_9-Lys(Phos)NH_2 (**P22**) were also investigated by TEM (**Figure 3.38**). The data suggested that both the thiol group and the phosphonium salt in the PNA sequence are required to induce gold nanoparticles aggregation. In the absence of either of these, no aggregation of the gold nanoparticles was observed.
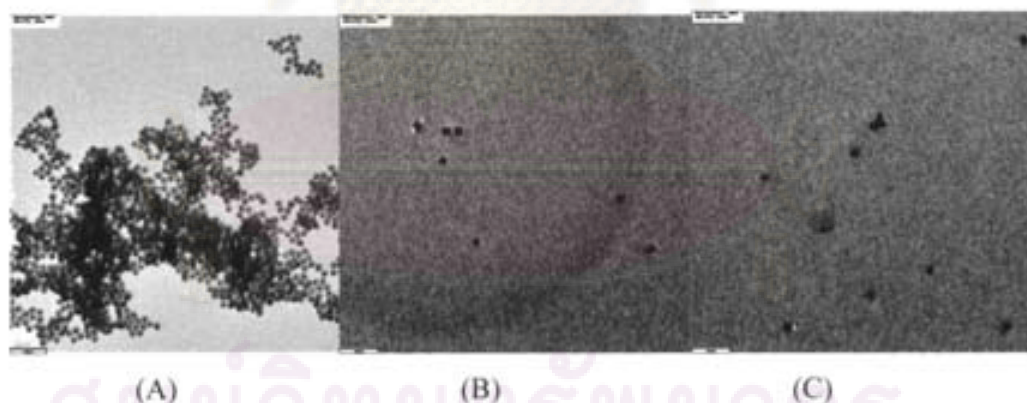

Figure 3.38 TEM images of gold nanoparticles after immobilization with (A) $BzS(CH_2)_2CO$-egl-T_9-Lys(Phos)NH_2 (**P20**), (B) $BzS(CH_2)_2CO$-egl-T_9-Lys(Ac)NH_2 (**P21**), and (C) Bz-egl-T_9-Lys(Phos)NH_2 (**P22**).

It is interesting to observe that the benzoylthiol PNA could be successfully immobilized onto the nanoparticles without the need for prior removal of the Bz group by treatment with ammonia. This is clearly and advantageous because BzS PNA are very stable compared to the HS PNA. However, it was unclear whether the benzoyl protected thiol group was immobilized onto the nanoparticles with simultaneous removal of the benzoyl group or as such, i.e. with the benzoyl group intact. To understand the nature of the immobilization, a mass spectrometric analysis was performed on the aggregated gold nanoparticles (**Figure3.39**). After digestion of the aggregated particles with KCN, the MALDI-TOF mass spectrum was taken. A mass peak at $m/z = 3822$ was observed which corresponded to the original PNA (**P19**) This result suggested that the S-Benzoyl PNA was immobilized on the gold nanoparticles with the benzoyl group in place. The same experiment with the non-thiolated Benzoyl PNA (**P22**) showed that this non-thiolated PNA could not be immobilized on the gold nanoparticles (**Figure3.39**).
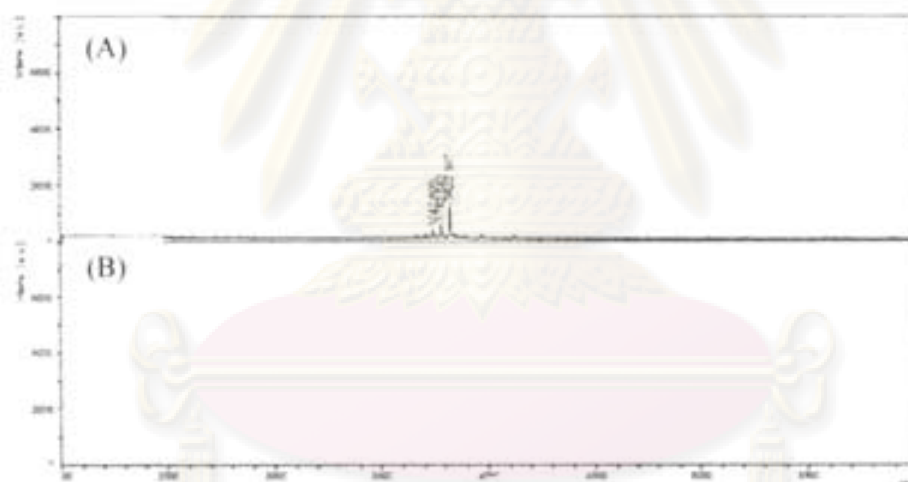

Figure 3.39 Mass spectrometric analysis of (A) BzS(CH$_2$)$_2$CO-egl-T$_4$AT$_4$-Lys(Phos)NH$_2$ (**P19**) and (B) Bz-egl-T$_9$-Lys(Phos)NH$_2$ (**P22**) after treatment with KCN.

Melting temperature of an equimolar quantities of PNA with DNA mixture of the PNA BzS(CH$_2$)$_2$CO-egl-T$_4$AT$_4$-Lys(Phos)NH$_2$ (**P19**) and its complementary DNA target (dA$_8$T) in the presence of gold nanoparticles (concentration PNA:gold nanoparticles = 810:1) was measured at 520 nm. A sigmoidal melting curve was

observed which correspond to a change from non-aggregated to aggregate state of the nanoparticles in a cooperative manner. The apparent T_m was 46 $^\circ$C which is somewhat lower than the T_m value of 73 $^\circ$C obtained from the free PNA·DNA with the same sequences in solution (**Figure 3.40**). The difference is not yet fully understood but may be due to aggregation induced PNA·DNA hybridization. The T_m value of thiolated-PNA·DNA differ from PNA·DNA although PNA and DNA have a same base sequences.
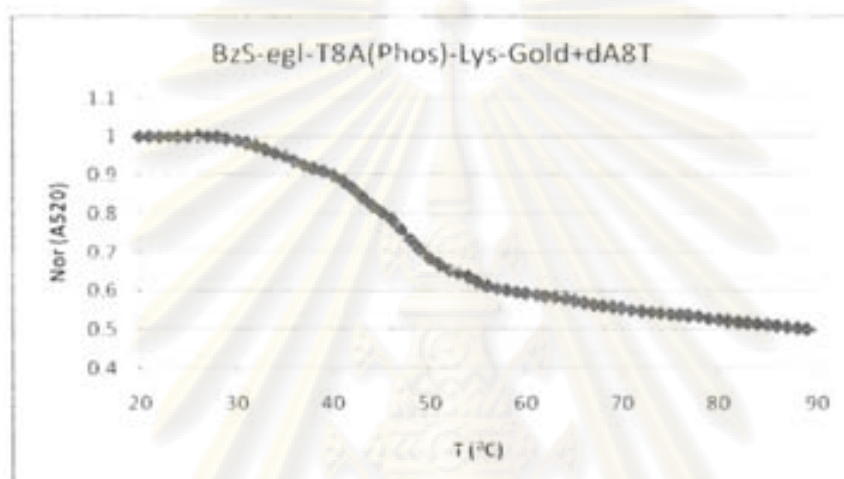

Figure 3.40 T_m of hybridization between BzS(CH$_2$)$_2$CO-egl-T$_4$AT$_4$-Lys(Phos)NH$_2$ (**P19**) and complementary DNA (dA$_8$T) in gold nanoparticles at 520 nm.

The same experiments as described for lipoic acid-T$_9$-Lys (**P8**) above were repeated using the new PNA BzS(CH$_2$)$_2$CO-egl-T$_9$-Lys(Phos)NH$_2$ (**P20**) under the same conditions. The amount of BzS(CH$_2$)$_2$CO-egl-T$_9$-Lys(Phos)NH$_2$ (**P20**) (5, 10, 20 and 50 pmol) were varied in 10 mM phosphate buffer pH 7, while the gold nanoparticles concentration was kept constant at 0.7 nM in a total volume 35 μL as shown in the **Figure 3.41**. It appears that the sensitivity was about the same as the lysine systems. i.e. at least 20 pmol of PNA (concentration PNA:gold nanoparticles = 810:1) was required to induce aggregation of the nanoparticles.

(A) (B) (C) (D)

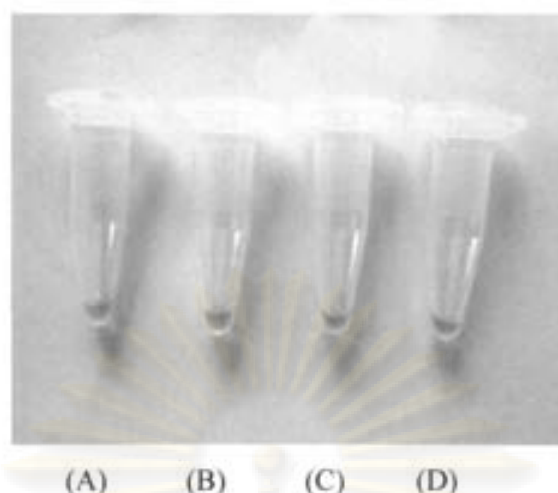**Figure 3.41** Aggregation behaviors of gold nanoparticles in the presence of BzS(CH$_2$)$_2$CO-egl-T$_9$-Lys(Phos)NH$_2$ (**P20**) at various quantities: (A) 50 pmol, (B) 20 pmol, (C) 10 pmol, and (D) 5 pmol.

Next, to determine the minimum amount of BzS(CH$_2$)$_2$CO-egl-T$_9$-Lys(Phos)NH$_2$ (**P20**) required to cause aggregation of the gold nanoparticles in the presence of DNA, two different BzS(CH$_2$)$_2$CO-egl-T$_9$-Lys(Phos)NH$_2$ (**P20**) concentrations were employed. When 10 pmol of BzS(CH$_2$)$_2$CO-egl-T$_9$-Lys(Phos)NH$_2$ (**P20**) (concentration PNA:gold nanoparticles = 405:1) was hybridized with 20 pmol DNA, only slight color changes were observed for both full match (dA$_9$) and single mismatch (dA$_8$T) (**Figure 3.42**).
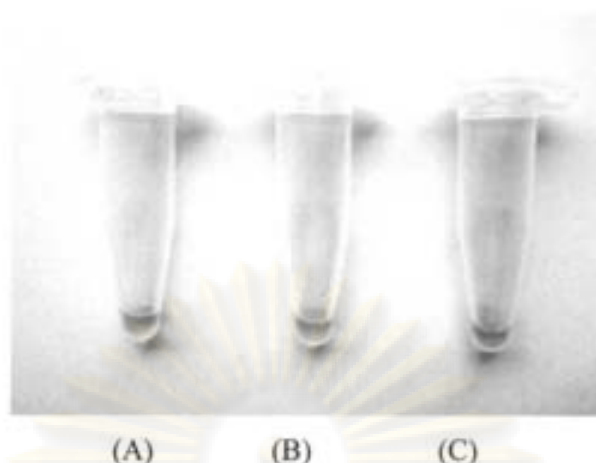
Figure 3.42 Aggregation behaviors of gold nanoparticels in the presence of 10 pmol BzS(CH$_2$)$_2$CO-egl-T$_9$-Lys(Phos)NH$_2$ (**P20**) and (A) no DNA (B) single base mismatch DNA and (C) complementary DNA.

At 20 pmol (concentration PNA:gold nanoparticles = 810:1), however, the color change from red to purple was clearly observed within a few minutes with 20 pmol single mismatched DNA (dA$_8$T). Unfortunately, although no color change was observed with 20 pmol complementary DNA (dA$_9$), the color change from red to purple was observed about 15 min later (**Figure 3.43**).
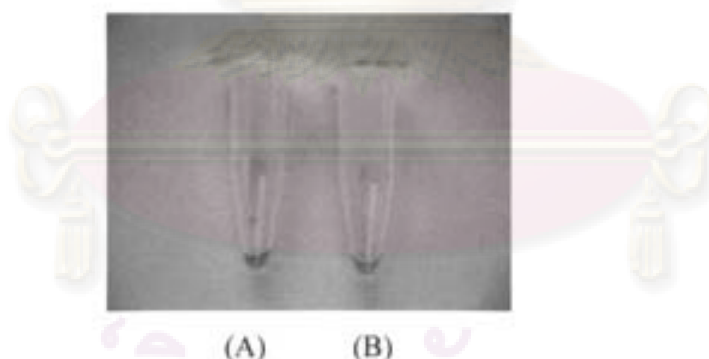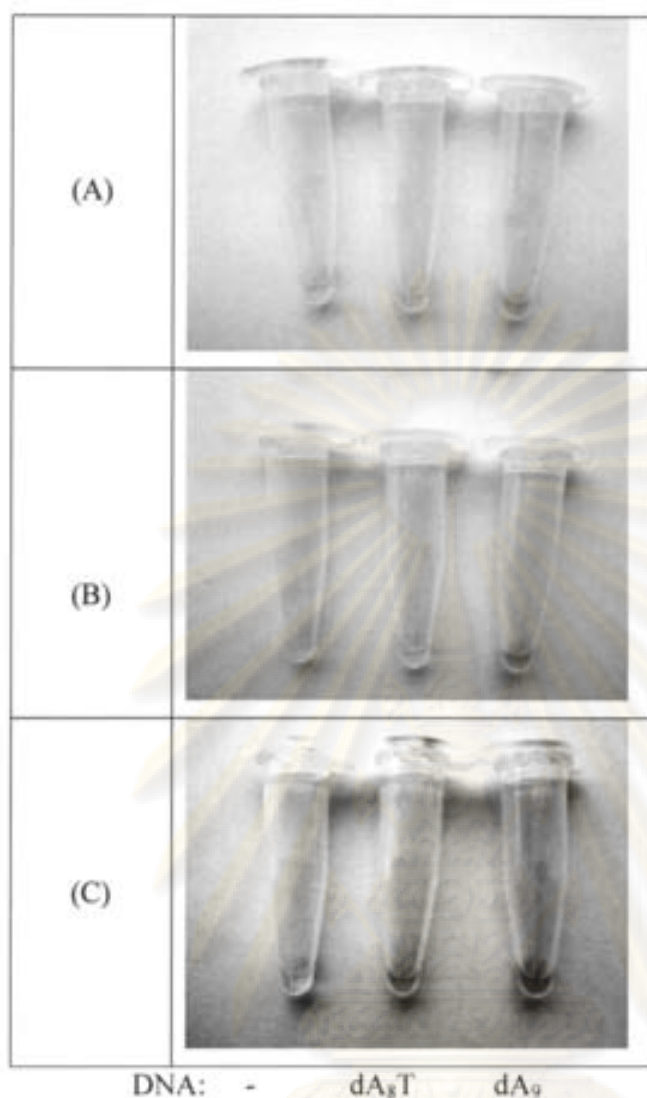

Figure 3.43 Aggregation behaviors of gold nanoparticles in the presence of 20 pmol BzS(CH$_2$)$_2$CO-egl-T$_9$-Lys(Phos)NH$_2$ (**P20**) and (A) complementary DNA and (B) single base mismatch DNA.

Increasing the amount of the DNA targets to 40 pmol resulted in a more stable color difference between complementary and single mismatched DNA targets over an

extended period. Therefore the suitable conditions for detection of PNA·DNA hybridization were 20 pmol PNA (concentration PNA:gold nanoparticles = 810:1) and 40 pmol DNA for detection of PNA·DNA hybridization.

iv) Effect of sodium phosphate buffer

To compare the aggregation behaviors due to hybridization under different phosphate buffer (pH 7.0), the hybridization between the BzS(CH₂)₂CO-egl-T₉-Lys(Phos)NH₂ (**P20**) and its complementary DNA (dA₉) and single base mismatch DNA (dA₈T) were studied at different phosphate buffer concentrations (100 mM, 10 mM and 1 mM).

The results showed that it was possible to discriminate between full match and single base mismatch at all buffer concentrations. The previously employed 10 mM phosphate buffer (pH 7) was therefore chosen for further experiments.
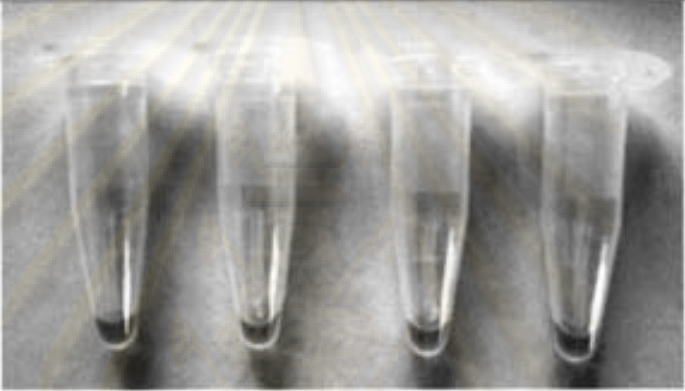
DNA: - dA_8T dA_9
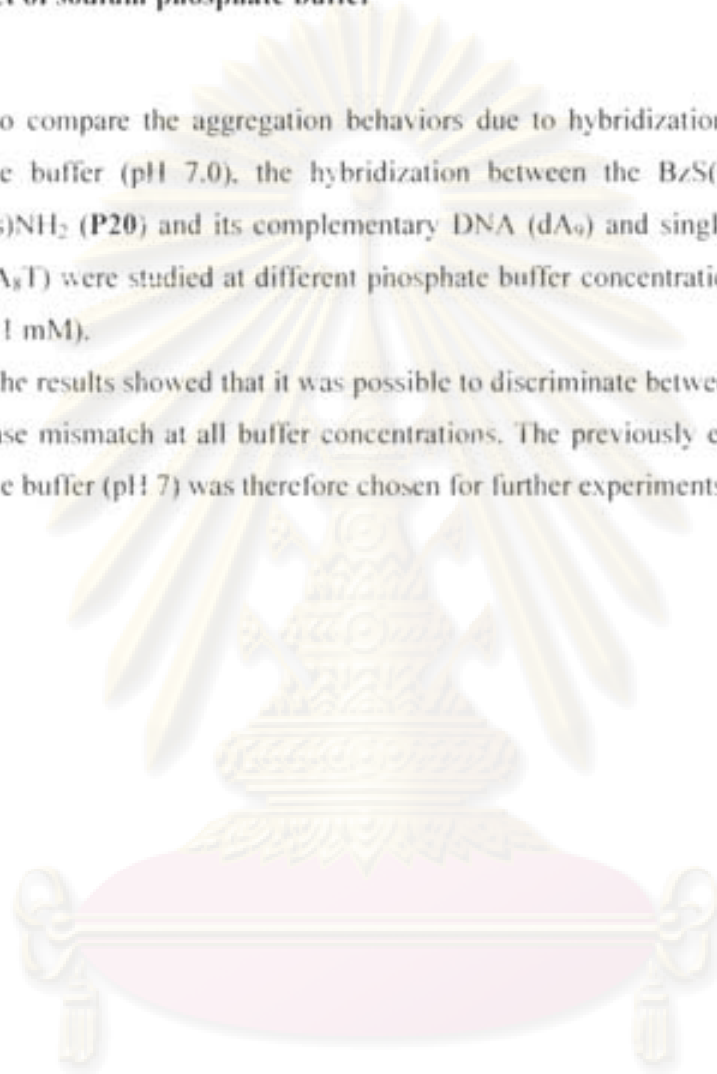
Figure 3.44 Aggregation behaviors of gold nanoparticles in the presence of 20 pmol $BzS(CH_2)_2CO$-egl-T_9-Lys(Phos)NH_2 (**P20**) and (left) no DNA (middle) complementary DNA and (right) single base mismatch DNA at various sodium phosphate buffer: (A) 100 mM, (B) 10 mM, and (C) 1 mM.

v) Effect of pH

To investigate the effect of pH, $BzS(CH_2)_2CO$-egl-T_9-Lys(Phos)NH_2 (**P20**) were hybridized with full match and single base mismatch DNA under the previously optimal hybridization conditions (10 mM phosphate buffer, 20 pmol of PNA and 40 pmol of DNA). The pH (4.5, 7 and 8) of 10 mM sodium phosphate buffer was varied

from 4.5 to 8. The best detection of hybridization efficiency by gold nanoparticles were achieved at 10 mM phosphate buffer (pH 7) because 10 mM phosphate buffer (pH 8) was unsuitable for detection PNA·DNA hybridization due to full match PNA·DNA duplex of unclearly color (**Figure 3.45**).
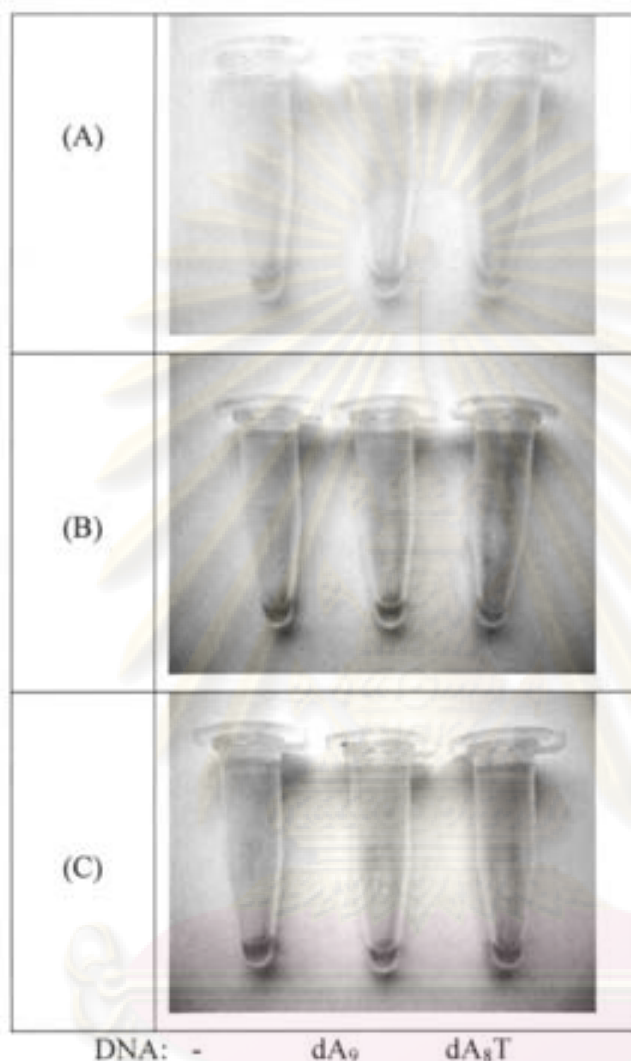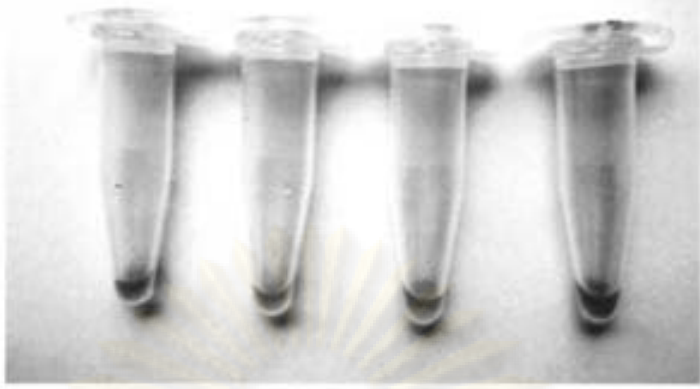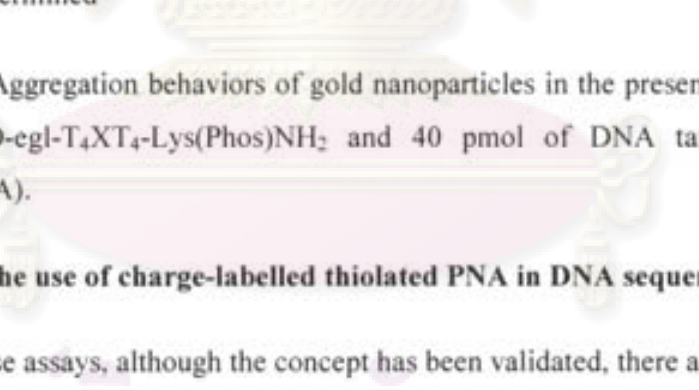

Figure 3.45 Aggregation behaviors of gold nanoparticles in the presence of 20 pmol BzS(CH$_2$)$_2$CO-egl-T$_9$-Lys(Phos)NH$_2$ (**P20**) and (left) no DNA (middle) complementary DNA and (right) single base mismatch DNA at various pH of 10 mM sodium phosphate buffer (A) pH 4.5, (B) pH 7.0, and (C) pH 8.0)

To investigate the specificity of the test, the hybridization experiments were repeated using BzS(CH$_2$)$_2$CO-egl-T$_4$XT$_4$-LysNH$_2$ (20 pmol) and DNA A$_4$YT$_4$ (X and Y = C,G,A,T) (40 pmol) (concentration PNA:gold nanoparticles = 810:1). The color

change due to aggregation of gold nanoparticles again suggested the high specificity of the assay (**Figure 3.46**). In all complementary cases, no aggregation of the gold nanoparticles was observed. However, in some single mismatched cases, the aggregation was only partial as observed from incomplete color change from red to purple. This is attributed to the relatively high stability of the PNA·DNA hybrids. This is confirmed by comparison with the reference T_m values obtained in solution experiments.

PNA	DNA			
	A_4CA_4	A_4GA_4	A_4TA_4	A_9
(P17) (X=G)				
T_m	57	N/D	N/D	34
(P18) (X=C)				
T_m	N/D	56	N/D	N/D

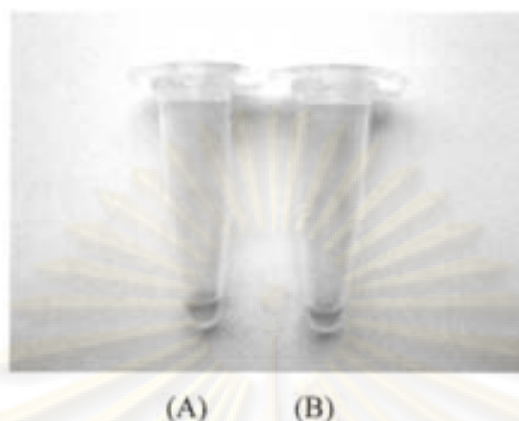|					
(P19) **(X=A)**					
	T_m	39	N/D	73	43
(P20) **(X=T)**					
	T_m	51	42	45	80

N/D = not determined

Figure 3.46 Aggregation behaviors of gold nanoparticles in the presence of 20 pmol $BzS(CH_2)_2CO$-egl-T_4XT_4-Lys(Phos)NH_2 and 40 pmol of DNA targets dA_4YA_4 (X,Y=C,G,T,A).

d) Towards the use of charge-labelled thiolated PNA in DNA sequence analysis

In these assays, although the concept has been validated, there are a number of practical issues to be considered. In real samples, the DNA target obtained from PCR is more likely to be much longer than the PNA probe. It is interesting to see whether the high specificity could still be obtained with these longer DNAs. To test this, two synthetic DNA carrying a complementary (CGC GGC GTA CAA AAA AAA AGC ATG CCC TGG) and non-complementary (CCA GGG CAT GCT TTT TTT TTG TAC GCC GCG) sequences in the middle of the strands were hybridized with the PNA $BzS(CH_2)_2CO$-egl-T_9-Lys(Phos)NH_2 (**P20**) under the optimized conditions

obtained above. The results clearly showed that the same specificity was still observed with longer DNA targets (**Figure 3.47**).

(A)   (B)

Figure 3.47 Aggregation behaviors of gold nanoparticles in the presence of 20 pmol BzS(CH$_2$)$_2$CO-egl-T$_9$-Lys(Phos)NH$_2$ (**P20**) and 40 pmol (A) complementary DNA and (B) single base mismatch DNA.
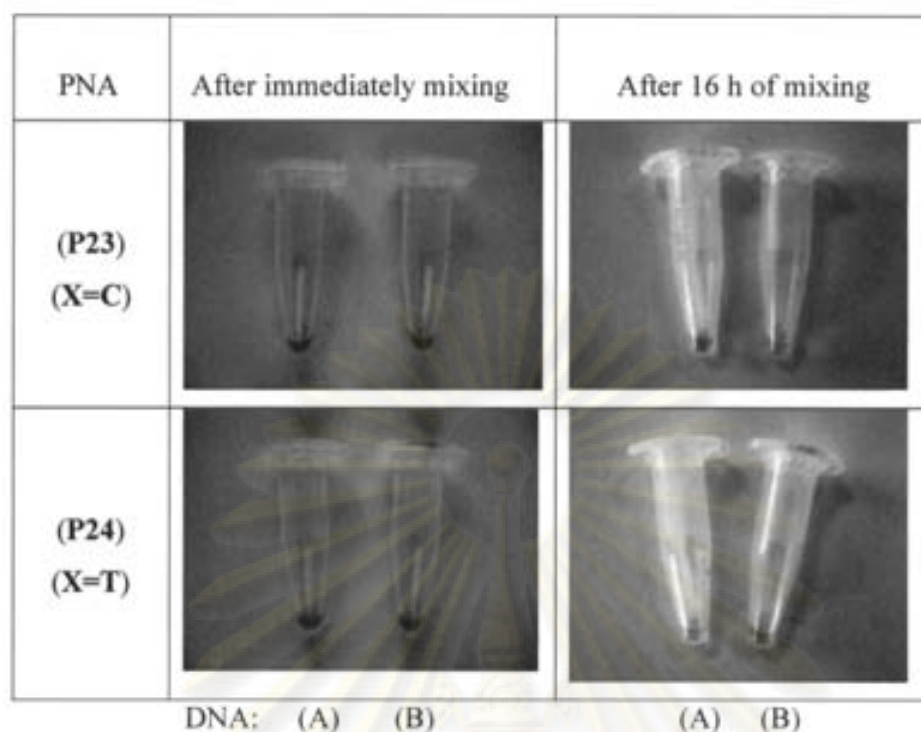
Aggregation behaviors of gold nanoparticles in the presence of 10 pmol BzS(CH$_2$)$_2$CO-egl-TTCCCCXTCCCAA-Lys(Phos)NH$_2$ (X=C,T) (**P23,P24**) and (A) complementary DNA and (B) single base mismatch DNA.

To apply this technique to biological-relevant target sequences, a pair of 13base sequence corresponding to a single nucleotide polymorphism (SNP) site -1082[G/A] in a human gene of IL10 promoter. The site is shown to be associated with a genetic disordered called SLE (Lupus Erythematosus)[65]. To test this, two thiolated PNA BzS(CH$_2$)$_2$CO-egl-TTCCCCCTCCCAA-Lys(Phos)NH$_2$ (**P23**) and BzS(CH$_2$)$_2$CO-egl-TTCCCCTTCCCAA-Lys(Phos)NH$_2$ (**P24**) were synthesized. The aggregation behaviours of gold nanoparticles in the presence of the PNA in the presence and absence of complemantary DNA targets were studied under the optimized conditions obtained above. Clear results were obtained even when lower quantities of PNA were used (10 pmol). In both cases, the presence of complementary and single base mismatch DNA targets could be clearly distinguished (**Figure 3.48**).
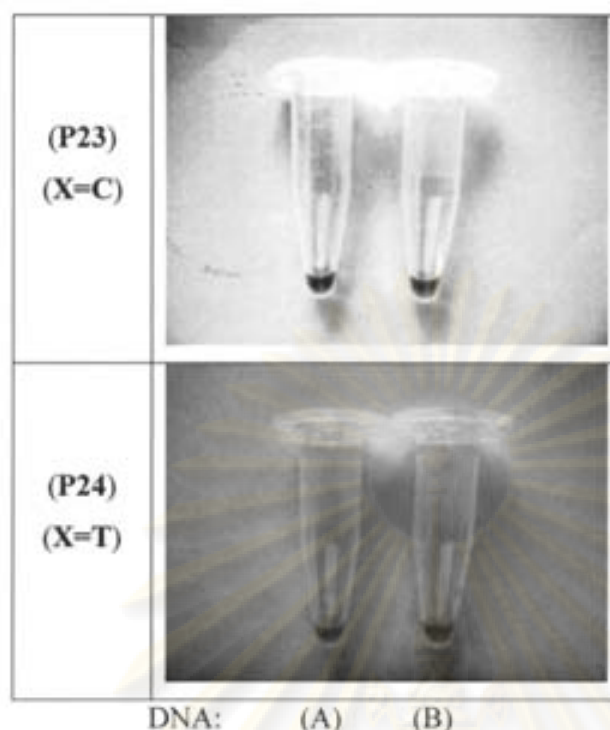
Figure 3.48 Aggregation behaviors of gold nanoparticles in the presence of 10 pmol BzS(CH$_2$)$_2$CO-egl-TTCCCCXTCCCAA-Lys(Phos)NH$_2$ (X=C,T) (**P23,P24**) and (A) complementary DNA and (B) single base mismatch DNA.

Although a clear color difference was observed, the difference was not stable. Gradual aggregation of the complementary hybrid was observed upon prolonged storage. To overcome this problem, a longer DNA targets were used. This is hoped to stabilize the nanoparticles further especially when the sequence of the target was complementary to the probe. When the DNA targets length was increased to 30 bases, the color change was still obvious as shown earlier. Furthermore, the color was stable for an extended period of at least 16 h at room temperature (**Figure 3.49**). In real samples, the target DNA is expected to be much longer than the PNA probe (see above) therefore the stability of the color should be even greater than this.

PNA	After immediately mixing	After 16 h of mixing
(P23) **(X=C)**		
(P24) **(X=T)**		
	DNA: (A) (B)	(A) (B)

Figure 3.49 Aggregation behaviors of gold nanoparticles in the presence of 10 pmol BzS(CH$_2$)$_2$CO-egl-TTCCCCXTCCCAA-Lys(Phos)NH$_2$ (X=C,T) (**P23,P24**) and (A) (ACGCATCC<u>TTGGGAGGGGGAA</u>TCCATGCTA) DNA and (B) (ACGCATCC<u>TTGGGAAGGGGAA</u>TCCATGCTA) DNA.

The data strongly suggested that the hybridization between PNA·DNA hybridization were highly sequence-specific by observing colorimetric of gold nanoparticles aggregation. Although the detection of PNA·DNA hybridization can be accomplished. In the case of real samples, the sensitivity for detection should be higher. This may be done increasing the particle size of gold nanoparticles.

CHAPTER IV

CONCLUSION

In this research, thiol-modified polyamide nucleic acid (PNA) nonamers $HS(CH_2)_2CO$-egl-T_9-LysNH$_2$ (**P1**), $HS(CH_2)_2CO$-egl-T_9-SerNH$_2$ (**P2**), and $HS(CH_2)_2CO$-egl-T_9-AspNH$_2$ (**P3**) were synthesized by solid phase peptide synthesis and was directly immobilized on 20 nm gold nanoparticles by self assembly monolayer (SAM) formation via S atom. As characterized by UV/ViS-spectroscopy, Transmission Electron Microscopy, and Photon Correlation Spectroscopy, the positively charged $HS(CH_2)_2CO$-egl-T_9-LysNH$_2$ (**P1**) caused a greater extent of gold nanoparticles aggregation than the neutral $HS(CH_2)_2CO$-egl-T_9-SerNH$_2$ (**P2**) and the negatively charged $HS(CH_2)_2CO$-egl-T_9-AspNH$_2$ (**P3**). Attempts to detect the hybridization between the nanoparticles immobilized PNA and complementary target DNA in solution by UV melting studies and fluorescence spectroscopy failed to show any evidences of hybridization.

Nevertheless, based upon the aggregation behaviour of gold nanoparticles caused by positively charged thiol-modified PNA, a novel colorimetric detection of hybridization event between the PNA and DNA had been successfully developed. When thiol-modified PNA carrying positive charge was hybridized with complementary DNA followed by addition of gold nanoparticles, no visible color changes was observed. On the other hand, when the same PNA was hybridized with non-complementary DNA, a distinct color changes from red to purple color due to the aggregation of the gold nanoparticles was evident. The presence of the negatively charged complementary DNA prevented aggregation of the nanoparticles induced by the positively charged thiol-modified PNA. The effect is more pronounced with longer DNA targets. The techniques have been sucessfully used to discriminate between full match and single base mismatch DNA targets with length in a range of 9-13 bases.

From the results, it can be demonstrated that the use of PNA sequences modified with a permanent charge tag (phosphonium salt) and a benzoyl protected thiol are critical to the success of the assay based on aggregation of the gold nanoparticles. The optimal PNA·DNA hybridization condition obtained was PNA: 20

pmol and DNA:40 pmol with 10 mM sodium phosphate buffer (pH 7) in total volume of 35 µL (concentration PNA:gold nanoparticles = 810:1).

The specificity of the technique was tested with hybridization of four model PNA $BzS(CH_2)_2CO$-egl-T_4XT_4-LysNH$_2$ or $BzS(CH_2)_2CO$-egl-T_4XT_4-Lys(Phos)NH$_2$ (X=A,T,C,G) and four DNA targets (dA_4YA_4, Y= A,T,C,G) in the presence of gold nanoparticles. The results showed that the only perfect match PNA-DNA sequences displayed no visible color change of the gold nanoparticles. In all other cases, the color of the nanoparticles changed from red to purple or blue as a result of aggregation caused by the positively charged PNA. The same results were obtained with more complex mixed base 13mer PNA sequences $BzS(CH_2)_2CO$-egl-TTCCCCCTCCCAA-Lys(Phos)NH$_2$ (P23) and $BzS(CH_2)_2CO$-egl-TTCCCCTTCCCAA-Lys(Phos)NH$_2$ (P24) at 10 pmol.

It can be concluded that although the PNA immobilized on gold nanoparticles failed to show detectable hybridization with DNA, a combination of positively-charged, thiol modified Vilaivan's PNA (ACPC system) and gold nanoparticles can be used to differentiate between complementary and single-mismatch target DNA by a new concept of positive charge induced aggregation of gold nanoparticles discovered in this work. This system should be an important prototype for development of a DNA biosensor which does not require labeling of the DNA in the future.
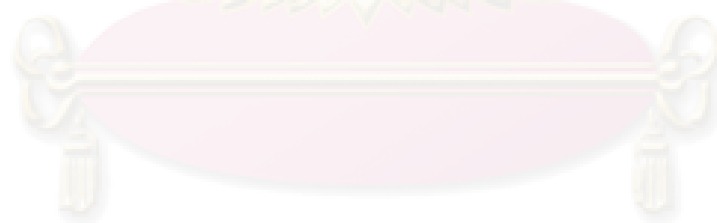
REFERENCES

1. Nielsen, P. E.; Egholm, M.; Berg, R. H.; Buchardt, O. Sequence-selective   recognition of DNA by strand displacement with a thymine-substituted polyamide. *Science.* **1991**, *254*, 1497.

2. Hyrup, B., Egholm, M., Nielsen, P. E., Wittung, P., Norden, B., and Buchardt, O. Structure-activity studies of the binding of modified peptide nucleic acid   (PNAs) to DNA. J. Am. Chem. Soc. 116 (1994) : 7964.

3. Hamilton, S. E., Simmons, C. G., Kathiriya, I. S., and Corey, D. R. Cellular   delivery of peptide nucleic acids and inhibition of human telomerase. Chem. Biol. 6 (1999) : 343.

4. Nielsen, P. E. Peptide nucleic acid: a versatile tool in genetic diagnostics and molecular biology. Curr. Opin. Biol. 12 (2001) : 16.

5. Suparpprom, C., Srisuwannaket, C., Sangvanich, P., and Vilaivan, T. Synthesis and oligodeoxynucleotide binding properties of pyrrolidinyl peptide nucleic acids bearing prolyl-2-aminocyclopentanecarboxylic acid (ACPC) backbones. Tetrahedron Lett. 46 (2005) : 2833.

6. West, J. L.; Halas, N. J. Engineering nanomaterials for biophotonics applications: improving sensing, imaging, and therapeutics. *Annu. Rev. Biomed. Eng.* **2003**, *5*, 285.

7. Kreibig, U.; Vollmer, M. *Optical Properties of Metal Clusters*; Springer: Berlin, 1995.

8. Kerker, M. The Scattering of light and Other Electromagnetic Radiation; Academic Press: New York, 1969.

9. Bohren, C. F.; Huffman, D. R. *Absorption and Scattering of light by Small Particle*; *Wiley*: New York, 1983.

10. Creighton, J. A.; Eadon, D. G. Ultraviolet-visible absorption spectra of the colloidal metallic elements. *J. Chem. Soc., Faraday Trans.* **1991**, *87*, 3881.

11. Mulvaney, P. Surface plasmon spectroscopy of nanosized metal particles. *Langmuir* **1996**, *12*, 788.

12. www.nbi.dk/~pmhansen/gold_color_size.jpg

13. Grabar, K. C.; Freeman, R. G.; Hommer, M. B.; Natan, M. J. Preparation and characterization of Au colloid monolayers. *Anal. Chem.* **1995**, *67*, 735.

14. Mirkin, C. A. Invited contribution from recipient of ACS award in pure   chemistry. *Inorg. Chem.* **2000**, *39*, 2258.

15. Love, J. C.; Estroff, L. A.; Kriebel, J. K.; Nuzzo, R. G.; Whitesides, G. M. Self-assembled monolayers of thiolates on metals as a form of nanotechnology. *Chem. Rev.* **2005**, *105*, 1103.

16. Nuzzo, R. G.; Allara, D. L., Adsorption of bifunctional organic disulfides on gold surfaces. *J. Am. Chem. Soc.* **1983**, *105*, 4481.

17. Giersig, M.; Mulvaney, P. Preparation of ordered colloid monolayers by electrophoretic deposition. *Langmiur.* **1993**, *9*, 3408.

18. Weisbecker, C. S.; Merritt, M. V.; Whitesides, G. M. Molecular self-assembly of aliphatic thiols on gold colloids. *Langmuir,* **1996**, *12*, 3763.

19. Rongchao Jin, Z. L.; Mirkin, C. A.; Letsinger, R. L. Mulitple thiol-anchor capped DNA-gold nanoparticle conjugates. *Nucleic Acids Research,* **2002**, 30.1558.

20. Lavan, D. A.; Lynn, D. M.; Langer, R. Moving smaller in drug discovery and delivery. *Nat. Rev. Drug Discovery.* **2002**, *1*, 77.

21. Chan, W. C. W.; Maxwell, D. J.; Gao, X.; Bailey, R. E. Han, M. Y.; Nie, S. Water-soluble quantum dots for multiphoton fluorescence imaging in vivo. *Curr. Opin. Biotechnol.* **2002**, *13*, 40.

22. Niemeyer, C. M. Nanoparticles, Proteins, and Nucleic acids: Biotechnology meets materials science. *Angew. Chem., Int. Ed.* **2001**, *40*, 4128.

23. Whaley, S. R.; English, D. S.; Hu, E. L.; Barbara, P. F.; Belcher, A. M. A. Selection of peptides with semiconductor binding specificity for directed nanocrystal assembly. *Nature.* **2000**, *405*, 665.

24. Bruchez, M., Jr.; Moronne, M.; Gin, P.; Weiss, S.; Alivisatos, A. P. semiconductor nanocrystals as fluorescent biological labels. *Science.* **1998**, *281*, 2013.

25. Chan, W. C. W.; Nie, S. M. Quantum dot bioconjugates for ultrasensitive nonisotopic detection. *Science.* **1998**, *281*, 2016.

26. Mattoussi, H.; Mauro, J. M.; Goldman, E. R.; Anderson, G. P.; Sundar, V. C.; Mikulec, F. V.; Bawendi, M. G. Self-assembly of CdSe-ZnS quantum dot bioconjugates using an engineered recombinant protein. *J. Am. Chem. Soc.* **2000**, *122*, 12142.

27. Mitchell, G. P.; Mirkin, C. A.; Letsinger, R. L. Hydroxylated quantum dots as luminescent probes for in situ hybridization. *J. Am. Chem. Soc.* **2001**, *123*, 4103.

28. Reynolds, R. A., Mirkin, C. A.; Letsinger, R. L. Homogeneous, nanoparticle based quantitative colorimetric detection of oligonucleotides. *J. Am. Chem. Soc.* **2000**,

122, 3795.

29. Mirkin, C. A.; Letsinger, R. L.; Mucic, R. C.; Storhoff, J. J. A DNA-based method for rationally assembling nanoparticles into macroscopic material. *Nature.* **996**, *382*, 607.

30. Storhoff, J. J.; Mirkin, C. A. Programmed material synthesis with DNA. *Chem. Rev.* **1999**, *99*, 1849.

31. Alivisatos, A. P.; Johnsson, K. P.; Peng, X.; Wilson, T. E.; Loweth, C. J.; Bruchez, M. P., Jr.; Schultz, P. G. Organization of 'nanocrystal molecules' using DNA. *Nature.* **1996**, *382*, 609.

32. Dubertret, B.; Calame, M.; Libchaber, A. J. Single-mismatch detection using gold-quenched fluorescent oligonucleotide. *Nature Biotechnol.* **2001**, *19*, 365.

33. Curtis, A.; Wilkinson, C. Nantotechniques and approaches in biotechnology. *Trends Biotechnol.* **2001**, *19*, 97.

34. Gref, R.; Minamitake, Y.; Peracchia, M. T.; Trubetskoy, V.; Torchilin, V.; Langer, R. Nanometerials: A membrane-based synthetic approach. *Science.* **1994**, *263*, 1600.

35. Chakrabarti, R.; Klibanov, A. M. Nanocrystals modified with peptide nucleic acids (PNAs) for selective self-assembly and DNA detection. *J. Am. Chem. Soc.* **2003**, *125*, 12531.

36. Cardenas, M.; Barauskas, J.; Schillen, K.; Brennan, J. L.; Brust, M.; Nylander, T. Thiol-specific and nonspecific interactions between DNA and gold nanoparticles. *Langmuir.* **2006**, 22, 3294.

37. Shorhoff, J. J.; Elghanian, R.; Mucic, R. C.; Mirkin, C. A.; Letsinger, R. L. One pot colorimetric differentiation of polynucleotides with single base imperfection using gold nanoparticles probes. *J. Am. Chem. Soc.* **1998**, *120*, 1959.

38. Elghanian, R.; Storhoff, J. J.; Mucic, R. C.; Letsinger, R. L.; Mirkin, C. A. Selective colorimetric detection of polynucleotides based on the distance dependent optical properties of gold nanoparticles. *Science.* **1997**, *277*, 1078.

39. Mirkin, C. A.; Letsinger, R. L.; Mucic, R. C.; Storhoff, J. J. *Nature.* **1996**, *121*, 8122.

40. Mucic, R. C.; Storhoff, J. J.; Mirkin, C. A.; Letsinger, R. L. DNA-directed synthesis of binary nanoparticles network materials. *J. Am. Chem. Soc.* **1998**, *120*, 12674.

41. Abigail, K. R.; Lytton, J.; Mirkin, C. A. A thermodynamic investigation into

the binding properties of DNA functionalized gold nanoparticles probes and molecular fluorophore probes. *J. Am. Chem. Soc.* **2005**, *127*, 12754.

42. Sato, K.; Hosokawa, K.; Maeda, M. Rapid aggregation of gold nanoparticles induced by non-cross-linking DNA hybridization. *J. Am. Chem. Soc.* **2003**, *125*, 8102.

43. Demers, L. M.; Mirkin, C. A.; Mucic, R. C.; Reynolds, R. A.; Letsinger, R. L.; Elghanian, R.; Viswanadham, G. A. fluorescence-based method for determining the surface coverage and hybridization efficiency of thiol-capped oligonucleotide bound to gold thin films and nanoparticles. *Anal. Chem.* **2000**, *72*, 5535.

44. Maxwell, D. J.; Taylor, J. R.; Nie, S. Self-assembled nanoparticles probes for recognition and detection of biomolecules. *J. Am. Chem. Soc.* **2002**, *124*, 9606.

45. Dubertret, B.; Calame, M.; Libchaber, A. J. Single-mismatch detection using gold-quenched fluorescent oligonucleotides. *Nature Biotechnology.* **2001**, *19*, 365.

46. Murphy, D.; Redmond, G.; Torre, B. G.; Eritja, R. Hybridization and melting behavior of peptide nucleic acid (PNA) oligonucleotide chimeras conjugated to gold nanoparticles. *Helvetica Chimica Acta.* **2004**, *87*, 2727.

47. Gourishankar, A.; Shukla, S; Hanesh, K. N.; Sastry, M. Isothermal titration calorimetry studies on the binding of DNA bases and PNA base monomers to gold nanoparticles. *J. Am. Chem. Soc.* **2004**, *126*, 13186.

48. Lowe, G., and Vilaivan, T. Amino acid bearing nucleobases for the synthesis of novel peptide nucleic acid. *J. Chem. Soc., Perkin Trans I.* **1997**, 539.

49. Lowe, G., and Vilaivan, T. Amino acid bearing nucleobases for the synthesis of novel peptide nucleic acid. *J. Chem. Soc., Perkin Trans I.* **1997**, 547.

50. Lowe, G., and Vilaivan, T. Solid phase synthesis of novel peptide nucleic acid. *J. Chem. Soc., Perkin Trans I.* **1997**, 555.

51. Miller, J. B. Preparation of Crystalline Diphenyldiazomethane. *J. Org. Chem.* **1959**, *24*, 560-561.

52. Ananthanawat, C., Synthesis and attachment of polyamide nucleic acid on gold surface. Master degree Thesis, Chulalongkorn University, **2005**.

53. Keating, C. D.; Musick, M. D.; Keefe, M. H.; Natan, M. J. Kinetics and

thermodynamics of Au colloid monolayer self-assembly: Undergraduate experiments in surface and nanomaterials chemistry. *J. Chem. Educ.* **1999**, *76*, 949.

54. Xiao, Y.; Ju, H.; Chen, H. Hydrogen peroxide sensor based on horseradish preoxidase-labeled Au colloids immobilized on gold electrode surface by cysteamine monolayer. *Analytical Chimica Acta.* **1999**, *391*, 73.

55. Srisuwannaket, C. Synthesis and DNA-binding properties of pyrrolidinyl peptide nucleic acids bearing (1S, 2S)-2-aminocyclopentane carboxylic acids spacer. (Doctoral dissertation, Graduate School, Chulalongkorn University, **2005**).

56. Ngamviriyavong, P., Synthesis of peptide nucleic acid containing aminoethyl linker. Master degree Thesis, Chulalongkorn University, **2004**.

57. Vilaivan, T., and Lowe, G. A novel pyrrolidinyl PNA showing high sequence specificity and preferential binding to DNA over RNA. *J. Am. Chem. Soc.*, **2004**, *124*, 9326.

58. LePlace, P. R.; Umezawa, N.; Lee, H.-S.; Gellman, S. H. An Efficient Route to Either Enantiomer of *trans*-2-Aminocyclopentanecarboxylic Acid. *J. Org. Chem.* **2001**, *66*, 5629.

59. Vilaivan, T. Synthesis and Properties of Novel Nucleopeptides. Doctoral Dissertation, University of Oxford, **1996**.

60. Liu, Z.; Sayre, L. M. Synthesis of *N,N*-dimethyl-2,4-dinitro-5-fluorobenzylamine and its reactions with amino acids and peptides. *Tetrahedron.* **2004**, *60*, 1601.

61. Marinakos, S.M.; Novak, J. P.; Brousseau, L. C.; House, A. B.; Edeki, E. M.; Feldhaus, J. C.; Feldheim, D. C. Gold particles as template for the synthesis of hollow polymer capsules. Control of capsule dimensions and guest encapsulation. *J. Am. Chem. Soc.* **1999**, *121*, 8518-8522.

62. Huret, J. L. DNA: molecular structure. Atlas genet cytogenet oncol haematol, **2006**.

63. Chadwick, S.; Englich, U.; Noll, B.; Ruhlandt-Senge, K. Syntheses and structure determinations of calcium thiolates. *Inorg. Chem.* **1998**, *37*, 4718.

64. Kocienski, P. J. Protecting groups 3 rd edition. **1994**.

65. Lupus research unit, department of microbiology, faculty of medicine, Chulalongkorn University, Bangkok, 10330, Thailand.

APPENDIX

Example of data from UV analysis in T_m experiments

Table A1 Data from UV analysis of $HS(CH_2)_2CO$-cgl-T_9-LysNH$_2$ (P1) & dA$_9$ at 20.0-

90.0 ^{o}C

Entry	Temperature (^{o}C)	Absorbance	Correct Temp.* (^{o}C)	Normalized Abs.
1	19.9	0.1373	18.9	1.0000
2	20.9	0.1370	19.9	0.9978
3	21.9	0.1376	20.8	1.0017
4	23.0	0.1376	21.9	1.0017
5	24.0	0.1378	22.8	1.0037
6	25.0	0.1379	23.8	1.0045
7	26.0	0.1381	24.8	1.0055
8	27.0	0.1386	25.8	1.0092
9	27.9	0.1389	26.7	1.0112
10	29.0	0.1392	27.7	1.0136
11	29.9	0.1394	28.6	1.0154
12	30.9	0.1398	29.6	1.0177
13	32.0	0.1403	30.7	1.0216
14	32.9	0.1406	31.6	1.0238
15	34.0	0.1410	32.6	1.0266
16	35.0	0.1414	33.6	1.0296
17	36.0	0.1417	34.6	1.0318
18	36.9	0.1420	35.5	1.0343
19	37.9	0.1423	36.5	1.0364
20	39.0	0.1427	37.5	1.0392
21	40.0	0.1432	38.5	1.0430
22	41.0	0.1435	39.5	1.0448
23	41.9	0.1439	40.4	1.0479
24	43.0	0.1442	41.4	1.0501
25	44.0	0.1446	42.4	1.0532
26	44.9	0.1450	43.3	1.0558
27	46.0	0.1453	44.4	1.0581
28	46.9	0.1458	45.3	1.0615

Entry	Temperature (°C)	Absorbance	Correct Temp.* (°C)	Normalized Abs.
29	48.0	0.1461	46.3	1.0641
30	48.9	0.1465	47.2	1.0666
31	50.0	0.1469	48.3	1.0695
32	51.0	0.1473	49.2	1.0724
33	52.0	0.1477	50.2	1.0756
34	52.9	0.1482	51.1	1.0794
35	54.0	0.1487	52.2	1.0825
36	55.0	0.1493	53.2	1.0869
37	56.0	0.1497	54.1	1.0901
38	56.9	0.1502	55.1	1.0940
39	57.9	0.1509	56.0	1.0986
40	59.0	0.1514	57.1	1.1025
41	60.0	0.1520	58.0	1.1071
42	61.0	0.1527	59.0	1.1122
43	62.0	0.1534	60.0	1.1169
44	63.0	0.1539	61.0	1.1210
45	63.9	0.1546	61.9	1.1257
46	65.0	0.1553	62.9	1.1310
47	66.0	0.1561	63.9	1.1364
48	67.0	0.1567	64.9	1.1409
49	68.0	0.1575	65.9	1.1468
50	69.0	0.1583	66.8	1.1524
51	69.9	0.1590	67.8	1.1576
52	71.0	0.1598	68.8	1.1636
53	71.9	0.1606	69.7	1.1697
54	73.0	0.1614	70.8	1.1754
55	74.0	0.1623	71.7	1.1818
56	75.0	0.1632	72.7	1.1886
57	75.9	0.1641	73.6	1.1948
58	77.0	0.1650	74.7	1.2013
59	78.0	0.1658	75.6	1.2077

Entry	Temperature (°C)	Absorbance	Correct Temp.* (°C)	Normalized Abs.
60	79.0	0.1668	76.6	1.2143
61	79.9	0.1676	77.6	1.2207
62	81.0	0.1686	78.6	1.2276
63	82.0	0.1694	79.6	1.2335
64	83.0	0.1702	80.5	1.2397
65	83.9	0.1710	81.5	1.2452
66	85.0	0.1718	82.5	1.2507
67	86.0	0.1725	83.5	1.2559
68	87.0	0.1730	84.4	1.2601
69	88.0	0.1736	85.4	1.2645
70	89.0	0.1742	86.4	1.2687
71	89.9	0.1746	87.3	1.2713

* The equation for determining the corrected temp was obtained by measuring the actual temp in the cuvette using a temperature probe and plotting against the set temperature (T_{block}) from 20-90 °C. A linear relationship was obtained with $T_{actual} = 0.978T_{block}-0.6068$ and $r^2 > 0.99$. (T_{actual} = Actual temperature as measured by the built-in temperature probe. T_{block} = Temperature of the heating block)

Correct temperature and normalized absorbance are defined as follows.

$$\text{Correct Temp.} = (0.978 \times T_{block}) - 0.6068$$
$$\text{Normalized Abs.} = Abs_{obs}/Abs_{init}$$

In entry 1: T_{obs} = 19.9 °C, Abs_{init} = 0.1373. Abs_{obs} = 0.1373;

$$\text{Correct Temp.} = (0.978 \times T_{obs}) - 0.6068$$
$$\text{Correct Temp.} = (0.978 \times 19.9) - 0.6068$$
$$= 18.9 \,°C$$
$$\text{Normalized Abs.} = Abs_{obs}/Abs_{init}$$
$$= 0.1373/0.1373$$
$$= 1.0000$$

In entry 25; T_{obs} = 44.0 °C, Abs_{init} = 0.1373. Abs_{obs} = 0.1446;

$$\text{Correct Temp.} = (0.978 \times T_{obs}) - 0.6068$$
$$\text{Correct Temp.} = (0.978 \times 44.0) - 0.6068$$
$$= 42.4 \,°C$$

$$\text{Normalized Abs.} = \text{Abs}_{obs}/\text{Abs}_{init}$$
$$= 0.1446/0.1373$$
$$= 1.0532$$
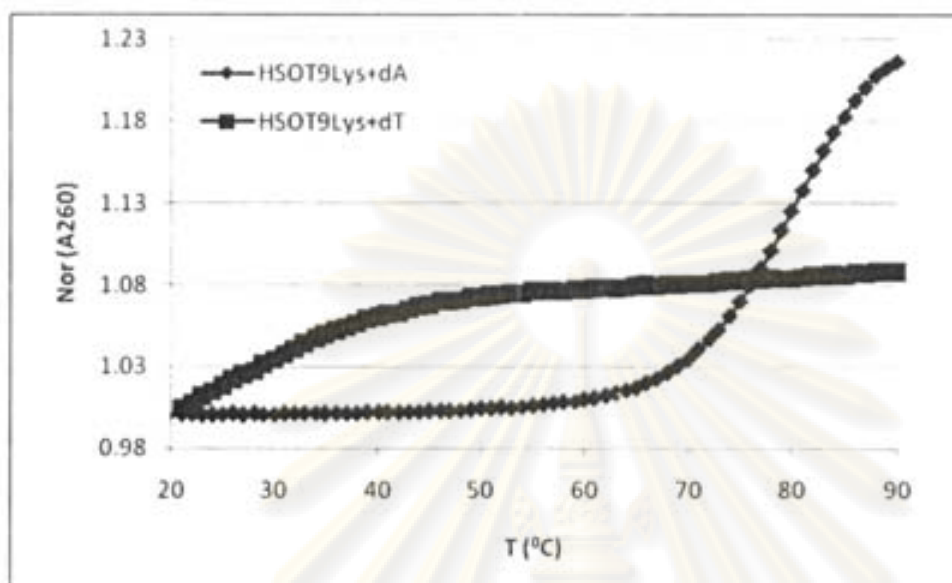
Figure A-1 T_m curves of HS(CH$_2$)$_2$CO-egl-T$_9$-LysNH$_2$ **(P1)** with d(AAAA$\underline{X}$AAAA) (X = T and A): Condition PNA:DNA = 1:1. [PNA] = 1 μM. 10 mM sodium phosphate buffer, pH 7.0, heating rate 1.0 °C/min.
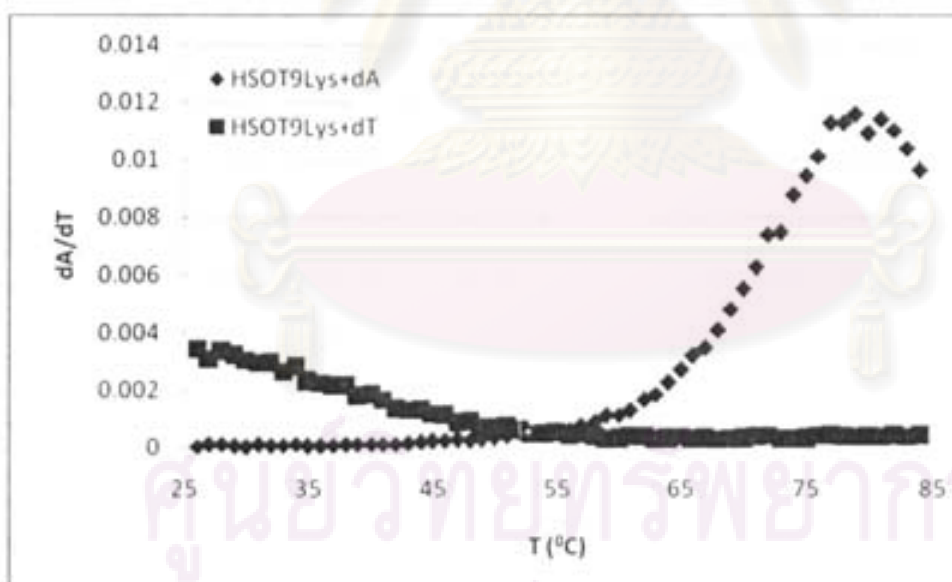
Figure A-2 First-derivative normalized UV-T_m plots between HS(CH$_2$)$_2$CO-egl-T$_9$-LysNH$_2$ **(P1)** with d(AAAA$\underline{X}$AAAA) (X = T and A): Condition PNA:DNA = 1:1. [PNA] = 1 μM. 10 mM sodium phosphate buffer, pH 7.0, heating rate 1.0 °C/min.
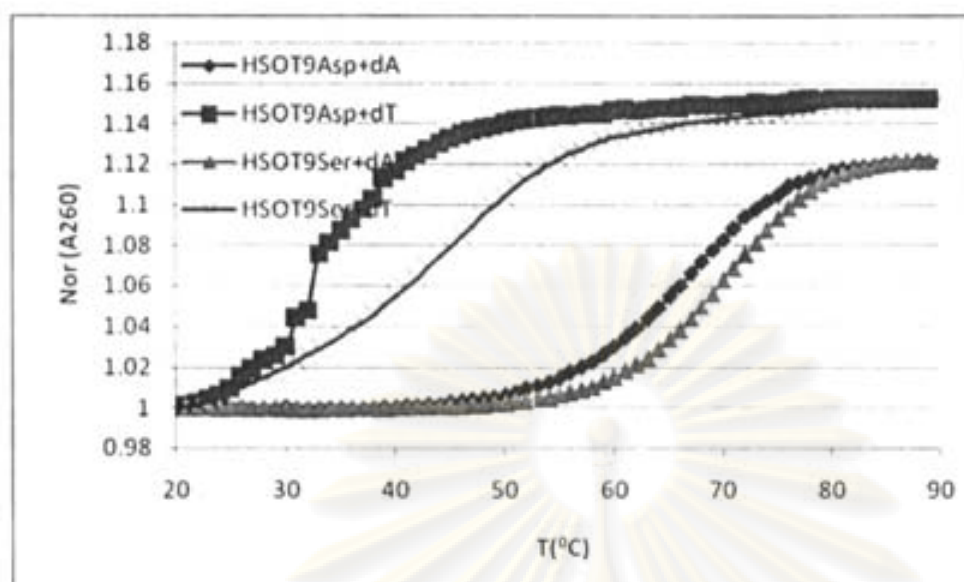
Figure A-3 T_m curves of HS(CH$_2$)$_2$CO-egl-T$_9$-SerNH$_2$ **(P2)** and HS(CH$_2$)$_2$CO-egl-T$_9$-AspNH$_2$ **(P3)** with d(AAAA$\underline{X}$AAAA) (X = T and A): Condition PNA:DNA = 1:1, [PNA] = 1 μM, 10 mM sodium phosphate buffer, pH 7.0, heating rate 1.0 °C/min.
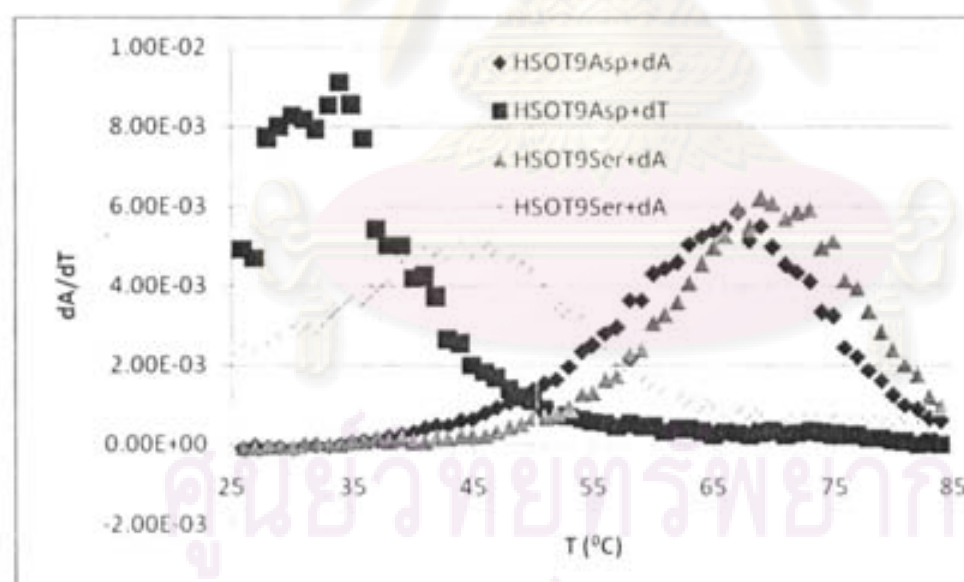
Figure A-4 First-derivative normalized UV-T_m plots between HS(CH$_2$)$_2$CO-egl-T$_9$-SerNH$_2$ **(P2)** and HS(CH$_2$)$_2$CO-egl-T$_9$-AspNH$_2$ **(P3)** with d(AAAA$\underline{X}$AAAA) (X = T and A): Condition PNA:DNA = 1:1, [PNA] = 1 μM, 10 mM sodium phosphate buffer, pH 7.0, heating rate 1.0 °C/min.
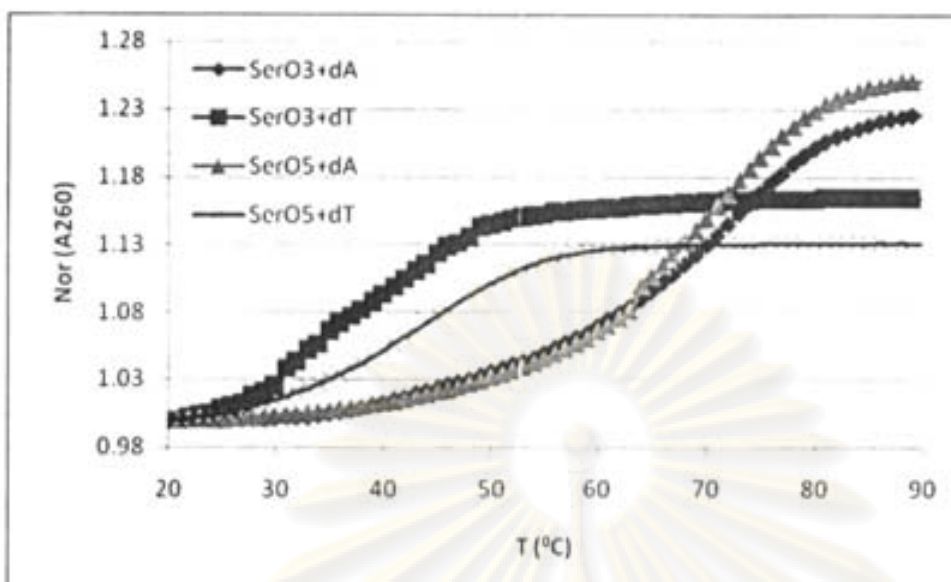
Figure A-5 T_m curves of HS(CH$_2$)$_2$CO-egl$_3$-T$_9$-LysNH$_2$ **(P4)**, HS(CH$_2$)$_2$CO-egl$_5$-T$_9$-LysNH$_2$ **(P5)** with d(AAAA$\underline{X}$AAAA) (X = T and A): Condition PNA:DNA = 1:1, [PNA] = 1 μM, 10 mM sodium phosphate buffer, pH 7.0, heating rate 1.0 °C/min.
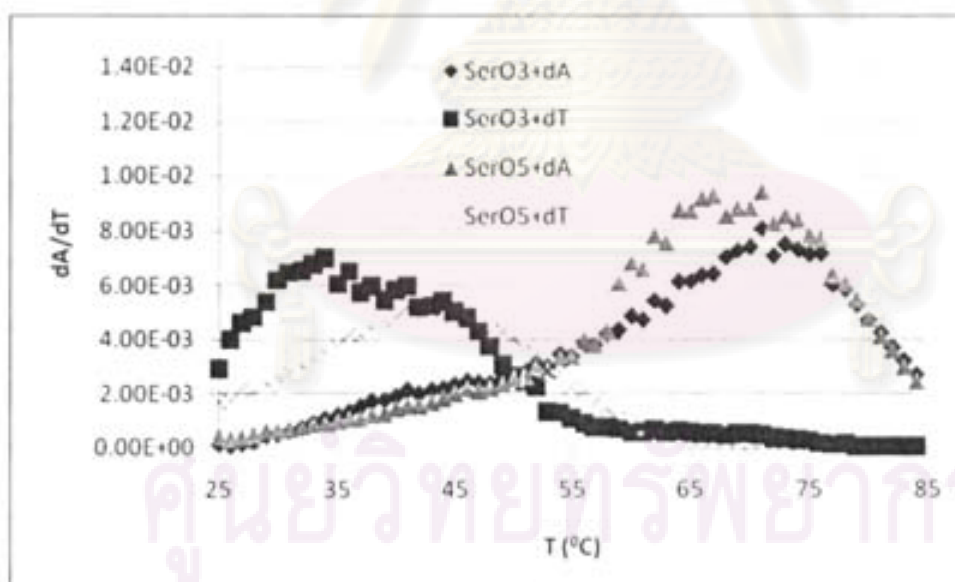
Figure A-6 First-derivative normalized UV-T_m plots between HS(CH$_2$)$_2$CO-egl$_3$-T$_9$-LysNH$_2$ **(P4)**, HS(CH$_2$)$_2$CO-egl$_5$-T$_9$-LysNH$_2$ **(P5)** with d(AAAA$\underline{X}$AAAA) (X = T and A): Condition PNA:DNA = 1:1, [PNA] = 1 μM, 10 mM sodium phosphate buffer, pH 7.0, heating rate 1.0 °C/min.
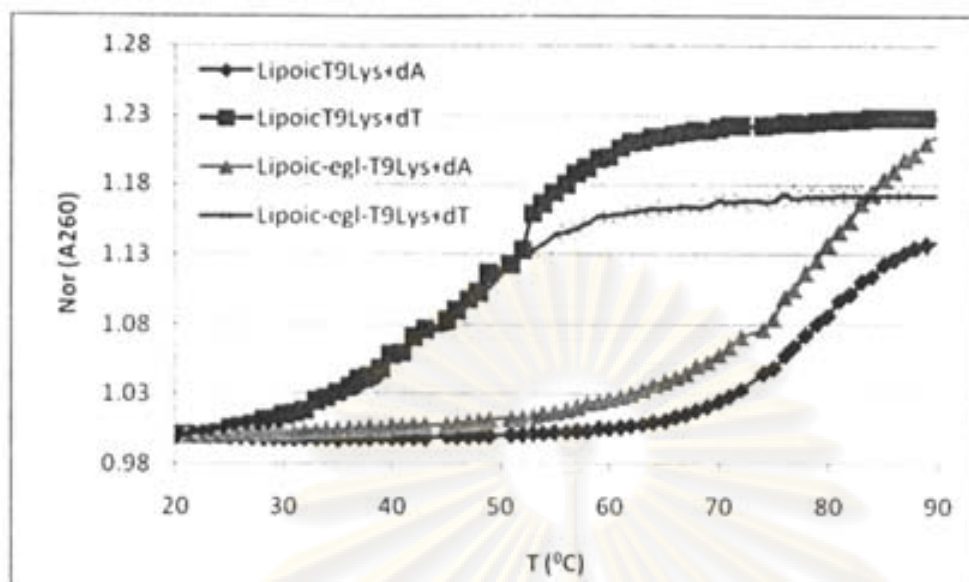
Figure A-7 T_m curves of Lipoic-T_9-LysNH$_2$ **(P8)**, Lipoic-egl-T_9-LysNH$_2$ **(P9)** with d(AAAAXAAAA) (X = T and A): Condition PNA:DNA = 1:1, [PNA] = 1 μM, 10 mM sodium phosphate buffer, pH 7.0, heating rate 1.0 °C/min.
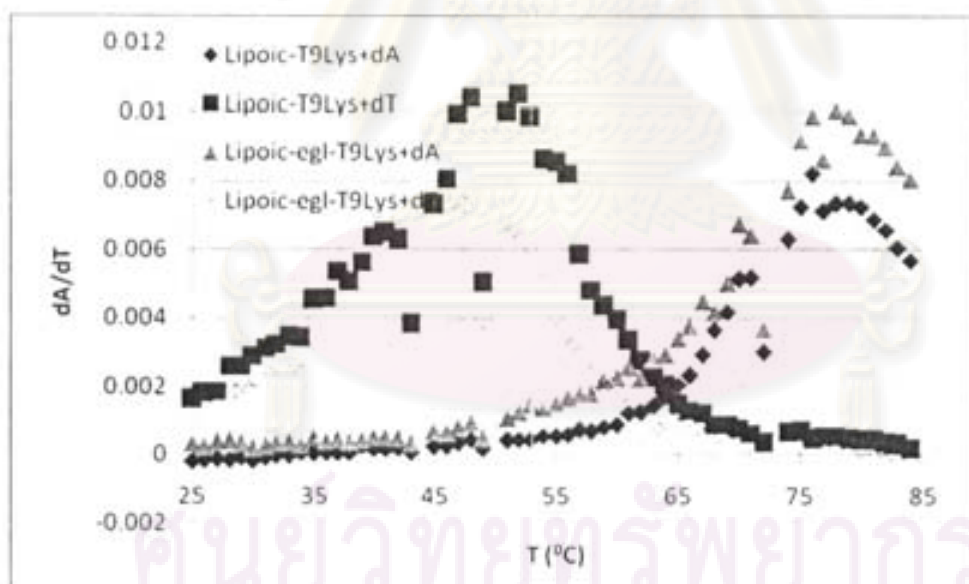
Figure A-8 First-derivative normalized UV-T_m plots between Lipoic-T_9-LysNH$_2$ **(P8)**, Lipoic-egl-T_9-LysNH$_2$ **(P9)** with d(AAAAXAAAA) (X = T and A): Condition PNA:DNA = 1:1, [PNA] = 1 μM, 10 mM sodium phosphate buffer, pH 7.0, heating rate 1.0 °C/min.
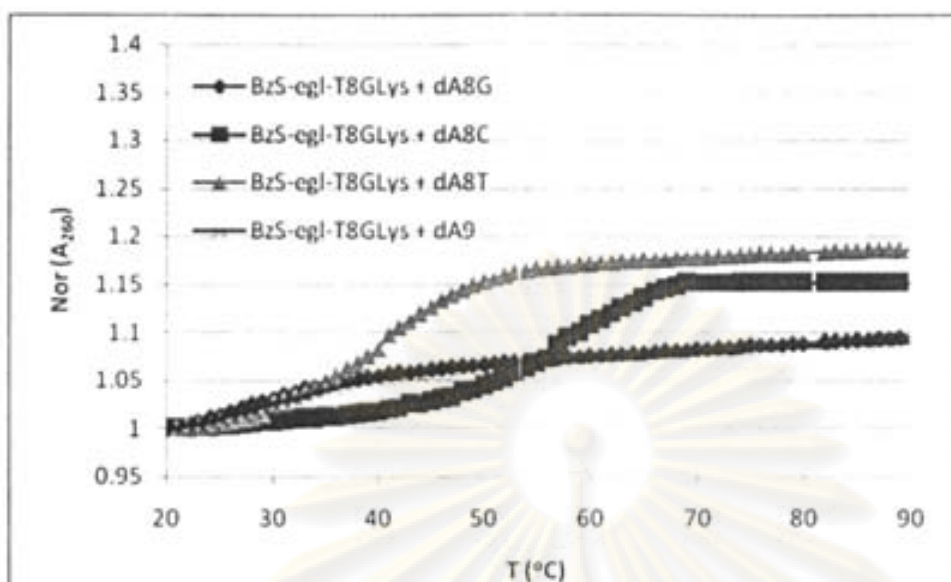
Figure A-9 T_m curves of BzS(CH$_2$)$_2$CO-egl-T$_4$GT$_4$-LysNH$_2$ **(P13)** with d(AAAAXAAAA) (X = G, C, T, and A): Condition PNA:DNA = 1:1, [PNA] = 1 µM, 10 mM sodium phosphate buffer, pH 7.0, heating rate 1.0 °C/min.
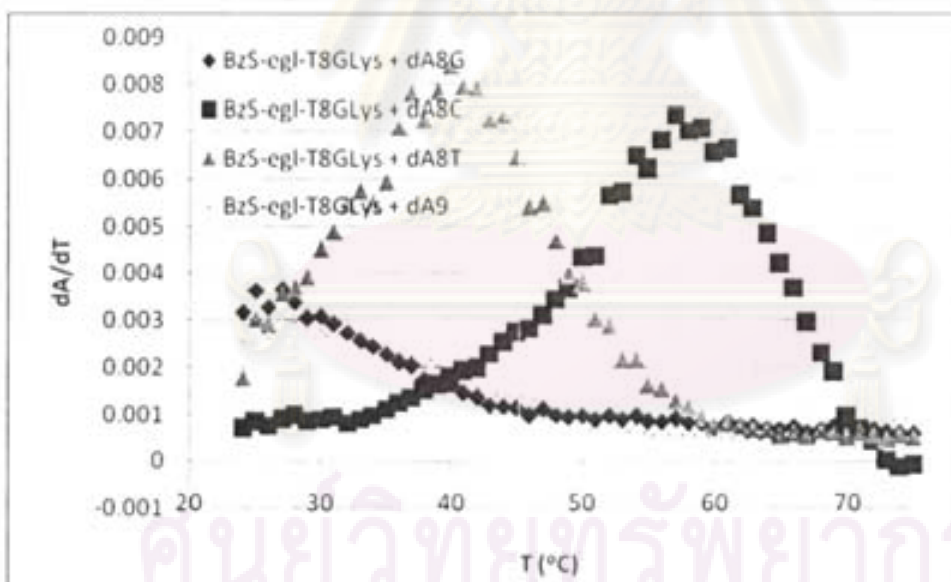
Figure A-10 First-derivative normalized UV-T_m plots between BzS(CH$_2$)$_2$CO-egl-T$_4$GT$_4$-LysNH$_2$ **(P13)** with d(AAAAXAAAA) (X = G, C, T, and A): Condition PNA:DNA = 1:1, [PNA] = 1 µM, 10 mM sodium phosphate buffer, pH 7.0, heating rate 1.0 °C/min.
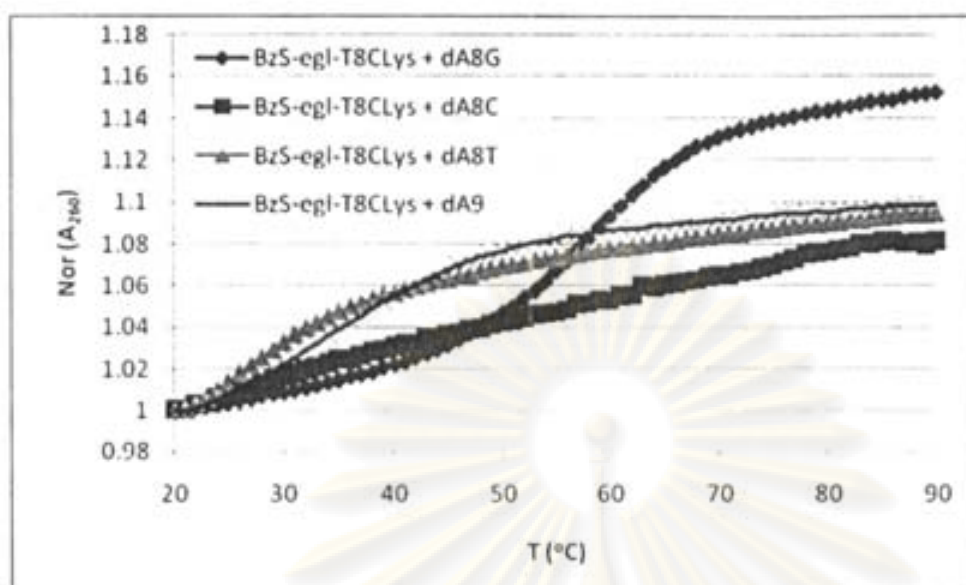
Figure A-11 T_m curves of $BzS(CH_2)_2CO$-egl-T_4CT_4-LysNH$_2$ **(P14)** with d(AAAA$\underline{X}$AAAA) (X = G, C, T, and A): Condition PNA:DNA = 1:1, [PNA] = 1 µM, 10 mM sodium phosphate buffer, pH 7.0, heating rate 1.0 °C/min.
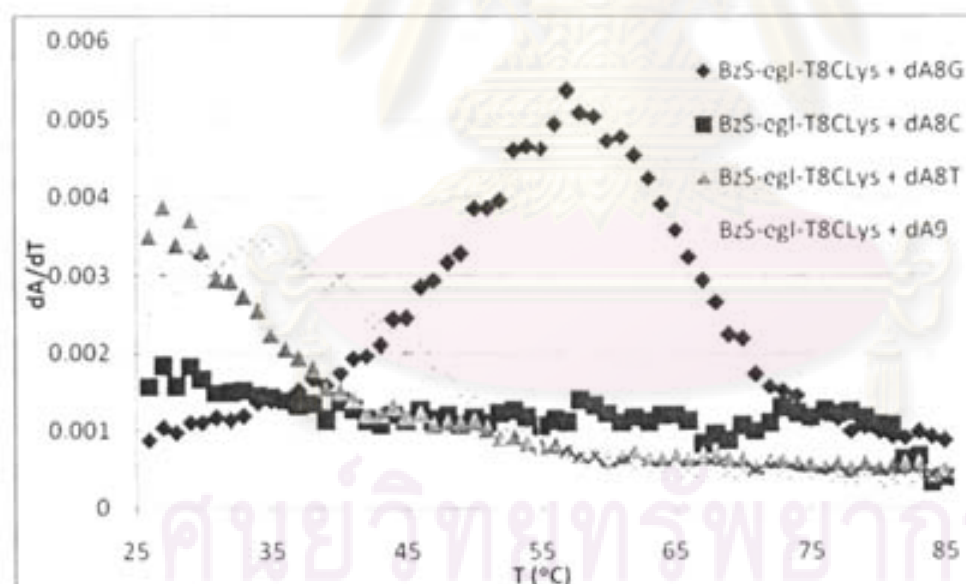
Figure A-12 First-derivative normalized UV-T_m plots between $BzS(CH_2)_2CO$-egl-T_4CT_4-LysNH$_2$ **(P14)** with d(AAAA$\underline{X}$AAAA) (X = G, C, T, and A): Condition PNA:DNA = 1:1, [PNA] = 1 µM, 10 mM sodium phosphate buffer, pH 7.0, heating rate 1.0 °C/min.
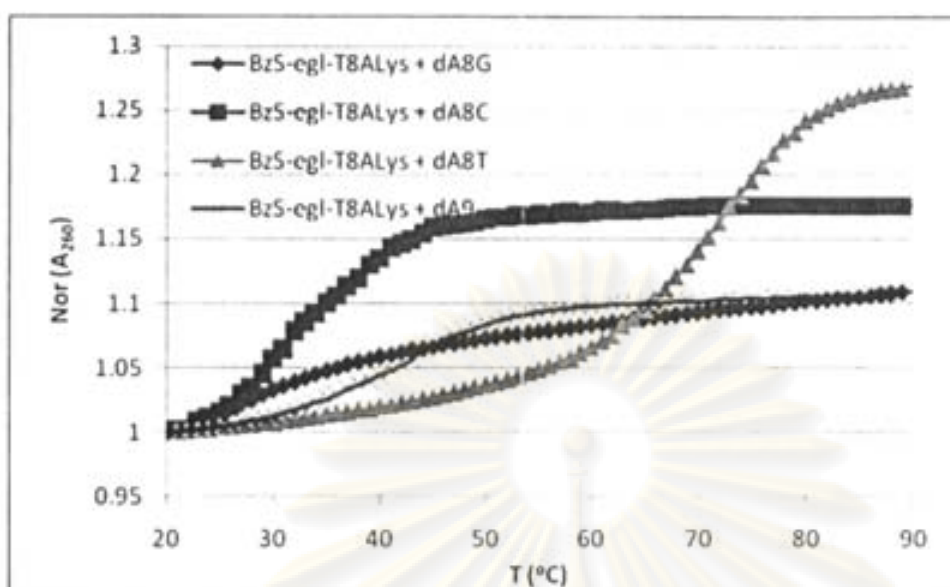
Figure A-13 T_m curves of BzS(CH$_2$)$_2$CO-egl-T$_4$AT$_4$-LysNH$_2$ **(P15)** with d(AAAA$\underline{X}$AAAA) (X = G, C, T, and A): Condition PNA:DNA = 1:1, [PNA] = 1 µM, 10 mM sodium phosphate buffer, pH 7.0, heating rate 1.0 °C/min.
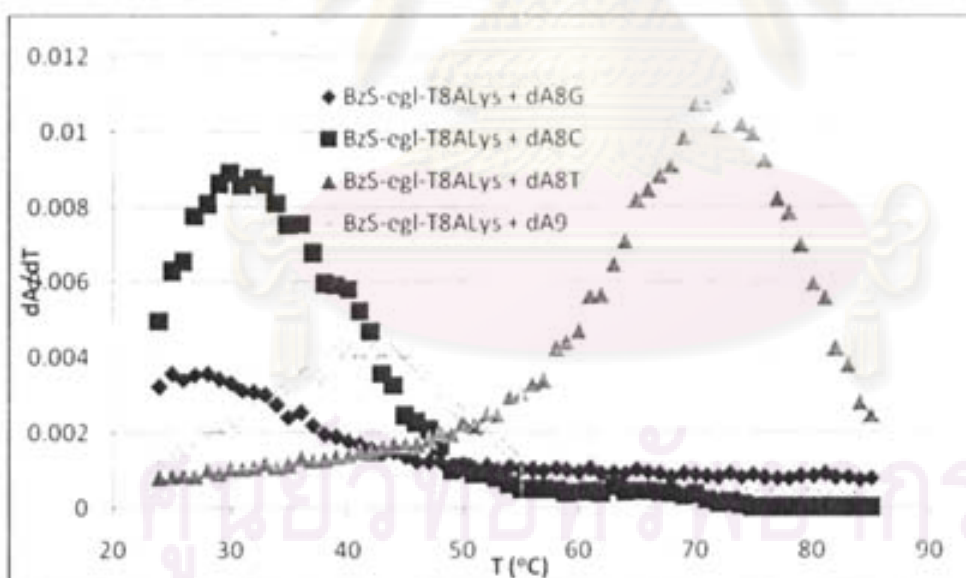
Figure A-14 First-derivative normalized UV-T_m plots between BzS(CH$_2$)$_2$CO-egl-T$_4$AT$_4$-LysNH$_2$ **(P15)** with d(AAAA$\underline{X}$AAAA) (X = G, C, T, and A): Condition PNA:DNA = 1:1, [PNA] = 1 µM, 10 mM sodium phosphate buffer, pH 7.0, heating rate 1.0 °C/min.
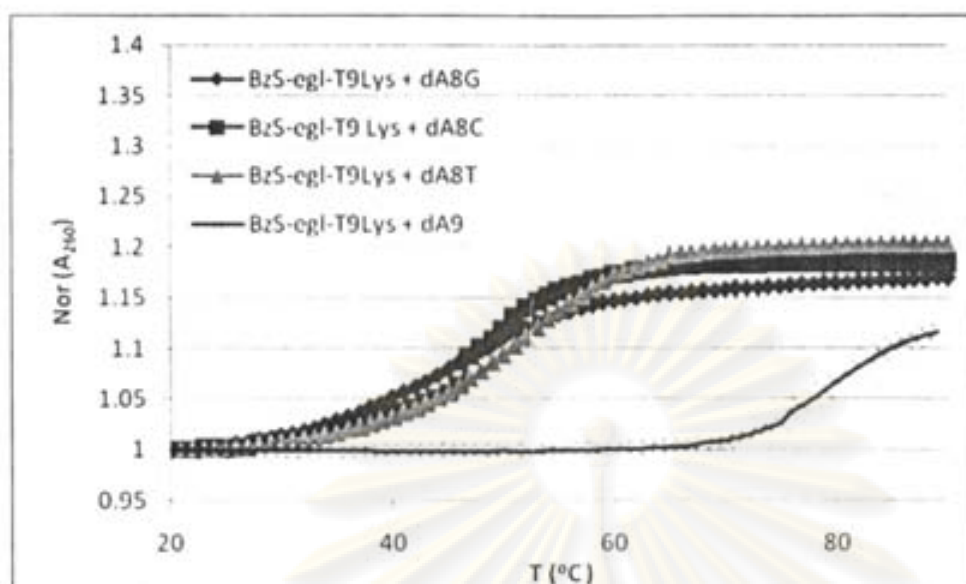
Figure A-15 T_m curves of BzS(CH$_2$)$_2$CO-egl-T$_9$-LysNH$_2$ **(P16)** with d(AAAA$\underline{X}$AAAA) (X = G, C, T, and A): Condition PNA:DNA = 1:1, [PNA] = 1 μM, 10 mM sodium phosphate buffer, pH 7.0, heating rate 1.0 °C/min.
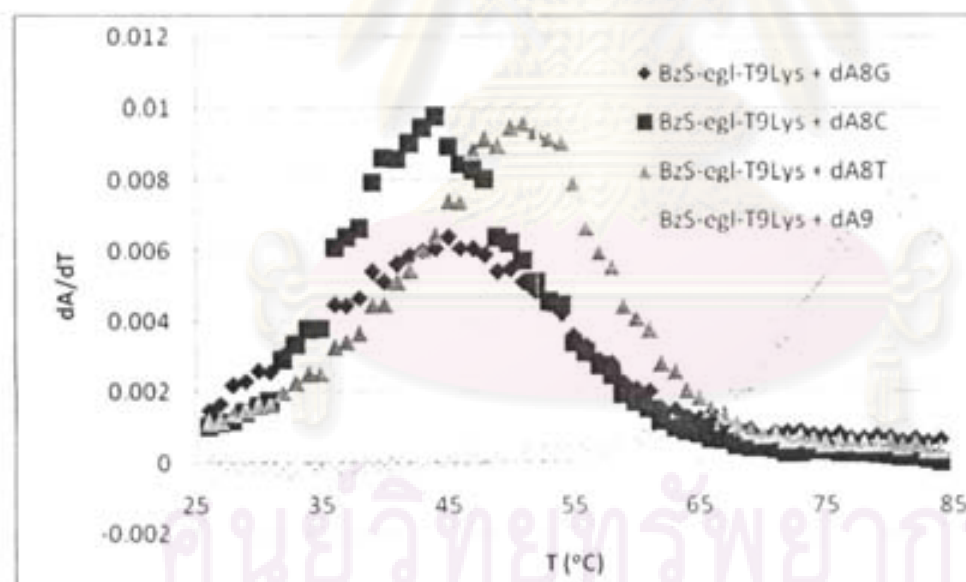
Figure A-16 First-derivative normalized UV-T_m plots between BzS(CH$_2$)$_2$CO-egl-T$_9$-LysNH$_2$ **(P16)** with d(AAAA$\underline{X}$AAAA) (X = G, C, T, and A): Condition PNA:DNA = 1:1, [PNA] = 1 μM, 10 mM sodium phosphate buffer, pH 7.0, heating rate 1.0 °C/min.
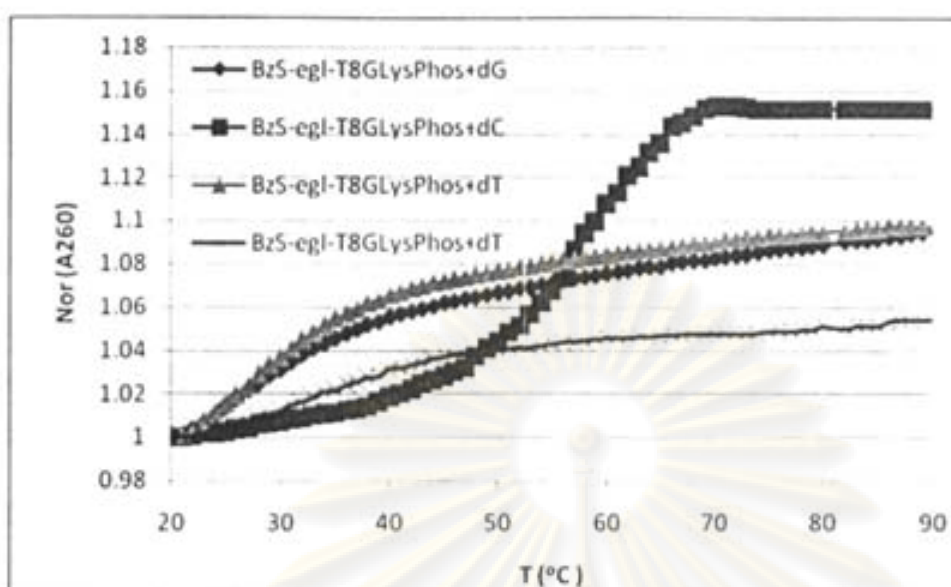
Figure A-17 T_m curves of BzS(CH$_2$)$_2$CO-egl-T$_4$GT$_4$-Lys(Phos)NH$_2$ **(P17)** with d(AAAA$\underline{X}$AAAA) (X = G, C, T, and A): Condition PNA:DNA = 1:1, [PNA] = 1 μM, 10 mM sodium phosphate buffer, pH 7.0, heating rate 1.0 °C/min.
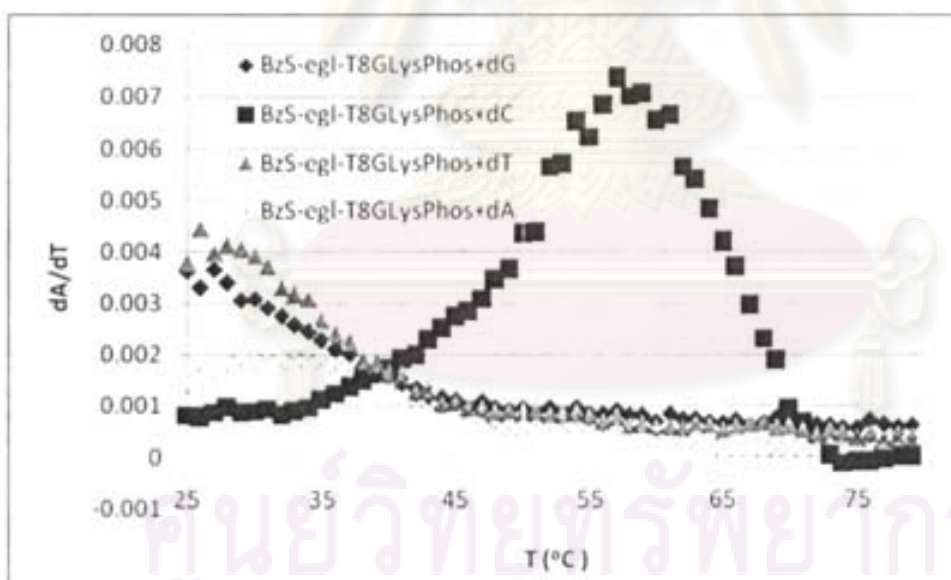
Figure A-18 First-derivative normalized UV-T_m plots between BzS(CH$_2$)$_2$CO-egl-T$_4$GT$_4$-Lys(Phos)NH$_2$ **(P17)** with d(AAAA$\underline{X}$AAAA) (X = G, C, T, and A): Condition PNA:DNA = 1:1, [PNA] = 1 μM, 10 mM sodium phosphate buffer, pH 7.0, heating rate 1.0 °C/min.
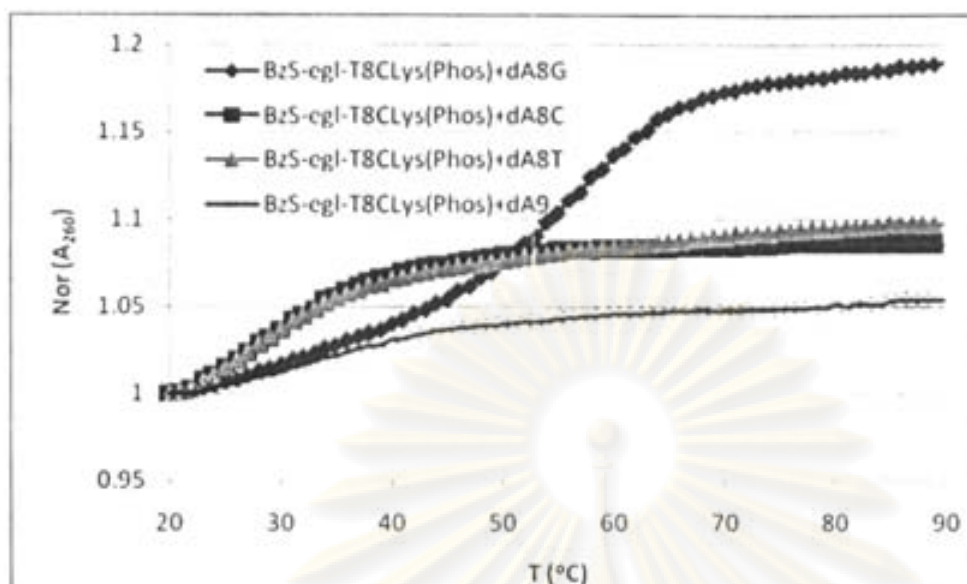
Figure A-19 T_m curves of BzS(CH$_2$)$_2$CO-egl-T$_4$CT$_4$-Lys(Phos)NH$_2$ **(P18)** with d(AAAAXAAAA) (X = G, C, T, and A): Condition PNA:DNA = 1:1, [PNA] = 1 µM, 10 mM sodium phosphate buffer, pH 7.0, heating rate 1.0 °C/min.
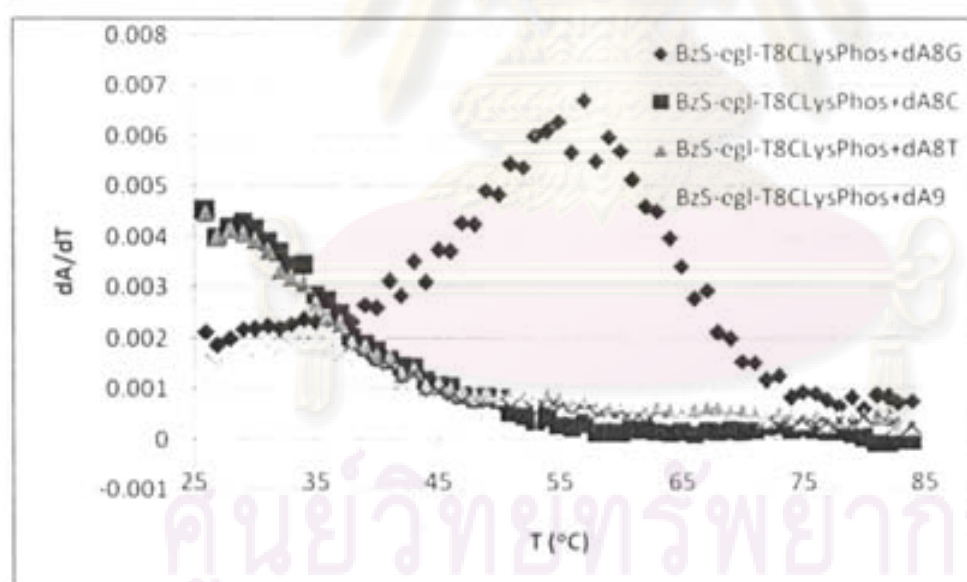
Figure A-20 First-derivative normalized UV-T_m plots between BzS(CH$_2$)$_2$CO-egl-T$_4$CT$_4$-Lys(Phos)NH$_2$ **(P18)** with d(AAAAXAAAA) (X = G, C, T, and A): Condition PNA:DNA = 1:1, [PNA] = 1 µM, 10 mM sodium phosphate buffer, pH 7.0, heating rate 1.0 °C/min.
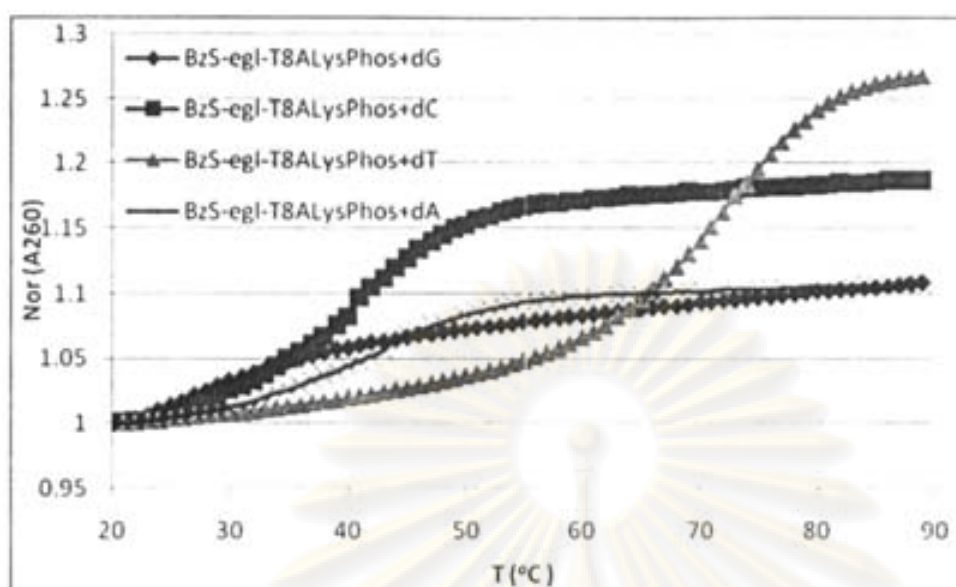
Figure A-21 T_m curves of BzS(CH₂)₂CO-egl-T₄AT₄-Lys(Phos)NH₂ **(P19)** with d(AAAA$\underline{X}$AAAA) (X = G, C, T, and A): Condition PNA:DNA = 1:1, [PNA] = 1 μM, 10 mM sodium phosphate buffer, pH 7.0, heating rate 1.0 °C/min.
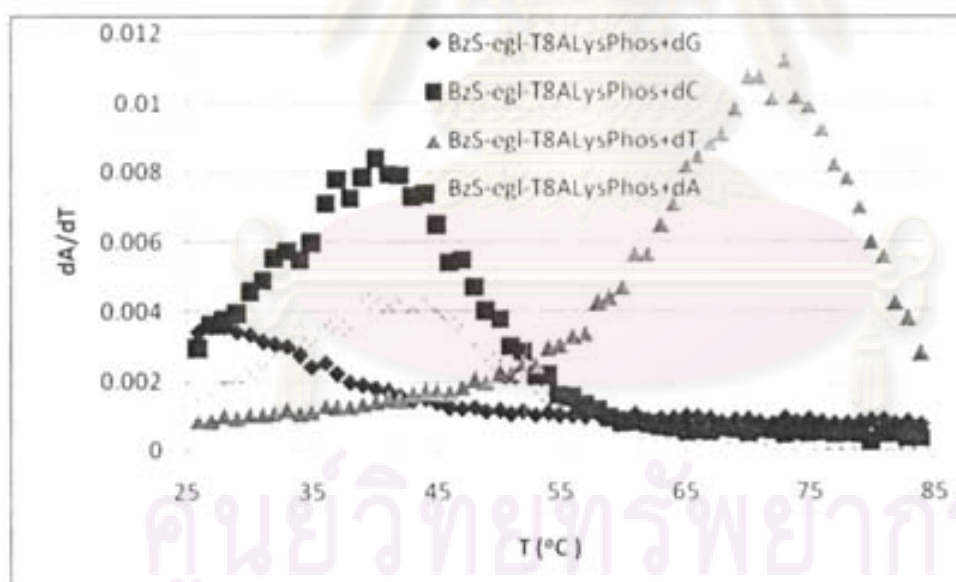
Figure A-22 First-derivative normalized UV-T_m plots between BzS(CH₂)₂CO-egl-T₄AT₄-Lys(Phos)NH₂ **(P19)** with d(AAAA$\underline{X}$AAAA) (X = G, C, T, and A): Condition PNA:DNA = 1:1, [PNA] = 1 μM, 10 mM sodium phosphate buffer, pH 7.0, heating rate 1.0 °C/min.
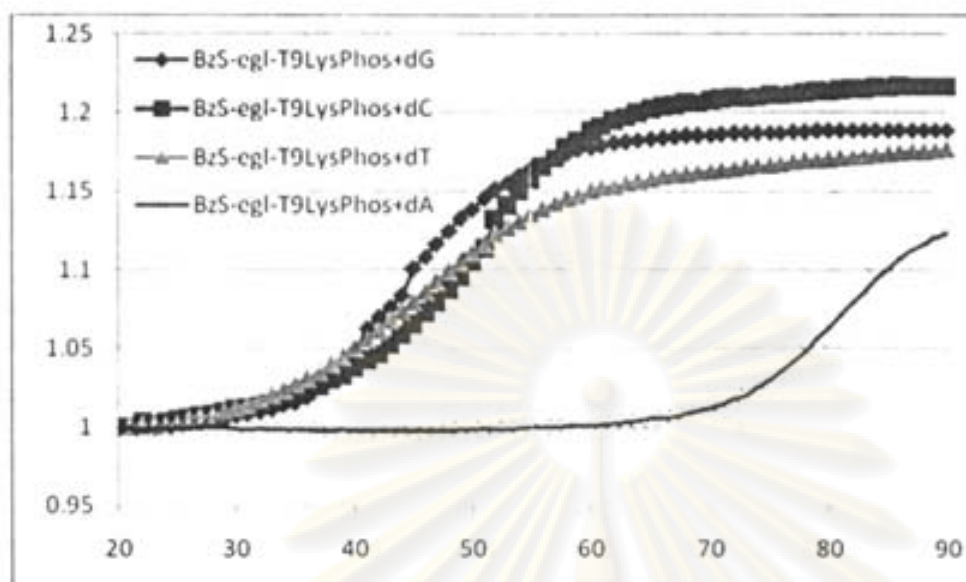
Figure A-23 T_m curves of BzS(CH$_2$)$_2$CO-egl-T$_9$-Lys(Phos)NH$_2$ **(P20)** with d(AAAA$\underline{X}$AAAA) (X = G, C, T, and A): Condition PNA:DNA = 1:1, [PNA] = 1 μM, 10 mM sodium phosphate buffer, pH 7.0, heating rate 1.0 °C/min.
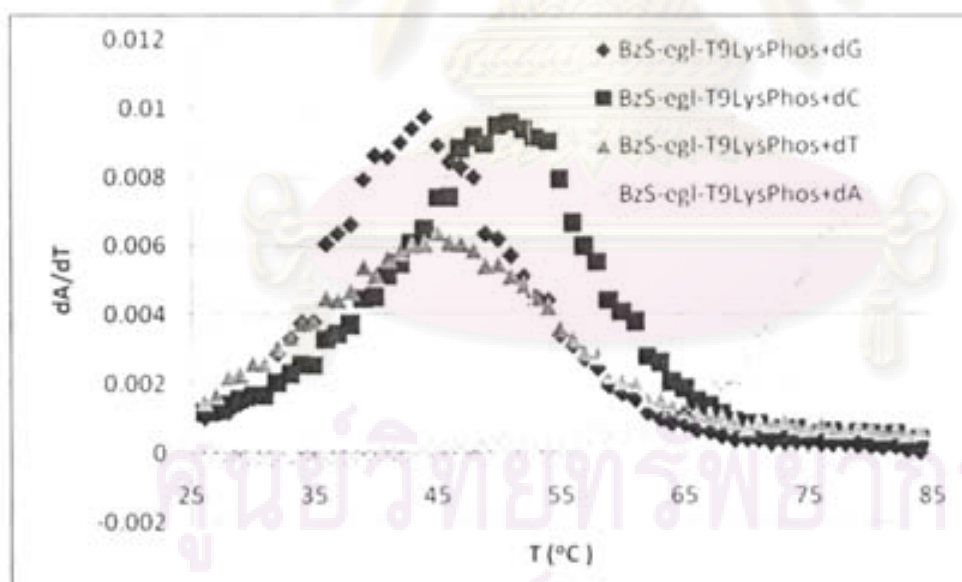
Figure A-24 First-derivative normalized UV-T_m plots between BzS(CH$_2$)$_2$CO-egl-T$_9$-Lys(Phos)NH$_2$ **(P20)** with d(AAAA$\underline{X}$AAAA) (X = G, C, T, and A): Condition PNA:DNA = 1:1, [PNA] = 1 μM, 10 mM sodium phosphate buffer, pH 7.0, heating rate 1.0 °C/min.
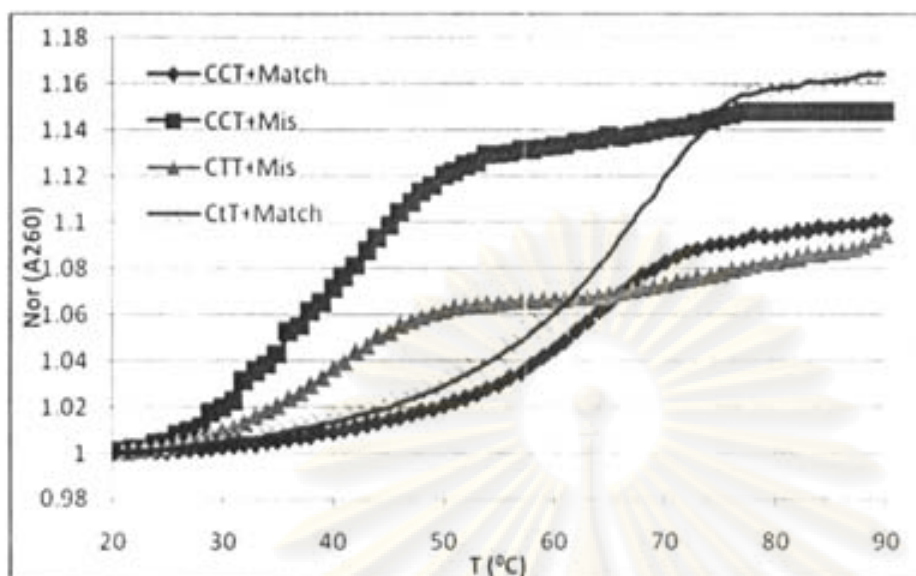
Figure A-25 T_m curves of BzS(CH$_2$)$_2$CO-egl-TTCCCCCTCCCAA-Lys(Phos)NH$_2$ **(P23)** and BzS(CH$_2$)$_2$CO-egl-TTCCCCTTCCCAA-Lys(Phos)NH$_2$ **(P24)** with d(TTGGGA<u>X</u>GGGGAA) (X = G and A): Condition PNA:DNA = 1:1, [PNA] = 1 μM, 10 mM sodium phosphate buffer, pH 7.0, heating rate 1.0 °C/min.
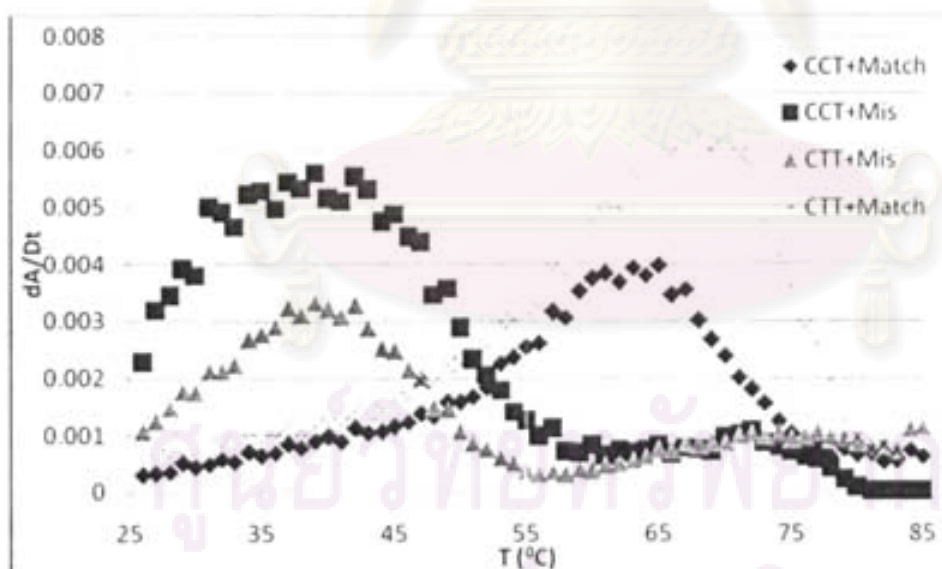
Figure A-26 First-derivative normalized UV-T_m plots between BzS(CH$_2$)$_2$CO-egl-TTCCCCCTCCCAA-Lys(Phos)NH$_2$ **(P23)** and BzS(CH$_2$)$_2$CO-egl-TTCCCCTTCCCAA-Lys(Phos)NH$_2$ **(P24)** with d(TTGGGA<u>X</u>GGGGAA) (X = G and A): Condition PNA:DNA = 1:1, [PNA] = 1 μM, 10 mM sodium phosphate buffer, pH 7.0, heating rate 1.0 °C/min.
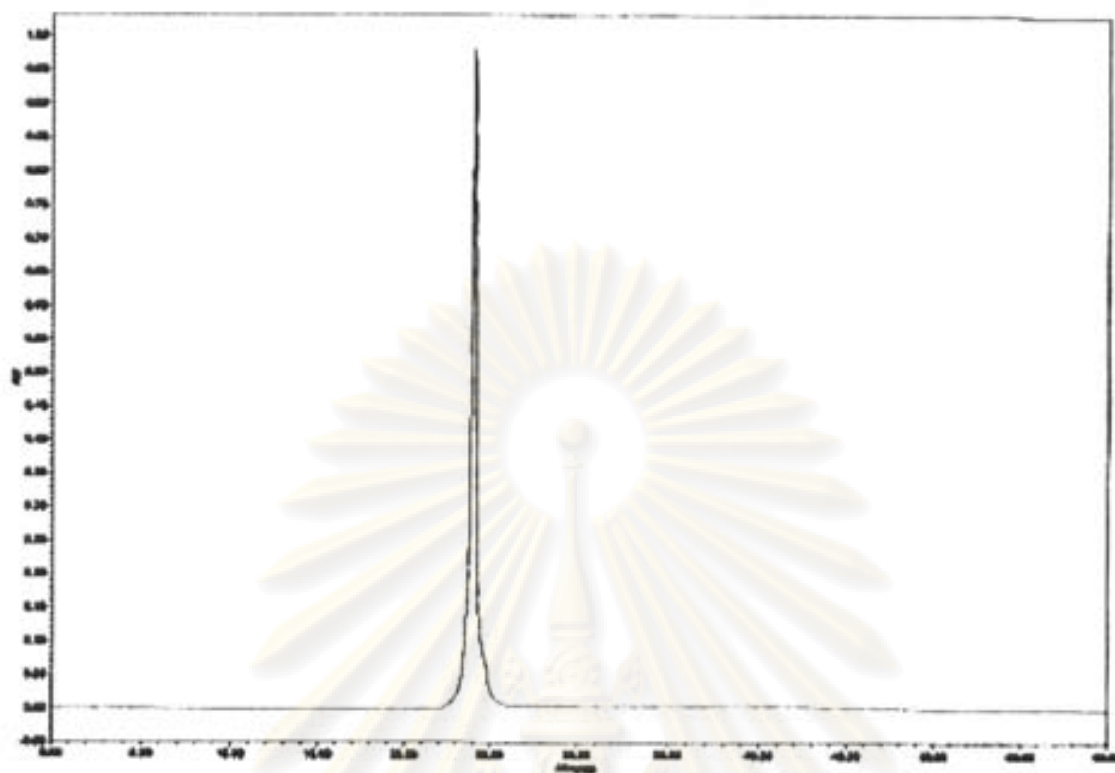
Figure B-1 : HPLC chromatogram of $HS(CH_2)_2CO$-egl-T_9-LysNH$_2$ (**P1**)
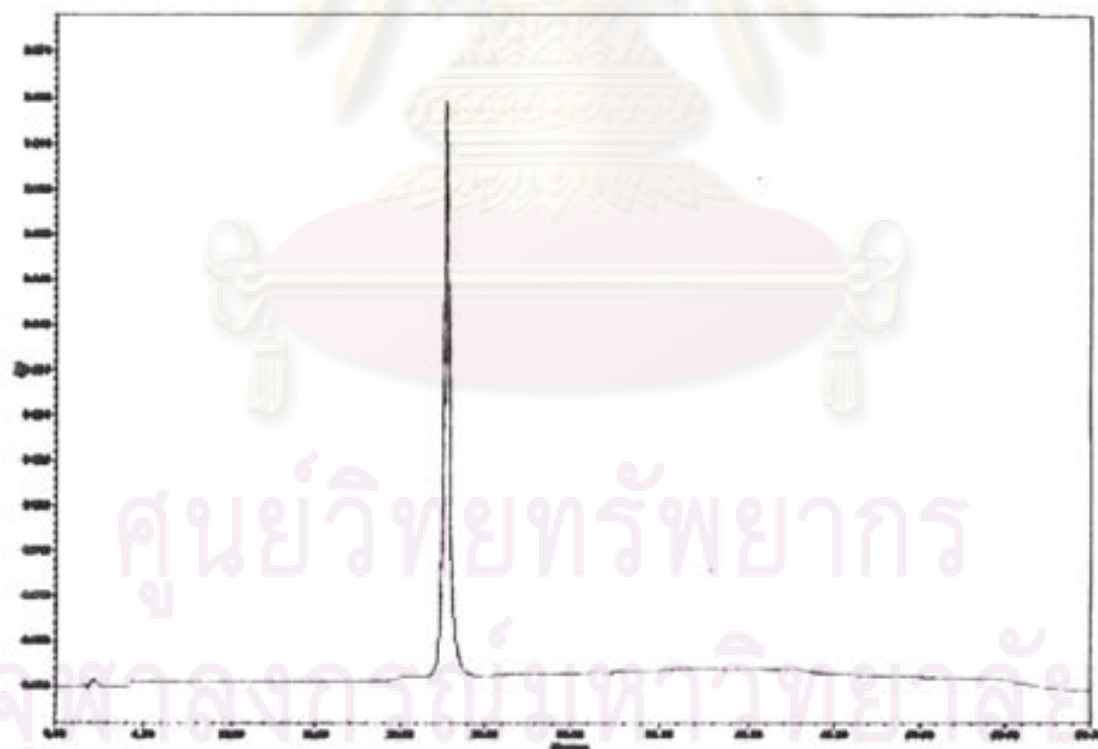
Figure B-2 : HPLC chromatogram of $HS(CH_2)_2CO$-egl-T_9-SerNH$_2$ (**P2**)
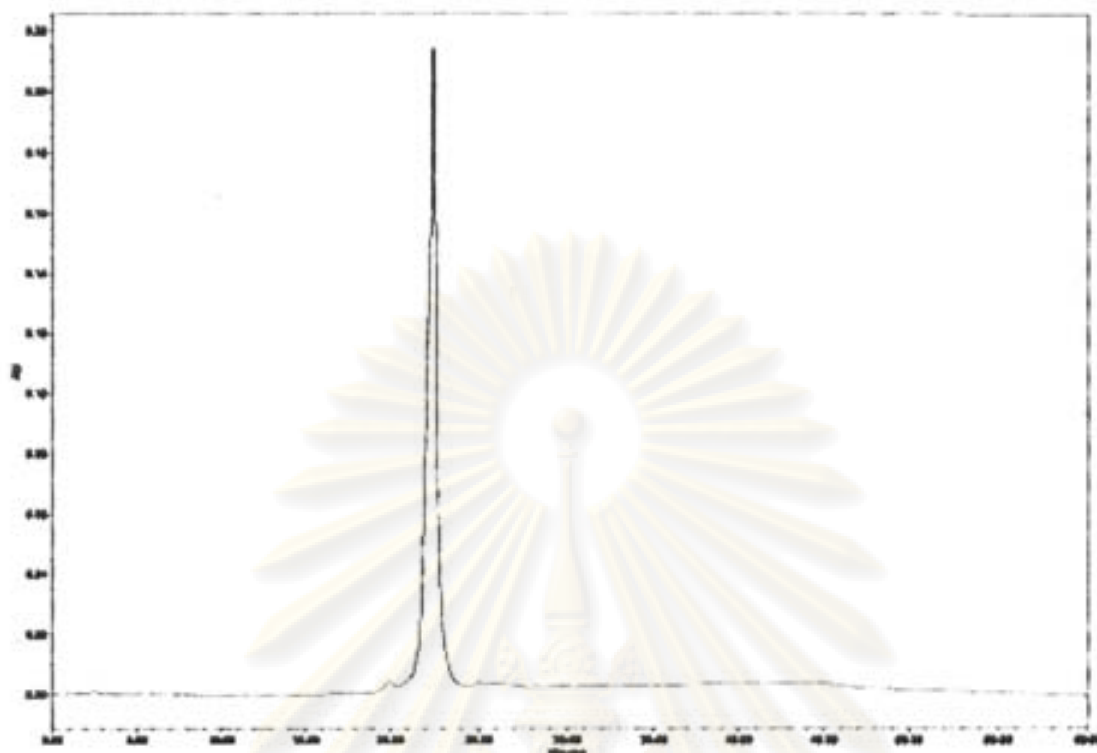
Figure B-3 : HPLC chromatogram of HS(CH₂)₂CO-egl-T₉-AspNH₂ (P3)
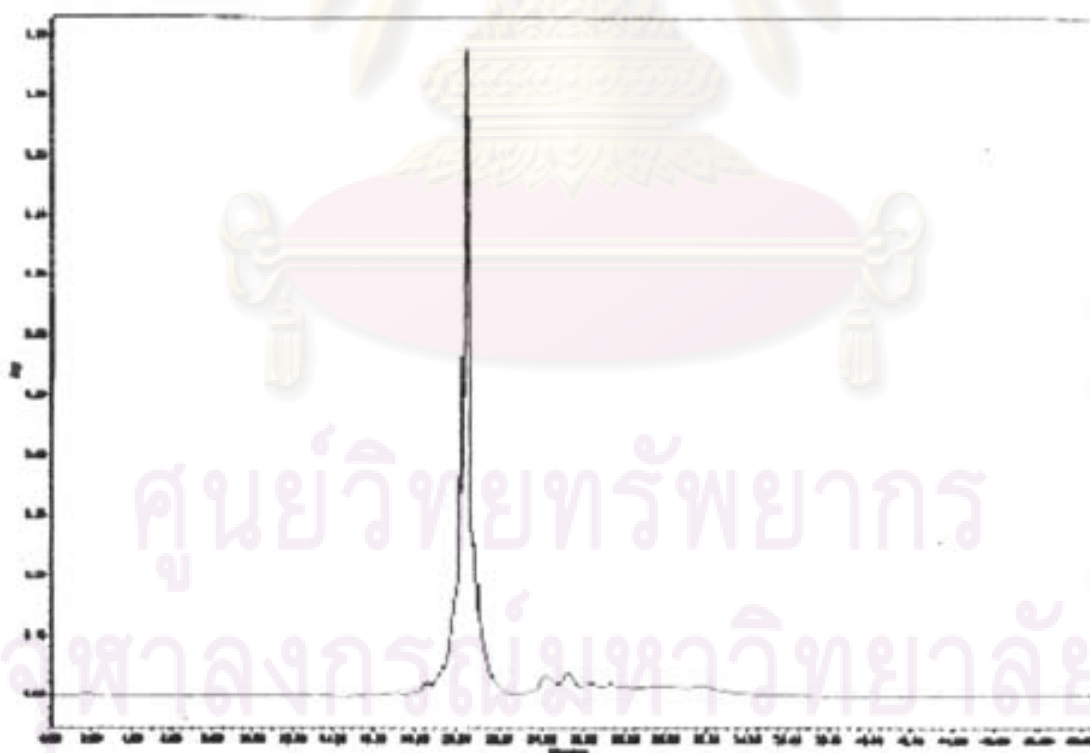
Figure B-4 : HPLC chromatogram of HS(CH₂)₂CO-egl₃-T₉-SerNH₂ (P4)
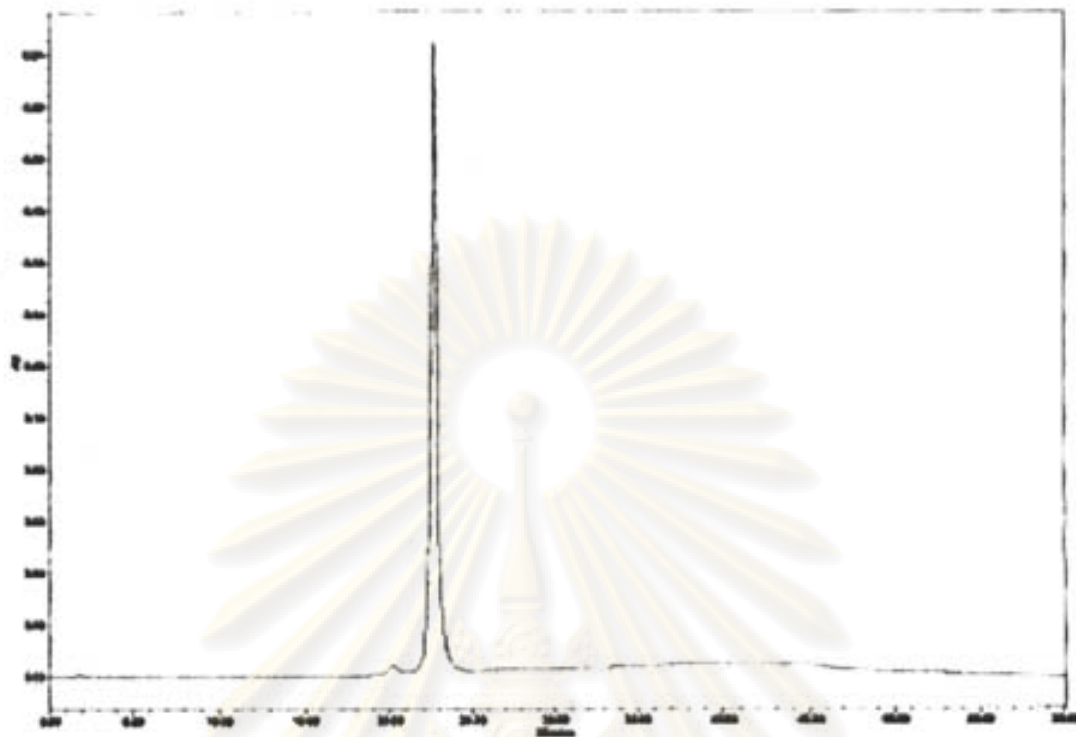
Figure B-5 : HPLC chromatogram of HS(CH$_2$)$_2$CO-egl$_5$-T$_9$-SerNH$_2$ (P5)

Figure B-6 : HPLC chromatogram of Ac-T$_9$-LysNH$_2$ (P6)
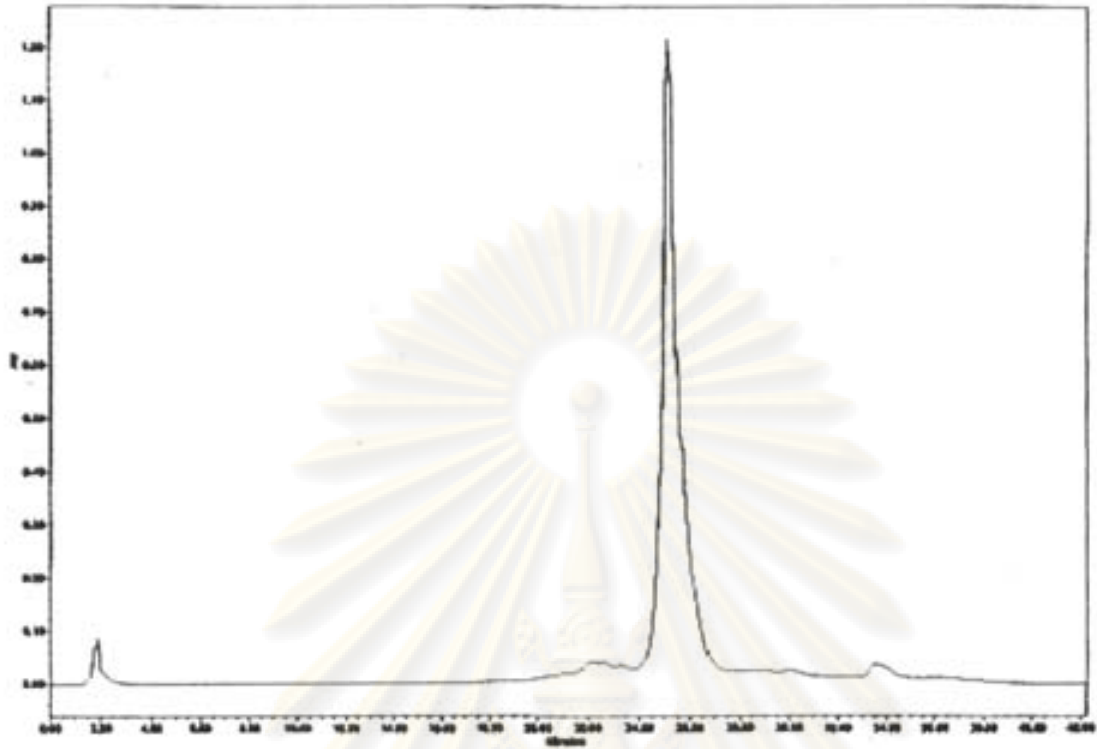
Figure B-7 : HPLC chromatogram of Ac-T$_9$-SerNH$_2$ (P7)

Figure B-8 : HPLC chromatogram of Lipoic-T$_9$-LysNH$_2$ (P8)
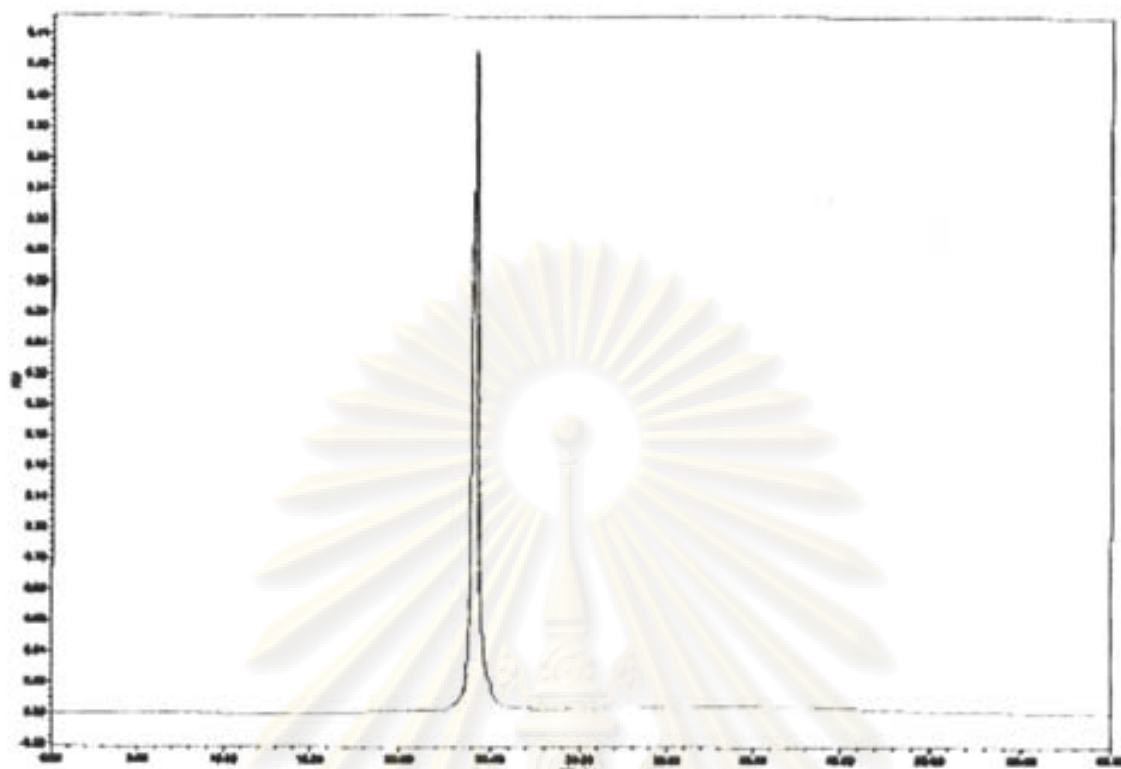
Figure B-9 : HPLC chromatogram of Lipoic-egl-T$_9$-LysNH$_2$ (**P9**)
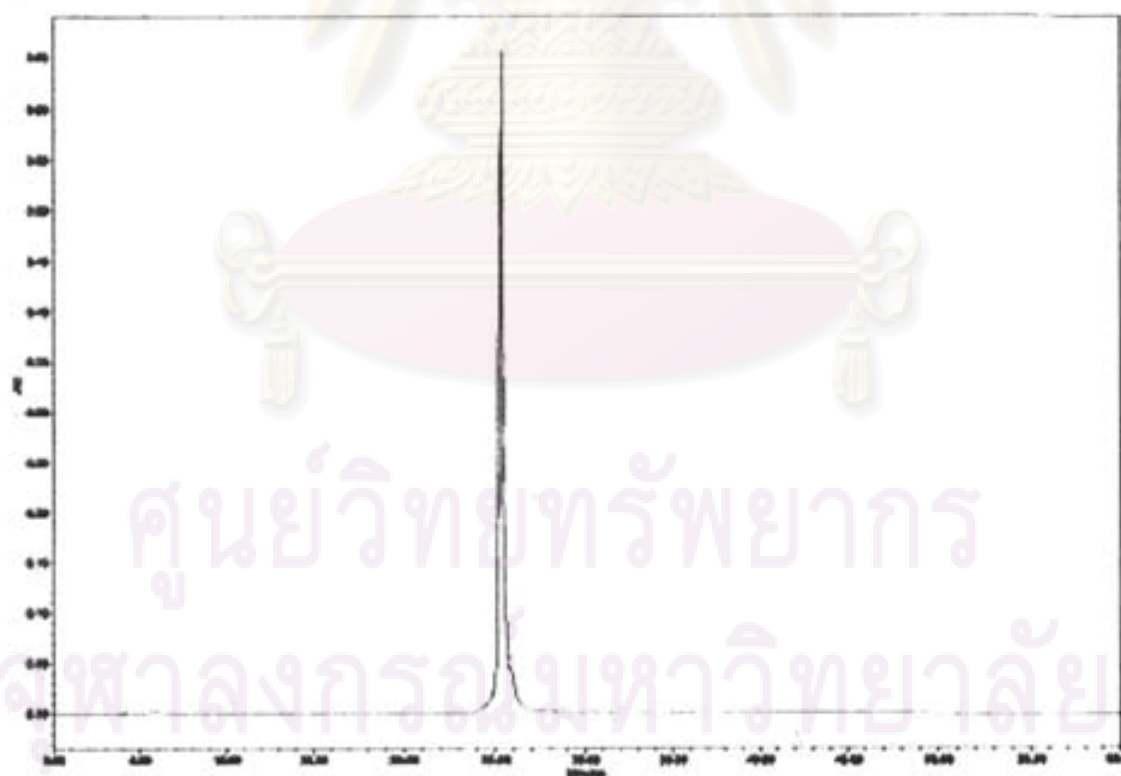
Figure B-10 : HPLC chromatogram of Lipoic-egl-T$_9$-SerNH$_2$ (**P10**)
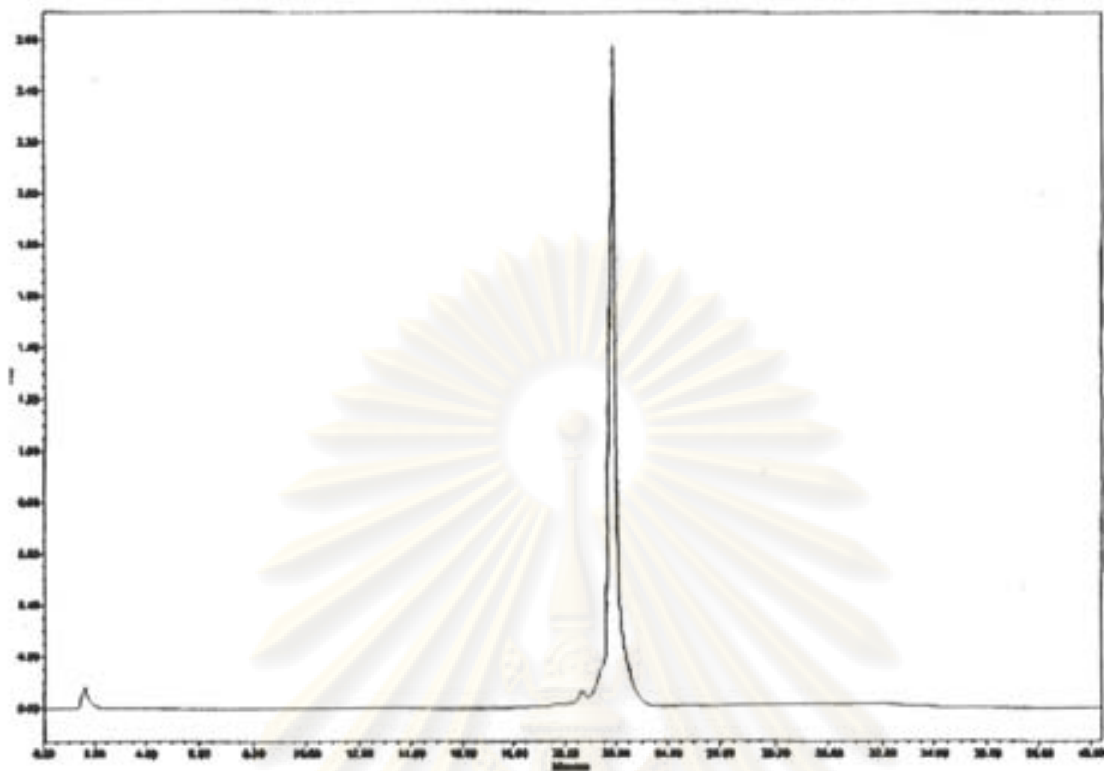
Figure B-11 : HPLC chromatogram of DNP-S(CH₂)₂CO-egl-T₉-LysNH₂ (**P12**)

Figure B-12 : HPLC chromatogram of BzS(CH₂)₂CO-egl-T₄GT₄-LysNH₂ (**P13**)
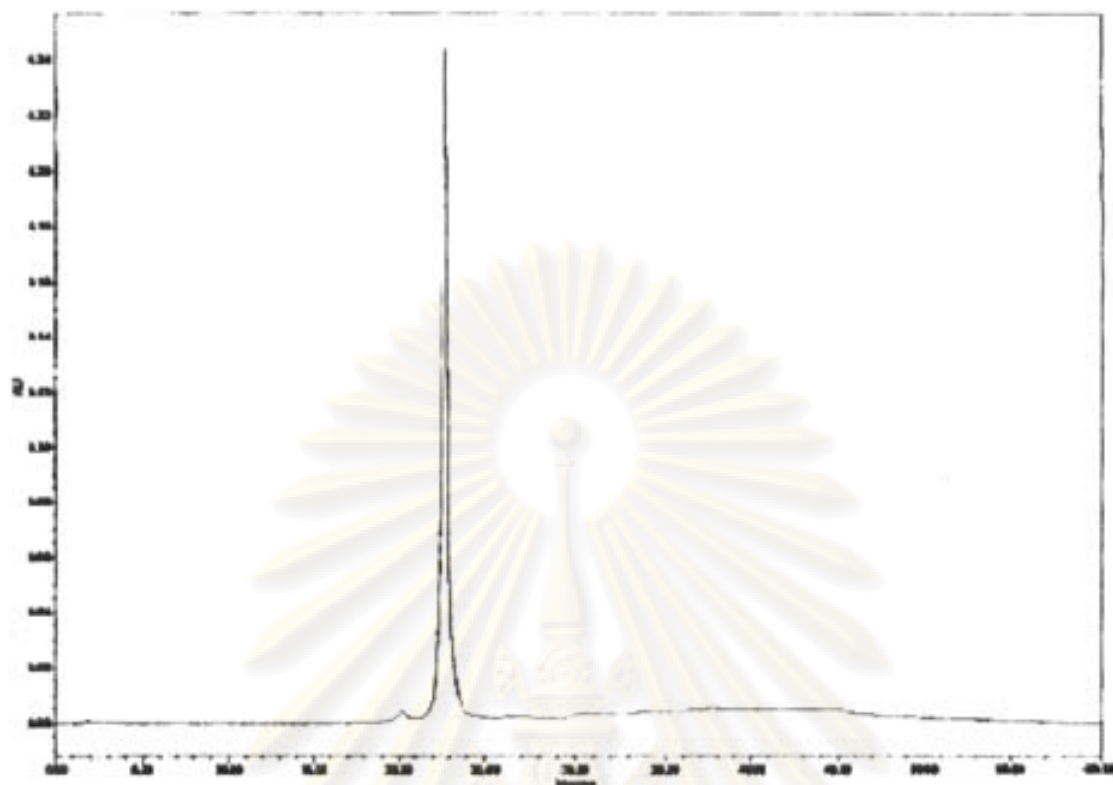
Figure B-13 : HPLC chromatogram of BzS(CH$_2$)$_2$CO-egl-T$_4$CT$_4$-LysNH$_2$ (**P14**)
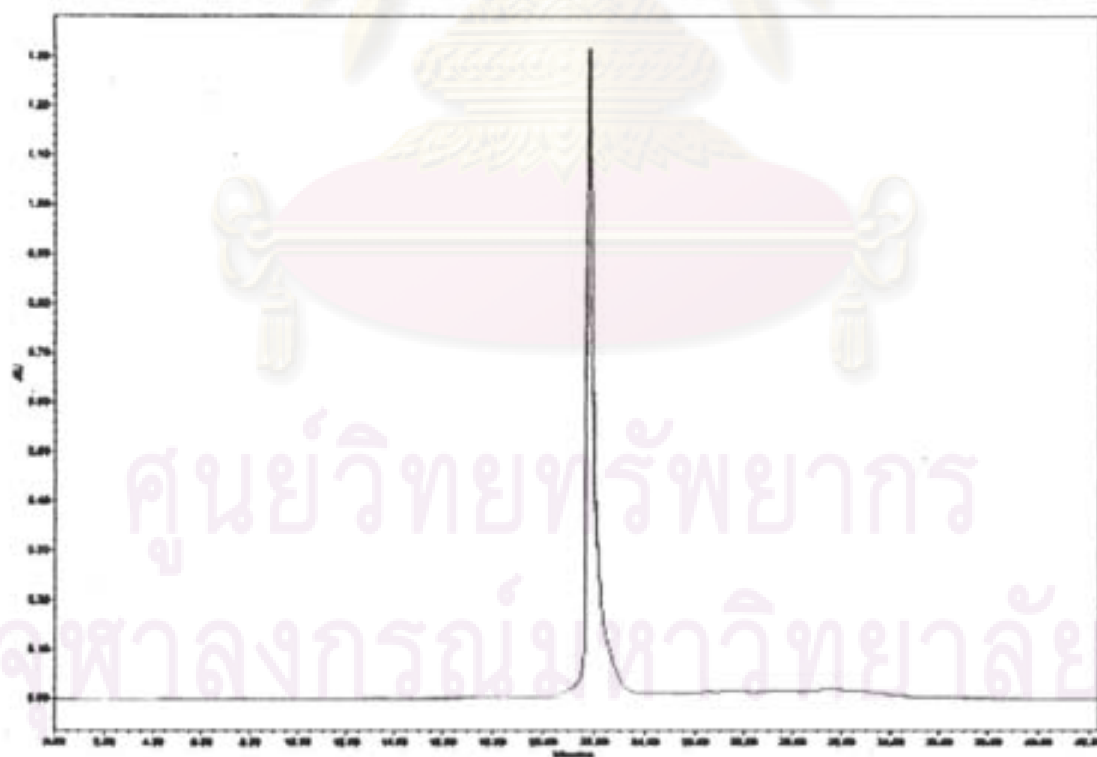
Figure B-14 : HPLC chromatogram of BzS(CH$_2$)$_2$CO-egl-T$_4$AT$_4$-LysNH$_2$ (**P15**)
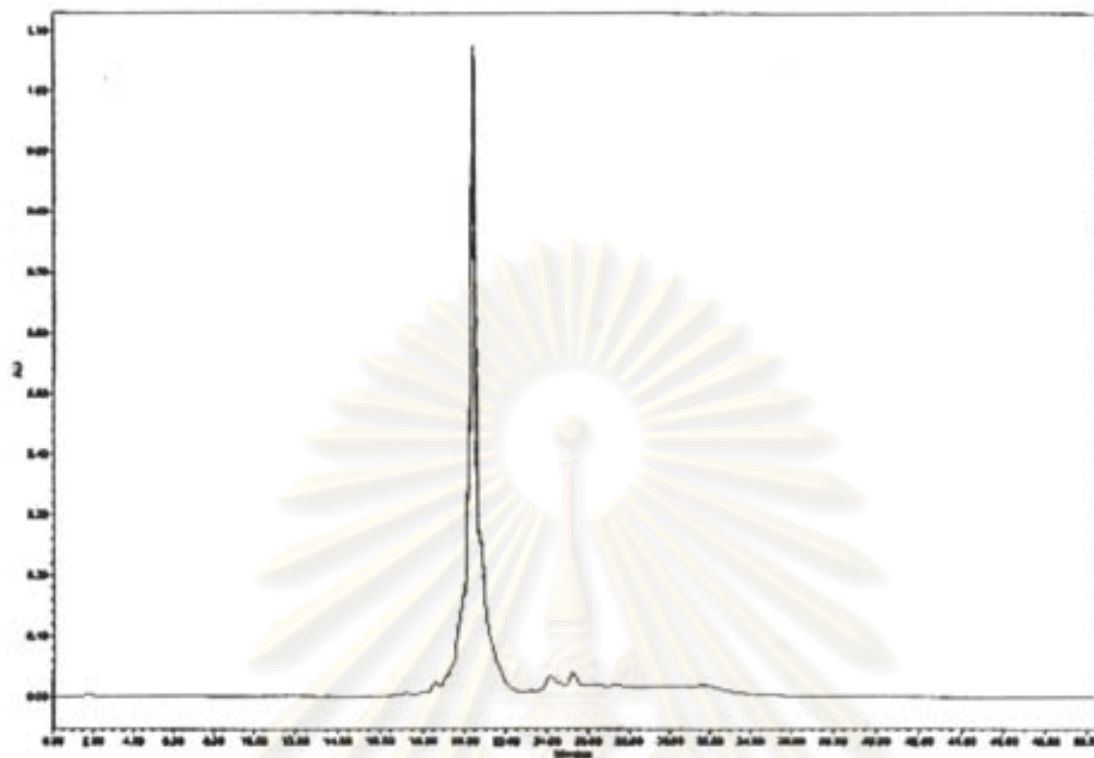
Figure B-15 : HPLC chromatogram of BzS(CH$_2$)$_2$CO-egl-T$_9$-LysNH$_2$ (**P16**)
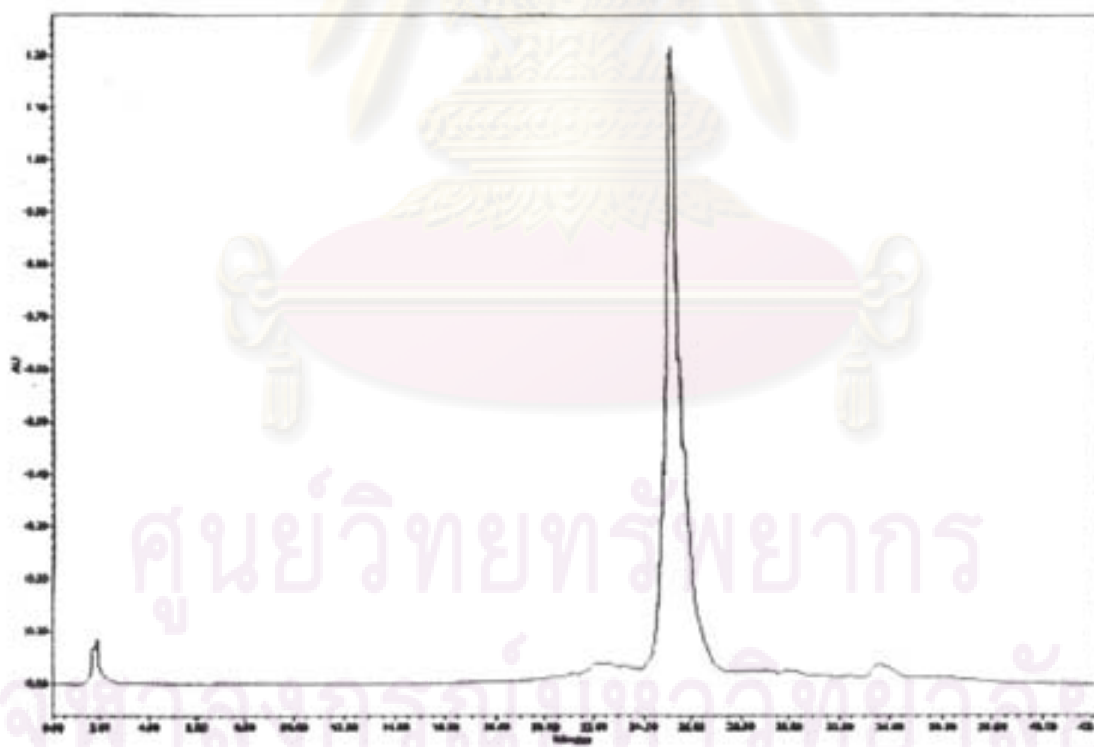
Figure B-16 : HPLC chromatogram of BzS(CH$_2$)$_2$CO-egl-T$_4$GT$_4$-Lys(Phos)NH$_2$ (**P17**)
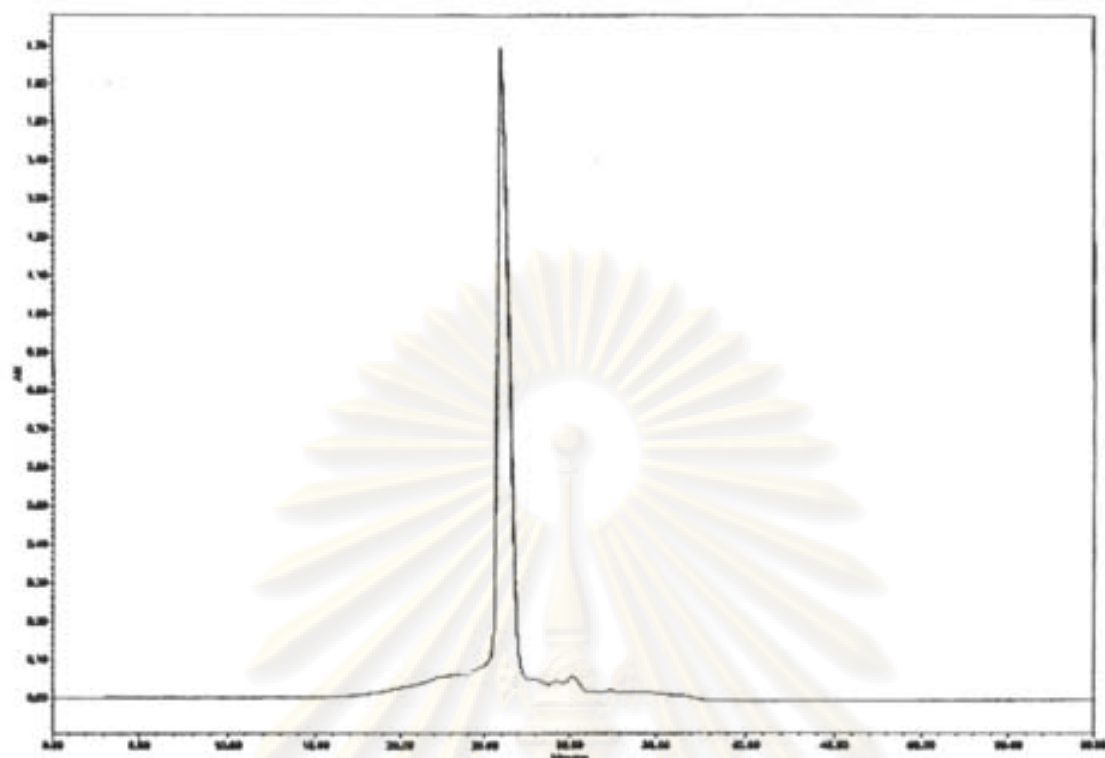
Figure B-17 : HPLC chromatogram of BzS(CH₂)₂CO-egl-T₄CT₄-Lys(Phos)NH₂
(P18)
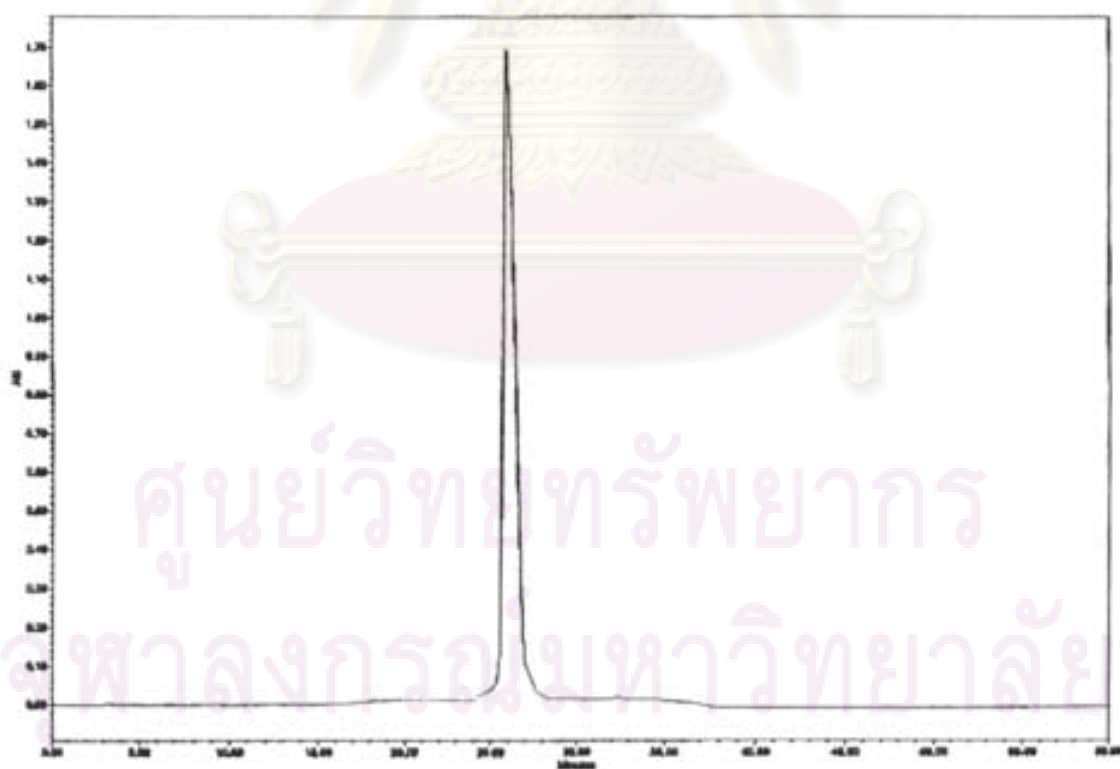
Figure B-18 : HPLC chromatogram of BzS(CH₂)₂CO-egl-T₄AT₄-Lys(Phos)NH₂
(P19)
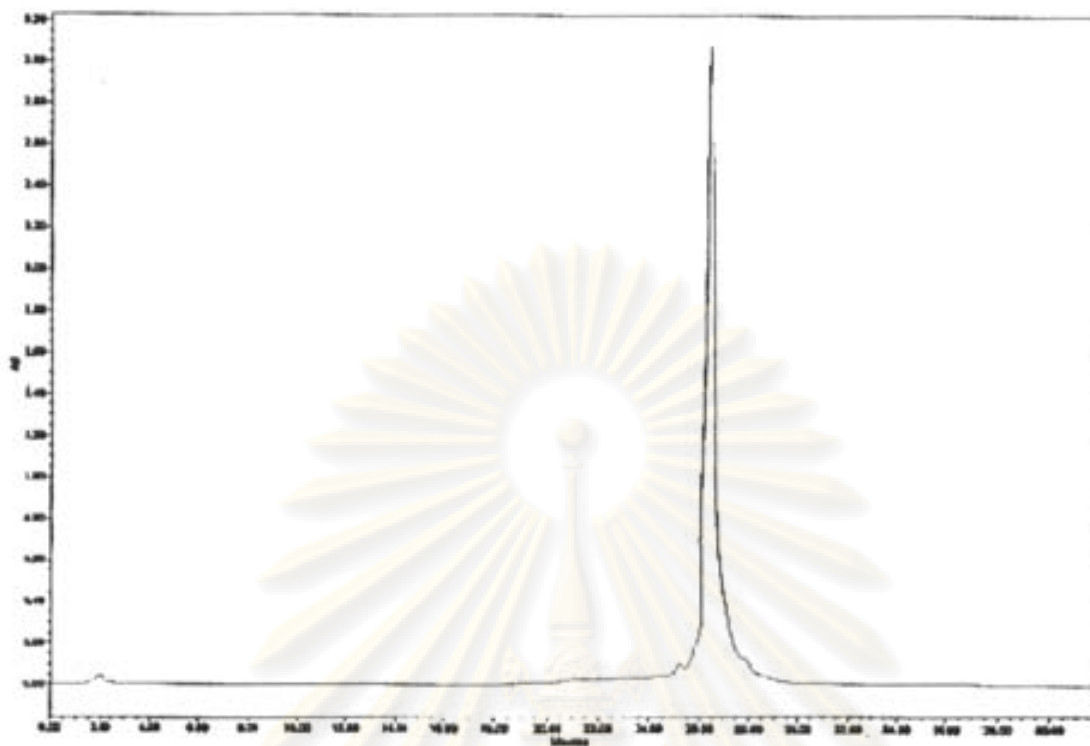
Figure B-19 : HPLC chromatogram of BzS(CH$_2$)$_2$CO-egl-T$_9$-Lys(Phos)NH$_2$ (**P20**)
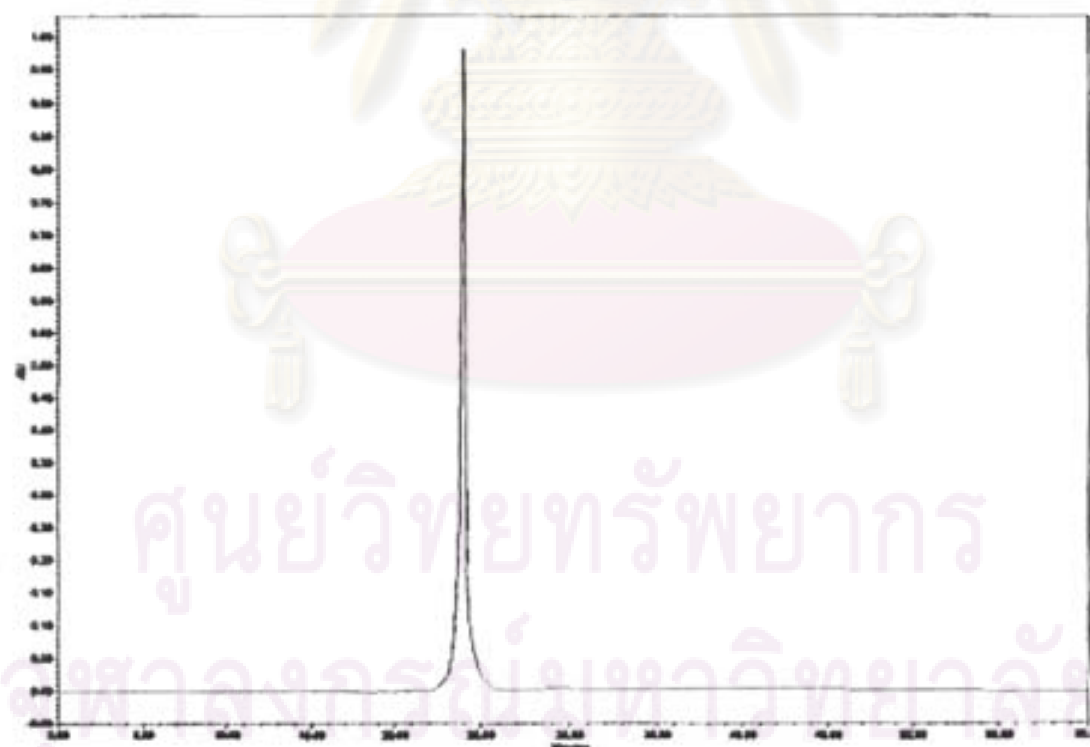
Figure B-20 : HPLC chromatogram of BzS(CH$_2$)$_2$CO-egl-T$_9$-Lys(Ac)NH$_2$ (**P21**)
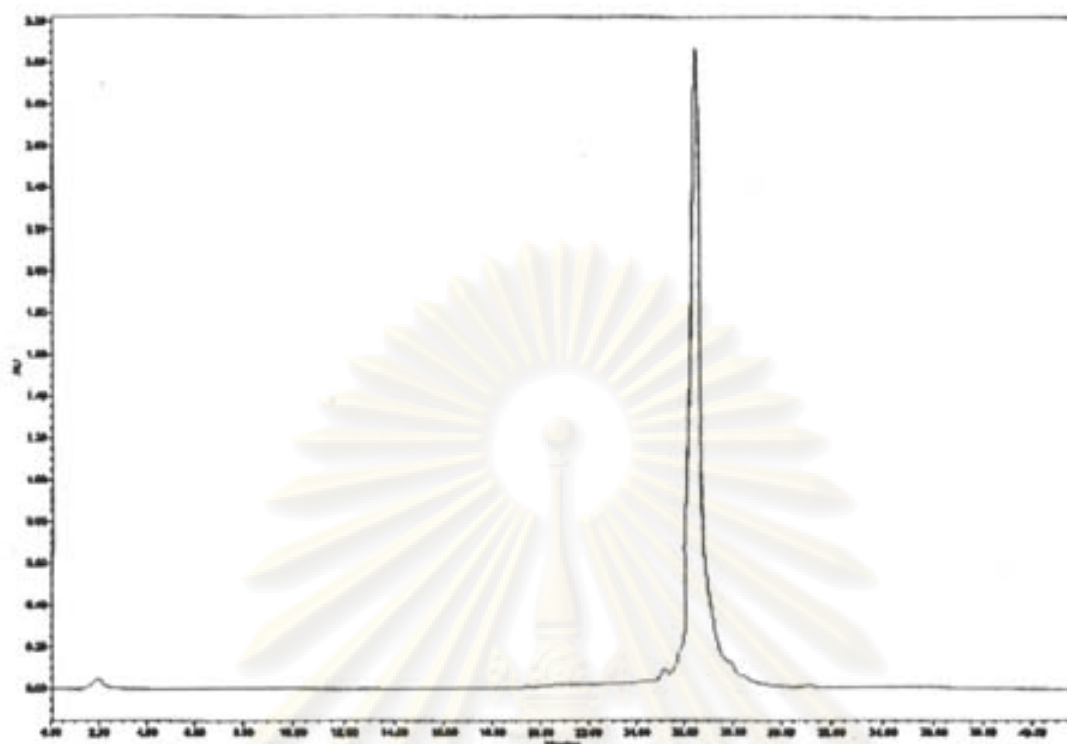
Figure B-21 : HPLC chromatogram of Bz-egl-T₉-Lys(Phos)NH₂ (**P22**)
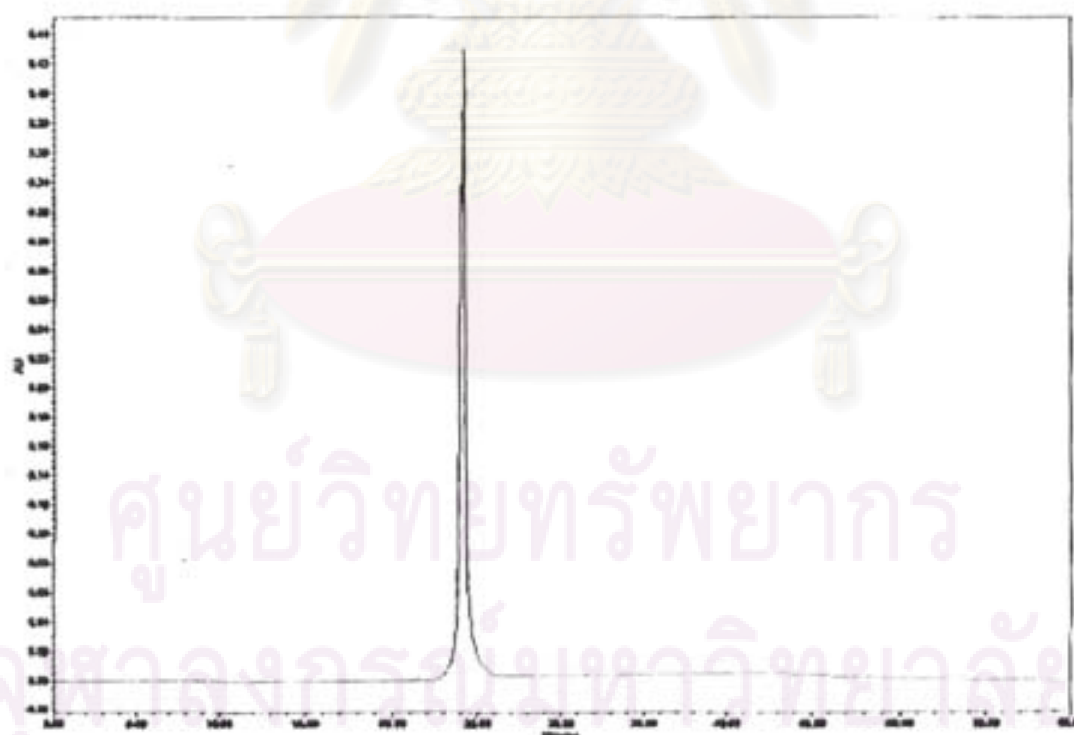
Figure B-22 : HPLC chromatogram of BzS(CH₂)₂CO-egl-TTCCCCCTCCCAA-Lys(Phos)NH₂ (**P23**)
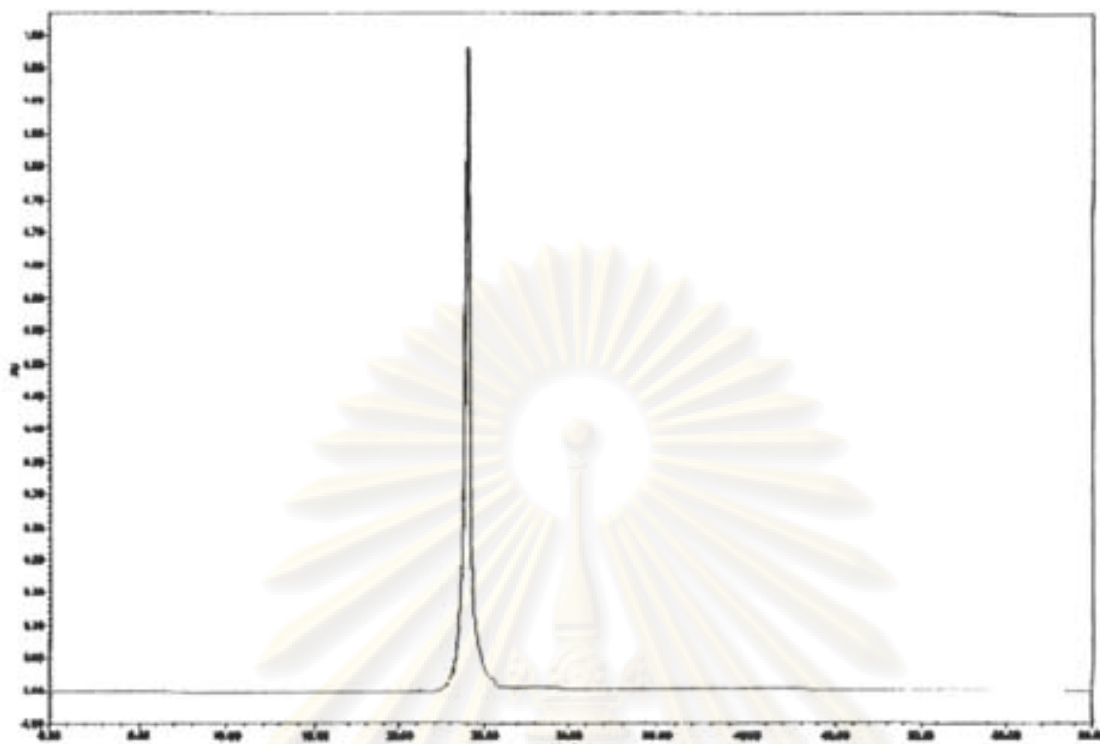
Figure B-23 : HPLC chromatogram of BzS(CH$_2$)$_2$CO-egl-TTCCCCTTCCCAA-Lys(Phos)NH$_2$ **(P24)**
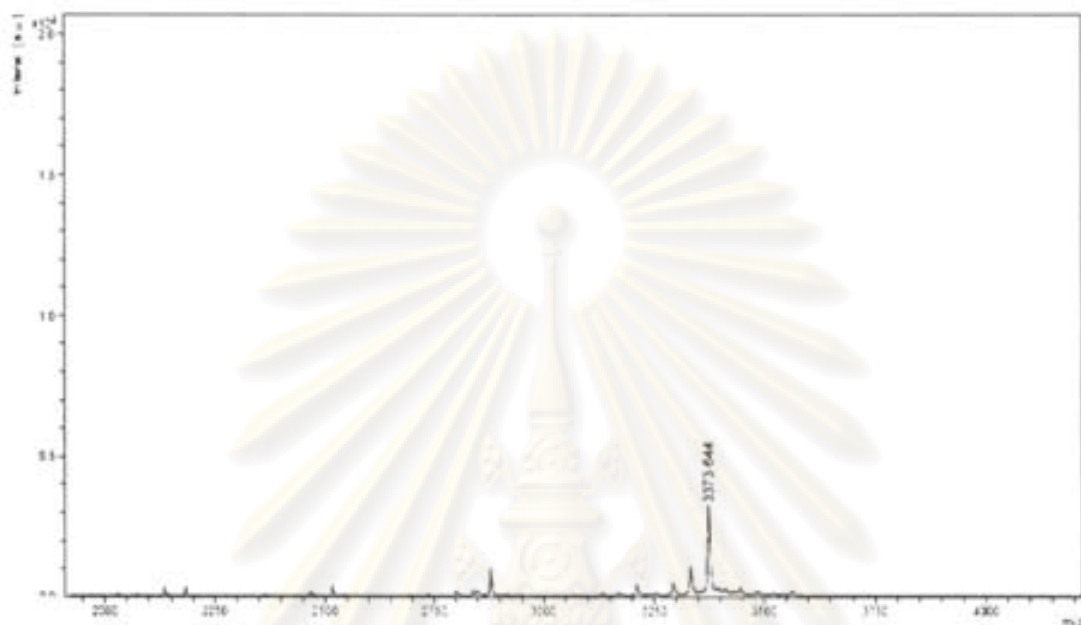
Figure C-1 : MALDI-TOF mass spectrum of HS(CH$_2$)$_2$CO-egl-T$_9$-LysNH$_2$ (**P1**)
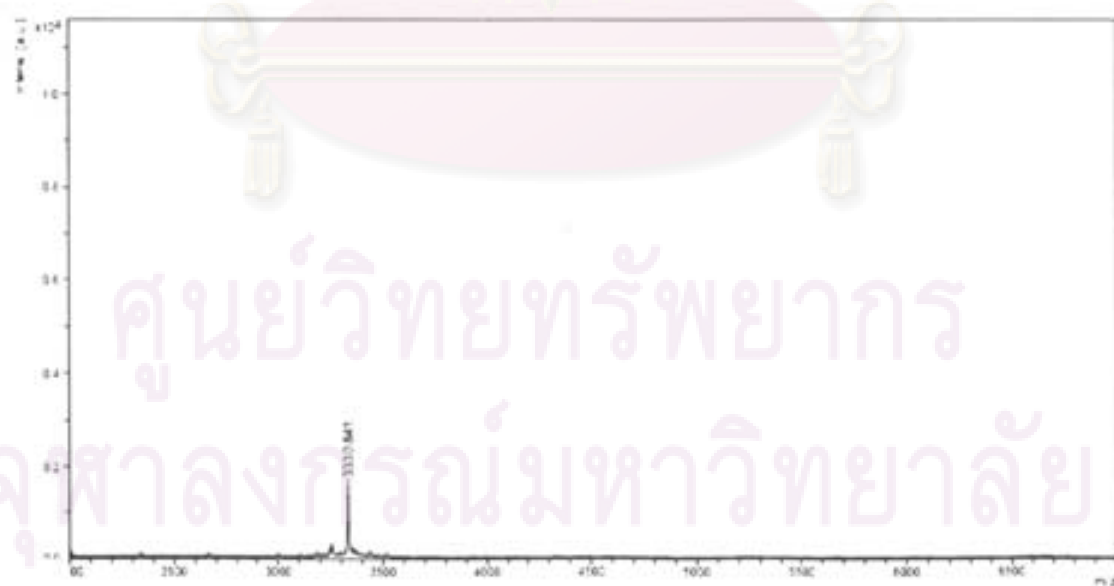
Figure C-2 : MALDI-TOF mass spectrum of HS(CH$_2$)$_2$CO-egl-T$_9$-SerNH$_2$ (**P2**)
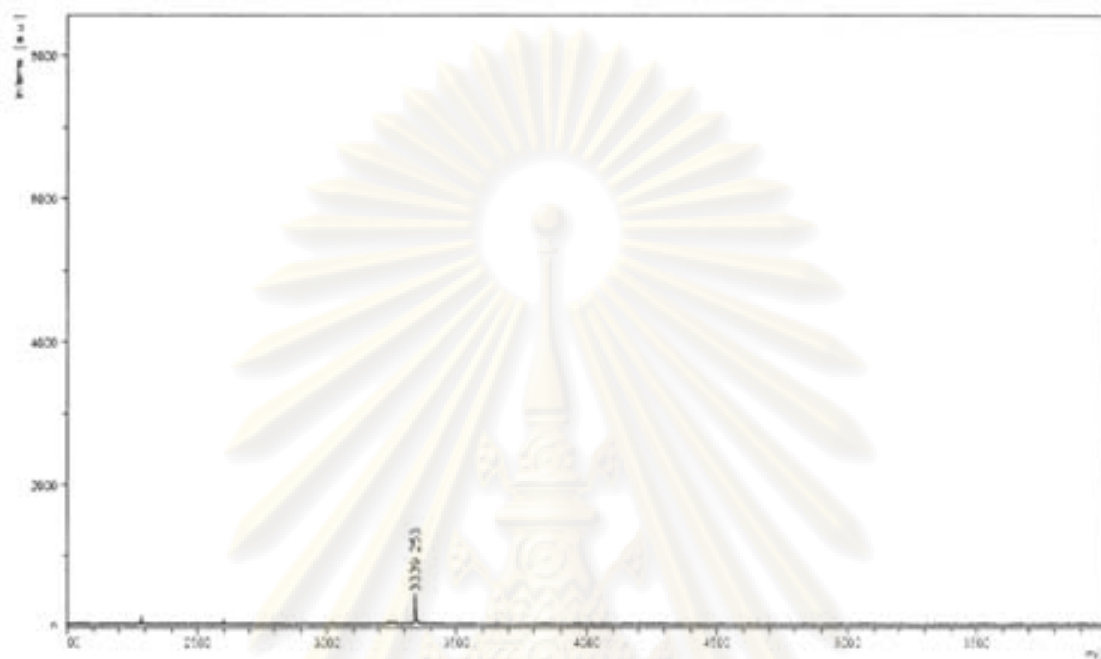
Figure C-3 : MALDI-TOF mass spectrum of HS(CH$_2$)$_2$CO-egl-T$_9$-AspNH$_2$ (**P3**)

Figure C-4 : MALDI-TOF mass spectrum of HS(CH$_2$)$_2$CO-egl$_3$-T$_9$-SerNH$_2$ (**P4**)
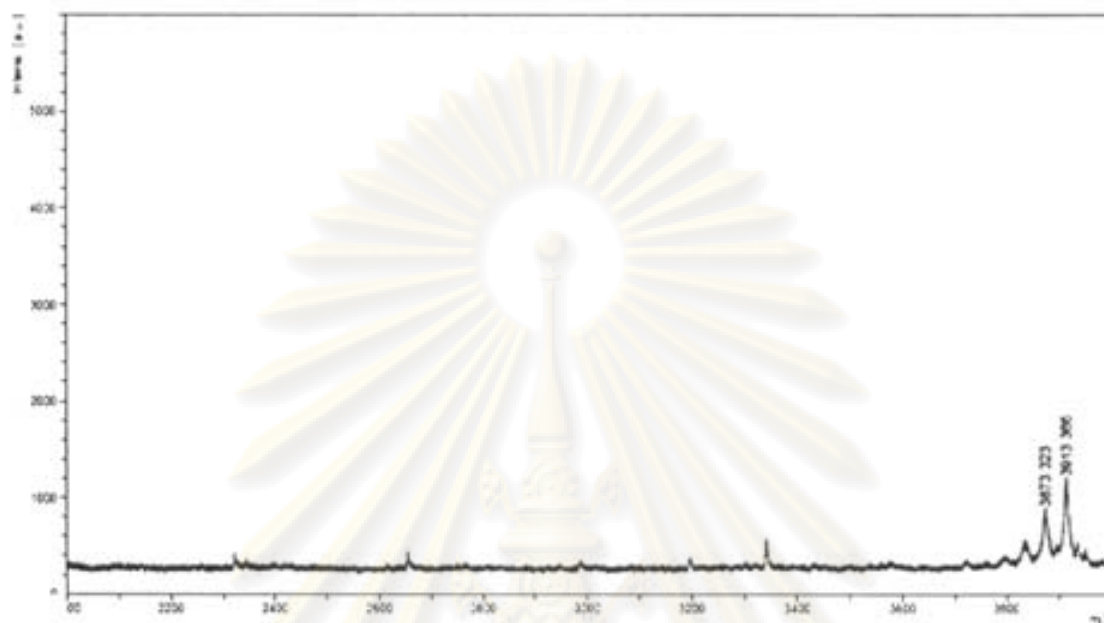
Figure C-5 : MALDI-TOF mass spectrum of HS(CH$_2$)$_2$CO-egl$_5$-T$_9$-SerNH$_2$ **(P5)**
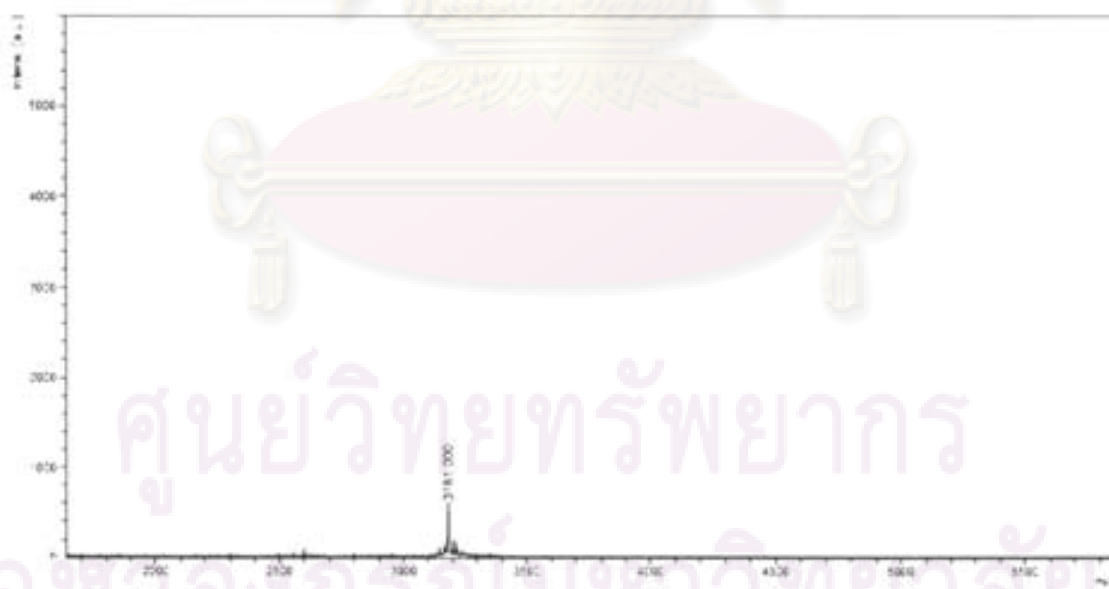
Figure C-6 : MALDI-TOF mass spectrum of Ac-T$_9$-LysNH$_2$ **(P6)**
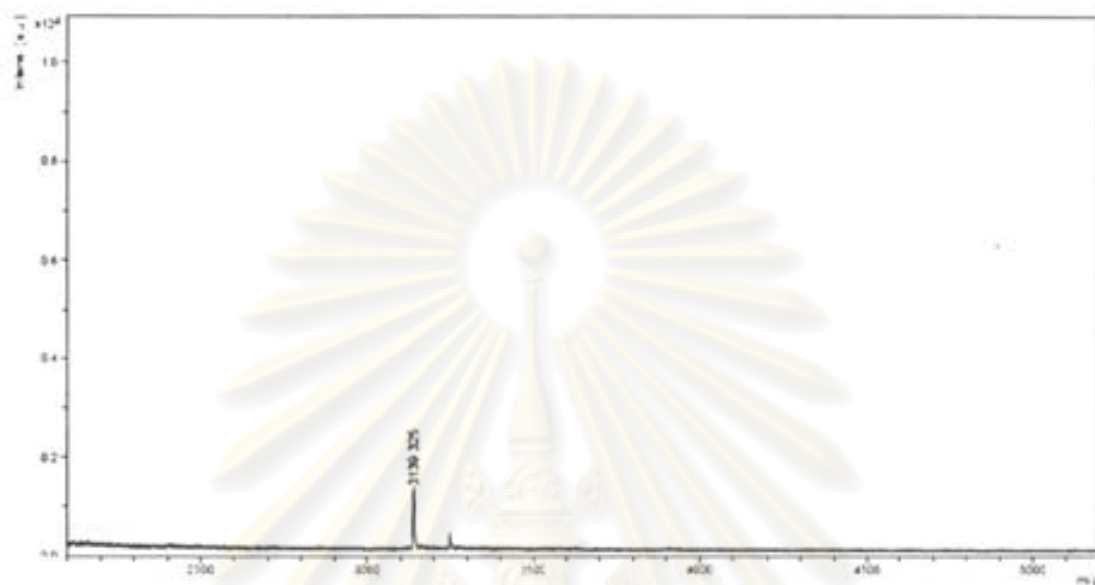
Figure C-7 : MALDI-TOF mass spectrum of Ac-T$_9$-SerNH$_2$ (**P7**)
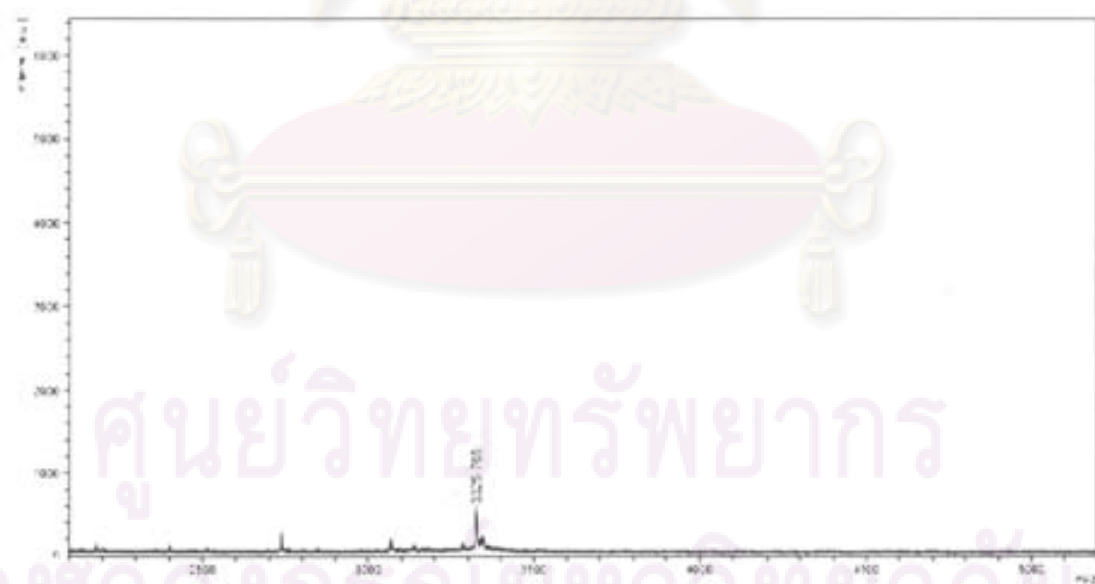
Figure C-8 : MALDI-TOF mass spectrum of Lipoic-T$_9$-LysNH$_2$ (**P8**)
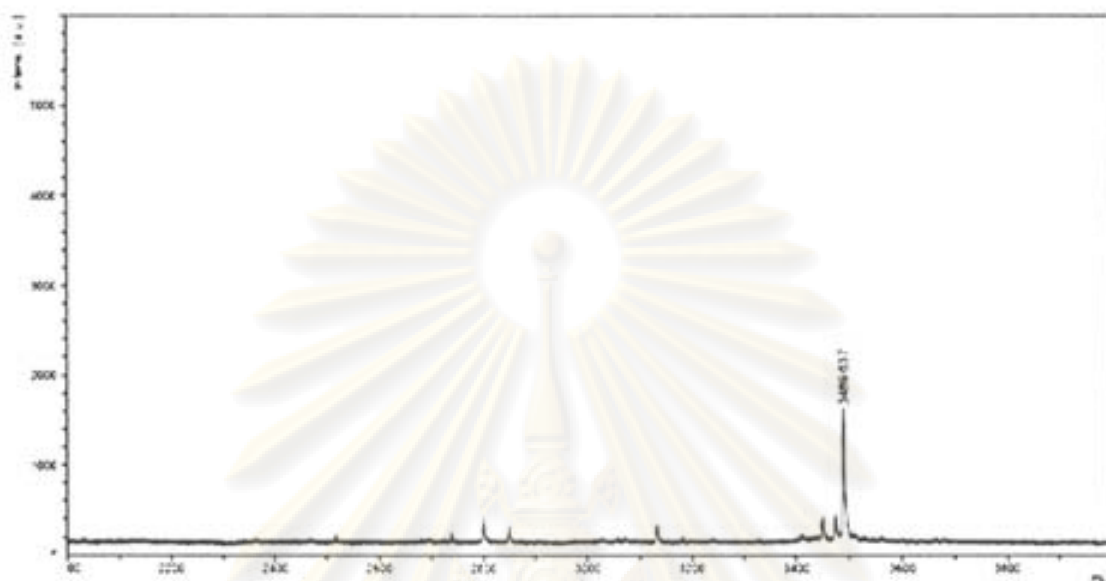
Figure C-9 : MALDI-TOF mass spectrum of Lipoic-egl-T$_9$-LysNH$_2$ (**P9**)
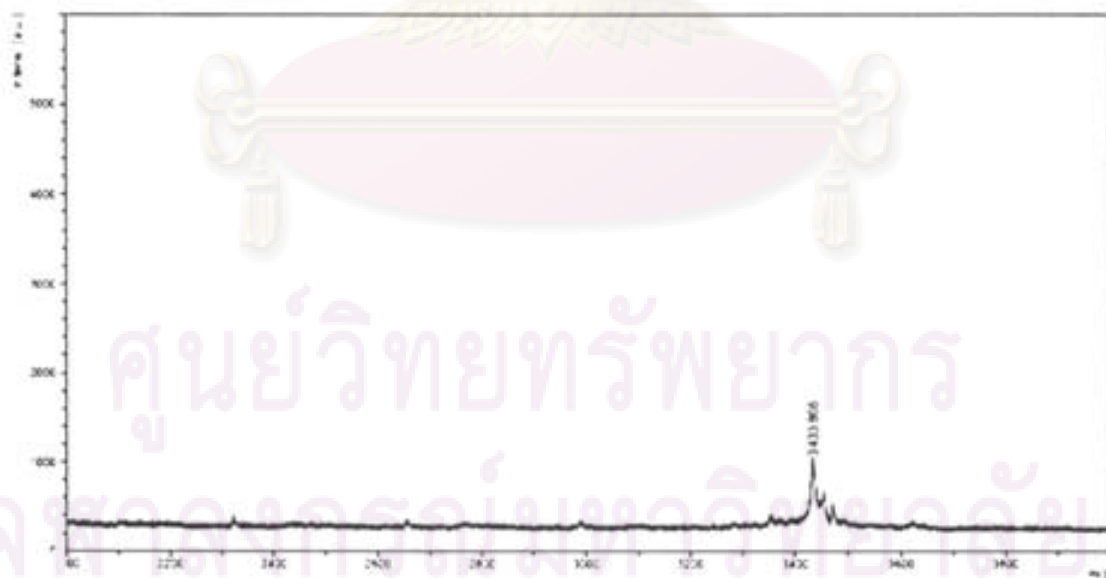
Figure C-10 : MALDI-TOF mass spectrum of Lipoic-egl-T$_9$-SerNH$_2$ (**P10**)
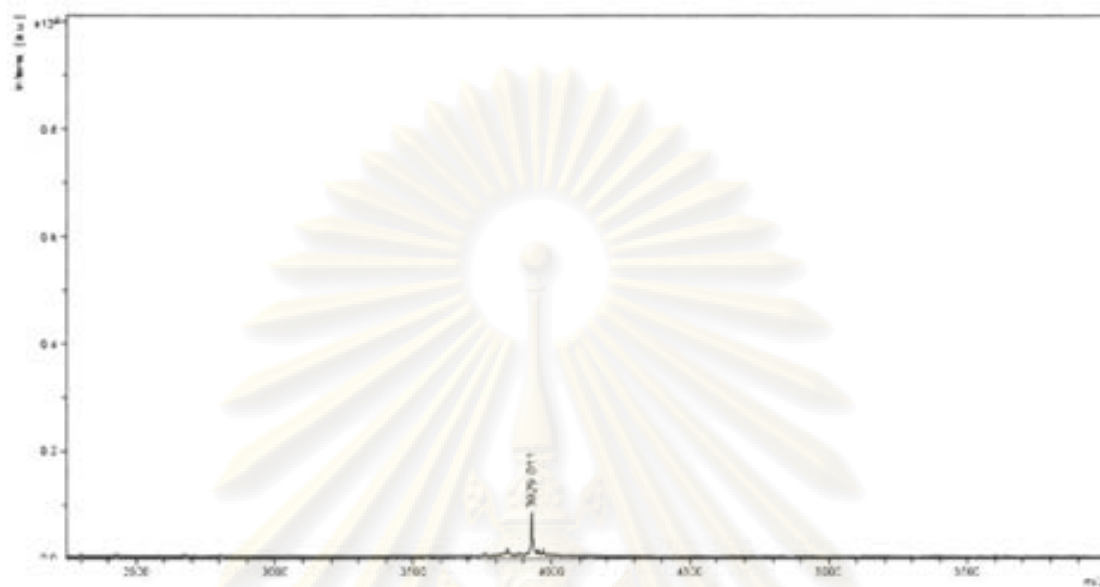
Figure C-11 : MALDI-TOF mass spectrum of Lipoic-egl-T$_9$-Lys(Fluorescien)NH$_2$
(P11)
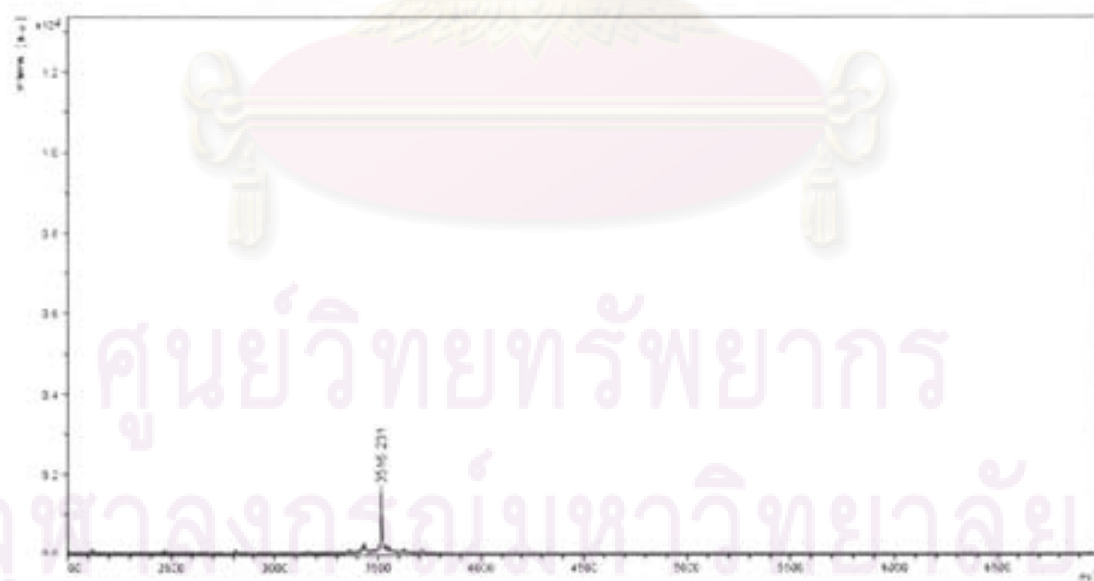
Figure C-12 : MALDI-TOF mass spectrum of DNP-S(CH$_2$)$_2$CO-egl-T$_9$-LysNH$_2$ (P12)
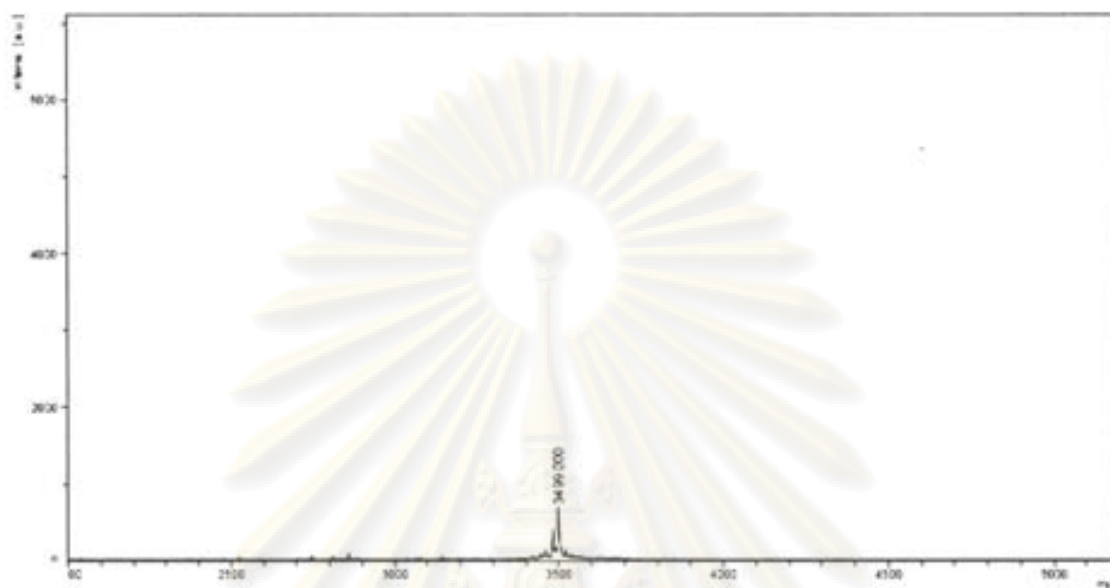
Figure C-13 : MALDI-TOF mass spectrum of BzS(CH$_2$)$_2$CO-egl-T$_4$GT$_4$-LysNH$_2$
(P13)
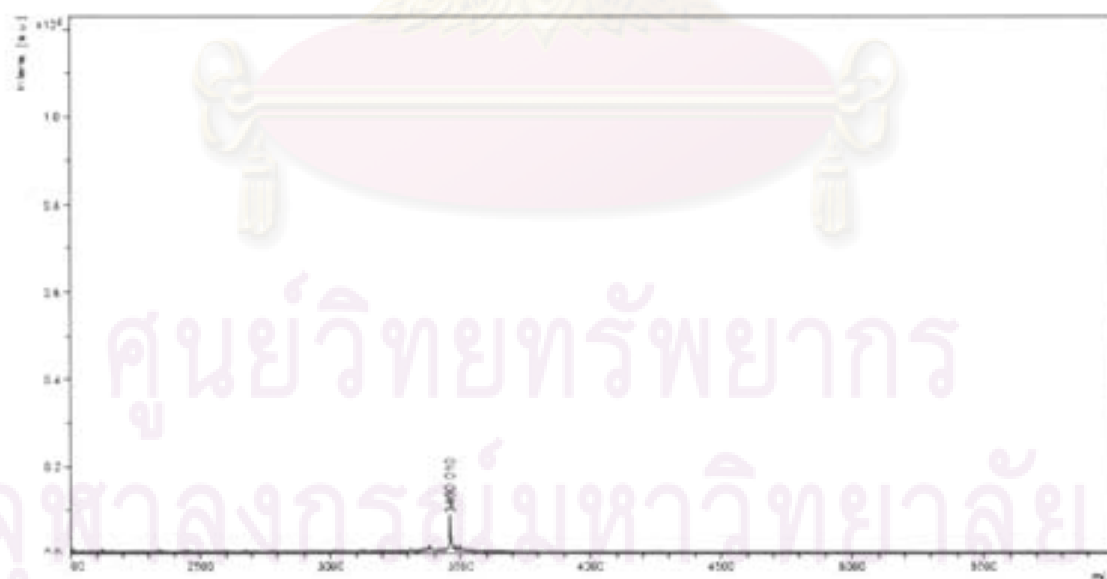
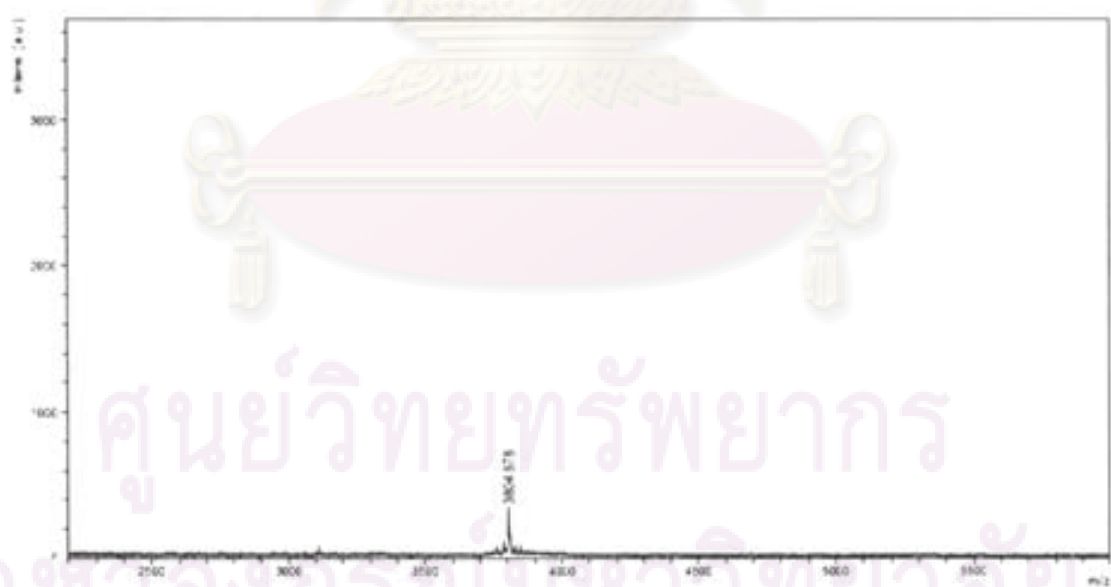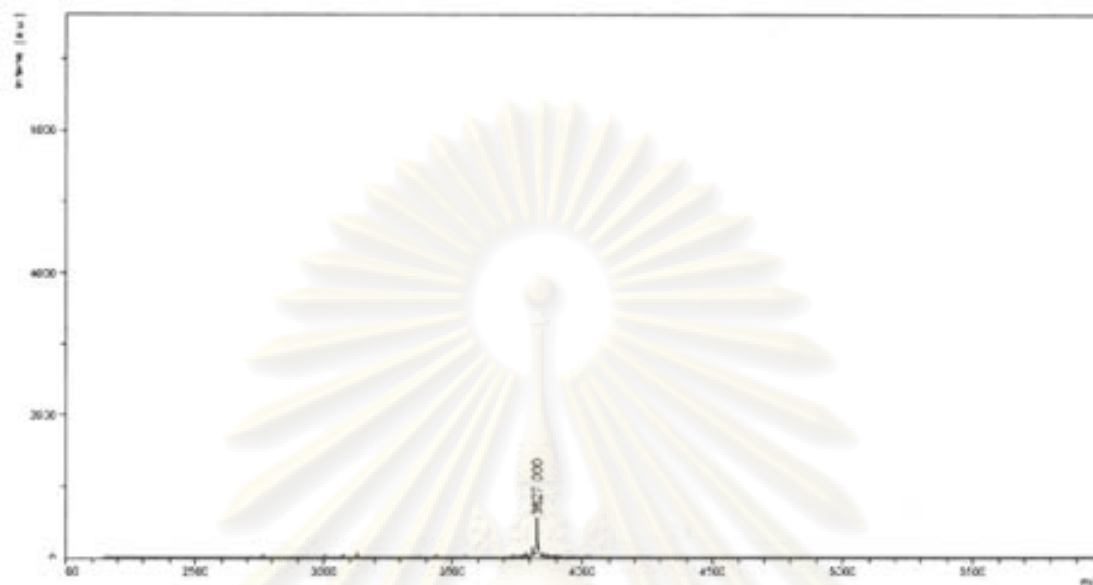**Figure C-14** : MALDI-TOF mass spectrum of BzS(CH$_2$)$_2$CO-egl-T$_4$CT$_4$-LysNH$_2$
(P14)
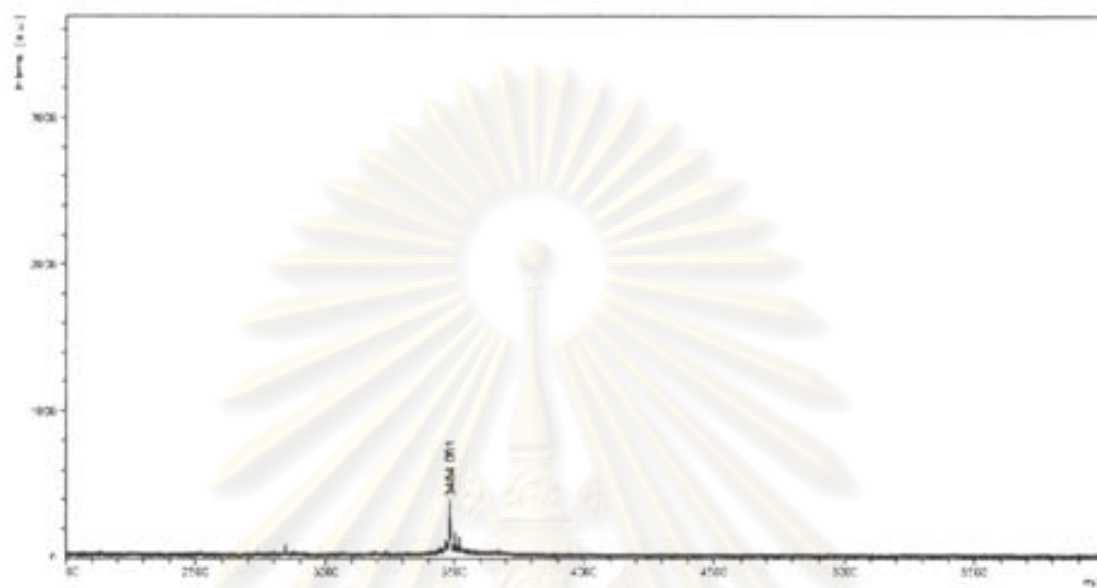
Figure C-15 : MALDI-TOF mass spectrum of BzS(CH₂)₂CO-egl-T₄AT₄-LysNH₂ (P15)
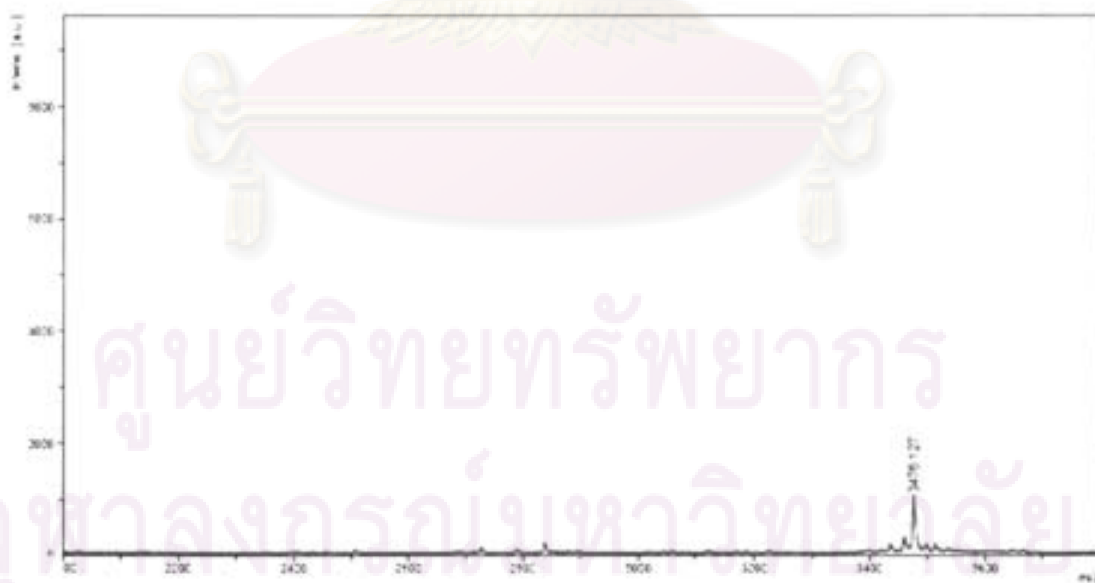
Figure C-16 : MALDI-TOF mass spectrum of BzS(CH₂)₂CO-egl-T₉-LysNH₂ (P16)
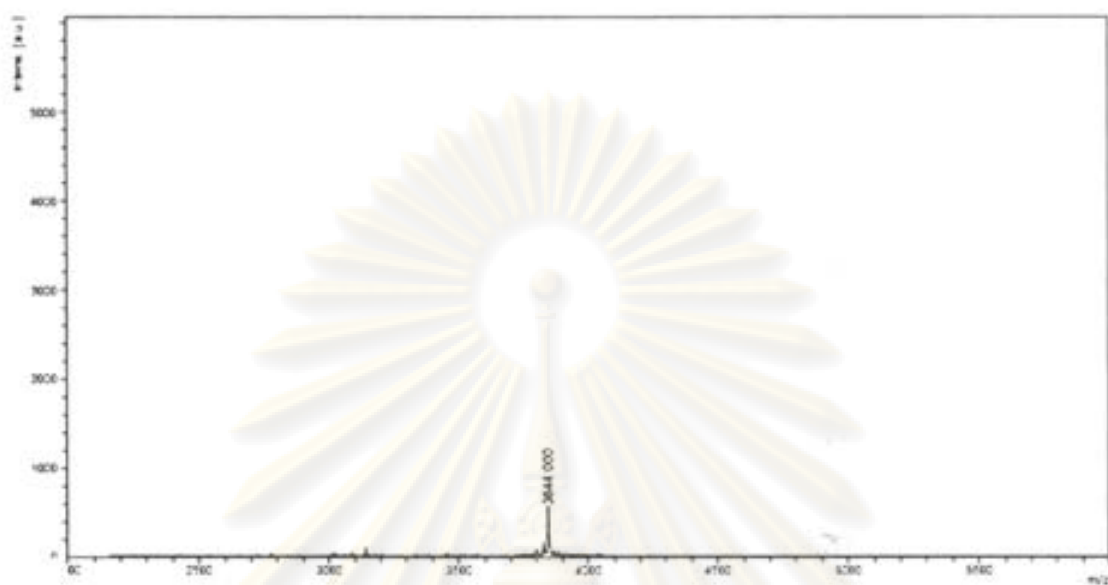
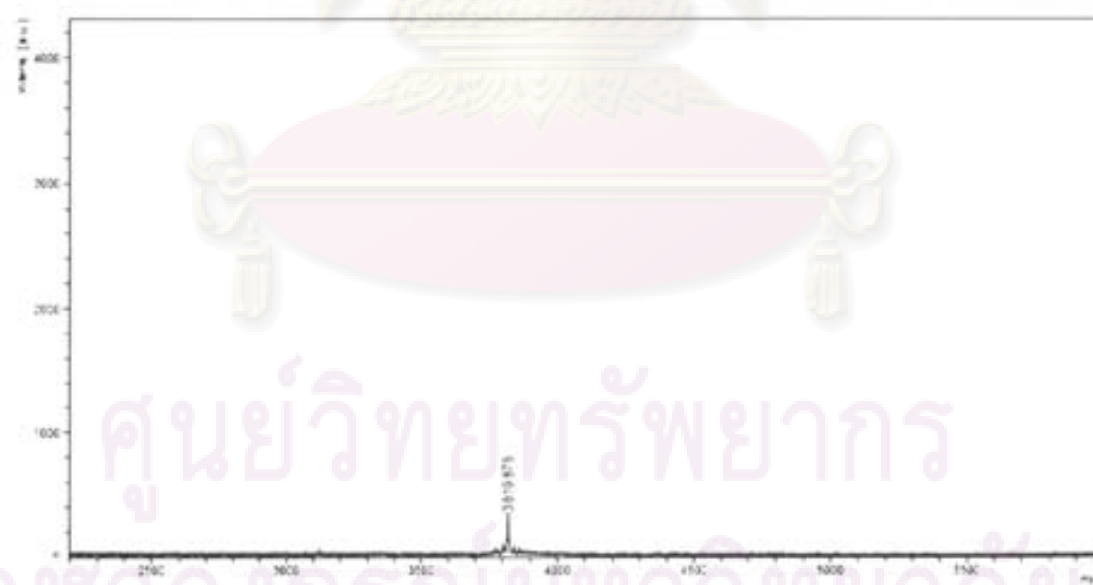**Figure C-17** : MALDI-TOF mass spectrum of BzS(CH$_2$)$_2$CO-egl-T$_4$GT$_4$-Lys(Phos)NH$_2$ (**P17**)

Figure C-18 : MALDI-TOF mass spectrum of BzS(CH$_2$)$_2$CO-egl-T$_4$CT$_4$-Lys(Phos)NH$_2$ (**P18**)

Figure C-19 : MALDI-TOF mass spectrum of BzS(CH₂)₂CO-egl-T₄AT₄-
Lys(Phos)NH₂ **(P19)**

Figure C-20 : MALDI-TOF mass spectrum of BzS(CH₂)₂CO-egl-T₉-Lys(Phos)NH₂
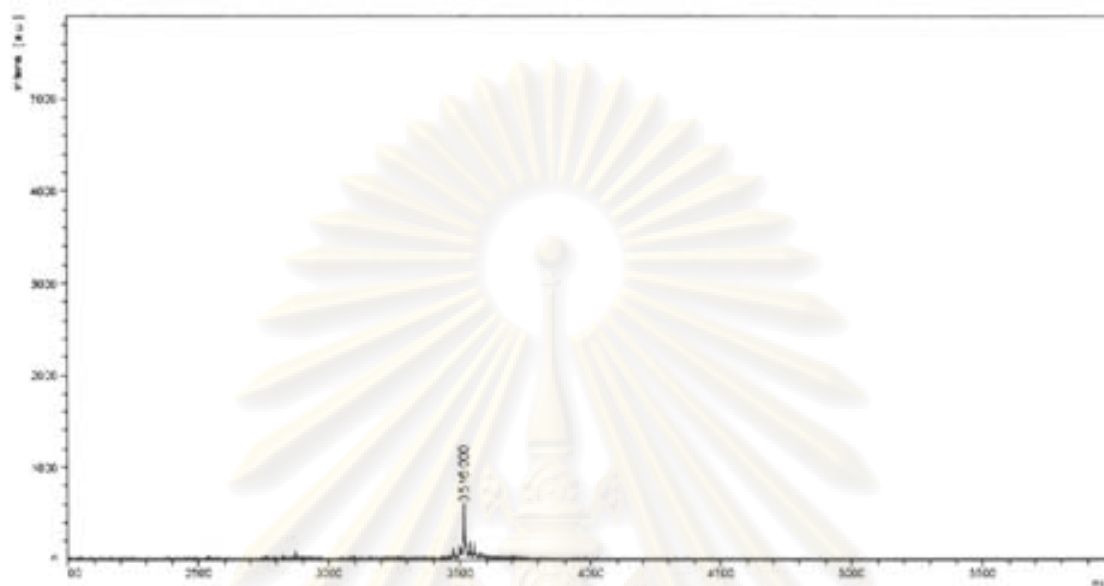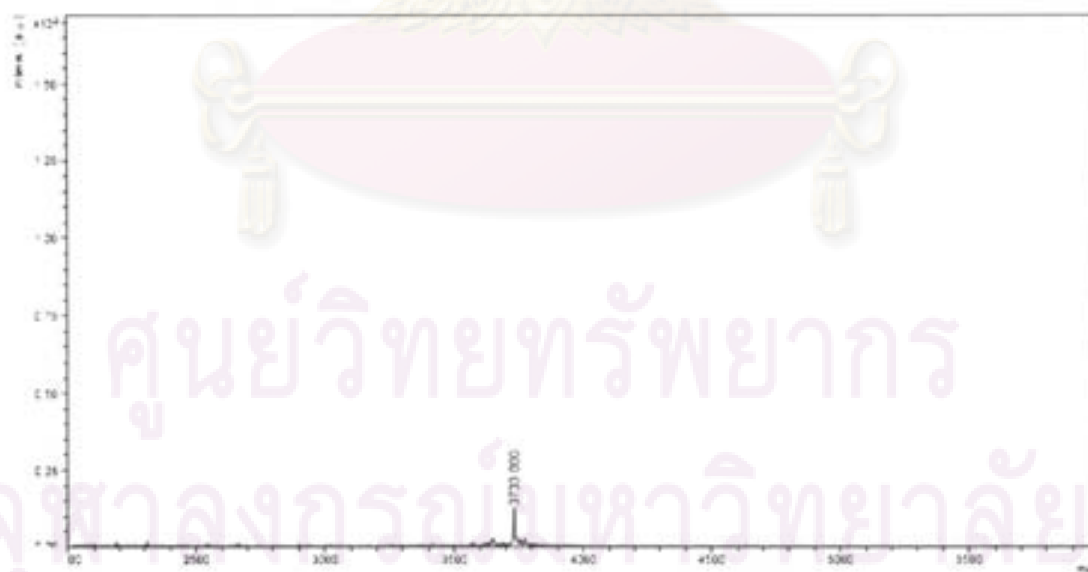**(P20)**

Figure C-21 : MALDI-TOF mass spectrum of BzS(CH$_2$)$_2$CO-egl-T$_9$-Lys(Ac)NH$_2$ (**P21**)

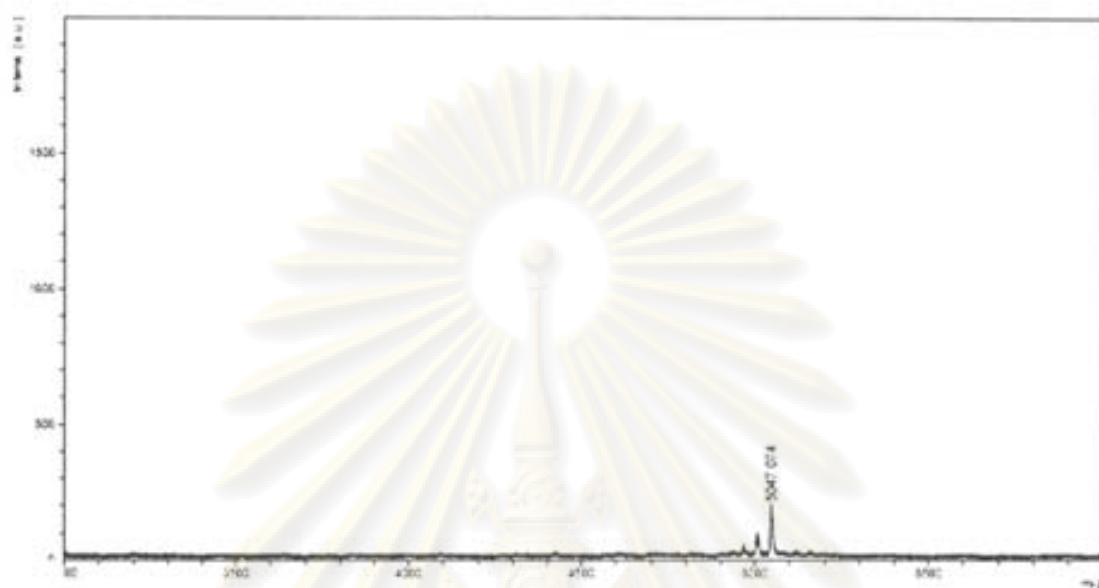**Figure C-22** : MALDI-TOF mass spectrum of Bz-egl-T$_9$-Lys(Phos)NH$_2$ (**P22**)

Figure C-23 : MALDI-TOF mass spectrum of BzS(CH$_2$)$_2$CO-egl
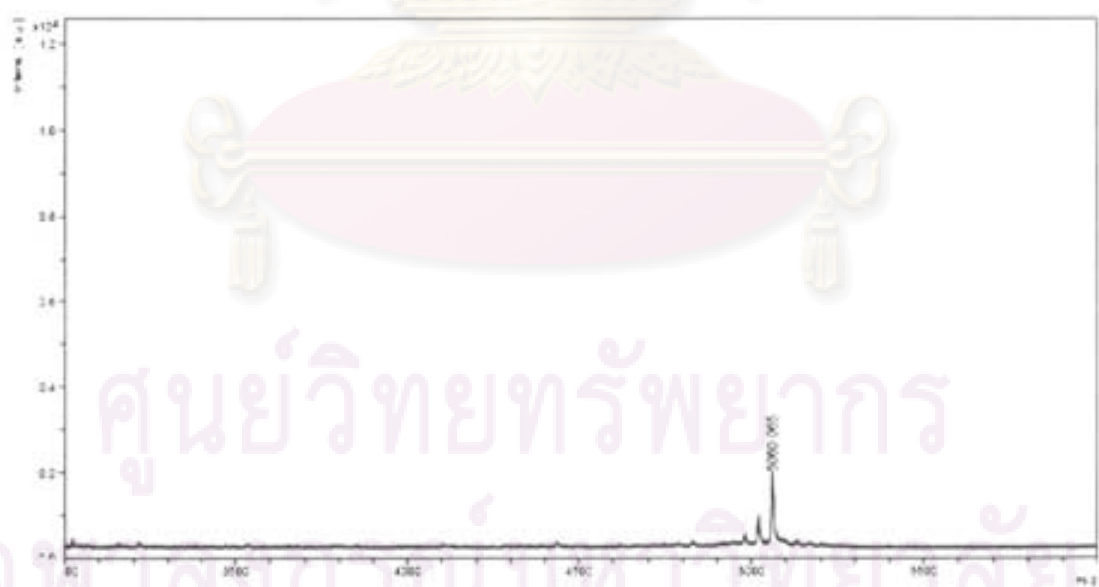TTCCCCCTCCCAA-Lys(Phos)NH$_2$ (**P23**)

Figure C-24 : MALDI-TOF mass spectrum of BzS(CH$_2$)$_2$CO-egl
TTCCCCTTCCCAA-Lys(Phos)NH$_2$ (**P24**)

VITAE

Miss Roejarek Kanjanawarut was born on June 16th, 1983 in Bangkok, Thailand. She graduated a Bachelor Degree of Science, majoring in Chemistry from Chulalongkorn University in 2005. In the same year, she was admitted to the Master's degree of Science, program in Petrochemistry and Polymer Science, at Chulalongkorn University and graduated in the academic year of 2007.